

The Role of N1-Src in Neuronal Development

Sarah Jane Wetherill

PhD

University of York

Biology

May 2016

Abstract

Protein phosphorylation by tyrosine kinases evolved in multicellular organisms to regulate intracellular signalling pathways associated with proliferation, differentiation and migration. In most tissues, basal protein tyrosine phosphorylation is maintained at low levels, but in the brain, basal tyrosine kinase activity is high and regulates key processes in the developing and mature brain and is dysregulated in neurological disorders. N1-Src is a neuronal splice variant of the ubiquitous proto-oncogene C-Src tyrosine kinase, which differs by a six amino acid insert in its SH3 domain. Since the SH3 domain confers substrate specificity, it is anticipated that both C- and N1-Src will have different substrates and functions. Specifically, N1-Src is highly active in the developing brain and has been implicated in neuronal differentiation. Studies also suggest a role for N1-Src in ion channel regulation, however, the mode of action of N1-Src remains poorly understood. The primary aim of this study was to further clarify the role of N1-Src in both the developing and adult brain. To achieve this, a multidisciplinary approach was adopted, which sought to 1) identify novel N1-Src substrates 2) determine the function of N1-Src in developing neurons and 3) dissect the signalling pathways downstream of N1-Src.

Recombinant, active Src kinases were generated to undertake *in vitro* kinase assays with putative N1-Src substrates. Src-dependent phosphorylation of HCN1, a pacemaker channel identified as an N1-Src interactor in a yeast 2-hybrid screen, could not be detected. This result was not conclusive as surprisingly, the assay did not detect Src or PKC phosphorylation of NR2A, an NMDA receptor subunit, previously characterised as a robust Src and PKC substrate. However, a screen of several putative N1-Src SH3 binding peptides revealed some encouraging candidates to pursue as substrates. To address the function of N1-Src in neuronal development, N1-Src was overexpressed or knocked down in cultured hippocampal neurons. Both manipulations were detrimental to neurite outgrowth and neuronal polarization, suggesting that N1-Src activates cytoskeletal remodelling pathways and precise levels of N1-Src are required for normal cellular development *in vitro*. The molecular mechanism of this phenomenon was investigated in a fibroblast cell line, in which N1-Src overexpression induces neurite-like processes. Using this model, an investigation into the role of N1-Src in RhoA signalling implied that N1-Src does not drive process outgrowth via the inhibition of RhoA, however constitutive activation of RhoA, prevented N1-Src mediated process extension. Preliminary results suggested that N1-Src overexpression enhances RhoA activation, which could form part of a negative feedback loop. Taken together, I have implicated N1-Src in neurite outgrowth, which provides a starting point for understanding the mechanistic role of N1-Src in pathways that dictate neuronal morphology.

Table of Contents

Abstract	2
Table of Contents.....	3
Table of Tables	8
Table of Figures	9
Acknowledgements.....	13
Declaration	14
Chapter 1. Introduction.....	16
1.1 Protein Phosphorylation	16
1.1.1 Tyrosine Phosphorylation.....	17
1.2 The Structure and Regulation of Src Family kinases (SFKs)	18
1.2.1 The SH4 Domain.....	20
1.2.2 The Unique Domain	20
1.2.3 The SH3 Domain.....	21
1.2.4 The SH2 Domain.....	24
1.2.5 The SH1 (Kinase) Domain	26
1.2.6 The C-terminal Domain (CTD)	27
1.2.7 The Autoregulation of SFKs	27
1.3 Cellular Functions of C-Src.....	30
1.3.1 C-Src Functions in the Brain	31
1.3.1.1 The Role of C-Src in the Developing Brain	31
1.3.1.2 The Role of C-Src in the Adult Brain	33
1.4 SFKs in Health and Disease.....	38
1.5 Neuronal Src Kinases.....	38
1.5.1 The Spatiotemporal Expression of N1-Src.....	41
1.5.2 Physiological Functions of the Neuronal Srcs.....	42
1.5.3 Neuronal Src Kinases in Neuroblastoma	43
1.5.4 Substrates and Binding Partners of N1-Src	44
1.6 Aims	49
Chapter 2. Materials and Methods	51
2.1 Materials.....	51
2.1.1 Molecular Biology Reagents	51
2.1.2 Protein Biochemistry Reagents.....	51
2.1.3 Cell Biology Reagents	52

2.2	Molecular Biology	52
2.2.1	Polymerase Chain Reaction (PCR).....	52
2.2.2	Agarose Gel Electrophoresis	52
2.2.3	Restriction Digest of Deoxyribonucleic Acid (DNA)	53
2.2.4	Agarose Gel Extraction of DNA Fragments	53
2.2.5	Annealing of Complimentary Oligonucleotides	53
2.2.6	Ligation of PCR Product into pJET1.2	53
2.2.7	DNA Ligation	53
2.2.8	Bacterial Transformation	53
2.2.9	PCR Colony Screening	54
2.2.10	Preparation of Plasmid DNA from Bacterial Cultures	54
2.2.11	Sequencing of Plasmid Constructs	54
2.2.12	Preparation of Glycerol Stocks for Storage of Plasmid DNA	55
2.2.13	Cloning	55
2.2.13.1	Src-pmCherry Constructs.....	55
2.2.13.2	pGEX-6P-1: hHCN1-CTD	55
2.2.13.3	pGEX-6P-1: rNR2A-CTD	55
2.2.13.4	pGEX-4T-1: CTD Constructs	55
2.2.13.5	pGEX-6P-1 Constructs Encoding GST-fusion Peptides.....	55
2.3	Protein Biochemistry	58
2.3.1	Protein Expression	58
2.3.2	Purification of Recombinant Proteins	58
2.3.3	Cleavage of the GST Tag from GST Fusion Proteins.....	59
2.3.4	SDS-Polyacrylamide Gel Electrophoresis (PAGE)	60
2.3.5	Wet Transfer.....	60
2.3.6	Western Blotting	60
2.3.7	<i>In Vitro</i> Kinase Assays with GST-hHCN1- and GST-rNR2A- Purified Proteins..	61
2.3.8	<i>In Vitro</i> γ - ³² P ATP Kinase Assays with hHCN1- and rNR2A-CTD	61
2.3.9	<i>In Vitro</i> Protein Kinase C-zeta (PKC-zeta) Kinase Assays with hHCN1- or rNR2A-CTD	62
2.3.10	<i>In Vitro</i> His Δ 80-N1-Src Kinase Assays with Putative GST-fusion Peptide Substrates	62
2.3.11	Immunoprecipitation (IP)	63
2.3.12	RhoA Pull-down Activation Assay	63
2.4	Cell Biology Techniques	64
2.4.1	Culture of Mammalian Cell Lines	64
2.4.1.1	Revival of Cell Stocks	64
2.4.1.2	Passage of Mammalian Cell Lines.....	64
2.4.1.3	Cell Storage.....	65
2.4.1.4	Plating Cells	65
2.4.2	L1-CAM Process Outgrowth Assay.....	65

2.4.3	Cell Line Transfections using EcoTransfect Reagent	65
2.4.4	Preparation of Rat Hippocampal Neurons	65
2.4.4.1	Transfection of Rat Hippocampal Neurons	66
2.4.5	Immunocytochemistry	66
2.4.5.1	Cell Fixation and Staining	66
2.5	Cell Imaging	67
2.5.1	Image Capture Using a Fluorescence Microscope	67
2.5.2	Coverslip Tiling Using the Zeiss Slidescanner	67
2.6	Analysis of Cell Morphology Data	67
2.6.1	Morphological Analysis Using NeuronJ	67
2.6.2	Statistical Analysis of Cell Data.....	68
Chapter 3.	Discovery of Novel N1-Src Substrates.....	70
3.1	Introduction	70
3.1.1	Aims	72
3.2	Results	73
3.2.1	The Purification of Recombinant Src kinases	73
3.2.2	The Expression and Purification of GST-hHCN1- and GST-rNR2A-CTD	75
3.2.3	The <i>In Vitro</i> Phosphorylation of GST-hHCN1-CTD and GST-rNR2A-CTD Could not be Detected via Western Blotting.....	78
3.2.4	Expression and Purification of Untagged hHCN1- and rNR2A-CTD.	80
3.2.5	hHCN1-CTD and rNR2A-CTD Phosphorylation was not Detected by Autoradiography.....	80
3.2.6	Phosphorylation of the rNR2A- and hHCN1-CTD by PKC was not Detected by Autoradiography.....	85
3.2.7	Prospective N1-Src Substrates Identified Through a Peptide Substrate Screen.....	87
3.3	Discussion	97
3.3.1	A Lack of <i>In Vitro</i> Phosphorylation of rNR2A-CTD and hHCN1-CTD by C- and N1-Src.	97
3.3.2	The Design of an <i>In Vitro</i> Kinase Assay Peptide Substrate Screen to Identify Putative Novel N1-Src Peptides.....	101
3.3.3	Alternative Methods for Discovering Novel N1-Src Substrates.	103
Chapter 4.	The Role of N1-Src in Neuronal Development.....	106
4.1	Introduction	106
4.1.1	N1-Src and Neuronal Development.	106
4.1.2	The Role of N1-Src in L1-CAM Mediated Neurite Outgrowth.	106
4.1.3	Using Rodent Model Systems for Studying the Effects of N1-Src on Neuronal Morphology.....	107
4.1.4	Aims	109

4.2	Results	109
4.2.1	Measuring the Morphological Parameters of Rat Hippocampal Neurons.....	109
4.2.2	N1-Src Overexpression in Hippocampal Neurons Leads to Aberrant Neuronal Morphology.....	113
4.2.3	N1-Src Overexpression Affects the Development of Cultured Rat Hippocampal Neurons.	116
4.2.4	N1-Src can be Specifically Knocked Down Using shRNA.	118
4.2.5	Knockdown of N1-Src with shRNA A Reduces the Length of Longest Neurite.	120
4.2.6	N2-Src shRNA B Increases Neurite Branching.....	123
4.2.7	A Time-course of N1-Src Shrna Transfection Reveals the Length of Longest Neurite Further Decreases with Time.	126
4.2.8	The Role of N1-Src in L1-CAM Mediated Neurite Outgrowth.	128
4.3	Discussion	133
4.3.1	The Experimental Use of Primary Hippocampal Neurons.	133
4.3.2	N1-Src Overexpression Resulted in Aberrant Neurite Outgrowth.	134
4.3.3	The Specificity of the N1-Src Targeting shRNAs.	136
4.3.4	Depletion of N1-Src Expression by shRNA A Resulted in Reduced Neurite Outgrowth.....	137
4.3.5	The Overexpression and Knockdown of N1-Src Display Similar Effects on Neuronal Morphology.....	139
4.3.6	The Effect of shRNA B on the Primary Branching of Neurites.....	140
Chapter 5.	<i>Dissecting the Role of N1-Src in RhoA Signalling</i>	142
5.1	Introduction	142
5.1.1	RhoA as a Regulator of Cell Morphology.....	142
5.1.2	The Molecular Mechanism and Regulation of the Small GTPase RhoA	142
5.1.3	Aims	145
5.2	Results	146
5.2.1	Dissecting the Role of N1-Src in RhoA Signalling Using RhoA Mutants.	146
5.2.2	Manipulating RhoA-N1-Src Signalling via the Inhibition of Rho.....	155
5.2.3	Overexpression of GFP-RhoA-WT, -Q63L and -T19N did not Affect N1-Src-FLAG Activity in COS7 Cells.....	161
5.2.4	N1-Src and C-Src-FLAG Interacted with Active GFP-RhoA-WT in COS7 Cells.....	164
5.3	Discussion	168
5.3.1	Dissecting the Role of N1-Src and RhoA in the Regulation of Process Outgrowth in COS7 Cells.....	168
5.3.1.1	The Effect of N1-Src-mCherry on Cell Morphology	168
5.3.1.2	The Effect of RhoA Inactivation on Cell Morphology	168
5.3.1.3	The Effect of the RhoA/B/C Inhibition on Cell Morphology	169

5.3.1.4	The Effect of Constitutively Active RhoA on Cell Morphology.	170
5.3.1.5	The Effect of N1-Src-on the Activation of RhoA.....	171
5.3.2	The Alternate Roles of C- and N1-Src in RhoA Signalling.....	173
5.3.2.1	The Differential Activation of RhoA by N1 and C-Src	173
5.3.3	RhoA as a Binding Partner for N1-Src	174
5.3.4	Concluding Remarks.....	175
Chapter 6. Conclusions and Future Directions.....		177
6.1	N1-Src as a Regulator of Ion Channel Signalling	177
6.2	The Role of N1-Src in Neuronal Development and Cytoskeletal Dynamics	178
6.3	Different Roles of C-, N1- and N2-Src.....	180
6.4	Future Directions.....	180
Abbreviations.....		183
References.....		188

Table of Tables

Table 1.1: A Summary of C- and N1-Src SH3 Binding Partners and their Relative Ability to Bind to each Kinase.....	46
Table 2.1: The Oligonucleotide Sequences Used to Generate GST-fusion Peptide Substrates for C- and N1-Src.....	57
Table 2.2: Antibiotic and Growth Conditions for <i>E.Coli</i> Expressing Various pGEX Constructs	59
Table 2.3: Western Blotting Antibodies and Blocking Conditions	61
Table 2.4: Kinase Buffers Used for <i>In Vitro</i> Kinase Assays Containing GST-hHCN1-CTD and GST-rNR2A-CTD.....	62
Table 2.5: Primary and Secondary Antibodies Used in Immunocytochemistry	67
Table 3.1: Prospective N1-Src Substrate Candidates that were Selected for the <i>In Vitro</i> Kinase Assay Screen.....	92

Table of Figures

Figure 1.1: Schematic Diagram Illustrating the Modular Structure of SFKs.	19
Figure 1.2: The Structure of the C-Src SH3 Domain in Complex with a Class I Ligand.	23
Figure 1.3: The Structure of the V-Src SH2 Domain.	25
Figure 1.4: A Schematic Illustrating SFK Activation.	29
Figure 1.5: Schematic Diagram Illustrating the Mini-exon Inserts in the SH3 Domains of Neuronal Src Kinases.	39
Figure 3.1: Purification of Recombinant C- and N1-Src Kinases	74
Figure 3.2: Optimisation of GST-hHCN1- and GST-rNR2A-CTD Expression and Purification.....	77
Figure 3.3: Attempted Detection of GST-hHCN1-CTD and GST-rNR2A-CTD Phosphorylation by C- and N1-Src.....	79
Figure 3.4: Recombinant Expression and Cleavage of GST-hHCN1- and GST-rNR2A- CTD.....	81
Figure 3.5: Neither rNR2A-CTD nor hHCN1-CTD Phosphorylation by C- or N1- Src were Detected by Autoradiography.....	83
Figure 3.6: Increasing the Reaction Content of rNR2A-CTD and hHCN1-CTD did not Result in Detectable Phosphorylation by C- or N1- Src by Autoradiography.	84
Figure 3.7: Neither Full Length rNR2A-CTD nor hHCN1-CTD were Phosphorylated by PKC-Zeta when Incubated with γ -32P ATP for 3 h.....	86
Figure 3.8: GST-Fusion Peptide Substrates Contained the Proposed N1-Src SH3 Binding Consensus Sequence Linked to the 'Ideal Src Substrate'.	88
Figure 3.9: Differential Phosphorylation of PD1-P5A and PD1 was Observed at a Substrate Concentration of 5 μ M.	90
Figure 3.10: Expression and Purification of GST-Fusion Peptides P1-P13.	93
Figure 3.11: Assessment of the Tyrosine Phosphorylation of Putative N1-Src GST- Fusion Peptide Substrates by Western Blotting	95
Figure 4.1: The Neuronal Polarization of Rat Hippocampal Neurons in Culture (Dotti's Classification System).....	108
Figure 4.2: Schematic Diagram Depicting the Method of Hippocampal Neuronal Morphology Analysis Using NeuronJ.	110
Figure 4.3: The Length of Rat Hippocampal Neurons Varied Between Cultures.	112
Figure 4.4: Overexpression of N1-Src-mCherry in Hippocampal Neurons Resulted in Aberrant Neuronal Morphology.....	114
Figure 4.5: N1-Src-mCherry Overexpression in Hippocampal Neurons Resulted in Aberrant Neurite Outgrowth.	115

Figure 4.6: The Overexpression of N1-Src-mCherry Disrupted Hippocampal Neuron Development in Culture.	117
Figure 4.7: shRNAs A and B Largely Depleted N1- and N2-Src Expression Respectively.	119
Figure 4.8: Representative Images of the Morphological Effects of shRNAs A and B in Hippocampal Neurons.	121
Figure 4.9: Knockdown of N1-Src by Two Independent shRNAs (A and B) Resulted in Atypical Neuronal Morphology.	122
Figure 4.10: N1-Src Knockdown by Two Independent shRNAs had Little Effect on the Primary Branching of Neurites in Hippocampal Neurons.....	124
Figure 4.11: N1-Src Knockdown by Two Independent shRNAs did not Affect the Percentage of Hippocampal Neurons with Secondary and Tertiary Branches.....	125
Figure 4.12: The Effect of N1-Src Depletion by shRNA A on the Length of Longest Neurite Increased with Respect to Time.	127
Figure 4.13: N1-Src-mCherry Co-localised with L1-CAM in the Perinuclear Region of COS7 Cells that were Grown in the Absence or Presence of L1-Fc.....	129
Figure 4.14: Preliminary Results Indicated that Homophilic L1-CAM Signalling did not Enhance Process Outgrowth in COS7 Cells.	130
Figure 5.1: Schematic Diagram Illustrating the Mechanism of RhoA Activation and Inactivation.	143
Figure 5.2: Schematic Diagram Illustrating the Dominant Negative and Constitutively Active RhoA Mutants.	147
Figure 5.3: N1-Src Co-localises with RhoA WT and T19N in the Perinuclear Region of COS7 Cells, which is Less Apparent in RhoA Q63L Expressing Cells.	148
Figure 5.4: The Effects N1-Src-mCherry and the GFP-RhoA Mutants on Process Extension in COS7 Cells.....	150
Figure 5.5: Process and Branch Formation is Enhanced in Cells Co-expressing N1-Src-mCherry and GFP-RhoA-T19N.....	152
Figure 5.6: The Effects of N1-Src-mCherry and the GFP-RhoA Mutants on the Cell Area and Circularity of COS7 Cells.	153
Figure 5.7: Schematic Diagram Illustrating the Inhibition of RhoA-C by C3.....	156
Figure 5.8: Overexpression of N1-Src-mCherry did not Enhance C3 Mediated Process Formation.	157
Figure 5.9: Process and Branch Formation, as well as the Length of Longest Process was Comparable in Cells Co-expressing C3 and empty-, C- or N1-Src-mCherry.	159
Figure 5.10: The Effects of the mCherry-Srcs and C3 Inactivation of Rho on the Cell Area and Circularity of COS7 Cells.	160

Figure 5.11: Overexpression of GFP-RhoA-WT, -Q63L or -T19N had Little Effect on C- or N1-Src-FLAG Activity.....	163
Figure 5.12: N1-Src-FLAG neither Interacted with nor Phosphorylated GFP-RhoA-WT.	165
Figure 5.13: C- and N1-Src have Differential Effects on the Activation Status of GFP-RhoA.	167
Figure 5.14: Schematic of the Proposed N1-Src/RhoA Signalling Pathway Regulating COS7 Cell Morphology.	172

I would like to dedicate this thesis to

Zoe Kilby (1989-2007)

A school friend that was taken too soon and whose strength and determination was truly inspiring.

Acknowledgements

I would like to thank both of my supervisors Gareth and Will, for their invaluable expertise and support that they have provided throughout this project for which, I am extremely grateful. Thank you to my TAP panel, Sangeeta and Frans for their input and support over the years. Phil, Clare, Laura and Ines, thank you for your wonderful company, help in the lab and ingenious humour. I would also like to thank the whole community in the Biology department, for their help, support, friendship and kindness. I would particularly like to thank Jenny and Jo from cookies, for their encouragement, friendship and support, and for supplying me with copious amounts of hot chocolate and cookies in my times of need.

To my amazing family and friends, thank you for your kindness, generosity and support, which has been greatly appreciated. Mum and Dad, thank you for your love and for getting me through the hard times. To my sister Laura, thank you for your immense encouragement, generosity, brilliant advice and for being the best sister ever. Thank you to my brilliant brother in law, Glen, for your wonderful support and letting me stay whilst I was writing. I cannot wait to welcome 'bump' to the world (I love you already) and I will endeavour to be the best aunty possible.

Charlotte you have been an amazing flat mate and a treasured friend, we have made a brilliant team and I know that we will be friends for life. Clare, your friendship has been indispensable; thank you for your support, the laughs, fantastic dancing and for being you. Laura S, Kelsey, Dan, Gemma, Laura W, Ines, Alice, Katy, Henry and Hannah, thank you for being wonderful friends and for your brilliant company.

Last but not least, I have to thank my sister's pet hamster Doug Doug (aka Dougalugs) who has been the best thesis buddy in the world. Thank you Dougers for your company whilst I have been writing and for keeping me vaguely sane.

Thank you.

Declaration

The work presented in this thesis was performed by the author (Sarah Jane Wetherill) between July 2012 and October 2016 in the Department of Biology, University of York, within the laboratory of Dr Gareth Evans. All experiments were performed by the author, with the exception of the cloning that has been listed below and referenced appropriately throughout this thesis. Neither this thesis nor any part of it has previously been submitted for acceptance of a higher degree.

* The *pSuper-shRNA-A* and *pSuper-shRNA-B* constructs were designed by Dr Gareth Evans and prepared by Katharina Mahal.

* The constructs *pGEX-6P-1-YA* and *pGEX-6P-1-PD1* were created by Dr Sarah Keenan.

Chapter 1

Introduction

Chapter 1. Introduction

1.1 Protein Phosphorylation

Protein phosphorylation is a post-translational modification (PTM), which alters protein function. The phenomenon of protein phosphorylation was first observed by Burnett and Kennedy in 1954, who demonstrated that casein was phosphorylated by the liver enzyme, casein kinase. Since this initial discovery, the field has expanded greatly with approximately 17,000 proteins known to be phosphorylated at one or more sites. Protein phosphorylation is therefore acknowledged as a key regulator of many cell biological mechanisms including proliferation, differentiation, migration, and trafficking, as well as many neuronal and immunological processes.

Phosphorylation is a reversible covalent modification that involves the transfer of a phosphoryl group to a hydroxylated amino acid residue (serine (Ser), threonine (Thr) or tyrosine (Tyr)) on a protein substrate. In cells, the forward phosphorylation reaction is catalysed by enzymes called kinases, which use adenosine triphosphate (ATP) molecules as phosphoryl donors. Phosphatase enzymes catalyse the reverse, dephosphorylation reaction, which remove the phosphoryl group from the amino acid residue.

As one of the largest gene families, the protein kinases make up 1.7 % of the human genome, with 518 members, most of which contain a conserved protein kinase catalytic domains that facilitate phosphoryl transfer (Manning et al., 2002). There are two main types of kinases; the Ser/Thr kinases and Tyr- kinases. Although, dual specificity kinases with both Ser/Thr and Tyr- kinase activity, also exist (e.g. (Roskoski, 2012)). The proportion of Ser, Thr, and Tyr phospho-sites within the phosphoproteome varies. Of the 6,600 phosphorylation sites derived from 2,244 proteins in the phosphoproteome of HeLa cells, 86.4 % of the sites were phosphoserine residues, 11.8 % were phosphothreonine residues and 1.8 % were phosphotyrosine residues (Olsen et al., 2006).

A further class of kinase, termed the pseudokinases, has also been described (reviewed in (Zeqiraj and van Aalten, 2010)). These kinases lack residues present in the active site of the conserved eukaryotic kinase domain that are critical for catalysis. For example, the pseudokinase STRAD, which forms part of a tumour suppressing complex with the adaptor protein MO25 and the kinase LKB1, serves to activate LKB1 via a phosphorylation independent mechanism. When bound as a pseudosubstrate in complex with LKB1, STRAD acts as an allosteric activator of the kinase (Zeqiraj et al., 2009). The pseudokinase is thought to have lost its ability to catalyse substrate

phosphorylation throughout evolution (Zeqiraj and van Aalten, 2010). Further examples of pseudokinases, whose functions are mediated via the formation of protein-protein interactions, include ILK (Fukuda et al., 2009), HER3 (Jura et al., 2009) and VRK3 (Kang and Kim, 2008). Whilst all pseudokinases were widely considered in the field to be inactive, in the past decade studies have emerged that have demonstrated that several pseudokinases are in fact catalytically active (Taylor and Kornev, 2010), although they are still the subject of much controversy.

Phosphorylation can exert its effects by modifying the activity, stability or localization of the target protein. In addition, protein phosphorylation can also facilitate or disrupt protein-protein interactions (Sopko and Andrews, 2008). This places both kinases and phosphatases at the centre of many diverse signalling networks, which regulate virtually all cellular processes. Given that protein phosphorylation is linked to such a broad range of functions in cell biology, it is unsurprising that the deregulation of both kinases and phosphatases can result in a variety of disease pathologies. For example multiple types of cancer (Mammoto et al., 2016), vascular diseases (Nakamura et al., 2016) and neurodegenerative diseases (Gatta et al., 2016) have been linked to aberrant protein phosphorylation.

1.1.1 Tyrosine Phosphorylation

Whilst tyrosine phosphorylation accounts for the lowest proportion of protein phospho-sites in comparison to Ser/Thr, this does not make it any less important. The human kinome contains 90 tyrosine kinases, which can be categorised into two families: receptor tyrosine kinases (RTKs) and non-receptor tyrosine kinases (nRTKs) (Manning et al., 2002).

RTKs account for 58 of the 90 tyrosine kinases and are type 1 transmembrane proteins that contain three distinct domains: an N-terminal extracellular domain, a single transmembrane domain and a C-terminal cytoplasmic domain (Manning et al., 2002). Generally, RTKs are activated upon ligand binding to the extracellular domain, which results in receptor dimerization (or in some cases oligomerisation), triggering the transphosphorylation of tyrosines in their cytosolic C-terminal domain. This in turn, creates binding sites for proteins containing Src homology 2 (SH2) domains (discussed in Section 1.2.4) or phosphotyrosine binding (PTB) domains. The subsequent RTK phosphorylation of various docking proteins, such as Gab1, can also facilitate the recruitment of other signalling proteins that act in downstream signalling transduction pathways (Lemmon and Schlessinger, 2010). Therefore, in effect, the intracellular domains of activated RTKs act as junctions where multiple signalling pathways can be triggered (Lemmon and Schlessinger, 2010).

Two of the major downstream signalling pathways that are triggered downstream of RTK activation include the Ras/Map kinase (MAPK) and the PI-3K/Akt pathways. Both of these pathways are initiated through the recruitment of the adaptor protein Grb2, which binds to the phosphorylated C-terminal tail of RTKs (Lemmon and Schlessinger, 2010). To stimulate the Ras/MAPK pathway, the two SH3 domains of Grb2 bind to SOS, a guanine nucleotide exchange factor (GEF) that catalyses the activation of the GTPase Ras. Activated Ras recruits and activates RAF, which triggers a MAPK cascade involving the subsequent activation of MEK and ERK (English et al., 1999). To activate the PI-3K pathway, Grb2 recruits the docking protein Gab1, which becomes phosphorylated and binds to the p85 subunit of PI-3K, resulting in the activation of the kinase. PI-3K catalyses the production of the lipid, phosphoinositide-3,4,5-triphosphate (PIP3). PIP3 recruits Akt to the membrane via its pleckstrin-homology (PH) domain, where it is activated and phosphorylates downstream targets (Cantley, 2002). These pathways together with others, form an interconnected complex signalling network that regulate key cellular processes including cell proliferation, differentiation and survival (Lemmon and Schlessinger, 2010).

Dissimilar to RTKs, nRTKs are mainly cytosolic intracellular proteins, although some are membrane localised since they contain an N-terminal lipid modification. Many act as additional subunits of cell surface receptors that do not have catalytic tyrosine kinase domains themselves (reviewed in Hunter, 2009) whilst some kinases, such as Src, are recruited to activated RTKs. Therefore, in response to receptor ligand binding, nRTKs are capable of triggering downstream signalling events (Neet and Hunter, 1996). Whilst there are nine families of nRTKs, the Src family of kinases will be the point of discussion in the remainder of this introduction.

1.2 The Structure and Regulation of Src Family kinases (SFKs)

Src family kinases (SFKs) are nRTKs, which comprise 11 known individual members (Manning et al., 2002). Eight of the family members, namely Blk, C-Src, Fgr, Fyn, Hck, Lck, Lyn and Yes, have been the most comprehensively studied and over the years, structural studies have revealed that SFKs share the same conserved modular structure, differing only by the N-terminal regions of the protein (Figure 1.1). The modular domains, termed Src homology (SH) domains, have since been described to occur in many other types of protein. The SFKs each comprise the following six domains: the SH4, unique, SH3, SH2, SH1 (or kinase domain) and the C-terminal domains (Figure 1.1; reviewed in Engen *et al.*, 2008). The role of each of these domains in both the function and regulation of the kinase is discussed below.

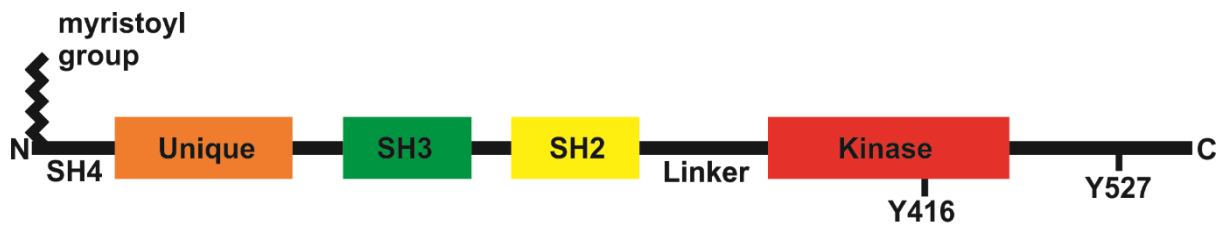


Figure 1.1: Schematic Diagram Illustrating the Modular Structure of SFKs.

The structure of each family member contains an N-terminal SH4 domain, followed by the unique, SH3, SH2 and catalytic kinase domains. The SH4 domain contains a lipid modification, which facilitates membrane tethering. Both the SH3 and SH2 domains confer substrate specificity by binding PXXP or phosphotyrosine motifs respectively, whereas the kinase domain catalyses the phosphorylation of bound substrates. The phosphorylation of Y-416 in the kinase domain promotes catalytic activity. Adjacent to the kinase domain is the C-terminal tail, which contains the highly conserved Y-527 and regulates the autoinhibition of SFKs upon phosphorylation.

1.2.1 The SH4 Domain

The N-terminal region of SFKs, comprising the SH4 and unique domains, is the least conserved area of the protein and its structure is intrinsically disordered. Lipid modification of the SH4 domain facilitates tethering to the plasma membrane, as well as other intracellular membrane compartments and is required for SFK function *in vivo* (Resh, 1994). All SFKs are myristoylated and many undergo additional palmitoylation (Resh, 1994, Koegl et al., 1994). Indeed, the myristoylation and palmitoylation sites, Gly-2 and Cys-3 (except in C-Src and Blk) respectively, are two of just a few conserved residues at the N-terminus (Koegl et al., 1994).

The sole irreversible myristoylation of SFKs occurs promptly after translation, whereas palmitoylation is a more dynamic, reversible modification that is dependent upon myristoylation and can occur at multiple sites in some SFKs (e.g. Lck and Fyn; (Buss et al., 1984, Paige et al., 1993, Koegl et al., 1994). Whilst this secondary modification strengthens membrane binding, palmitoylation has also been reported to localise SFKs to caveolae in the plasma membrane and to regulate the trafficking of SFKs (Shenoy-Scaria et al., 1994, Sato et al., 2009). The basic residues that flank the lipid modification sites also promote the kinases' interaction with the negatively charged plasma membrane (Silverman et al., 1993). Localisation of SFKs to the membrane enables the kinases to interact with and phosphorylate other membrane-localised proteins, as well as cytoplasmic components. Therefore, this modification is intrinsic to the function of SFKs, which are key components of many different signalling pathways and regulate many cellular processes.

1.2.2 The Unique Domain

The unique domain is the intrinsically disordered region (IDR) situated between the SH4 and SH3 domains of SFKs, which typically consist of 50-80 residues. Whilst the unique domains are not conserved between the different SFK members, the domain of each individual kinase is conserved between species (Amata et al., 2014). This indicates a specific role of the unique domain in the regulation and function of each kinase. In support, the swapping of the unique domains of C-Src and Yes, effectively switches the functional properties of the kinases (Summy et al., 2003, Hoey et al., 2000).

Post-translational modification of the unique domain via phosphorylation has proved to be an important regulator of SFK function (Amata et al., 2014). In the literature there are many examples that demonstrate the divergent roles of the multiple phosphorylation events within the unique domains of SFKs (reviewed in Amata *et al.*, 2014). For example, phosphorylation of C-Src by PKA at Ser-17 has been implicated in the translocation of

the kinase to the cytosol in response to platelet-derived growth factor (PDGF) and the cAMP dependent activation of the small GTPase Rap1 (Walker et al., 1993, Obara et al., 2004). Whereas, Thr-37, Thr-46 and Ser-75 phosphorylation by cyclin-dependent kinase 1 (cdk1) promotes the activation of Src during mitosis, by disrupting regulatory intramolecular interactions (Shenoy et al., 1992).

In recent years, a novel regulatory mechanism involving unique-lipid interactions in C-Src has emerged. Whilst the unique domain has been defined as an IDR, NMR spectroscopy revealed the presence of two partially structured regions between residues 60-74 (Pérez et al., 2009). Perez and colleagues demonstrated using NMR that this region comprises an additional lipid binding site, which promotes intermolecular interactions with acidic lipids. Further experiments established that lipid binding by the unique domain could be regulated by the phosphorylation of Ser-37 and Thr-75, which largely diminished unique-lipid binding, with little effect observed on SH4-lipid interactions (Perez et al., 2013). In the same study, the unique domain was found to interact with the SH3 domain, which also displayed a degree of lipid binding. The binding of the SH3 domain to positively charged lipids and the unique domain occurred away from the substrate docking site, and interaction of the SH3 domain with a high affinity proline rich peptide resulted in the abolition of unique-SH3 contacts. In addition to this, the unique-SH3 interaction was perturbed by the binding of calcium-loaded calmodulin to the unique domain, which prevented unique-lipid interactions, suggesting this interaction is regulated by calcium signalling (Perez et al., 2013). It is now thought that the SH3 domain acts as a scaffold for the unique domain, which forms a disordered loop between the SH4 and SH3 domains (Maffei et al., 2015).

Together these data present a novel regulatory role for the unique domain, although thus far, these interactions have only been described *in vitro*. Nevertheless, the observation that C-Src mutants, defective in unique-lipid binding, negatively affected *Xenopus laevis* oocyte maturation, a process that is usually promoted by wild type (WT) C-Src, suggests unique-lipid interactions are required for C-Src function, and could be relevant to other SFKs.

1.2.3 The SH3 Domain

The SH3 domain, which consists of approximately 60 amino acid residues, is widely recognised throughout cell biology as a facilitator of protein-protein interactions. Whilst it was first described as one of the six modular domains of C-Src, almost 300 SH3-containing proteins have since been identified in humans (Kärkkäinen et al., 2006). In addition to their presence in eukaryotes, SH3 containing proteins also occur in prokaryotes and viruses (Whisstock and Lesk, 1999). Therefore, it is unsurprising that

SH3 domains are key players in many signal transduction pathways. Some of their main functions include promoting multiprotein complex formation, substrate recognition, and enzymatic regulation, as well as enhancing localised protein concentration (Mayer, 2001).

In SFKs, SH3 domains play multiple key roles. Primarily, the SH3 facilitates substrate docking and has an important role in the regulation of kinase activity via the formation of intramolecular interactions (discussed in Section 1.2.7). More recently, the SH3 was shown to act as a scaffold for the intrinsically disordered unique domain and is thought to interact with the lipid membrane (discussed in Section 1.2.2, (Perez et al., 2013)).

When the structure of the C-Src SH3 domain was solved in 1992, it was revealed that the protein consisted of two short three-stranded anti-parallel β -pleated sheets that were positioned at approximately right angles to each other (Figure 1.2, (Yu et al., 1992)). A hydrophobic core was identified at the interface between the two β -pleated sheets, which was flanked by connecting n-Src and RT loops (Feng et al., 1995, Yu et al., 1992, Noble et al., 1993, Xu et al., 1997). This conserved hydrophobic region, a flat surface populated mostly by aromatic residues, contains three shallow binding pockets and is the site of substrate recognition (Noble et al., 1993, Musacchio et al., 1994).

SH3 domains interact with substrate regions that contain short amino acid sequences, rich in proline residues, called PXXP motifs (where X is any amino acid residue). The motifs adopt the conformation of a left handed polyproline helix type 2 (PPII, (Musacchio et al., 1994)). Since all SH3 domains recognise a consensus centred around a PXXP motif, it is the flanking residues that confer specificity to individual proteins, ensuring that all SH3 domains do not recognise the same subsets of proteins. Whilst the third binding pocket, dubbed the 'specificity pocket', facilitates the binding of the flanking residues, further interactions with the n-Src and RT loops (the main sources of variation in SH3 domains) outside of the hydrophobic core, have also been described (Alexandropoulos et al., 1995, Ren et al., 1993, Weng et al., 1995, Rickles et al., 1995, Feng et al., 1995).

C-Src is capable of binding two types of sequence; the class I R/K Φ PX Φ P and class II P Φ XP Φ R/K motifs (where Φ and X represent a hydrophobic or any amino acid residue respectively; (Zarrinpar et al., 2003, Mayer, 2001)). These motif sequences reflect the ability of the SH3 hydrophobic core to bind the PPII substrates in two opposing conformations (Feng et al., 1994). Whilst two of the shallow substrate pockets on the binding interface form contacts with the two Φ P dipeptides, the third pocket, formed by the n-Src and RT loops, is typically occupied with the side chain of a positively charged residue (R/K, Figure 1.2, (Feng et al., 1995, Kay et al., 2000, Mayer, 2001)).

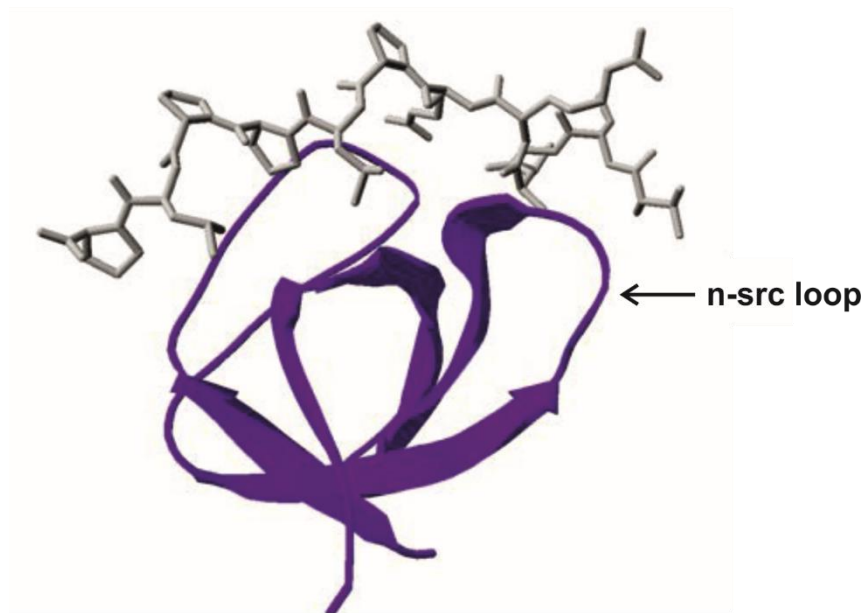


Figure 1.2: The Structure of the C-Src SH3 Domain in Complex with a Class I Ligand.

A diagram of the crystal structure of the C-Src SH3 domain (purple) in complex with a class I ligand (grey, R/KΦPXΦP). The ligand forms contacts with three pockets on the binding interface. The two ΦP dipeptides interact with two shallow pockets, whereas the third pocket, occupied with the side chain of the positively charged residue flanking the PXΦP motif. The position of the n-Src loop, which form part of the specificity pocket, is indicated. The n-Src loop is also the region of the SH3 domain in which N1 and N2 mini-exon inserts are incorporated, which gives rise to the neuronal splice variants of Src (discussed further in Section 1.5). The crystal structure was solved by Feng *et al.*, (1995) and the image was created by Dr Gareth Evans (University of York). PDB code 1QWF.

1.2.4 The SH2 Domain

The approximately 100 amino acid SH2 domain resides C-terminal to the SH3 domain and also recognises a specific short peptide motif. SH2 domains were first described by Sadowski and colleagues (1986) as a non-catalytic conserved domain observed in SFKs and fps . They speculated that the domain may facilitate protein-protein interactions. It is now known that there are 110 proteins in the human proteome, that contain at least one SH2 domain, which effectively link tyrosine kinases to a diverse array of signalling pathways, since they specifically bind phosphotyrosine containing motifs (Liu et al., 2006). In SFKs, the SH2 domain provides a site for substrate recognition but also plays a key role in their autoinhibition, by facilitating an intramolecular interaction with the C-terminal tail. This interaction will be discussed further in Section 1.2.7.

Pioneering studies established that SH2 domains, confer specificity for different binding partners, through the recognition of different phosphotyrosine containing consensus motifs (Zhou et al., 1993, Songyang et al., 1994). For example, the Abl SH2 domain recognises the motif pYENP (where p signifies a phosphorylated residue), whereas the Crk SH2 domain binds to pYDHP motifs (Songyang et al., 1994). Similar studies have also identified the SFK SH2 binding motif, pYEEI, which was determined from a phospho-peptide library screen, after it bound to the SH2 domain with high affinity (Zhou et al., 1993). Further studies confirmed that the phosphorylation of the tyrosine residue was critical for this high affinity interaction (Bradshaw et al., 1999). In addition to the canonical pYEEI binding motif, more comprehensive studies have highlighted the significance of other residues flanking the motif between residue positions -2 to +4, which may also confer binding specificity to SFKs (Bradshaw et al., 1999, Filippakopoulos et al., 2009).

Waksman and colleagues (1993) determined the crystal structure of the V-Src SH2 domain in complex with an 11-residue pYEEI peptide (Figure 1.3). The study likens the ligand to a 'two-pronged plug' that engages with the SH2 domain, which is described as the corresponding 'two holed socket'. The protein is composed of two β -sheets linked by a single β -strand, which are flanked at either side by an α -helix (Figure 1.3). The largest β -sheet is central to the domain and separates the SH2 into two functionally distinct areas.

The phosphotyrosine forms a series of interactions with a pocket at one side of the domain, consisting of one face of the central β -sheet, a loop and an α -helix. Whereas the distal Ile residue, occupies the hydrophobic pocket on the other side of the central β -sheet, which effectively engulfs the side chain of the residue. The remaining two central Glu residues are positioned on the surface of the SH2 domain and form contacts with

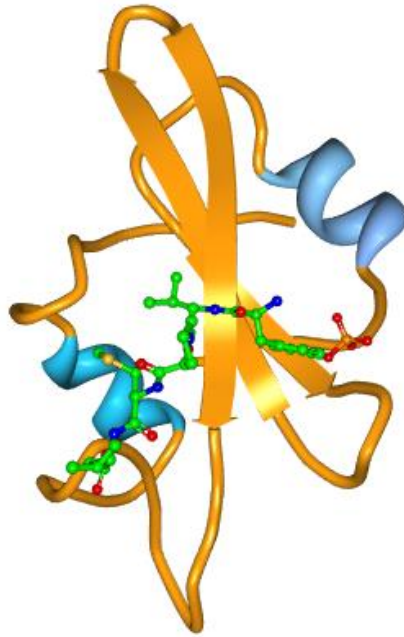


Figure 1.3: The Structure of the V-Src SH2 Domain.

A diagram of the crystal structure of the V-Src SH2 domain in complex with a phosphotyrosine ligand (green). The protein is composed of two β -sheets (orange) linked by a single β -strand, which are flanked at either side by an α -helix (blue). The SH2 is partitioned into two functionally distinct compartments by the largest β -sheet at the centre of the domain. The phosphotyrosine interacts with a binding pocket at one side of the domain, whereas the distal Ile residue forms contacts with the hydrophobic pocket on the other side of the central β -sheet. The two central Glu residues lie on the surface of the SH2 domain. The crystal structure was solved by Waksman et al. (1993). The image was generated in RCSB Protein Workshop, PDB code 1SHA.

basic residues (Waksman et al., 1993). These findings were further supported by a similar study in which the SH2 domain of a different SFK, Lck, was crystalised (Eck et al., 1993).

1.2.5 The SH1 (Kinase) Domain

The catalytic kinase domain is connected to the SH2 domain via a flexible regulatory linker, and houses the active site of the enzyme where substrate phosphorylation takes place. The crystal structures of dozens of catalytic domains obtained from different kinases have revealed that the domains are structurally similar (Nolen et al., 2004). In fact, Manning and colleagues (2002) were able to identify 478 kinases in the human genome on the basis that they shared structurally conserved features of a common catalytic domain. However, in a similar fashion to SH2 and SH3 domains, the kinase domain recognises a specific motif that also governs substrate binding. Songyang and colleagues (1995) demonstrated that whilst catalytic domains shared many conserved mechanistic properties, substrate recognition was dependent on differing sequence motifs for the kinases tested. Whilst both V- and C-Src recognised the sequence EEEIYGEF, the SFK Lck optimally bound to peptides containing the sequence XEXIYGVLV (where X is any amino acid, (Songyang et al., 1995)). This indicated that the kinase domain further contributes to the substrate specificity already conferred by SH2 and SH3 domains.

The kinase domain consists of two distinct lobes that are connected by a short linker region. The composition of the smaller N-terminal (N) lobe includes five antiparallel β -strands, as well as an α -helix and a glycine-rich loop. Whereas the larger C-terminal (C) lobe is comprised of seven α -helices, a four stranded β -sheet situated on the surface of a deep cleft that exists between the two lobes, and also a series of loops including a catalytic and an important regulatory activation loop. The cleft that occurs between the lobes facilitates nucleotide binding and substrate phosphorylation. Here, the terminal phosphoryl group of ATP is added to a tyrosine residue. Whilst the N-lobe is predominantly concerned with Mg-ATP binding at the base of the cleft which exposes a transferrable phosphate group, the C-lobe is associated with substrate recognition and catalysis (Knighton et al., 1991, Boggon and Eck, 2004).

The N- and C- lobes work in synchrony during catalysis, facilitating 'open' and 'closed' conformations (Yamaguchi and Hendrickson, 1996). In the open conformation, which is promoted and stabilised by the phosphorylation of Tyr-416 (chicken C-Src nomenclature) on the C-lobe's activation loop, ATP and substrate binding occurs (Breitenlechner et al., 2005, Huse and Kuriyan, 2002, Roskoski, 2004). When the two lobes effectively 'close' together, the phosphorylation event occurs and ADP is released upon the 're-opening'

of the complex (Roskoski, 2004). The phosphorylation at Tyr-416 can either occur as a result of auto- or trans-phosphorylation, the latter of which occurs between SFK molecules, indicating that Tyr-416 phosphorylation is a self-regulatory event amongst SFKs (Sugimoto et al., 1985, Imamoto and Soriano, 1993). This mechanism of regulation has also been observed for multiple other unrelated kinases, whereby phosphorylation of the activation loop propagates increased kinase activity (Huse and Kuriyan, 2002).

1.2.6 The C-terminal Domain (CTD)

The C-termini of SFKs contain between 15-17 residues, including the highly conserved Tyr-527 residue. The phosphorylation of Tyr-527 by the tyrosine kinases Csk or Chk, promotes an autoregulatory structural conformation that inhibits kinase activity (discussed further in Section 1.2.7). Importantly, phosphatases that facilitate the dephosphorylation of this residue, such as PTP1B, PTP α and SHP1/2, facilitate the activation of the kinase (Bjorge et al., 2000, Harder et al., 1998, Somani et al., 1997, Zhang et al., 2004).

1.2.7 The Autoregulation of SFKs

Whilst SFK activity can be regulated by myristoylation, palmitoylation and phosphorylation, which are outlined above, the autoinhibition of SFKs is probably the most studied and best characterised regulatory mechanism and is described below.

Phosphorylation of Tyr-527 in the C-terminal region of SFKs generates an SH2 domain binding motif that facilitates an intramolecular interaction between the C-terminal tail and the SH2 domain of the kinase (Xu et al., 1997, Schindler et al., 1999, Sicheri et al., 1997, Williams et al., 1997). The importance of this interaction has been demonstrated on multiple occasions, including in a study on C-Src, whereby the substitution of Tyr-527 with a Phe residue, resulted in the constitutive activation of C-Src and cellular transformation (Reynolds et al., 1987). Such studies indicated that the SH2:Y527 interaction forms part of an autoinhibitory mechanism. Tyrosine phosphorylation at Tyr-527 is coordinated by C-terminal Src kinase (Csk), whose major role in maintaining SFKs in the inactive conformation was highlighted by gene knock-out studies in mice. A large increase in the activity of C-Src, Fyn and Lyn was observed in Csk^{-/-} mice, which was thought to contribute to the resultant embryonic lethal phenotype (Imamoto and Soriano, 1993, Nada et al., 2003).

In addition to the SH2:Y527 interaction, crystal structures of C-Src, Hck and Lck revealed that a second interaction occurs simultaneously between the SH3 domain and a PPII helix present in the linker region connecting the SH2 and kinase domains (Xu et al., 1997, Schindler et al., 1999, Sicheri et al., 1997). The SH3:linker interaction is thought to stabilise the SH2:Y527 interaction. Mutations of critical proline residues in the PPII

helix of the linker responsible for SH3 binding in Hck, resulted in elevated kinase activity and increased transforming capabilities in mouse fibroblasts (Briggs and Smithgall, 1999). This indicated the importance of this interaction in conjunction with SH2:Y527 binding.

The result of both the SH2:Y527 and SH3:linker interactions is the subsequent effects on the catalytic kinase domain. In this 'closed' inhibitory conformation (Figure 1.4), both the SH2 and SH3 domains apply pressure on the kinase domain, at the opposite side to the active site, which alters the orientation of both the N- and C-lobes. In the active site cleft, a catalytically important α -helix is displaced and the activation loop is forced into a partially helical conformation that is incompatible with substrate binding, and prevents autophosphorylation at Tyr-416 (Xu et al., 1997, Schindler et al., 1999, Sicheri et al., 1997).

The interaction formed between the C-terminal tail and the SH2, as well as those formed between the SH3 and the linker are relatively weak. This is because the SH2 and SH3 binding motifs present in the linker and C-terminal tail respectively, do not conform exactly to the specific motifs described above (i.e. SH3: PXXP; SH2: YEEI). This means that higher affinity substrates are capable of displacing these interactions (Figure 1.4). The binding of an SH2 or SH3 containing substrate partially activates the kinase and promotes Tyr-416 phosphorylation, although whether the displacement of one of the intermolecular interactions results in the disruption of the second to promote the open active kinase conformation is still uncertain (Figure 1.4).

The significance of this autoregulatory mechanism, which has been alluded to in the above paragraphs, lies in the ability of constitutively activated C-Src to transform 'normal' cells into 'cancerous' cells, in which cell proliferation and survival mechanisms are upregulated. For example, a strain of the closely related viral oncogene V-Src promotes cell transformation due to its high constitutive activity, which is attributed to the deletion of a portion of the C-terminus or the mutation of Tyr-527. The absence of the Tyr-527 residue, is therefore thought to prevent the autoinhibition of the kinase, which promotes cellular phenotypes that would usually be tightly regulated. Examples demonstrating the critical nature of this mechanism in the context of typical SFKs are outlined above whereby the mutation of Tyr-527 or the critical proline in PPII helix linker resulted in cell transformation (Reynolds et al., 1987, Briggs and Smithgall, 1999).

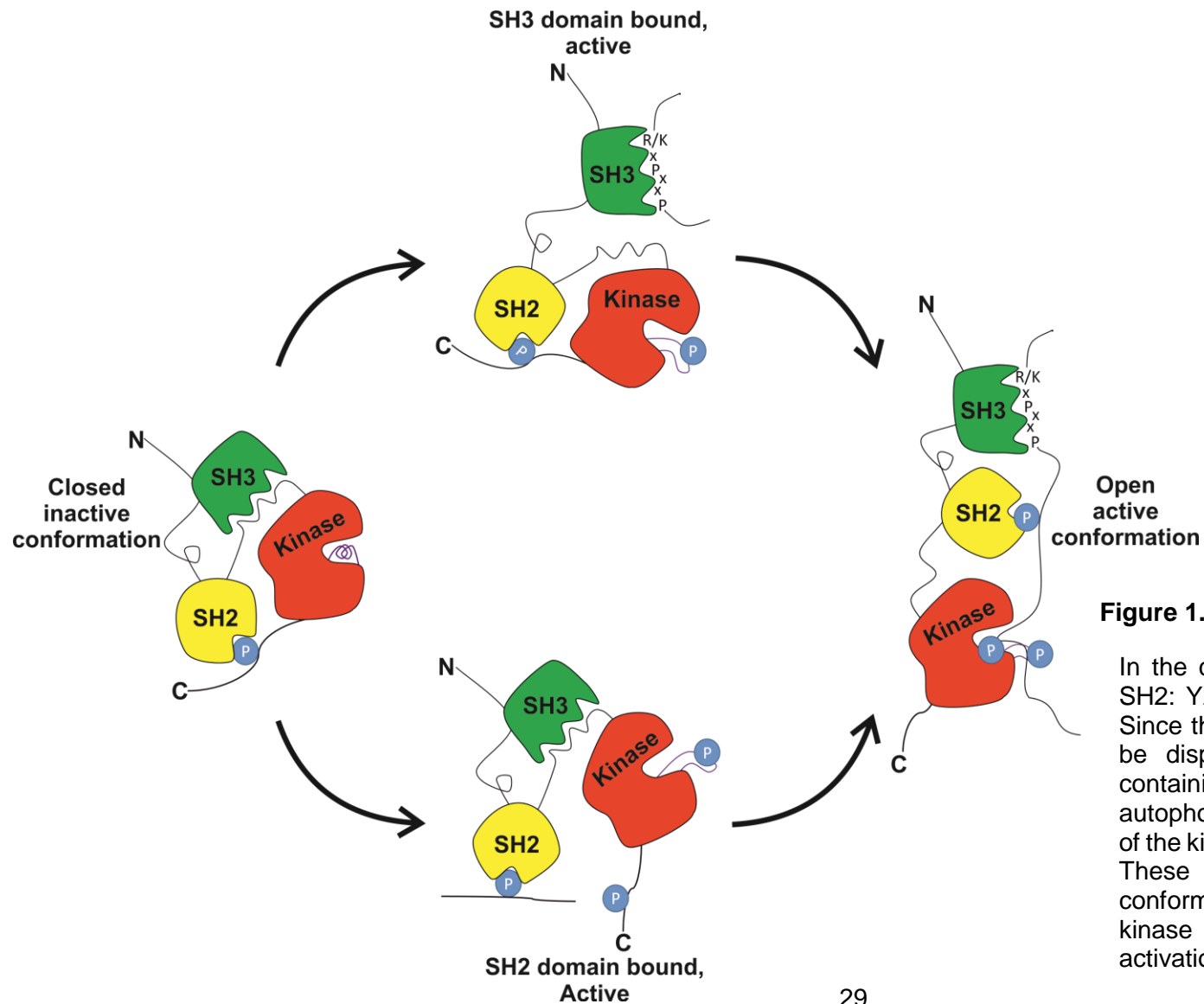


Figure 1.4: A Schematic Illustrating SFK Activation.

In the closed inactive complex, SH3: linker and SH2: Y257 interactions prevent catalytic activity. Since these interactions are low affinity, they can be displaced by higher affinity SH3 or SH2 containing substrates, which facilitates the autophosphorylation of Tyr-416 at the active site of the kinase domain, resulting in partial activation. These SH2 and SH3 substrate bound conformations are thought to promote the open kinase conformation, resulting in full kinase activation.

1.3 Cellular Functions of C-Src

The founding member of SFKs, C-Src, is a proto-oncogene that was first discovered after its viral counterpart V-Src, a retroviral oncogene accountable for sarcomas caused by the Rous sarcoma virus, was found to have been captured from its host genome (Stehelin et al., 1976, Shalloway et al., 1981, Takeya and Hanafusa, 1983). Since its discovery, a large number of C-Src substrates have been identified and a diverse range of functions have since emerged for the kinase, including roles in cell proliferation, differentiation, motility and survival. In addition to this, C-Src has been implicated in the mechanisms governing learning and memory (Engen et al., 2008). Therefore, it is unsurprising that C-Src activity lies at the heart of a diverse range of signalling networks, due to its ability to phosphorylate and recognise a plethora of substrates.

Upstream of C-Src, kinase activity has been shown to be upregulated in response to a range of cell surface receptor signals. For example, multiple mitogen activated growth factor receptors (e.g. epidermal growth factor receptors (EGFR) and PDGFRs), Integrins, G-protein coupled receptors (GPCRs e.g. β -adrenergic receptor) and receptor tyrosine phosphatases (e.g. PTP α) have all been linked to C-Src activation and subsequent signalling events (Gould and Hunter, 1988, Luttrell et al., 1999, Schaller et al., 1999, Zheng et al., 2000). These studies, amongst others, have shown or suggested that C-Src is involved in the intracellular relay of cell-cell and cell-matrix signals; a phenomenon that is now widely acknowledged and has been investigated a great deal.

Perhaps one of the most well-known roles of C-Src is its participation in focal adhesion signalling and cell spreading. In both C-Src^{-/-} fibroblasts and osteoclasts, as well as epithelial cells treated with an SFK inhibitor, both integrin-dependent cell-matrix adhesion and cell spreading are reduced (Kaplan et al., 1995, Felsenfeld et al., 1999, Lakkakorpi et al., 2001, Jones et al., 2002). Active C-Src localises at focal adhesions at sites of integrin clustering on the cell membrane, which is triggered by ECM stimuli (Kaplan et al., 1994, Playford and Schaller, 2004). However, this localisation is abolished in the absence of the SH4 or SH3 domains of the kinase, which highlights the necessity of membrane association and the likely role of the SH3 domain in substrate recognition (Kaplan et al., 1994). At focal adhesions, C-Src is found in complex with multiple other proteins including Focal adhesion kinase (FAK), p130^{CAS} and paxillin, which have also been shown to be phosphorylated by the kinase (Glennay and Zokas, 1989, Kanner et al., 1990).

During cell spreading, integrin engagement results in the autophosphorylation of FAK at Tyr-397, which recruits C-Src by providing an SH2 binding site (Schaller et al., 1994). C-Src phosphorylates FAK at multiple sites, enabling the recruitment of other focal

adhesion complex components (Calalb et al., 1995, Calalb et al., 1996). This triggers a series of signalling events that regulate Rho GTPase-mediated cytoskeletal dynamics. The recruitment and phosphorylation of the scaffolding protein p130^{CAS}, paves the way for the further recruitment of Crk, DOCK180 and ELMO1. A complex between the latter two proteins activates Rac1 via guanine nucleotide exchange factor (GEF) activity (Chodniewicz and Klemke, 2004). In a parallel pathway, Rac1 activation is also promoted via the FAK/Src complex component Paxillin, whose phosphorylation recruits Paxillin kinase linker (PKL) and subsequently β -PIX, which is also a Rac1 GEF (ten Klooster et al., 2006). Simultaneously, the transient inactivation of RhoA is promoted via the FAK/Src complex, through the recruitment and phosphorylation of p190rhoGAP. The latter, is a GTPase activating protein (GAP) that renders RhoA inactive by stimulating GTP hydrolysis (Arthur et al., 2000, Ren et al., 2000). Whilst Rac1 activation promotes cell protrusion, RhoA inactivation suppresses contractility of the actin cytoskeleton. Therefore, through co-ordinating the activities of Rac1 and RhoA, the FAK/Src complex facilitates cell spreading (Huvneers and Danen, 2009).

In conjunction with integrin-dependent FAK/Src signalling, considerable crosstalk with growth factor receptors and cell adhesion molecules also plays a role in the regulation of cell spreading. For example, the integrin-dependent Src-mediated phosphorylation of EGFR promotes cell spreading upon the stimulation PI3K signalling, which results in Vav1-mediated Rac1 activation (Moro et al., 2002, Marcoux and Vuori, 2003). Since C-Src was first discovered, a clearer picture has emerged whereby a range interconnected networks involving different types of cell surface receptors, co-ordinate downstream Rho GTPase-mediated cytoskeletal dynamics, via a combination of intermediate signals in which C-Src is a key player. Together, such networks are capable of regulating cell-matrix adhesion and cell-cell adhesion to coordinate processes that include cell migration, proliferation and survival (Huvneers and Danen, 2009).

1.3.1 C-Src Functions in the Brain

1.3.1.1 The Role of C-Src in the Developing Brain

In the 1980's, a body of work investigating the relative expression of C-Src in various organisms, indicated that in both frogs and fish, C-Src expression was at its highest in both the developing and mature brain (Schartl and Barnekow, 1984). Further studies demonstrated that in some areas of the rat brain including the cerebellum, hippocampus and striatum, maximal C-Src expression was between 6 to 20 times higher in comparison to the corresponding adult tissues. It was observed that these increases in C-Src activity largely correlated with peak times of neurogenesis and neuronal growth, suggesting a potential role for C-Src in neuronal development (Cartwright et al., 1988). Manness and

colleagues proposed that C-Src expression occurs in two phases during neuronal development (Maness et al., 1986, Fults et al., 1985). Firstly, C-Src expression becomes elevated in the neuroectoderm of gastrulating embryos, which coincides with the period when cells commit to a specific cell lineage (Maness et al., 1986). The second phase, described in cerebellar neuronal progenitor cells, occurs during neuronal differentiation (Fults et al., 1985).

Since these observations were made, C-Src has been implicated in multiple roles during neuronal development. The enrichment of activated C-Src in neuronal growth cone membranes indicated a potential role for the kinase in axonal outgrowth and guidance, which was confirmed in later studies (Maness et al., 1989). Growth cones are the dynamic structures present at the tip of growing axons, which facilitate the directional outgrowth of axons in response to external stimuli including a variety of guidance cues, as well as cell adhesion molecules present on neighbouring cells. SFKs have been implicated downstream of multiple cell surface receptors including EphA, Trk, DCC and PlexinA, which are stimulated by the following guidance cues: ephrins, neurotrophins, netrin and semaphorins respectively to promote neurite outgrowth (Knoll and Drescher, 2004, Liu et al., 2004, Falk et al., 2005). However, the specific mechanisms through which the kinases act are largely uncharacterised. Specifically, the recruitment of both C-Src and FAK to the activated netrin receptor DCC has been shown to be required for netrin mediated neurite outgrowth (Liu et al., 2004). Whilst the direct mechanism involved is unknown, netrin mediates neurite outgrowth via the modulation of PI3K, ERK and Rho GTPases; therefore, it is likely that Src/FAK signalling acts upstream of these signalling components (Liu et al., 2004).

C-Src mediated neurite outgrowth can also be regulated by cell adhesion receptors, in particular L1-CAM. Ignelzi and colleagues (1994) demonstrated that neurite outgrowth was reduced in Src^{-/-} cerebellar granule neurons (CGNs) that were cultured on L1-CAM. Neurite outgrowth on the extracellular matrix component laminin, which stimulates integrin signalling, was unaffected (Ignelzi Jr et al., 1994). This pointed towards a specific role for C-Src in L1-CAM-mediated neurite outgrowth, since laminin failed to evoke a response. However, it is possible that the functional redundancy between SFKs could mask a potential role for C-Src.

The neuronal specific cell-cell adhesion molecule L1-CAM, consists of an N-terminal extracellular domain (6 x immunoglobulin-like domains connected to 5 x fibronectin type III repeats), a transmembrane domain and a cytoplasmic domain c-terminal domain (CTD), which contains multiple phosphorylation sites that are thought to regulate L1-CAM-cytoskeletal interactions (Crossin and Krushel, 2000). To date, three sites on the

cytoplasmic CTD of L1-CAM have been implicated in L1-CAM cytoskeletal interactions and C-Src is thought to be involved in the regulation of these interactions, either directly or indirectly (Nagaraj and Hortsch, 2006).

L1-CAM is thought to interact with the actin-spectrin cytoskeleton by binding ankyrin B via the FIGQY motif in the cytoplasmic CTD. By generating L1-CAM^{-/-} cerebellar neurons that expressed a L1-CAM-CTD truncation mutant (110 of 114 CTD amino acids deleted) whilst growing on a wild type L1-CAM substrate, Cheng *et al.*, (2005) showed that L1-CAM-CTD was unnecessary for neurite outgrowth. This agrees with findings by (Gil *et al.*, 2003), who demonstrated that L1-CAM/ankyrin binding renders L1-CAM stationary in the membrane, preventing L1-CAM mediated neurite outgrowth. Thus when the ankyrin binding motif is absent, L1-CAM can stimulate neurite outgrowth. However, contradictory evidence published by (Nishimura *et al.*, 2003) suggests L1-CAM/ankyrin interactions stimulate neurite initiation. Nevertheless, tyrosine phosphorylation of the FIGQY motif prevents L1-CAM binding to ankyrin, although it is not thought that this motif is directly phosphorylated by SFKs under basal conditions (Whittard *et al.*, 2006a). Despite this, epidermal growth factor (EGF), neural growth factor (NGF) and fibroblast growth factor (FGF) receptors and the MAP kinase pathway have been implicated in FIGQY phosphorylation pathways, and often involve Src kinase.

In cerebellar neurons, neurite branching but not neurite outgrowth is mediated by L1-CAM interaction with cytoskeletal component ezrin-moesin-radixin (ERM). Both a juxtamembrane ERM binding motif and the RSLE endocytosis motif were demonstrated to be required for the regulation of neurite branching (Cheng *et al.*, 2005). The tyrosine (Tyr-1176) that precedes the RSLE region is phosphorylated by C-Src (demonstrated *in vivo*), and prevents clathrin-mediated endocytosis of L1-CAM by prohibiting AP-2 binding to the L1-CTD (Schaefer *et al.*, 2002). Phosphorylation of Tyr-1176 by Src may also be a means of perturbing L1-CAM/ERM interactions.

A further occasion, whereby C-Src has been implicated in the regulation of neurite outgrowth is in relation to p190rhoGAP, which promotes neurite extension by downregulating the activity of RhoA. The study demonstrated that both C-Src and Fyn are the primary kinases in both the developing and mature brain that phosphorylate p190rhoGAP and C-Src-mediated phosphorylation of p190rhoGAP is known to promote the inactivation of RhoA (Brouns *et al.*, 2001). However, this study did not directly link Src to the effects of p190rhoGAP on axon outgrowth and guidance.

1.3.1.2 The Role of C-Src in the Adult Brain

In the adult nervous system, C-Src regulates synaptic transmission and plasticity. Synaptic transmission facilitates the relay of information between neurons. This form of

communication is dependent upon the release of chemical messengers (neurotransmitters) from the pre-synapse, which bind to post-synaptic ion-channel receptors. Neurotransmitters can have an excitatory (e.g. glutamate) or inhibitory effect (γ -aminobutyric acid; GABA), resulting in the depolarisation or hyperpolarisation of the post-synaptic membrane respectively. Synaptic plasticity is defined by the ability of synapses to strengthen or weaken. This can manifest for example, as an increase or decrease in the amount of neurotransmitter released at the pre-synapse (short-term plasticity) or the number of receptors present at the post-synapse (a factor in long-term plasticity).

Short-term synaptic plasticity, which may last between tens of milliseconds to minutes, can manifest as synaptic depression, facilitation or augmentation/posttetanic potentiation (PTP). During short-term depression and facilitation, the deliverance of two stimuli in close succession gives rise to a response to the second, which is either smaller (depression) or greater (facilitation) than the first. Whereas, synaptic augmentation or PTP occurs in response to sustained presynaptic activation and can occur for up to several minutes (Regehr, 2012). Such mechanisms of short-term synaptic plasticity regulate the mobilisation of neurotransmitter from the pre-synapse into the synaptic cleft, resulting in a reduction (depression; (Betz, 1970)) or increase (facilitation and augmentation; (Katz and Miledi, 1968, Magleby and Zengel, 1975)) in their release. For example, facilitation takes place, when pre-synaptic calcium levels become elevated due to the arrival of two closely spaced action potentials at the pre-synapse. Since pre-synaptic calcium levels regulate membrane-vesicle fusion, more neurotransmitter is released after the second action potential, which strengthens the synapse (Katz and Miledi, 1968). On the other hand, depression occurs when the pool of readily releasable vesicles has become depleted. Therefore, synaptic strength declines until neurotransmitter levels are restored by the reserve pool of vesicles (Betz, 1970).

The most commonly studied types of long-term synaptic plasticity, are long-term potentiation (LTP) and long-term depression (LTD). These forms of plasticity are largely regulated at the postsynapse via the modulation of glutamate receptors (Traynelis et al., 2010). The activation of ionotropic NMDA receptors (NMDARs) in the postsynapse is often required for triggering both LTP and LTD. However, in order to relieve the Mg^{2+} channel blockade of glutamate bound NMDARs, sustained membrane depolarisation must be achieved through either high frequency stimulation (LTP) or prolonged low frequency stimulation (LTD) at the post-synapse (Malenka, 1994). Once activated, the second messenger Ca^{2+} enters through the channel, activating either protein kinases (e.g. CAMKII) in LTP or protein phosphatases (e.g. calcineurin) in LTD (Soderling and Derkach, 2000, Mulkey et al., 1993). The resulting, complex downstream signalling

cascades regulate events that either serve to strengthen (LTP) or weaken (LTD) at the synapse. For example, one of the main pathways through which synaptic strength is determined, is through the regulation of AMPA receptor (AMPA) trafficking to the postsynaptic membrane (Malinow and Malenka, 2002). AMPARs are a further class of ionotropic receptor that are activated upon glutamate binding, resulting in Na⁺ influx and membrane depolarisation. During LTP or LTD, AMPARs are inserted into the membrane (Shi et al., 1999) or removed by endocytosis (Carroll et al., 1999), respectively.

In addition to the involvement of ionotropic receptors in the regulation of long-term synaptic plasticity, a second class of receptor, termed the metabotropic receptors, also contribute to its maintenance (Mukherjee and Manahan-Vaughan, 2013). Metabotropic receptors differ from ionotropic receptors in that they do not contain an ion channel pore (for example many are G-protein-coupled receptors (GPCRs)), however, they are still activated upon neurotransmitter (e.g. glutamate) binding. This class of receptor is indirectly linked with ion channel function at the post-synapse through the regulation of downstream intracellular signalling pathways. Therefore, the mode of action of metabotropic receptors on synaptic activity is slower in comparison to ionotropic receptors (Mukherjee and Manahan-Vaughan, 2013). During long-term synaptic plasticity, multiple types of glutamate metabotropic receptors (e.g. mGluR1 and mGluR5), have been implicated in the regulation of ion channel activity, including NMDARs (e.g. Trepanier et al., 2013), AMPARs (e.g. Kelly et al., 2009) and SK channels (e.g. Tigaret et al., 2016).

At the post-synapse, C-Src regulates ion channel signalling. In particular, ionotropic glutamate NMDARs and AMPARs, voltage-gated potassium and calcium channels, GABA_A receptors and nicotinic acetylcholine receptors can all be regulated by C-Src (Wang and Salter, 1994, Fadool et al., 1997, Cataldi et al., 1996, Moss et al., 1995, Wang et al., 2004). The regulation of NMDARs by Src is probably the most widely studied, given the high profile role of NMDARs in learning, memory and synaptic development, which is due to their modulation of excitatory synaptic transmission and plasticity (Sanz-Clemente et al., 2013).

NMDARs are heterotetrameric complexes, which consist of two NR1 subunits and two NR2 (NR2A-D) or NR3 (NR3A-B) subunits. Differential phosphorylation of the NR2 subunits mediated by SFKs plays a key role in their modulation (Salter and Kalia, 2004).

Over the past couple of decades, the role of C-Src in the regulation of NMDARs has been characterised in terms its biochemical, molecular and physiological roles. Src regulation of NMDARs stimulates long term potentiation in CA1 hippocampal neurons (Yang et al., 2012) and could potentially be a therapeutic target for the treatment of

inflammatory and neuropathic pain, schizophrenia and the damaging effects of ischemia and reperfusion (Liu et al., 2008, Trepanier et al., 2013).

Protein tyrosine kinases enhance NMDAR currents in hippocampal and spinal dorsal horn neurons and it has been demonstrated that NR2A and NR2B subunits are tyrosine phosphorylated via Western blot analysis of immunoprecipitated NR2A and NR2B from isolated rat cortical synaptic membranes (Lau and Huganir, 1995, Wang and Salter, 1994). Furthermore, electrophysiological experiments on human embryonic kidney cells (HEK-293) expressing NMDARs containing NR1 and NR2A-D subunits confirmed the activating effects of Src on NR2A containing channels, and demonstrated the necessity of the CTD for Src-mediated effects (Kohr and Seeburg, 1996). Biochemical characterisation of the NR2A subunit phosphorylation by V-Src, when co-expressed alongside the NR1 subunit in HEK-293 cells, defined the regions where NR2A was phosphorylated, using CTD truncation mutants of NR2A. This enabled the identification of specific tyrosine mutants that reduced NR2A phosphorylation. Three individual tyrosines, Tyr-1292, Tyr-1325, and Tyr-1387, were identified as V-Src targets (Yang and Leonard, 2001). Thus extensive evidence exists implicating Src in NMDAR regulation.

In addition, there is an increasing amount of research placing Src regulation of NMDARs in the context of signalling pathways. For example, Lu et al. (1999) demonstrated that the enhancement of NMDAR currents mediated indirectly by GPCR ligand binding (i.e. muscarine and lysophosphatidic acid) and the subsequent activation of PKC, was prevented upon the inhibition of Src. These results indicated that Src acts downstream of the muscarinic and lysophosphatidic acid GPCRs and PKC, to positively regulate NMDAR activity (Lu et al., 1999). It is speculated that PKC may activate Src indirectly, by modifying the tyrosine kinases CAK β /PYK2, which in turn phosphorylate and activate Src, although this is yet to be confirmed.

More recently, differential roles of Src and Fyn kinases in LTP and LTD, acting through different signalling pathways has been shown. In CA1 hippocampal neurons, Src phosphorylation of NR2A in NR1/NR2A NMDARs enhances channel activity and stimulates LTP. However, Fyn kinase phosphorylates NR2B in NR1A/NR2B NMDARs, increasing channel activity and enhancing LTD (Yang et al., 2012). This differential stimulation of either LTP or LTD by either NR2A or NR2B containing channels respectively, is thought to be a consequence of the differences between the resultant Ca²⁺ currents that flow through the channels (Erreger et al., 2005). NR1/NR2A channels activate and deactivate more quickly than NR1/NR2B channels, resulting in a considerable, yet transient influx of Ca²⁺ ions. Whereas, NR1/NR2A ion channels open and close more slowly, enabling a much greater volume of Ca²⁺ entry (Erreger et al.,

2005). In the same study, roles for different GPCRs, namely the pituitary adenylate cyclase activating peptide 1 receptor and dopamine 1 receptor, in the selective activation of Src and Fyn kinases respectively, are also defined (Yang et al., 2012, Macdonald et al., 2005).

Not only do these findings clearly implicate GPCRs and PKC as key players in Src regulation of NMDARs, they also indicate an important role for Src in the regulation of synaptic plasticity in the hippocampus, supporting its importance for learning and memory.

A further mode of NMDAR regulation by Src has been reported, whereby activation of group 1 (mGluR1 and mGluR5) and 2 (mGluR2/3) metabotropic glutamate receptors enhance NMDAR currents via Src activation (Heidinger et al., 2002, Benquet et al., 2002, Yang et al., 2012, Trepanier et al., 2013). Ca²⁺ calmodulin dependent activation of Src, Fyn and Pyk2 kinases triggered by mGluR1 activity led to increased NR2A and NR2B phosphorylation and enhanced NMDAR currents in cortical neurons (Heidinger et al., 2002). Benquet *et al.* reported similar findings in relation to mGluR1 but also realised that activation of mGluR5 stimulates a GPCR-dependent mechanism, which acts via the PKC signalling pathway to increase Src activity and enhance NMDAR currents in CA1 neurons (Benquet et al., 2002). Furthermore and also in CA1 neurons, inhibition of the protein kinase A (PKA) post-mGluR2 activation stimulates Src and thus increases subtype specific NR1/NR2A receptor currents (Trepanier et al., 2013).

In addition to these regulatory mechanisms, activation of C-Src via receptor tyrosine kinase, cytokine receptor and integrin pathways can also influence NMDAR function. It is thought that these pathways converge at the point of C-Src activation to effect changes in NMDAR regulation that ultimately controls synaptic transmission and plasticity (Salter and Kalia, 2004).

A role for C-Src has also been described at the pre-synapse. Synaptosomes (isolated nerve terminals) derived from the hippocampi of rats that were subject to spacial maze learning contained increased levels and activity of C-Src. In addition to this, interactions with proteins including synapsin1 and synaptophysin were promoted (Zhao et al., 2000). These proteins along with dynamin1, are known to interact with C-Src on presynaptic vesicles, which is thought to regulate mechanisms involved in synaptic vesicle endocytosis (synaptophysin/dynamin1) and recycling (synapsin1) (Barnekow et al., 1990, Foster-Barber and Bishop, 1998, Evans and Cousin, 2005, Messa et al., 2010). Therefore, in conjunction with regulating synaptic transmission and plasticity at the post-synapse, C-Src also appears to have an important role in maintaining synaptic transmission at the pre-synapse.

1.4 SFKs in Health and Disease

Given that C-Src is expressed ubiquitously and has been implicated in multiple cellular fundamental processes, it was widely anticipated that Src^{-/-} mice would not be viable or at the very least display serious pathological defects. However, studies revealed that the C-Src knockout mouse was viable and the only abnormality that was detected was in relation to bone re-modelling, since the mice developed osteoporosis (Soriano et al., 1991). Interestingly, no neurological impairments were detected, which was surprising since C-Src is highly expressed in the brain. It was thought that the reason that so few abnormalities were observed in C-Src^{-/-} mice, was a result of the functional redundancy occurring between the kinases. This theory was supported by the fact that double knockout mice of both C-Src and Fyn or C-Src and Yes are not viable, which suggested that the kinases regulate overlapping functions that are essential for life (Stein et al., 1994).

In addition to osteoporosis, the dysregulation of C-Src has since been linked to multiple disease pathologies, associated with its regulation of the NMDA receptor (discussed in Section 1.3.1.2) and has also been linked to glutamate induced neurodegeneration (Liu et al., 2008, Trepanier et al., 2013, Khanna et al., 2007). C-Src is also inextricably linked to many types of cancer, including breast (Picon-Ruiz et al., 2016), colon (Xiao et al., 2016), skin (Choi et al., 2015), lung (Karachaliou et al., 2016) and ovarian (Sun et al., 2016). This is unsurprising, given that C-Src's major cellular roles include promoting cell proliferation, motility, invasion and survival. When constitutively activated, C-Src, like its viral counterpart V-Src, possesses the ability to transform cells, which is one of the reasons why C-Src activity is so tightly regulated (Cartwright et al., 1987). In cancer, the aberrant upregulation of C-Src activity is not typically related to genetic mutations in the kinase, although this has been observed in some cases. Instead, it is thought that kinase activity is promoted by increased protein levels or in response to cellular stimuli, such as its recruitment to EGFRs (Ishizawa and Parsons, 2004). Currently, there are multiple therapeutic C-Src inhibitors in development, which are reviewed by (Kim et al., 2009).

1.5 Neuronal Src Kinases

In 1985, Brugge and colleagues first observed that neurons expressed a variant of Src that was biochemically distinct from C-Src. They demonstrated that Src expressed in neurons had a higher specific activity in comparison to the Src expressed in astrocyte cultures, and saw that the neuronal variant displayed a shift in electrophoretic mobility with respect to C-Src (Brugge et al., 1985). It was later revealed that two neuronal splice variants of C-Src exist, named N1- and N2-Src, which contain a 6 and 17 amino acid residue insert in their SH3 domains respectively (Figure 1.5; (Martinez et al., 1987, Pyper and Bolen, 1990, Pyper and Bolen, 1989).

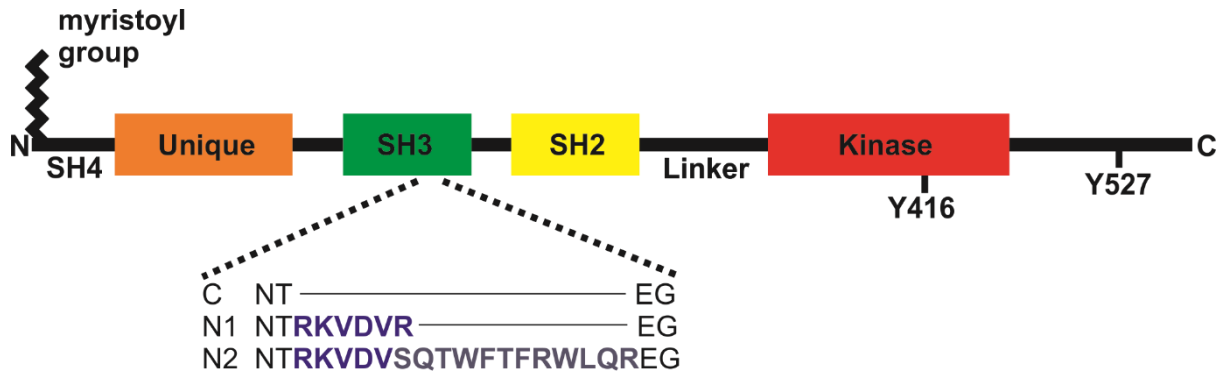


Figure 1.5: Schematic Diagram Illustrating the Mini-exon Inserts in the SH3 Domains of Neuronal Src Kinases.

N1-Src and N2-Src are splice variants derived from C-Src, which differ only by short inserts in their SH3 domains. Whilst N1-Src contains a 6 amino acid insert, N2-Src contains a 17 amino acid insert, which includes the first 5 amino acids of the N1-Src insert. The sequences of the amino acid inserts are indicated above.

Both kinases demonstrated increased catalytic activity in comparison to C-Src, although N2-Src appeared to have higher constitutive activity with respect N1-Src (Brugge et al., 1985, Levy and Brugge, 1989, Keenan et al., 2015). This is thought to be a consequence of the placement of the N-Src inserts in the n-Src loop of their SH3 domains. The importance of the n-Src loop in the autoregulation of V-Src kinase activity, was demonstrated, when mutation of the n-Src loop resulted in increased kinase activity (Brábek et al., 2002). Since both N1- and N2-Src demonstrated a reduced affinity for an SH3:kinase linker peptide *in vitro*, it is proposed that the observed increased kinase activity may be caused by disrupted intramolecular interactions between the SH3 domain and kinase linker, which are crucial for the autoinhibitory regulation of the kinases (Keenan et al., 2015). This idea is supported by a further study, in which N1-Src activity remained high, despite the kinase being predominately phosphorylated at Tyr-527; the residue on the C-terminal tail that promotes autoinhibition (Levy and Brugge, 1989).

The mRNA of N1-Src incorporates an 18 nucleotide mini-exon insert that arises due to a splicing event that occurs between exons 3 and 4 of the C-Src gene (Martinez et al., 1987). The N2-Src mRNA sequence contains a 51 nucleotide insert, which is the product of two splicing events. In N2-Src mRNA, both the N1 and N2 mini-exon inserts are included and the N1 mini-exon acts as a splice acceptor for the N2 mini-exon. This results in a change in the final amino acid of the N1-Src insert from an Arg residue to a Ser

residue (Pyper and Bolen, 1990). These splicing events are regulated by positive and negative regulatory elements in a tissue specific manner. In non-neuronal tissues, the splicing events described above are skipped (Levy et al., 1987, Martinez et al., 1987). This is thought to be regulated by the polypyrimidine tract binding protein (PTB), which binds to negative regulatory elements that lie upstream of the N1 exon and represses the N1 splicing event (Chan and Black, 1997). Since the N1 exon splicing event is required for the inclusion of the N2 exon, this would prevent the expression of both N1- and N2-Src in non-neuronal tissues. In neuronal cells, N1 exon splicing is dependent upon the presence of a conserved enhancer sequence downstream of the N1 exon and repression of N1 splicing by PTB is lifted however, the mechanisms involved require further investigation (Black, 1991, Modafferi and Black, 1997, Chou et al., 2000).

The discovery that N1-Src is evolutionarily conserved in mammals, birds, reptiles and fish lead to the belief that N1-Src expression is required for neural processes characteristic of 'higher' organisms (Raulf et al., 1989, Yang et al., 1989). Since C-Src expression has been detected in the most basic of organisms such as the sponge, the evolution of the N1- and N2-Src genes suggests their involvement in more complex brain specific functions (Ottillie et al., 1992). The presence of a similar neuronal splice variant

of C-Src was also identified in frogs. *Xenopus laevis* produces a neuronal C-Src variant that contains a five amino acid insert instead of six. At both ends of the frog insert lie Arg residues that are conserved amongst other animals, whilst the remaining residues are divergent (Collett and Steele, 1992). This suggests that these conserved charged residues may be key to role of N1-Src. However, Collet and Steele (1992) did not find an N2-Src homologue present in frogs, indicating that their divergence from other vertebrates must have occurred before the evolution of the N2 mini-exon.

1.5.1 The Spatiotemporal Expression of N1-Src

Wiestler and Walter (1988) first described the pattern of expression of N1-Src in the developing mouse brain. They observed that N1-Src expression first became visible at embryonic day 10 (E10) and subsequently monitored the expression level of the kinase in the mouse forebrain, midbrain and cerebellum between E9 to postnatal day 28 (P28). In both the forebrain and midbrain, the level of N1-Src expression was considerably higher than C-Src. N1-Src expression peaked at E18 and declined thereafter, but remained at a higher level than C-Src in the forebrain, whereas in the cerebellum, C- and N1-Src expression was comparable between E14 to P28. Given that in the period between E14-18 an increasing number of cells become post-mitotic and differentiated, it is thought that N1-Src could play a role in these processes (Wiestler and Walter, 1988). In support of these data, Ross and colleagues demonstrated that N1-Src mRNA was prevalent in the rat central nervous system (CNS) between E15-19, signifying a prominent role for N1-Src in the developing brain (Ross et al., 1988).

Studies indicate that N1-Src also plays an important role in the adult brain. The immunostaining of adult rat brain slices revealed that N1-Src is widely expressed in the mature brain, but is particularly enriched in the midbrain, hippocampus, cerebellum, pons, medulla and the cerebral cortex (Sugrue et al., 1990). A second study, which investigated the localisation of N1-Src mRNA by *in situ* hybridisation, supported these findings (Ross et al., 1988). N1-Src mRNA was most noticeably present in the forebrain, in the pyramidal layers and dentate gyrus of the hippocampus, the granule layer of the cerebellum and the olfactory bulb region of the brain. Interestingly, Le Beau and colleagues (1987) also measured heightened N1-Src activity in the majority of these structures in comparison to other brain regions. Since enhanced Src kinase activity can be linked with neuronal plasticity, it is thought that N1-Src could be a key component in driving this process. Notably, whilst both C- and N1-Src appeared to display high levels of mRNA in the cerebellum, N1-Src mRNA levels were markedly higher in the hippocampus, cerebral cortex as well as other regions of the forebrain (Ross et al., 1988). Taking these data into account, and the fact that differential levels of C- and N1-Src expression levels have been observed in the developing brain, this highlights the

spatial and temporal differences that exist in C- and N1-Src expression in both the mature and adult brain. Therefore, these data support the theory that both kinases will have different functions.

In the foetal rat brain N1-Src is enriched in growth cone membrane extracts, suggesting a potential role for N1-Src in axonal extension and guidance (Maness et al., 1988). Whereas, in the adult brain, Sugrue and colleagues (1990) reported that N1-Src expression was present in all neuronal compartments i.e. the cell soma, axon, dendrites and nerve terminals, suggesting widespread roles for N1-Src within cells. Despite only containing a single lipid modification, N1-Src has also been placed at lipid rafts, which are signalling hubs rich in multiple types of cell surface receptors and cellular signalling components (Mukherjee et al., 2003). Moreover, the N1-Src detected in the lipid raft fractions of mouse brain lysates displayed increased kinase activity, suggesting that N1-Src may play a role in signalling events directed from lipid rafts (Mukherjee et al., 2003). Interestingly, lipid rafts have been implicated in multiple neuronal functions including cell adhesion, axonal guidance and synaptic transmission, which are all processes that N1-Src is predicted to partake in when considering the spatiotemporal expression of the kinase (Tsui-Pierchala et al., 2002).

1.5.2 Physiological Functions of the Neuronal Srcs

There are very few studies in the literature that have addressed the functional relevance of the two neuronal splice variants of Src. Whilst no specific neuronal roles have been assigned to N2-Src, only a couple of studies have investigated the effects of N1-Src overexpression in different subsets of neurons. Kotani and colleagues (2007) explored the role of N1-Src during the morphogenesis of Purkinje neurons, a class of GABAergic neuron present in the Purkinje layer of the cerebellum, which are characterised by their large dendritic arbours. In transgenic mice overexpressing N1-Src (WT) and constitutively active N1-Src (Y527F), the organisation of the Purkinje cell layer in their cerebellum was disrupted. This effect was more profound in the Y527F mice. In addition to this, a large proportion of Y527F cells at postnatal day 7 (P7) had polarization defects, since the multiple dendritic shafts characteristic of earlier stages in development, failed to converge into a single shaft. Investigations into the molecular basis for these observations revealed that these morphological defects were linked to the aberrant arrangement of microtubules present in the dendritic shafts of the unpolarised neurons (Kotani et al., 2007). This study directly linked the effects of N1-Src to altered cytoskeletal dynamics, which are integral to the processes governing neuronal morphogenesis.

A second study, from Worley and colleagues (1997), compared the effects of both C- and N1-Src in multiple cell types from the developing *Xenopus laevis* retina. Whilst

axonal outgrowth was markedly reduced in retinal ganglion cells overexpressing the constitutively active mutants of both C- and N1-Src, their effects were different in ventral forebrain neurons. Conversely, the over expression of both WT and Y527F N1-Src in ventral forebrain neurons resulted in an increase in neurite outgrowth, whereas Y527F C-Src had the opposite effect. The effects of both C- and N1-Src Y527F on photoreceptor differentiation were also monitored, which was severely reduced in the presence of both kinases (Worley et al., 1997). These results, in conjunction with those observed by Kotani and colleagues, suggest a role for N1-Src during neuronal morphogenesis, which varied between different neuronal types. In addition to this, whilst C- and N1-Src overexpression appears to have similar effects on neuronal development in some cell types, they also appear to differ in others. This indicates that both C- and N1-Src could have different functions in some subclasses of neurons in the brain.

Worley and colleagues (1997) also demonstrated that *Xenopus* epithelial cells overexpressing N1-Src projected neurite-like processes, whereas C-Src transfected cells were predominantly adopted a rounded and more spread morphology. Whilst these findings demonstrated the different roles for both kinases in a non-neuronal cell type, they also re-enforced the observation made by Kotani which suggested that N1-Src modulates cytoskeletal dynamics to direct changes in cell morphology.

1.5.3 Neuronal Src Kinases in Neuroblastoma

Whilst no neuronal functions or *bona fide* substrates of N2-Src have been reported, the kinase has been shown to be associated with the positive prognosis of neuroblastoma cancer patients at stage IV-S of the disease (Bjelfman et al., 1990, Matsunaga et al., 1998). The childhood cancer, neuroblastoma, is derived from immature neuroblasts in the sympathetic nervous system that fail to differentiate and undergo uncontrolled proliferation. Like many others, the cancer is defined by a series of tumorigenic stages, which in this case range from stages I-IV, but can also manifest as stage IV-S (Evans et al., 1971). However, unlike the majority of other cancer types, neuroblastoma cells possess the ability to differentiate and mature. The degree of cellular differentiation that occurs within tumours, which is a determinant of the prognosis outcome, appears to be dependent on the age of the child and the stage of the cancer. For example, tumour cells in younger patients (under 12 months) tend to be more likely to terminally differentiate, making the cancer less aggressive. For the same reason, tumours at stage IV-S, can spontaneously regress and are therefore associated with a positive prognosis (Rudolph et al., 1997).

Bjelfman and colleagues (1990) observed that neuronal Src was elevated in neuroblastoma cases, which had a positive prognosis. Further investigations revealed

that whilst N1-Src expression was upregulated in differentiating neuroblastoma cells, its sole expression in the absence of N2-Src was not a sufficient marker for positive prognosis. However, cells that had undergone or were undergoing terminal differentiation expressed high levels of N2-Src, similar to those observed in human brain tissue, which correlated with the spontaneous regression of the cancer (Matsunaga et al., 1998). Therefore, N2-Src was identified as a promising prognostic marker for neuroblastoma patients, as well as a potential therapeutic target in the treatment of the disease. Since there is little published data describing the functional role of N2-Src, it remains unclear whether N2-Src plays a causative role in the differentiation of neuroblastoma cells. Although it is tempting to speculate that the kinase may prove to be an important therapeutic target, since the closely related N1-Src has been implicated in the processes of neuronal differentiation by regulating cytoskeletal dynamics (see sections 1.5.1 and 1.5.2) (Kotani et al., 2007, Maness et al., 1988, Wiestler and Walter, 1988, Worley et al., 1997).

1.5.4 Substrates and Binding Partners of N1-Src

The N1- and N2-Src mini-exon inserts occur in the SH3 domain of the kinases, which are important for substrate binding. The precise site of insertion lies in the n-Src loop, which forms an integral part of the 'specificity' pocket that typically interacts with the positively charged residue flanking the PXXP core of the substrate binding motif. The n-Src loop, which in addition to the RT loop is the site of most variation in the SH3 domains of SFKs, has also been implicated in forming alternative interactions with binding partners. Therefore, it is sensible to predict that the SH3 domains of both N1- and N2-Src would bind a different subset of substrates in comparison C-Src. In support of this prediction, a recent study published by the Evans lab demonstrated that both N1-Src and N2-Src displayed a reduced affinity for traditional class I and II C-Src SH3 binding ligands (discussed further in Section 3.1, (Keenan et al., 2015)).

Whilst no N2-Src SH3 binding partners have been identified, there are a number of studies in the literature that have performed C- and N1-Src SH3 pull-down studies with candidate binding partners. The outcome of these studies, amongst others, are summarised in Table 1.1. The ability of both the C- and N1-Src SH3 domains to bind to the proteins of interest, was determined by blotting for the kinase SH3 domains in the pulldown assays and comparing the relative intensities of their protein bands. Several proteins, including ASAP1, RICH1, dynamin, SNP70 and the well-known C-Src substrate FAK (discussed in Section 1.3) bound to the C-Src SH3 domain but did not appear to interact with N1-Src. In addition to this, the N1-Src SH3 domain seemed to have a reduced affinity for 3BP-1, CR16, Daam1 and Sam68 in comparison to the C-Src SH3 domain. These findings further support the theory that as a result of the N1-Src SH3

mini-exon insertion, the kinase has a reduced or complete lack of affinity for C-Src substrates.

It is particularly interesting that the N1-Src SH3 does not appear to interact with FAK, since the C-Src/FAK complex is integral to many cellular signalling transduction pathways that regulate proliferation, motility, survival and neurite outgrowth in neurons. However, a study, performed by Ruest and colleagues (2001), demonstrated the N1-Src precipitated with FAK when both kinases were co-expressed in COS7 cells. Furthermore, the study suggested that N1-Src recruitment by FAK facilitated the phosphorylation of p130CAS. In addition to this, they demonstrated that in their model, N1-Src mediated phosphorylation of CAS was greater than C-Src (Ruest et al., 2001). Therefore, these observations suggest that the interaction of N1-Src with FAK via an alternative mechanism could be sufficient to recruit the kinase. Indeed, it has been documented that the autophosphorylation of FAK at Y397 creates a C-Src SH2 binding motif (Schaller et al., 1994). In this instance, it could be possible that N1-Src substrate specificity governed by the SH2 domain overrides that of the SH3 domain. Alternatively, N1-Src could be interacting indirectly with FAK via a different binding partner.

Table 1.1: A Summary of C- and N1-Src SH3 Binding Partners and their Relative Ability to Bind to each Kinase.

Protein	Protein type	Binds to:		Comparison of C- and N1-Src interaction	Reference
		C-Src SH3 (Y/N)	N1-Src SH3 (Y/N)		
ASAP1	Arf1 GAP	Y	N	-	(Brown et al., 1998)
3BP-1	Rac GAP	Y	Y	C>N1	(Cicchetti et al., 1992)
CR16	MAPK substrate	Y	Y	C>N1	(Weiler et al., 1996)
Daam1	Formin	Y	Y	C>N1	(Aspenstrom et al., 2006)
Delphilin	Formin	-	Y	N.D	(Miyagi et al., 2002)
Dynamin	GTPase localised at the pre-synaptic membrane	Y	N	-	(Foster-Barber and Bishop, 1998)
EVL	Actin-associated protein	Y	Y	N1>C	(Lambrechts et al., 2000)
FAK	Kinase	Y	N	-	(Messina et al., 2003)
HCN1	Ion channel	-	Y	N.D	(Santoro et al., 1997)
NR2A	Ion channel	-	Y	N.D	(Grovesman et al., 2011)
Rich1	Rho/Rac/cdc42 GAP	Y	N	-	(Richnau and Aspenstrom, 2001)
Sam68	Adaptor protein	Y	Y	C>N1	(Finan et al., 1996)
SNP70	Nuclear protein, co-localises with splicing factors	Y	N	-	(Craggs et al., 2001)
Synapsin	Protein localised at synaptic vesicles	Y	N	-	(Foster-Barber and Bishop, 1998)
Tau	Microtubule associated protein	Y	N	-	(Reynolds et al., 2008)

N.D=not determined

One protein in particular, Ena/Vasp like protein (EVL), was demonstrated to show preferable binding to the N1-Src SH3 in comparison to C-Src *in vitro* (Lambrechts et al., 2000). EVL is a member of the Ena/Vasp family of proteins, which are known to play a role in axon guidance by regulating actin cytoskeletal dynamics, however the functional implications of the N1-Src SH3 domain binding to EVL require further investigation. In addition, the relatively poorly understood formin, Delphilin, has also been identified as a binding partner of the N1-Src SH3 domain *in vitro* (Miyagi et al., 2002). Delphilin acts as a scaffolding protein expressed in the neuronal post-synaptic density that binds the glutamate receptor GluR δ 2, which plays a role in motor coordination, synapse formation and synaptic plasticity (Kashiwabuchi et al., 1995). Whilst the exact roles of Delphilin have not been defined, it is possible that it also serves to regulate cytoskeletal dynamics, which appears to be the main role of other members of the formin family (Wallar and Alberts, 2003). To date, the physiological relevance of the interaction between N1-Src and Delphilin has not been reported in the literature.

N1-Src has also been shown to interact with the C-terminal domain (CTD) of the hyperpolarization-activated cyclic nucleotide-gated channel 1 (HCN1) in rat brain lysates (Santoro et al., 1997). HCN1 belongs to a family of four HCN channels (HCN1-4) that are expressed throughout the peripheral and central nervous systems, as well as in cardiac tissue. They are homotetrameric voltage gated pore loop channels known as 'pacemakers', since they are responsible for the rhythmic excitation of neurons and cardiac pacemaker cells. The structure of each subunit has two main portions; the transmembrane core and the CTD. A hyperpolarization activated current (I_h) passes through the channels in response to membrane hyperpolarization and cAMP binding (Wahl-Schott and Biel, 2009). HCN1 channels have been implicated in multiple, diverse functions including learning and memory (Nolan et al., 2004, Nolan et al., 2003), balance controlled by the inner ear (Horwitz et al., 2011), resting potentials in neurons and the regulation of presynaptic neurotransmitter release (Southan et al., 2000). HCN1 is also thought to be involved in various disease pathologies including epilepsy (Santoro et al., 2010) and Alzheimer's disease (Saito et al., 2012).

Little is known about the interaction and effects of neuronal Src on the HCN1 channel. Santoro *et al.* (1997) first discovered HCN1 by identifying the channel as a binding partner of the N1-Src SH3 domain, which was used as bait in a yeast two-hybrid experiment. Subsequently, there have been no reports of N1-Src regulation of HCN1, although there is literature describing a role for C-Src in the regulation of the HCN family of channels. Whole cell patch clamp experiments performed on HEK-293 cells transfected with HCN2 or HCN4 exhibited decelerated activation kinetics and in HCN4 transfected cells, decreased whole cell conductance when treated with the C-Src

inhibitor, 4-5-amino-(4-chlorophenyl)-7-(t-butyl)pyrazolo[3-4-d]pyrimidine (PP2) (Li et al., 2008a, Zong et al., 2005). The same effects were shown in dominant negative Src mutants (Arinsburg et al., 2006, Zong et al., 2005), suggesting C-Src is involved in HCN channel regulation.

Site-directed mutagenesis (SDM) experiments revealed that conserved Tyr-531 and Tyr-554 phosphorylation sites (confirmed by mass spectrometry) in the CTD of HCN4 alter channel activation (Li et al., 2008a) and channel activation kinetics (Li et al., 2008a, Aktories et al., 2004) respectively. Li and colleagues (2008a) reported that Y531F mutants almost abolished the effects of PP2 on voltage dependent channel activation, whereas Tyr-554 mutants had unaltered activation kinetics in the presence of PP2. Zong and colleagues (2005) gained the same results in relation to Tyr-554 for both HCN2 and HCN4. This group however did not show that C-Src had an effect on voltage dependent activation of HCN channels or a role for Tyr-531. Despite these conflicting discoveries, it is apparent that Tyr phosphorylation by C-Src plays a role in HCN channel activation.

In addition to N1-Src binding to the HCN1 channel, Groveman and colleagues confirmed that the CTD of the NR2A subunit in NMDA receptors (described in Section 1.3.1.2) can be phosphorylated by and bind N1-Src *in vitro*. They also demonstrated that NR1/NR2A receptor currents are enhanced in HEK-293 cells when co-expressed with N1-Src, indicating that similar to C-Src, N1-Src is capable of activating NMDAR currents (Groveman et al., 2011). However, this study did not investigate the differences, if any, between their phosphorylation of, or binding affinities to, the NR2A-CTD, nor did it report the effects of C- vs N1-Src on NMDAR currents. Furthermore, whether the kinases activate the channels via the same or different mechanisms *in vivo* remains to be discovered.

1.6 Aims

Whilst little is known about the precise functions and substrates of N1-Src, the literature suggests that N1-Src is important in the developing brain, potentially regulating cytoskeletal dynamics during neuronal morphogenesis (Kotani et al., 2007, Worley et al., 1997). In addition to this, N1-Src localization data and the interactions observed between N1-Src and several ion channels (Santoro et al., 1997, Groveman et al., 2011) indicate that the kinase may also play an important role in the adult brain. The primary aim of this project was to therefore clarify the roles of N1-Src in neuronal signalling through three specific approaches:

1) Identify novel N1-Src substrates:

Firstly, experiments were focussed on discovering novel N1-Src substrates. To identify whether HCN1 was an N1-Src substrate, *in vitro* kinase assays were performed using purified recombinant protein. In addition, the ability of N1-Src SH3 binding peptides, selected from putative N1-Src substrates, to enhance phosphorylation of an ideal Src substrate sequence, was investigated.

2) Determine the function of N1-Src in developing neurons:

With the aim of further understanding the role of N1-Src in neuronal development, the morphology of primary rat hippocampal neurons in N1-Src overexpression and shRNA knockdown studies were examined.

3) Dissect the signalling pathways downstream of N1-Src:

The signalling mechanisms through which N1-Src acts were also investigated, focussing specifically on L1-CAM and RhoA signalling pathways using a fibroblast cell model.

Chapter 2

Materials and Methods

Chapter 2. Materials and Methods

2.1 Materials

2.1.1 Molecular Biology Reagents

Oligonucleotides were purchased from Integrated DNA technologies (Leuven, Belgium). Pfu DNA polymerase was purchased from Thermo Scientific (Waltham, MA) and Taq DNA polymerase was a kind gift from Dr Dani Ungar (University of York). DNA ligase and ligase buffer were obtained from Promega (Fitchburg, WI). All restriction enzymes were purchased from New England Biolabs (NEB, Ipswich, MA). Both NucleoSpin® Plasmid mini- and midi-prep kits were sourced from Machery-Nagel (Düren, Germany) and gel extraction kits were purchased from Qiagen (Venlo, Netherlands). DNA HyperLadder I and SYBR®Safe were obtained from BioLine (London, UK) and Life Technologies (Paisley, UK), respectively. XL10 Gold supercompetent *E coli* were from Stratagene (Stockport, UK). XL10 Gold ultra-competent cells were purchased from Agilent Technologies (Stockport, UK). BL21-DE3 cells were a kind gift from Dr Daniel Ungar, and both the Rosetta 2 and Rosetta GamiB cell strains were a kind gift from Dr Wayne Paes.

The *pLINK*, *pLINK-C3*, *pmCherry-N1*, *pRK7-NR2A* vectors were a kind gift from Dr Sangeeta Chawla (University of York) (Grant et al., 1998). The *pGEX-6P-1* plasmids encoding YA, PD1 were made in house by Dr Sarah Keenan and the P1-13 GST-fusion peptides by Dr Gareth Evans (University of York). The pSUPER N-Src shRNA constructs A and B were designed in the Evans lab and prepared by Katharina Mahal. The *pcDNA3-eGFP-RhoA* constructs were gifts from Gary Bokoch (plasmid numbers #12965 (WT RhoA), #12968 (Q63L) and #12967 (T19N) (Subauste et al., 2000). L1-4A (*pcDNA3-L1-CAM*) was a gift from Vance Lemmon (plasmid number #13268) (Cheng et al., 2005).

2.1.2 Protein Biochemistry Reagents

Protein ladders were purchased from BioRad, Hercules (CA). The PVDF and Immobilon Western enhanced chemiluminescence (ECL) solution were both obtained from Millipore (Watford, UK). Glutathione agarose beads were purchased from GenScript (Piscataway, NJ) and 3C protease was sourced from the Technology Facility in the Department of Biology, University of York. The RhoA pull down activation assay kit was purchased from Cytoskeleton Inc. (Denver, CO) and the GFP conjugated protein G beads used were a kind gift from Dr Paul Pryor (University of York). The recombinant PKC-zeta and MBP proteins were sourced from Millipore (Watford, UK) and Sigma (Dorset, UK) respectively.

The following antibodies were purchased from: Actin B from Abcam (Cambridge), FLAG (M2) from Sigma (Dorset, UK), PY20 from BD Bioscience (San Diego, CA) and pY416

and GFP(a) were from Cell Signalling Technologies (Boston, MA). In addition, both α -mouse and α -rabbit horseradish peroxidase (HRP) antibodies were purchased from Sigma (Dorset, UK).

2.1.3 Cell Biology Reagents

Dulbecco's Modified Eagle Medium (DMEM) and Alexa Fluor® conjugated secondary antibodies were obtained from GIBCO, Invitrogen (Paisley, UK). EcoTransfect and Lipofectamine® transfection reagents were purchased from OZ Biosciences (Marseille, France) and Invitrogen (Paisley, UK). The GFP(b) antibody that was used solely for immunofluorescence experiments was a kind gift from Dr Paul Pryor (University of York).

Unless otherwise stated all other chemicals and reagents were purchased from Sigma (Dorset, UK).

2.2 Molecular Biology

2.2.1 Polymerase Chain Reaction (PCR)

The rat NR2A-CTD (C-terminal domain) was PCR amplified from the pRK7:NR2A construct. The PCR reaction contained 100 ng of pRK7:NR2A, 1X polymerase buffer, 0.2 mM dNTPs, 1 μ M of the forward (5' CGGAATTCAAGGACTGTAGCGATGTTGAC 3') and reverse (5' AGTATCGAATCTGATGTTTAACTCGAGGCG 3') primers, 0.5 U of Pfu DNA polymerase and distilled water (dH₂O) to 50 μ l. To amplify the rat NR2A-CTD, the PCR reaction was subjected to the following conditions: an initial denaturation step of 95 °C for 5 min, 25 repeated cycles of 95 °C for 30 seconds (s) (denaturation), 53 °C for 45 s (primer annealing) and 72 °C for 1 minute (min) (extension), as well as a final extension step at 72 °C for 10 min.

2.2.2 Agarose Gel Electrophoresis

Agarose gels were used to visualise and quantify DNA bands. To prepare an agarose gel (0.7-2 %), agarose was dissolved in 60 ml of 1X TAE buffer (40 mM Tris, 20 mM acetic acid, and 1 mM EDTA) using a microwave oven. The molten agarose was briefly cooled and SYBR®Safe DNA stain was added at a 1 in 20,000 dilution (v/v). The solution was poured into a gel cassette and a suitable well comb was secured into the cassette to form wells. After setting at room temperature, the gel was immersed in 1X TAE and DNA samples were diluted with 5X Orange G loading buffer (0.5 % (w/v) Orange G and 25 % glycerol (v/v) in dH₂O) and loaded into the gel. The DNA was separated by electrophoresis by applying a potential difference of ~ 80 V across the gel for ~ 30 min. DNA within the gel was visualised under a blue safelight.

2.2.3 Restriction Digest of Deoxyribonucleic Acid (DNA)

Restriction digests were performed using restriction endonucleases (NEB or Promega) and were carried out according to the manufacturers' instructions. Typically, a double restriction digest reaction (30 μ l) contained 100-500 ng of plasmid DNA, an appropriate reaction buffer (1X), 0.1 mg ml⁻¹ of BSA, 1 μ l of each restriction enzyme and dH₂O. The reactions were incubated for 1 hour (h) at 37 °C.

For subcloning, a preparative digest reaction (60 μ l) was performed, in which 2-6 μ g DNA was digested by 2 μ l of each restriction enzyme for 1 hour (h) at 37 °C. In this case, the whole reaction was loaded and separated by agarose gel electrophoresis. The relevant bands were excised and gel extracted (Section 2.2.4).

2.2.4 Agarose Gel Extraction of DNA Fragments

DNA bands were excised from an agarose gel under safelight, using a scalpel and DNA was extracted using a gel extraction kit, following the manufacturer's instructions. A sample of the extracted product was separated by agarose gel electrophoresis (Section 2.2.2), visualised and then quantified by comparing the band size to those of a known quantity from 5 μ l of HyperLadder I.

2.2.5 Annealing of Complimentary Oligonucleotides

Complimentary oligonucleotides (oligos) were annealed in a 10 μ l reaction containing 3.3 μ M of each oligonucleotide and 4 μ l of annealing buffer (100 mM NaCl and 50 mM HEPES, pH 7.4). The mixture was incubated in a PCR machine at 90 °C for 4 min followed by a 70 °C incubation for 10 minutes. The annealed oligos were slowly cooled to 10 °C (e.g. step-cool to 37 °C for 15-20 min, then to 10 °C or room temperature) before using or moving them to refrigerated storage.

2.2.6 Ligation of PCR Product into pJET1.2

A CloneJET PCR cloning kit (Thermo Fisher Scientific, Loughborough, UK) was used to ligate 50-100 ng of gel-extracted, blunt-ended PCR products into the propagation vector pJET1.2 according to the manufacturer's instructions.

2.2.7 DNA Ligation

To ligate restriction digested, gel-purified DNA, the insert was incubated with a gel-purified linearised plasmid in a 10 μ l reaction containing a 3:1 molar ratio of insert to vector (typically 100 ng of vector), 3 Units (U) of T4 DNA ligase, 1X ligation buffer and dH₂O. The reaction was incubated at room temperature for 3 h or overnight at 4 °C.

2.2.8 Bacterial Transformation

Plasmid DNA (~100 ng) was incubated with 50 μ l of XL10 Gold competent *E. coli* cells at 4 °C for 15-30 minutes. To facilitate the uptake of plasmid DNA, the bacteria were heat

shocked for 45 s at 42 °C, and subsequently placed on ice for a further 2 min. Sterile Lysogeny Broth (LB, 450 µl of 1 % NaCl, 1 % Tryptone and 0.5 % yeast extract (w/v) in dH₂O) was added to the bacteria, which were incubated at 37 °C with agitation. After 1 h, the bacteria were spread onto LB agar (1 % NaCl, 1 % Tryptone, 0.5 % yeast extract and 2 % agar (w/v) in dH₂O) plates containing the appropriate antibiotic(s) (ampicillin 100 µg/ml, kanamycin 50 µg/ml, chloramphenicol 34 µg ml⁻¹ or tetracycline 15 µg ml⁻¹). The plates were incubated overnight at 37 °C and subsequently stored at 4 °C. Aseptic technique was employed throughout the transformation process.

2.2.9 PCR Colony Screening

PCR was used to screen individual *E. coli* colonies for the successful inclusion of a DNA insert into a plasmid vector backbone. A PCR reaction (20 µl) contained 1X GoTaq buffer (Promega), 1 µM dNTPs, 2 µM of the forward and reverse primers, 0.1 µl of Taq polymerase and dH₂O. Finally, a scrape of each colony to be tested was mixed into separate PCR reactions using a sterile pipette tip. The PCR reaction conditions were as described in Section 2.2.1 however, the primer annealing temperature was changed to 55 °C and the extension time was extended to 1 min per kb of product during the repeated cycles. The PCR products were separated by agarose gel electrophoresis (Section 2.2.2) and successful clones were mini-prepped (Section 2.2.10).

2.2.10 Preparation of Plasmid DNA from Bacterial Cultures

Starter cultures containing 5 ml or 100 ml of selective LB medium were inoculated with a single colony (or a scrape from a glycerol stock) of *E. coli* transformed with the desired plasmid. The cultures were incubated overnight at 37 °C with agitation and then centrifuged at 4 °C, for 10 min, at 4500 *g*. Plasmid DNA was isolated from the bacteria using a Machery and Nagel NucleoSpin[®] Plasmid mini-prep kit (5 ml cultures) or a NucleoSpin[®] Midi-prep kit (100 ml cultures) according to the manufacturer's instructions. The quantity and quality of isolated DNA were analysed using a NanoDrop spectrophotometer (Thermo Scientific) in the University of York Technology Facility.

2.2.11 Sequencing of Plasmid Constructs

The sequences of all DNA plasmid constructs produced were confirmed by the sequencing service in the Genomics Unit of the Technology Facility, University of York. Pre-mixes contained 100-200 ng of plasmid DNA and 3.2 µM of a vector-specific forward or reverse primer. The sequencing data were subsequently analysed using the Applied Biosystems Sequence Scanner software v1.0. ClustalW2 software was used to generate sequence alignment (<http://www.ebi.ac.uk/Tools/msa/clustalw2/>).

2.2.12 Preparation of Glycerol Stocks for Storage of Plasmid DNA

For long-term storage, 1 ml of a bacterial culture containing XL10 Gold *E. coli*, transformed with plasmid DNA, was mixed with 1 ml of sterile 50 % (v/v) glycerol solution (in dH₂O) and stored at -80 °C in a cryovial.

2.2.13 Cloning

2.2.13.1 Src-pmCherry Constructs

Preparative digests (Section 2.2.3) were performed to excise the full length open reading frame (ORF) of C-, N1- and N2-Src from the relevant pFLAG-Src-plasmids and to linearise pmCherry-N1. The enzymes used were XhoI (5') and BamHI (3') with NEB buffer 3. The products were separated by agarose gel electrophoresis (Section 2.2.2) and gel extracted (Section 2.2.4). C-, N1- and N2-Src were ligated (Section 2.2.7) into linearised pmCherry-N1, transformed into XL10 Gold bacteria (Section 2.2.8) and the subsequent colonies were screened by colony PCR (Section 2.2.9). Successful colonies were mini-prepped and sequenced (Sections 2.2.10-11).

2.2.13.2 pGEX-6P-1: hHCN1-CTD

hHCN1-CTD was PCR amplified and cloned into the propagation vector *pJET1.2* by Dr Sarah Keenan. Using the restriction enzymes Sall (5') and NotI (3') with buffer 3, preparative digests were performed to excise *hHCN1-CTD* from *pJET1.2* and to linearise the plasmid *pGEX-6P-1*. Following the procedure outlined in Section 2.2.13.1 hHCN1-CTD was sub-cloned into *pGEX-6P-1* producing the construct *pGEX-6P-1:hHCN1-CTD*.

2.2.13.3 pGEX-6P-1: rNR2A-CTD

The *rNR2A-CTD* was PCR amplified from the vector *pRK7:NR2A*, which contained the ORF of the NR2A subunit of the NMDA receptor (NMDAR) (Section 2.2.1). The PCR product was gel extracted (Section 2.2.4), ligated into *pJET1.2* (Section 2.2.6) and a preparative digest (Section 2.2.3) was performed using the enzymes XhoI (5') and EcoRI (3') with buffer 3 to excise the rNR2A-CTD insert from the plasmid. The *rNR2A-CTD* was then sub-cloned into linearised *pGEX-6P-1* according to the procedure described in Section 2.2.13.1.

2.2.13.4 pGEX-4T-1: CTD Constructs

pGEX-6P-1:hHCN1-CTD and *pGEX-6P-1:rNR2A-CTD* were cut with Sall (5') and NotI (3') or XhoI (5') and EcoRI (3') respectively and the CTDs were individually sub-cloned into linearised *pGEX-4T-1* following the procedures described in Section 2.2.13.1.

2.2.13.5 pGEX-6P-1 Constructs Encoding GST-fusion Peptides.

The plasmid *pGEX-6P-1-'Y'* containing the ideal Src substrate (Y) was generated by ligating the appropriate annealed oligos (See Table 2.1) into linearised *pGEX-6P-1*,

which was pre-cut using the enzymes BamHI (5') and EcoRI (3'). Subsequently, the remaining annealed oligos corresponding to YA, PD1, PD1-P5A or P1-13 (See Table 2.1) were ligated into the linearised *pGEX-6P1-Y'* plasmid, which was pre-cut with the restriction enzymes Sall (5') and NotI (3'). This yielded plasmid constructs that contained the Y sequence, followed by the sequence of one of the remaining SH3 domain binding motifs. Both oligo sequences were separated by a short linker sequence that was 15 bp in length and corresponded to the sequence of the multiple cloning site of the plasmid between the 5' EcoRI and 3' Sall restriction sites. The constructs containing YA and PD1 were cloned by Dr Sarah Keenan (Keenan, 2012), whereas those containing peptides P1-13 were cloned by Dr Gareth Evans.

Table 2.1: The Oligonucleotide Sequences Used to Generate GST-fusion Peptide Substrates for C- and N1-Src

Name	Oligonucleotide Sequence	
Y	FWD	AATTCGGTGGCGGTGCAGAAGAGGAAATTTACGGTGAATTTGG
	REV	TCGAACAAATTCACCGTAAATTTCTCTTCTGCACCGCCACCG
YA	FWD	TCGACTCGGTGGCGGTGTGAGCCTGGCGCGTCTGCGCTGGCAGCTCTGGCGTAAGC
	REV	GGCCGCTTACGCCAGAGCTGCCAGCGCACGACGCGCCAGGCTCACACCGCCACCGAG
PD1	FWD	TCGACTCGGTGGCGGTGCGTGGCATCGCATGCCGGCGTATACCGCGAAATATCCGGC
	REV	GGCCGCCGGATATTTGCGGTATACGCCGGCATGCGATGCCAGCCACCGCCACCGAG
PD1-P5A	FWD	TCGACTCGGTGGCGGTGGCTGGCATCGCATGGCAGCGTATACCGCGAAATATCCGGC
	REV	GGCCGCCGGATATTTGCGGTATACGCTGCCATGCGATGCCAGCCACCGCCACCGAG
P1	FWD	TCGACTCGAAACAAGACCACCTGCAAATACTGCTAGGTTACAATAAGG
	REV	GGCCCCTTATTGTAACCTAGCAGTATTTGCAGGTGGTCTTTGTTTCGAG
P2	FWD	TCGACTCAAGGAAAAAGGACCAATATTAACACAAAGAGAAGCATAAAGG
	REV	GGCCCCTTATGCTTCTCTTTGTGTTAATATTGGTCTTTTTCTTGTAG
P3	FWD	TCGACTCATAGGAAGATGTCCAAGCGATCCTTATAAACATAGTTAAGG
	REV	GGCCCCTTAACTATGTTTATAAGGATCGCTTGGACATCTTCTATGAG
P4	FWD	TCGACTCCAACCTAAAACACCAGTACCAGCACAAAGAGAAAGGTAAGG
	REV	GGCCCCTTACCTTTCTCTTTGTGCTGGTACTGGTGTTTAGGTTG GAG
P5	FWD	TCGACTCCATAGGAGAACACCAAGTGAAGCAGATAGATGGTTATAAAGG
	REV	GGCCCCTTATAACCATCTATCTGCTTCACTTGGTGTCTCCTATGGAG
P6	FWD	TCGACTCTATTTAAGGCAACCATATTACGCAACAAGAGTAAATTAAGG
	REV	GGCCCCTTAAATTTACTCTTGTTCGTAATATGGTTGCCTTAAATAGAG
P7	FWD	TCGACTCAATTTAAAAGAACCATTATTAACATTTAGATTAAATTAAGG
	REV	GGCCCCTTAAATTTAATCTAAATGTTAATAATGGTTCTTTAAATTGAG
P8	FWD	TCGACTCACTCAAAGAGTCCAGCTACAGCACCTAAACCAATGTAAGG
	REV	GGCCCCTTACATTGGTTTAGGTGCTGTAGCTGGACTCTTTTGAGTGAG
P9	FWD	TCGACTCGTAAAGAAAAATCCAGGAATAGCTGCAAAATGGTGGTAAGG
	REV	GGCCCCTTACCACATTTTGCAGCTATTCCTGGATTTTCTTTACGAG
P10	FWD	TCGACTCTATAGCAAAATACCATTAGATACAAGTAGATTAGCATAAAGG
	REV	GGCCCCTTATGCTAATCTACTTGTATCTAATGGTATTTTGCTATAGAG
P11	FWD	TCGACTCGGACCAAGAGGCCTGGTAATACATTAAGAAAAATGGTAAGG
	REV	GGCCCCTTACATTTTCTTAATGTATTACCAGGCCTTTTGGTCCGAG
P12	FWD	TCGACTCGCTGCAAAGATACCAGATAAAACAGAAAGATTACATTAAGG
	REV	GGCCCCTTAATGTAATCTTTCTGTTTTATCTGGTATCTTTGCAGCGAG
P13	FWD	TCGACTCGGAGCAAGAAGTCCAGCTCCAACAAGAAAAGAATTTAAGG
	REV	GGCCCCTTAAATTTCTTTCTTGTGGAGCTGGACTTCTTGCTCCGAG

2.3 Protein Biochemistry

2.3.1 Protein Expression

GST-fusion proteins were expressed in *E. coli* cells and subsequently purified. Depending on the protein, different *E. coli* strains were used for expression (see Table 2.2). The majority of GST-fusion proteins were expressed in BL21 (DE3) *E. coli*, since they are deficient in the proteases Lon and OmpT, enhancing protein production from cloned genes. The Rosetta 2 *E. coli* strain was trialled or used for proteins whose corresponding gene sequences contained many rare *E. coli* codons, given that this strain contains plasmids that encode for several of the rare tRNAs. Additionally, Rosetta Gami B *E. coli*, which also express the rare tRNAs found in Rosetta 2 cells, were used for proteins containing disulphide bonds. This strain is also a double mutant in thioredoxin reductase (*trx*B) and glutathione reductase (*gor*), which creates a more oxidising cytoplasmic environment and enhances protein folding through stimulating the formation of disulphide bonds between cysteine residues.

A single colony of *E. coli* cells, transformed with a *pGEX* construct, was used to inoculate a starter culture of LB (50 ml) and incubated with agitation (200 rpm), overnight at 37 °C in the presence of the appropriate antibiotics (See Table 2.2). The starter culture was added to 1 L of LB under antibiotic selection and placed in a shaking incubator for 3-4 h until $OD_{600} = 0.6 - 1$. The culture was induced with isopropyl β -D-1-thiogalactopyranoside (IPTG; 1 mM) for 3 h at 37 °C (or overnight at 18 °C) with constant agitation. Cultured bacteria were pelleted in a Sorvall Evolution centrifuge at 5000 *g* for 10 min and the supernatant was discarded and the pellets were frozen at -80 °C.

2.3.2 Purification of Recombinant Proteins

Different bacterial cell lysis methods were used, for the purification of each GST fusion protein, in order to optimise the final protein yield and stability. Sonication (i) was used for the purification of GST, the GST-P1-13 and GST-PTP1B-His Δ 80Src kinase protein purification, whereas French press (ii) was used for the purification of GST-hHCN1-CTD and GST-rNR2A-CTD.

- (i) Frozen *E. coli* cell pellets were thawed on ice and resuspended in phosphate buffered saline (PBS, 30 ml) containing lysozyme (133 μ M final concentration), phenylmethanesulfonylfluoride (PMSF, 1 mM) and 1X protease inhibitor cocktail (Sigma-Aldrich). After incubating on ice for 30 min, Triton X-100 (1.5 % w/v) and dithiothreitol (DTT, 7 mM) were added. This solution was subjected to 6 x 1 min cycles of 30 s 10 kHz sonication and 30 s gentle agitation.
- (ii) Frozen *E. coli* cell pellets were thawed on ice and resuspended in breaking buffer (100 mM HEPES, 500 mM KCl, 2 mM β -Mercaptoethanol in dH₂O) containing

PMSF (1 mM) and 1 X protease inhibitor cocktail. Cells were lysed at 4 °C using a manual French press (Thermo Scientific).

Insoluble matter was removed from the lysate by centrifugation for 30 min at 17200 g and 4 °C. Cleared lysate was incubated with glutathione agarose (0.1-1 ml) for 1-2 h. Beads were washed five times with PBS, followed by one wash with 1.2 M NaCl in PBS and a further two washes with PBS. After each wash, the beads were centrifuged for 5 min at 720 g at 4 °C. Protein was eluted from the beads by the addition of 600 µl glutathione elution buffer per 0.5 ml beads and incubation at room temperature for 20-30 min with agitation. This elution process was repeated 3 times. Eluted protein was aliquoted and frozen at -80 °C following analysis by sodium dodecyl sulphate polyacrylamide gel electrophoresis (SDS-PAGE) (Section 2.3.4).

Table 2.2: Antibiotic and Growth Conditions for *E.Coli* Expressing Various pGEX Constructs

Construct	E-coli strain	Antibiotic resistance	Growth conditions post- IPTG induction
<i>pGEX-4T-1</i> <i>pGEX-6P-1</i> <i>pGEX-6P-1:Peptide constructs</i> <i>pGEX-6P-1:hHCN1-CTD</i> <i>pGEX-4T-1:rNR2A-CTD</i> <i>pGEX-6P-1:PTP1B-HisΔ80C-Src/N1-Src</i>	BL21	Ampicillin (100 µg ml ⁻¹)	3-4 h at 37 °C with shaking (200 rpm)
<i>pGEX-6P-1:hHCN1-CTD</i> <i>pGEX-4T-1:hHCN1-CTD</i> <i>pGEX-4T-1:rNR2A-CTD</i>	Rosetta 2	Ampicillin (100 µg ml ⁻¹) Chloramphenicol (34 µg ml ⁻¹)	16 h at 18 °C with shaking (200 rpm)
<i>pGEX-4T-1:rNR2A-CTD</i>	Rosetta Gami B	Ampicillin (100 µg ml ⁻¹) Chloramphenicol (34 µg ml ⁻¹) Tetracycline (12.5 µg ml ⁻¹) Kanamycin (15 µg ml ⁻¹)	16 h at 18 °C with shaking (200 rpm)

2.3.3 Cleavage of the GST Tag from GST Fusion Proteins

GST was cleaved from glutathione resin bound GST fusion proteins using PreScission protease (produced by York Technology Facility). Proteins were incubated with 50 µg PreScission protease for 48 h at 4 °C, rotating end over end.

2.3.4 SDS-Polyacrylamide Gel Electrophoresis (PAGE)

Sodium dodecyl sulphate (SDS) polyacrylamide gels comprising a resolving gel (10-15 % acrylamide, 0.05 % ammonium persulfate (APS), 0.01 % tetramethylethylenediamine (TEMED), 375 mM Tris, pH 8.8, and 0.1% SDS) and a stacking gel (5 % acrylamide, 0.05 % APS, 0.01 % TEMED, 125 mM Tris pH 6.8 and 0.1 % SDS) were prepared and transferred into a gel electrophoresis tank (BioRad) containing 1X SDS-PAGE buffer (25 mM Tris, 192 mM glycine, 0.1 % SDS). Protein samples were denatured at 95 °C for 10 min and separated alongside 5 µl of a protein ladder at 180 V for approximately 1 h. Gels were either stained with Coomassie Brilliant blue stain for 30 min, followed by de-staining (40 % (v/v) methanol, 10 % (v/v) glacial acetic acid in dH₂O) overnight to visualise protein bands or transferred to methanol-activated polyvinylidene fluoride (PVDF) membrane (Immobilon-P) for Western blot analysis.

2.3.5 Wet Transfer

Protein samples separated by SDS-PAGE were transferred onto PVDF by wet transfer. Briefly, 6 cm x 8 cm PVDF was pre-soaked for 1 min in methanol followed by distilled water for 1 min and then transfer buffer (25 mM Tris, 192 mM glycine, 20 % methanol). Two 6 cm x 8 cm sponges and sheets of filter paper were also soaked in transfer buffer. The SDS polyacrylamide gel and PVDF membrane were sandwiched between the filter papers and sponges in a transfer cassette and subjected to electrophoretic transfer at 66 V for 1 h (or 20 V overnight). Successful transfer of proteins was confirmed by Ponceau staining,

2.3.6 Western Blotting

Transferred proteins of interest were detected using the appropriate antibodies via Western blotting (see Table 2.3 for antibodies and their dilution factors). The PVDF membrane was blocked with 3 % BSA (for phosphotyrosine antibodies) or 3 % Marvel skimmed milk powder in PBS, followed by incubation with the appropriate primary antibody (Table 2.3). Incubations were carried out for 2 h at room temperature or overnight at 4 °C. The membrane was washed 3 x 5 min in PBS containing 0.5 % Tween-20 and subsequently incubated with a HRP-conjugated secondary antibody solution (3 % milk and 0.5 % Tween-20 in PBS) for 1 h. The membrane was subjected to 3 x 10 min washes with 0.5 % Tween-20 in PBS. All incubations were performed at room temperature with shaking unless specified otherwise. ECL substrate was added to the PVDF membrane, the membrane was blotted with 3 mm filter paper to remove excess liquid, wrapped in cling film and placed in a film cassette. Membranes were exposed to photo-sensitive film (Santa Cruz) for a relevant period of time. The film was developed, rinsed in water and fixed.

Table 2.3: Western Blotting Antibodies and Blocking Conditions

Antibody	Block	Primary antibody	Secondary antibody	
		Concentration	Antibody	Concentration
Actin B	3 % milk in PBS	1:10000	α -rabbit HRP	1:5000
FLAG	3 % milk in PBS	1:1000	α -mouse HRP	1:5000
GFP(a)	3 % milk in PBS	1:2000	α -mouse HRP	1:5000
PY20	3 % BSA in PBS	1:1000	α -mouse HRP	1:5000
pY416	3 % BSA in PBS	1:2000	α -rabbit HRP	1:5000
RhoA	5 % milk in PBS	1:500	α -mouse HRP	1:5000

2.3.7 *In Vitro* Kinase Assays with GST-hHCN1- and GST-rNR2A- Purified Proteins

In vitro C-Src and N1-Src kinase assay reactions (25 μ l) were performed using GST-hHCN1- (5 μ M) and GST-rNR2A-CTD (5 μ M) substrates in reaction buffer A (Table 2.4). The ideal Src substrate GST-YA (10 μ M) was used as the positive control and GST (10 μ M) alone as a negative control. The assays were performed in the absence or presence of 40 nM His Δ 80-C- or N1-Src for each substrate. Assays were performed at 30 °C for 1 h. Kinase reactions that were performed with glutathione agarose-bound protein substrates contained approximately 10 μ g of GST-tagged substrate. These reactions were performed with GST-hHCN1- and GST-rNR2A-CTD proteins that were expressed and purified from the pGEX-4T-1 plasmid constructs. Since these proteins contained a thrombin cleavage site in place of a PreScission protease cleavage site, residual PreScission protease present in His Δ 80-Src kinase stocks could not cleave the protein. The reactions were performed separately with reaction buffers B and C (Table 2.4) and were subjected to shaking (150 rpm) at 30 °C for 1 h. All reactions were terminated by the addition of 2 X Laemmli buffer (25 μ l) and stored at -20 °C. Kinase assay protein samples were separated by SDS-PAGE and analysed by Western blotting (Sections 2.3.4-6).

2.3.8 *In Vitro* γ -³²P ATP Kinase Assays with hHCN1- and rNR2A-CTD

In vitro kinase assays were performed in 50 μ l reactions containing 100 nM His Δ 80C- and N1-Src, 5 μ M untagged hHCN1- or rNR2A-CTD, 10 mM MgCl₂, 0.5 mM ATP, and 5 μ Ci γ -³²P ATP in 100mM Tris (pH 7.5). The reactions were incubated for 3 h at 30 °C. Every 1 h, 10 μ l of the reactions were removed, terminated with 2X Laemmli buffer and stored at -20 °C. Further *in vitro* kinase assays (25 μ l) with an increased concentration of hHCN1- (5.8 μ M) and rNR2A-CTD (7.2 μ M) were performed that also

Table 2.4: Kinase Buffers Used for *In Vitro* Kinase Assays Containing GST-hHCN1-CTD and GST-rNR2A-CTD

Reaction Buffer	A	B	C
	100 mM Tris 0.5 mM ATP 10 mM MgCl ₂ 40 nM Src pH 7.5	100 mM Tris 0.5 mM ATP 10 mM MgCl ₂ 50 µg/ml BSA 1 mM DTT 40 nM Src pH 7.5	100 mM Tris 0.5 mM ATP 10 mM MgCl ₂ 50 µg/ml BSA 1 mM DTT 200 µM NaVO ₄ ³⁻ 40 nM Src pH 7.5

contained 100 nM His Δ 80C- and N1-Src, 10 mM MgCl₂, 0.5 mM ATP, and 2 µCi γ -³²P ATP in 100 mM Tris (pH 7.5). The reactions were incubated at 30 °C and terminated after 3 h with 2X Laemmli buffer and stored at -20 °C. For both types of kinase assays, an identical reaction with the positive control GST-YA was performed. Kinase assay protein samples were separated by SDS-PAGE (Section 2.4.4) and then the gels were sandwiched between two acetate sheets and exposed to X-ray film for 24-48 h.

2.3.9 *In Vitro* Protein Kinase C-zeta (PKC-zeta) Kinase Assays with hHCN1- or rNR2A-CTD

In vitro kinase assays (25 µl) were performed in the presence or absence of the constitutively active form of protein kinase C (PKC-zeta; 50 ng) with the rNR2A- or hHCN1-CTDs (5 µM). Reactions also contained 10 mM MgCl₂, 0.5 mM ATP, and 2 µCi γ -³²P ATP in 100 mM Tris (pH 7.5) and were incubated at 30 °C for 3 h. Reactions were terminated with 2X Laemmli buffer and stored at -20 °C. Identical reactions containing myelin basic protein (MBP, 5 µM) were performed and served as a positive control for PKC-zeta kinase activity. Kinase assay samples were analysed as described in Section 2.3.8.

2.3.10 *In Vitro* His Δ 80-N1-Src Kinase Assays with Putative GST-fusion Peptide Substrates

In vitro His Δ 80-N1-Src kinase reactions (25 µl) containing PD1 (positive control; 1.7, 5 or 15 µM), PD1-P5A (negative control; 1.7, 5 or 15 µM) and the putative N1-Src GST-fusion peptide substrates P1-13 (5 µM) were performed using reaction buffer A, however, a kinase concentration of 5 nM was used (Table 2.4). The assays were incubated at 30 °C for 1 h and the reactions were terminated by the addition of 2X Laemmli buffer (25 µl) and stored at -20 °C. Kinase assay protein samples (5 µl) were separated by SDS-PAGE in duplicate. One set of gels were analysed by Western blotting (Sections 2.3.4-

6), whilst the other set were Coomassie stained and subsequently de-stained, to enable the comparison of GST-fusion peptide quantities between reactions.

To facilitate the comparison of substrates GST-P1-13 with both GST-PD1 (5 μ M) and GST-PD1-P5A (5 μ M), densitometry was performed on the resulting blots and Coomassie stained gels from three replicates in Image J. Within a single replicate, the two blots (blot 1 contained samples P1-6 and blot 2 contained samples P7-13) contained the same quantity of a GST-PD1 positive control. Therefore the densitometry values were normalised to the density of the same GST-PD1 band across blots. In addition, to account for potential differences in the amount of substrate in each reaction, densitometry bands obtained for each phospho-protein were normalised to the densitometry values from the corresponding Coomassie stained protein bands. Finally, the values within each experiment were normalised to PD1 to account for potential differences in the processing of blots and Coomassie gels between biological replicates. Differences between the data values obtained were assessed for significance using a one-way ANOVA.

2.3.11 Immunoprecipitation (IP)

For each condition, a T75 flask of cultured COS7 cells (3×10^6 cells) was transfected with the appropriate plasmid constructs according following the procedure outlined in Section 2.4.3. The cells in each T75 flask were lysed in 1 ml of ice cold 1X radioimmunoprecipitation assay buffer (RIPA) buffer (20 mM Tris-HCl (pH 7.5), 270 mM sucrose, 1 % Triton X-100, 5 % glycerol, 10 mM sodium β -glycerophosphate, 1 mM ethylene glycol tetraacetic acid (EGTA), 1 mM ethylenediaminetetraacetic acid (EDTA), 0.1 % β -mercaptoethanol, 1 mM sodium orthovanadate, 0.1 % phosphatase inhibitor, 1 mM PMSF). Cells were scraped from the bottom of the flasks and extracted on ice for 10 min. The cell lysates were then centrifuged for 10 min at 16,000 g at 4 $^{\circ}$ C to remove insoluble matter. Protein G agarose (20 μ l aliquots) conjugated to a GFP antibody was pre-washed in RIPA buffer and incubated end over end, overnight at 4 $^{\circ}$ C with the appropriate cell lysate. The following day, the beads were pelleted by centrifugation for 5 min at 16,000 g at 4 $^{\circ}$ C. The supernatant was removed and the beads were transferred into SPIN-X columns (Corning) and washed x 3 with 500 μ l of RIPA buffer. Proteins that were retained by the GFP resin were eluted upon the addition of 50 μ l of 2X Laemmli buffer (Sigma-Aldrich) to the SPIN-X columns.

2.3.12 RhoA Pull-down Activation Assay

The RhoA pull-down activation assays were performed using a commercial kit purchased from Cytoskeleton Inc. according to the manufacturer's instructions. For each condition, a 10 cm dish of COS7 cells (1×10^6 cells) was transfected with the appropriate plasmid

constructs according to the procedure outlined in Section 2.4.3. Cells were lysed in 500 μ l of the provided cell lysis buffer (50 mM Tris pH 7.5, 10 mM $MgCl_2$, 0.5 M NaCl, 2 % Igepal and 1 X protease inhibitor cocktail) and lysates were immediately clarified at 10000 g , for 10 min at 4 °C.

Clarified lysates were snap frozen and stored at -80 °C and the protein content of the lysates (~ 2 mg ml^{-1}) was assessed by Bradford assay (Bradford, 1976). Thawed protein lysate aliquots (500 μ l) were incubated separately with Rhotekin RhoA binding domain (RBD) beads (25 μ g) at 4 °C, rotating end over end. As a positive and negative control, cell lysates containing wild type RhoA, were pre-loaded with guanosine triphosphate (GTP) or guanosine diphosphate (GDP), respectively. After a 1 h incubation, the supernatant was removed, the beads were resuspended in the provided wash buffer (25 mM Tris pH 7.5, 30 mM $MgCl_2$, 40 mM NaCl) and transferred into SPIN-X columns, which had been prewashed. The SPIN-X columns were centrifuged at 5000 g for 1 min at 4 °C to pellet the beads and remove the wash buffer. Proteins that were pulled down by the Rhotekin RBD beads were eluted upon the addition of 20 μ l of 2X Laemmli buffer to the SPIN-X columns. Eluted samples were stored at -20 °C until use. Input (total protein lysate; 2 %) and eluted protein (10 μ l) samples were run on separate gels and subjected to Western blotting (Sections 2.3.4-6).

2.4 Cell Biology Techniques

2.4.1 Culture of Mammalian Cell Lines

The culture of mammalian cell lines was performed under sterile conditions in a Class 2 biological safety cabinet. COS7 and B104 cell lines were cultured in high glucose DMEM containing glutamine and pyruvate. The media was supplemented with 10 % foetal bovine serum (FBS) and 1 % penicillin-streptomycin (PenStrep). Cells were maintained in a 37 °C incubator with 5 % CO_2 .

2.4.1.1 Revival of Cell Stocks

Cells were removed from storage at -80 °C and thawed for 2 min in a 37 °C water bath. Cells were then placed in a T25 flask containing 5 ml of media pre-warmed to 37 °C. The media was replaced the following day.

2.4.1.2 Passage of Mammalian Cell Lines

Adherent cells were washed with PBS and incubated with 1X trypsin-EDTA (Invitrogen) for 2-5 min at 37 °C. The trypsin was inhibited with culture medium containing 10 % FBS and 1 % PenStrep. Cells were collected from the bottom of the flask and centrifuged at 130 g , for 5 min at room temperature. After centrifugation, the cells were resuspended in

culture medium and 1/5th of the suspension was replaced into a new flask containing pre-warmed media.

2.4.1.3 Cell Storage

For long term storage, cells resuspended after passage were added in equal proportion to freezing media (90% FBS, 10 % DMSO) and stored, in cryovials, at -80 °C.

2.4.1.4 Plating Cells

Passaged cells were counted using a haemocytometer and 2×10^4 or 1×10^5 cells were plated into single wells of a 24 or 6 well plate, respectively. For immunocytochemistry experiments, cells were plated on 13 mm coverslips in a 24 well plate.

2.4.2 L1-CAM Process Outgrowth Assay

The wells of 8 well chamber slides were pre-coated with L1-CAM protein dissolved in PBS (40 μ l; 50 μ g/ml) or PBS alone (40 μ l; control). 1×10^5 COS7 cells were plated in each well and subsequently transfected and processed for immunofluorescence. The plastic eight well chamber was removed from the slides using a tool provided by the manufacturer.

2.4.3 Cell Line Transfections using EcoTransfect Reagent

Mammalian cell lines were transfected with plasmid constructs using EcoTransfect according to the manufacturer's instructions. Briefly, DMEM containing plasmid DNA was incubated with DMEM containing EcoTransfect (at a ratio of 1 μ g DNA: 2 μ l EcoTransfect) for 20 min at room temperature. The transfection solution was applied dropwise to plated or flasks of cells and incubated for 48 h at 37 °C with 5 % CO₂. Cells were either fixed and stained or lysed for use in an immunoprecipitation assay (Section 2.3.11) or for Western blot analysis (Section 2.3.4-6).

2.4.4 Preparation of Rat Hippocampal Neurons

Rat hippocampi were dissected from euthanised new born (postnatal day 0, P0) Wistar rats by Dr Sangeeta Chawla. Dr Chawla's protocol for the preparation of hippocampal neurons from new born rats has been approved by the Biology Ethics Committee. The subsequent dissociation of cells was carried out by either myself, Dr Chawla or Christopher Ugboode according to a pre-published procedure (Belfield et al., 2006). Briefly, dissected hippocampi were incubated at 37 °C with papain enzyme solution for a total of 40 min, with additional fresh enzyme solution being added after 20 min. The hippocampi were washed x 3 with pre-warmed dissociation media containing kynurenic acid and magnesium chloride/sulphate. After washing, the hippocampi were incubated with 2 ml of trypsin inhibitor for 5 min at 37 °C. This procedure was repeated x 3 and followed by 3 washes with warmed growth medium. The hippocampi were dissociated

by trituration in growth medium and diluted in OPTI+ solution to give an equivalent concentration of one hippocampus per 2 ml of media. The cells were plated on coverslips that were pre-coated in poly-D-lysine (PDL; coverslips were incubated at RT with 15 $\mu\text{g ml}^{-1}$ PDL for 1-2 h end over end and air dried under sterile conditions). Cells were plated at a density of 2.5 - 5 $\times 10^5$ cells per well of a 24 well plate.

2.4.4.1 Transfection of Rat Hippocampal Neurons

P1 primary rat hippocampal neurons were transfected, 24 h after plating, with various DNA constructs using Lipofectamine® reagent in accordance with the manufacturer's instructions. Briefly, for a single well of a 24 well plate, midi-prepped DNA and 2.5 μl Lipofectamine® reagent were each added to 200 μl Neurobasal media (Gibco, Life technologies) in separate tubes (for shRNA experiments the ratio was 0.1 μg ShRNA: 2 μl Lipofectamine® and for mCherry constructs the ratio was 0.25 μg DNA to 2 μl of Lipofectamine®). The contents of both tubes were mixed and incubated at room temperature for 20 min. The growth medium from the hippocampal neurons was removed, and replaced with DNA/ Lipofectamine® solution. After a ~5 h incubation period at 37 °C with 5 % CO₂, the DNA/Lipofectamine® solution was aspirated from the cells and the previously removed growth medium was reapplied. Cells were cultured for a further 48 h (P3), fixed, stained and mounted onto slides (Section 2.4.5.1). For some experiments (Section 4.2.7), neurons were cultured until P7 before cells were fixed.

2.4.5 Immunocytochemistry

2.4.5.1 Cell Fixation and Staining

Cells were washed x 3 with PBS and fixed in a paraformaldehyde (PFA) solution (4 % PFA and 4 % sucrose in PBS, pH to 7.4) at room temperature. After 20 min, cells were washed x 3 with PBS. To permeabilise the cells, 0.1 % Triton X-100 dissolved in PBS, was applied for 30 min at room temperature. Cells were subsequently stained with an appropriate primary antibody at the required dilution for 2 h at room temperature (Table 2.5). After washing the cells x 3 with PBS, cells were incubated in the dark with an Alexa Fluor® secondary antibody raised in the correct species, at a dilution of 1:500 for 1 h (Table 2.5). After a further 3 washes in PBS and once in water, the coverslips were air dried and mounted onto slides in Mowiol mounting medium (10 % Mowiol, 25 % glycerol in 0.1 M Tris pH 8.5) containing 1 $\mu\text{g ml}^{-1}$ DAPI (4',6-diamidino-2-phenylindole) stain and stored at 4 °C prior to processing by microscopy.

Table 2.5: Primary and Secondary Antibodies Used in Immunocytochemistry

Primary Antibody		Secondary antibody	
Name	Concentration	Name	Concentration
GFP(b)	1:1000	α-rabbit Alexa Fluor®488	1:500
FLAG	1:1000	α-mouse Alexa Fluor®594	1:500
L1-CAM	1:1000	α-mouse Alexa Fluor® 488	1:500

2.5 Cell Imaging

2.5.1 Image Capture Using a Fluorescence Microscope

Fluorescence images were captured using a Nikon TE200 epifluorescence inverted microscope with a RoleraXR CCD (QImaging) camera controlled by SimplePCI Software (Hamamatsu). Images of COS7 cells or hippocampal neurons were acquired using a 40X or 20X objective lens.

2.5.2 Coverslip Tiling Using the Zeiss Slidescanner

Fluorescence images of whole coverslips containing transfected hippocampal neurons were acquired with a 20X objective lens, using a Zeiss AxioScan.Z1 slide scanner. Images were processed using the Zeiss image software analysis programme Zen Blue.

2.6 Analysis of Cell Morphology Data

2.6.1 Morphological Analysis Using NeuronJ

Image analysis of both COS7 and neuronal cells was performed using ImageJ. To compile tiled images of the same neuron where required, the stitching plugin for ImageJ was used (Preibisch et al., 2009). Neurite morphology data was extracted from images using the NeuronJ plugin, which allows the semi-automatic tracing of neurites, which were subsequently categorised into neurites/processes, primary branches, secondary branches and tertiary branches. The NeuronJ programme calculated the lengths of individual neurites/processes and branches, which were subsequently compiled in Microsoft Excel (Meijering et al., 2004). In a similar fashion, NeuronJ was used to trace and measure neurite-like extensions projected by COS7 cells under different cellular conditions.

To measure additional morphological parameters of COS7 cells, the perimeter of individual cells was manually traced in ImageJ and subsequently used to calculate the area (μm^2) and circularity of the cells. Circularity ($4\pi(\text{area}/\text{perimeter}^2)$) was used to describe the 'roundness' of the cells measured, whereby a value of 1 describes a perfect circle and a value of 0 represents an elongated oblong shape (Schneider et al., 2012).

2.6.2 Statistical Analysis of Cell Data

Statistical analysis was performed on data combined from experiments containing at least three biological replicates. Statistical tests were not performed when the experiment comprised fewer than three biological replicates.

Data are presented as mean \pm SEM. SigmaStat v12.5 software was used to perform all statistical analyses. Normal distribution was determined using a Shapiro-Wilk test. For normally distributed data, paired or unpaired Student's two-tailed t-test was used to compare two samples. Multiple comparisons on non-parametric data were made using Kruskal-Wallis tests (or one-way ANOVA on ranks) on the total number of cells from three biological replicates (unless stated otherwise). Where the outcome of the Kruskal-Wallis test was significant, a Dunn-Bonferroni post-hoc test was used for the pairwise comparison between the fixed variables. For experiments containing two factors, statistical significance was assessed using a two-way ANOVA on the total number of cells from three biological replicates (unless stated otherwise). A post-hoc Tukey test was used to facilitate the pairwise comparison between the fixed variables where necessary. Results were considered significant when $P < 0.05$ (*).

Chapter 3

Discovery of Novel N1-Src Substrates

Chapter 3. Discovery of Novel N1-Src Substrates

3.1 Introduction

The lack of tools available that enable the discrimination between C- and N1-Src kinases, such as N1-Src specific activators, inhibitors, antibodies and knock-out mice, has hampered the discovery of N1-Src substrates. It is therefore unsurprising that few *bona fide* N1-Src substrates have been identified since N1-Src's discovery by Levy and colleagues in 1987. For this reason, it is anticipated that the phosphorylation of some neuronal substrates that have previously been assigned to C-Src activity, are in fact attributable to N1-Src.

Given that N1-Src differs from C-Src by only a short insert in the SH3 domain, the area of the protein that co-ordinates substrate docking, it is highly likely that C- and N1-Src have different substrates. This was alluded to by Keenan *et al.*, (2015), who demonstrated that in relation to C-Src, both N1- and N2-Src had a low affinity for ideal Src substrates that were linked to the canonical C-Src SH3 binding motifs (Classes I and II). They also showed that *in vitro* phosphorylation of synaptophysin, a well-established substrate of C-Src in the brain, was greatly reduced when incubated with N1- and N2-Src compared to C-Src (Keenan *et al.*, 2015). Taken together, this evidence suggested that N1-Src has a reduced affinity for C-Src substrates and therefore may have different substrates to C-Src in neurons.

Of the few substrates known to be phosphorylated by N1-Src *in vitro*, the C-terminal domain (CTD) of the NMDA receptor (NMDAR) subunit, NR2A, has also been shown to be phosphorylated by V-Src and regulated by C-Src (Yang and Leonard, 2001, Yu *et al.*, 1997, Groveman *et al.*, 2011). However, phosphorylation of the NR2A-CTD by C- and N1-Src has not been compared and since ion channel CTD phosphorylation often occurs at multiple residues and by more than one kinase, it is possible that C- and N1-Src might phosphorylate the NR2A subunit at different sites. Whilst it has been shown that V-Src phosphorylates the NR2A-CTD at three individual tyrosine residues, the specific residues phosphorylated by N1-Src remain unknown. In addition, whilst Groveman *et al.*, (2011) showed that NR1-1A/NR2A receptor currents were enhanced in HEK-293 cells when co-expressed with N1-Src, the differential effects of C- and N1-Src were not investigated.

Amongst other proteins (see Section 1.5.4), a second type of neuronal ion channel, hyperpolarisation-activated cyclic nucleotide-gated 1 (HCN1), has been shown to interact with N1-Src, however phosphorylation of the protein by N1-Src has not been demonstrated (Santoro *et al.*, 1997). It was anticipated that HCN1 could be an N1-Src

substrate, since other HCN channels have been shown to be regulated and phosphorylated by C-Src (Li et al., 2008a, Arinsburg et al., 2006, Zong et al., 2005). For example, the direct phosphorylation of recombinant GST-HCN2-CTD was demonstrated in an *in vitro* kinase assay with C-Src (Rolli-Derkinderen et al., 2005).

Given that very few N1-Src substrates have been identified and recent studies suggest that N1-Src has a lower affinity for traditional C-Src substrates, further studies carried out in the Evans lab sought to identify an N1-Src SH3 binding consensus motif that would ultimately lead to the discovery of novel N1-Src substrates (Keenan, 2012). A consensus motif for N1-Src SH3 substrate binding was established after performing a phage display experiment, in which a library of short peptides, consisting of 12 amino acids each, were screened for preferential binding to the N1-Src SH3 domain. Notably, the N1-Src SH3 binding consensus motif deviated from the traditional proline rich PXXP motifs that bind the C-Src SH3 and instead, had preferential affinity for a PXXT/A sequence, that was flanked either side with a positive residue.

A follow-up bioinformatics study was performed with the aim of identifying putative N1-Src substrates. Proteins that contained the newly identified N1-Src SH3 binding motif, which were also predicted to be phosphorylated by a Src family kinase (SFK), were pinpointed as potential N1-Src substrates. Interestingly, after grouping the potential substrates into functional clusters, this revealed that a large proportion of the substrates identified were involved in processes that are crucial to neuronal development, including cell adhesion molecule signalling, Ras/Rho protein signalling and cytoskeletal rearrangement. This aligned with reports in the literature that N1-Src is involved in neuronal development (Kotani et al., 2007, Wiestler and Walter, 1988, Worley et al., 1997).

Whilst progress is being made, a huge gap remains in the literature with respect to our understanding of *bona fide* N1-Src substrates. This must be addressed in order to dissect the function of N1-Src. Given that N1-Src has been shown to be highly expressed in the developing brain (Wiestler and Walter, 1988) and the fact that there is evidence implicating N1-Src in ion-channel regulation (Grovesman et al., 2011), it appears that N1-Src could be an integral signalling component of neuronal processes taking place in both the developing and adult brain.

3.1.1 Aims

The principal aim of this chapter was to identify novel N1-Src substrates. It was hypothesised that N1-Src phosphorylates the HCN1-CTD, ultimately regulating the ion channel's activity. It was also predicted that both the HCN1- and NR2A-CTDs would be phosphorylated by C- and N1-Src to different extents, potentially at different tyrosine residues. Therefore, *in vitro* kinase assays were performed with both the GST tagged human (h) HCN1-CTD and rat (r) NR2A-CTDs.

In addition to this, a second approach was adopted, with the aim of validating predicted N1-Src substrates that were identified in the bioinformatics study described in Section 3.1 and which had known roles in the developing and adult brain. Peptides that were derived from putative N1-Src substrates and were predicted to bind the N1-Src SH3 domain, were linked with the ideal Src substrate motif (YGEF) that is phosphorylated by the kinase domain, and screened for enhanced phosphorylation by N1-Src.

3.2 Results

3.2.1 The Purification of Recombinant Src kinases

Recombinant C- and N1-Src kinases were expressed and purified for *in vitro* kinase assays (see Section 2.3.1-2), with the aim of discovering novel N1-Src substrates. Multiple studies have found that the bacterial expression of Src is problematic, delivering highly degraded protein, poor yields and protein aggregation resulting in the formation of inclusion bodies (Saya et al., 1993, Osusky et al., 1995). These poor results have been attributed to Src kinase activity, given that the bacterial expression of an inactive mutant of Src eradicated these problems (Wang et al., 2001a). Wang *et al.*, (2006) devised a strategy to overcome the effects of Src kinase activity on the quality of protein expression in bacteria. This was accomplished by fusing Src to a phosphatase catalytic domain (PTP1B), which is thought to counteract the aberrant phosphorylation caused by the kinases (Wang et al., 2006b). A similar approach has been successfully adopted by the Evans lab to express both C-Src and the neuronal Src kinases (Keenan et al., 2015).

C- and N1-Src kinases are routinely recombinantly expressed minus the first 80 residues ($\Delta 80$), since these residues are not required for kinase activity *in vitro* (Keenan et al., 2015). The $\Delta 80$ C- and N1-Src were expressed with a GST tag, tyrosine phosphatase catalytic domain (PTP1B) and HIS tag fused to the N-termini of the proteins (Figure 3.1A). The GST tag and PTP1B were cleaved from the Srcs, after the proteins had been isolated from the bacterial lysates, to yield His- $\Delta 80$ C- and N1-Src (~55 kDa) (Figure 3.1B). To achieve this, protein bound glutathione resin, was treated with PreScission protease (a fusion protein of human rhinovirus 3C protease and GST). Figure 3.1B shows an example of the cleavage reactions and the purified cleaved protein for His- $\Delta 80$ C- and N1-Src.

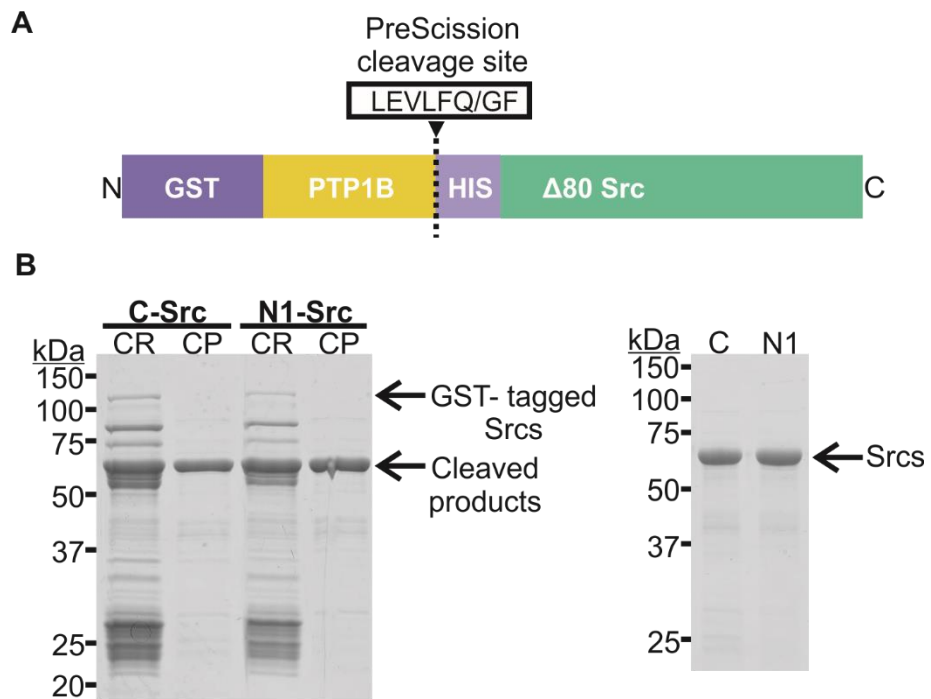


Figure 3.1: Purification of Recombinant C- and N1-Src Kinases

(A) Schematic diagram of recombinant Src kinases lacking the first 80 N-terminal residues ($\Delta 80$). The proteins were N-terminally tagged with GST, the phosphatase PTP1B and six histidine residues (HIS), to facilitate the expression and purification of the proteins. The PTP1B and HIS tag were separated by a PreScission protease site (LEVLFQ/GP) to allow for the release of GST-PTP1B from HIS- $\Delta 80$ -Src. **(B) Left panel** – Coomassie stained, 12.5 % SDS polyacrylamide gel showing preparations of GST-PTP1B-cleaved His $\Delta 80$ C- and N1-Src. Proteins were isolated from 1 L cultures of BL21 E. coli cells, purified using glutathione resin and subsequently cleaved from their GST-PTP1B tag with PreScission protease. The lanes correspond the whole cleavage reaction (CR) and purified cleaved protein (CP) for each kinase. **Right panel** – Coomassie stained, 12.5 % SDS polyacrylamide gel showing 1 μ g of purified C- and N1-Src kinases based on pre-determined protein concentrations.

3.2.2 The Expression and Purification of GST-hHCN1- and GST-rNR2A-CTD

Santoro *et al.*, (1997) found that the CTD of HCN1 binds to the N1-Src SH3 domain. Since there is also evidence in the literature for C-Src phosphorylation of HCN channel CTDs (Zong *et al.*, 2005), *in vitro* kinase assays were performed to determine whether the human HCN1-CTD (hHCN1-CTD) is an N1-Src substrate. Given that phosphorylation of the NR2A-CTD by C- and N1-Src has previously been documented (Grovesman *et al.*, 2011), this was used as a positive control for the assay, with a view to performing further studies to pinpoint the phosphorylated residues. Therefore, firstly, GST-hHCN1- (80.5 kDa) and GST-rNR2A-CTD (69.2 kDa) proteins were expressed and purified for use in *in vitro* kinase assays with recombinant His- Δ 80C- and N1-Src kinases (Figure 3.2).

The sequence encoding *hHCN1-CTD* was cloned into pGEX-6P1 and the induction of recombinant GST-hHCN1-CTD was achieved in BL21 *E. coli* upon IPTG induction for 3 h at 37 °C. Figure 3.2A (left panel) shows the protein recovered from the elution of GST-hHCN1-CTD from glutathione resin. The elution appeared successful, since there was a purified protein band in the region of 80.5 kDa, the molecular weight (MW) of the recombinant protein. However, the estimated concentration of intact GST-hHCN1-CTD protein was low (approximately 200 $\mu\text{g ml}^{-1}$).

With the aim of improving the protein yield and reducing the degradation of the protein, hHCN1-CTD was A) expressed in Rosetta 2 *E. coli* cells and B) induced at a lower temperature (18 °C) and over a longer period of time (overnight). Rosetta 2 cells differ from the BL21 strain because they contain plasmids that encode tRNAs for codons that are rare in *E. coli*, but which are often present in eukaryotic genes. Analysis of the *hHCN1-CTD* DNA sequence revealed that 72 of the 521 codons are low usage codons in *E. coli*, 17 of which are prolines; residues important for SH3 domain substrate interactions. In addition, a reduction in the rate of protein synthesis by expressing the protein overnight and at a reduced temperature, can often increase the yield of soluble mammalian proteins. Reducing the growth temperature also reduces the rate of proteolytic cleavage, which should ultimately improve the protein yield.

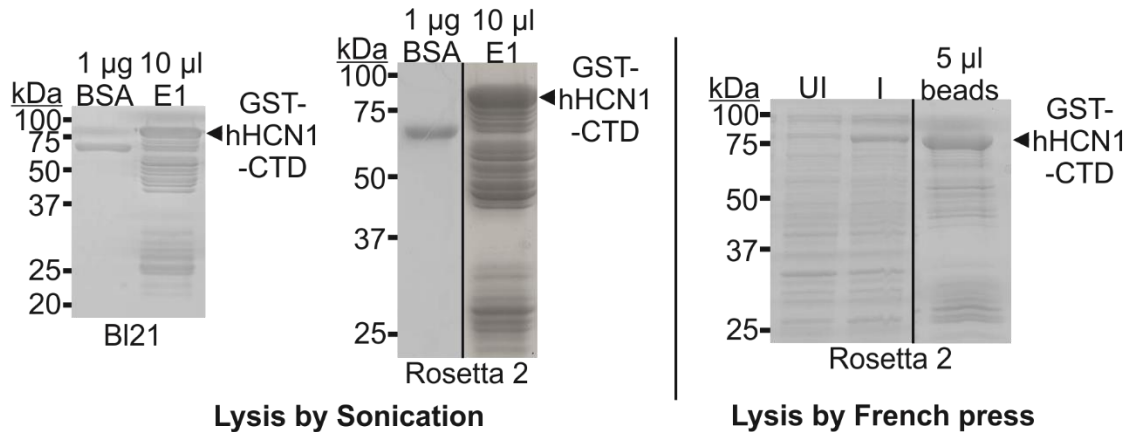
An improved yield of full length GST-hHCN1-CTD was achieved using Rosetta 2 cells and a reduced induction temperature, since the estimated concentration of eluted protein was approximately 300-400 $\mu\text{g ml}^{-1}$ (Figure 3.2 (middle panel)). In addition to the increase in GST-hHCN1-CTD, there also appeared to be an increase in contaminants and/or break down products of GST-hHCN1-CTD (Figure 3.2A middle panel – right lane) compared to protein purified from BL21 cells (Figure 3.2A left panel – right lane). Centrifugal protein concentrators with a molecular weight cut off of 30 kDa were used with the intention of increasing protein concentration, and removing the lower molecular

weight degradation products, however little improvement in protein concentration was achieved and it was found that a large proportion of protein was retained in the filtrate (data not shown).

In order to try to improve protein yield further, the method of cell lysis was modified. In place of sonication, a French press was used. After GST-hHCN1-CTD was expressed and bound to glutathione resin, the resulting protein appeared to contain a smaller proportion of lower molecular weight bands (Figure 3.2A, right panel – right lane), indicating that the French press lysis method resulted in reduced degradation of GST-hHCN1-CTD, however the protein yield remained unchanged. This protein was carried forward for use as a candidate substrate for His- Δ 80N1-Src in *in vitro* kinase assays.

GST-rNR2A-CTD was expressed in a variety of *E. coli* strains for 3 h at 37 °C or overnight at 18 °C to obtain optimal levels of expression (Figure 3.2 B). Cells were lysed using a French press and lysates were incubated with glutathione resin; after extensive washing of the beads, the protein was eluted. Figure 3.2 B (left panel) indicated that greater amounts of expressed protein were obtained using the following combination of conditions: BL21 cells induced for 3 h at 37 °C and overnight at 18 °C, Rosetta 2 cells induced for 3 h at 37 °C and Rosetta Gami B cells induced overnight at 18 °C. From each of these expression conditions, eluted protein obtained from Rosetta Gami B cells appeared to contain less fragmented protein (Figure 3.2B, right panel). Rosetta Gami B cells contain the same plasmids as Rosetta 2 cells that encode rare tRNAs in *E. coli* but also contain mutations in thioredoxin reductase and glutathione reductase genes. These mutated genes enhance disulphide bond formation in the cytoplasm, improving protein folding and stability. Similar to *hHCN1-CTD*, the *rNR2A-CTD* DNA sequence contains many rare codons (40/369 codons) and encodes eight cysteine residues. Thus, expression in Rosetta Gami B cells induced overnight at 18 °C was the method of expression selected for GST-rNR2A-CTD.

A GST-hHCN1-CTD purification



B GST-rNR2A-CTD expression and purification

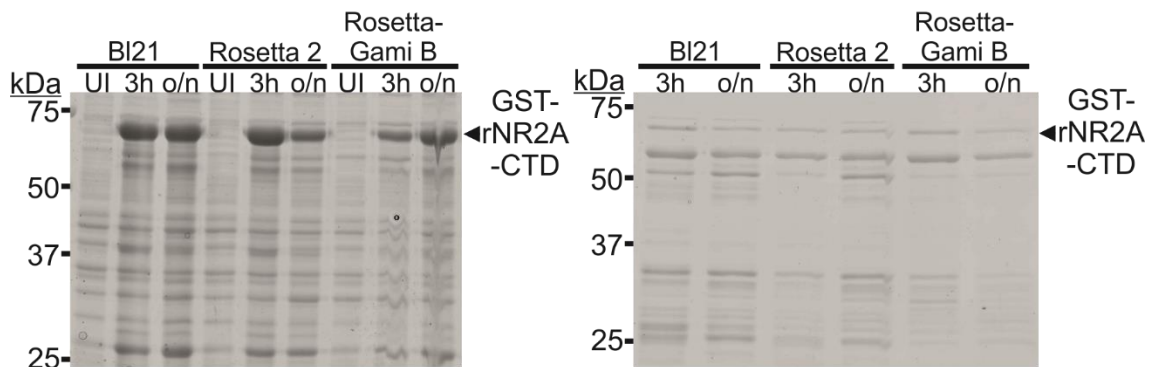


Figure 3.2: Optimisation of GST-hHCN1- and GST-rNR2A-CTD Expression and Purification

(A) Left panel - Coomassie stained, 12.5 or 10 % SDS-PAGE gels showing glutathione resin-purified GST-hHCN1-CTD (80.5 kDa) from sonicated BL21 (left gel) and Rosetta 2 (middle gel) E. Coli cells that had been cultured at 37 °C for 3 h or 18 °C overnight post-IPTG induction, respectively. Lanes correspond to 1 µg BSA and 10 µl eluate (E1) containing GST-hHCN1-CTD. **Right panel** - GST-hHCN1-CTD expressed in and isolated from Rosetta 2 E. coli cells that had been incubated at 18 °C overnight and subjected to the French press lysis method. Lanes correspond to uninduced (UI) and IPTG-induced (I) bacterial protein samples and 5 µl of glutathione resin bound GST-hHCN1-CTD (5 µl beads).

(B) Left panel- Samples (2 µl) of uninduced (UI) and induced (I) BL21, Rosetta 2 and Rosetta Gami B cells expressing GST-rNR2A-CTD (69.2 kDa) cultured at 37 °C for 3 h or 18 °C overnight post-IPTG induction, **Right panel**- GST-rNR2A-CTD isolated from cell types induced under conditions described for left panel and purified using glutathione resin. Protein was eluted using glutathione elution buffer. Lanes were loaded with 10 µl of each eluate containing GST-rNR2A-CTD.

3.2.3 The *In Vitro* Phosphorylation of GST-hHCN1-CTD and GST-rNR2A-CTD Could not be Detected via Western Blotting

To determine whether His Δ 80C- or N1-Src kinase phosphorylates GST-hHCN1-CTD, an *in vitro* kinase assay was performed using the recombinantly expressed proteins described in Sections 3.1.1 and 3.1.2. A GST tagged peptide (GST-YA, 31.5 kDa) containing the ideal Src substrate peptide sequence AEEIYGEF, was used as a positive control for C- and N1-Src activity (Keenan et al., 2015). GST-rNR2A-CTD was used as a second positive control, given that both C- and N1-Src have been shown to phosphorylate this protein, which is also the CTD of an ion channel expressed in the brain. To confirm that the GST tag was not phosphorylated, GST was incubated with both kinases.

GST, GST-YA, GST-rNR2A-CTD and GST-hHCN1-CTD (5 μ M) were incubated in individual kinase reactions with ATP (0.5 μ M) and MgCl₂ (10 mM) in 100 mM Tris (pH 7.5), and in the presence or absence of His Δ 80C- or N1- Src. The composition of this buffer has been adopted by the Evans lab in previous studies (Keenan et al., 2015) (Section 2.3.8, Table 2.4). Figures 3.3 A and B, show that the purified recombinant Src kinases (described in Section 3.2.1) were active in the phosphorylation reactions as tyrosine phosphorylation of the positive control GST-YA (31.5 kDa) was evident. It was apparent that in Figure 3.3 A, His Δ 80C-Src phosphorylation of GST-YA, was greater than that of His Δ 80N1-Src. Phosphorylation of GST-YA was shown to be specific as the purified kinases did not phosphorylate GST, which does not contain any known Src phosphorylation sites and served as a negative control. Unfortunately, tyrosine phosphorylation of GST-rNR2A-CTD and GST-hHCN1-CTD by His Δ 80C- or N1 Src was not detected by this method. The blots presented in Figure 3.3 represent short exposures (< 1 min), however longer exposures of up to 30 min did not show a PY20 signal for GST-rNR2A-CTD, GST-hHCN1-CTD or GST either (data not shown).

With the aim of optimizing the assay, the phosphorylation reaction buffer described by Keenan *et al.*, (2015) was adapted to incorporate elements of that used by Zong *et al.*, (2005), who demonstrated the *in vitro* phosphorylation of GST-HCN2-CTD by C-Src. In the reactions performed by Zong and colleagues, GST-HCN2-CTD was phosphorylated whilst still bound to glutathione resin. In addition to ATP (0.35 mM) and MgCl₂ (10 mM), their reaction buffer also contained the reducing agent DTT (1 mM) and the phosphatase inhibitor, pervanadate (200 μ M). Despite incorporating these changes into the kinase reactions (Figure 3.3 B), phosphorylation of neither the hHCN1-CTD nor the rNR2A-CTD were detected when incubated with His Δ 80C- or N1-Src. The blots shown in Figures 3.3

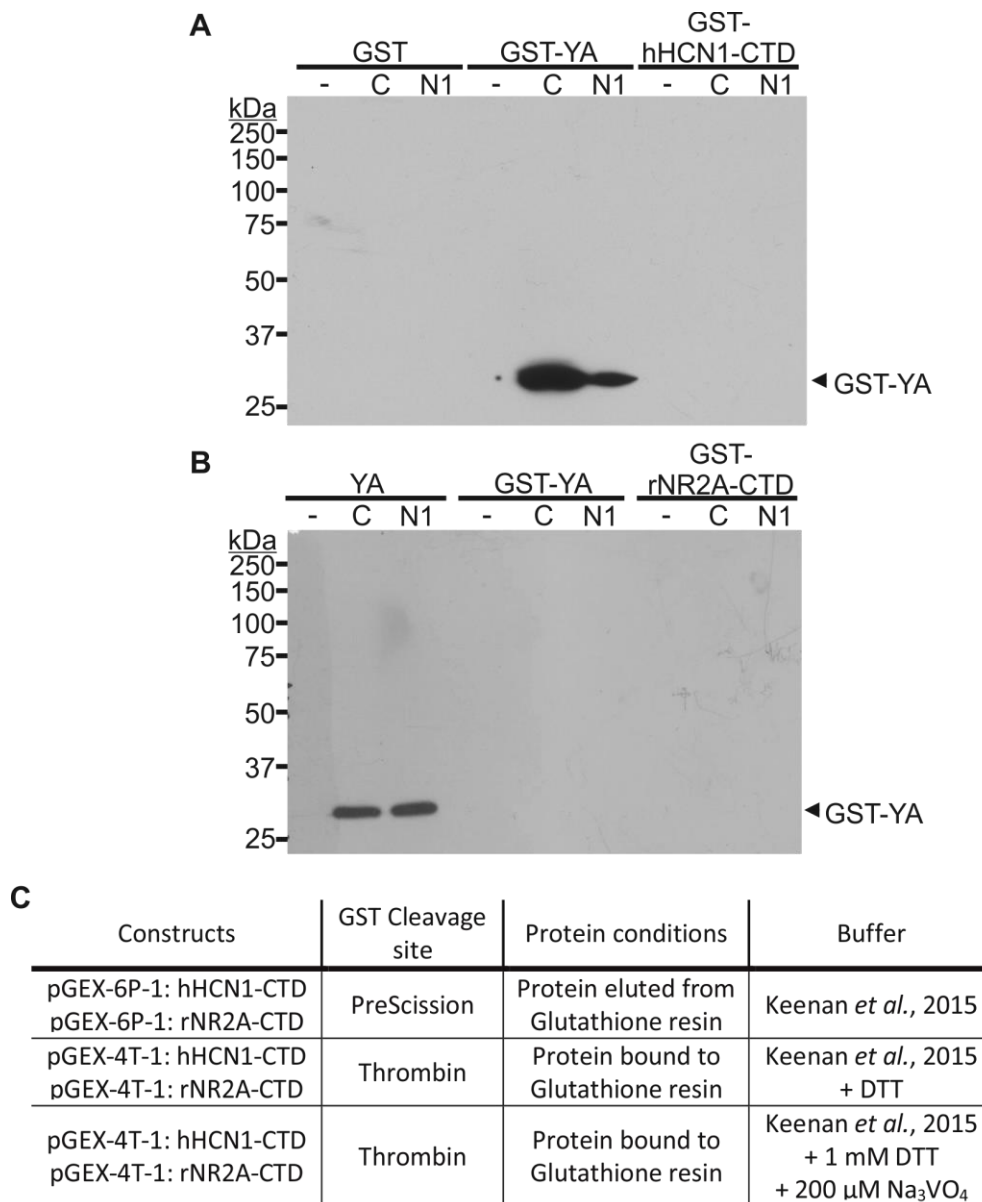


Figure 3.3: Attempted Detection of GST-hHCN1-CTD and GST-rNR2A-CTD Phosphorylation by C- and N1-Src.

GST, GST-YA and rNR2A-CTD (5 μ M; **A**) and hHCN1-CTD (5 μ M; **B**) were incubated with C-, N1-Src or no kinase (control) at 30 °C for 3 h with ATP (0.5 mM), MgCl₂ (10 mM) in Tris pH7.5 (100 mM). The reactions (25 μ l) were terminated with 2X Laemmli buffer. Samples were separated by SDS-PAGE, transferred onto PVDF and analysed by Western blotting using the primary antibody PY20 and anti-mouse HRP secondary antibody. The blots presented in **(A)** and **(B)** represent the results obtained using the different combinations of conditions described in **(C)**.

A and B were indicative of the results obtained across several experiments with different conditions (summarised in Figure 3.3 C).

3.2.4 Expression and Purification of Untagged hHCN1- and rNR2A-CTD.

In Section 3.2.2, GST-hHCN1- and GST-rNR2A-CTD were expressed and purified, however protein yield was low due to high levels of protein degradation and poor elution from the glutathione resin. In order to determine whether the strong interaction between GST and glutathione resin was restricting the yield of recombinant proteins, the GST tag was cleaved from the N-terminus of both proteins. Proteins expressed from the pGEX-6P-1 vector have a PreScission protease cleavage site (LEVLFQ/GP) separating the GST tag and the protein of interest (Figure 3.4A). To this end, PreScission protease was added to the glutathione resin-bound GST-hHCN1-CTD and GST-rNR2A-CTD and the GST tag was subsequently cleaved from each protein.

Figures 3.4 B and C show the expression and purification steps taken in the preparation of rNR2A- and hHCN1-CTD. GST-hHCN1-CTD migrated to the correct size with a molecular weight of approximately 80.5 kDa. Upon cleavage of the protein with PreScission protease, the cleaved protein migrated to a level that corresponded with the predicted molecular weight of 54.1 kDa. The GST-rNR2A-CTD protein band also migrated to the correct molecular weight, in the region of 69.2 kDa, however, upon cleavage of the GST tag (26.4 kDa), the band observed was approximately 10 kDa higher than the expected size of the cleaved protein (42.8 kDa). In addition to this, the untagged rNR2A-CTD appeared as a doublet band. The protein concentrations of both rNR2A-CTD and hHCN1-CTD were estimated to be approximately $400 \mu\text{g } \mu\text{l}^{-1}$, which was equivalent to 9.5 and 7.7 μM , respectively. Whilst there was little improvement in yield, it was evident from the Coomassie staining of both rNR2A- and hHCN1-CTD, that the preparations contained fewer contaminants than the preparations of the GST-tagged equivalents (Figure 3.2). Therefore, these protein preparations containing untagged protein, were carried forward for use in the γ - ^{32}P ATP kinase assays.

3.2.5 hHCN1-CTD and rNR2A-CTD Phosphorylation was not Detected by Autoradiography.

Whilst phosphorylation of the GST-YA positive control was detected in previous kinase assays (Figures 3.3 A and B), indicating that the method used (Section 2.3.1-3) to purify C- and N1-Src resulted in active kinases, phosphorylation of the second positive control, rNR2A-CTD, was not observed by Western blotting (Figures 3.3 A and B). Since phosphorylation of rNR2A-CTD by N1-Src has previously been observed by Groveman

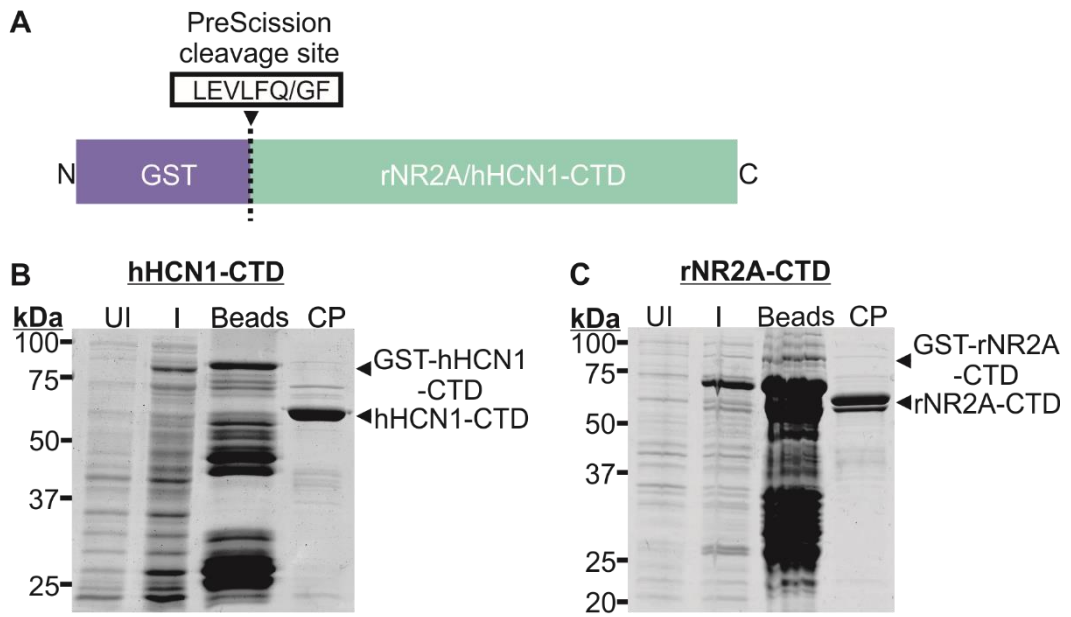


Figure 3.4: Recombinant Expression and Cleavage of GST-hHCN1- and GST-rNR2A-CTD.

(A) Schematic diagram of GST-rNR2A/hHCN1-CTDs (69.2 kDa/80.5 kDa) showing the presence of a PreScission protease cleavage site (LEVLFQ/GP) separating the GST tag (26.4 kDa) from the protein of interest. 10 % SDS polyacrylamide gels show preparations of GST-cleaved hHCN1-CTD (54.1 kDa) **(B)** and rNR2A-CTD (42.8 kDa) **(C)**. The GST-hHCN1-CTD and GST-rNR2A-CTD were isolated from 2 L cultures of Rosetta 2 or Rossetta Gami B E. coli cells respectively, bound to glutathione resin and subsequently cleaved from their GST tag with PreScission protease. The lanes correspond to Uninduced (UI) and IPTG induced (I) E. coli lysates, 2.5 μ l glutathione resin bound with rNR2A- or hHCN1-CTD and 5 μ l of eluate containing cleaved protein (CP).

et al., (2011) using ELISA, and phosphorylation by C-Src is documented in the literature (Yang and Leonard, 2001), further measures were taken to improve the assay. With the aim of increasing the sensitivity of phosphorylation detection, His Δ 80C- and N1-Src kinase assays were performed using γ -³²P ATP across a 3 h time course. It was anticipated that improving the purity of the proteins (Figure 3.4), together with increasing the sensitivity of the assay would optimise the observed output of the reaction. Phosphorylation of the positive control GST-YA was detected in both time courses (Figures 3.5 A and B, upper panels), indicated by a band that corresponded with the molecular weight of the protein (31.5 kDa). However, phosphorylation of both hHCN1-CTD and rNR2A-CTD by either C- or N1-Src was not detected (Figures 3.5 A and B, upper panels). The Coomassie stained SDS-PAGE gels for both experiments (Figures 3.5A and B, lower panels), indicated that equal amounts of protein (rNR2A-CTD and hHCN1-CTD) were present in the reaction contents removed at each time interval. However, it appeared that there was breakdown of the GST-YA positive control, since a large band at approximately 25 kDa (most likely GST) was observed. Yet despite this, phosphorylation of GST-YA was still detected.

A further kinase assay was performed (Figure 3.6), in which the largest amount of protein substrate achievable was added to a larger total reaction volume. This resulted in the maximum amount of protein being loaded onto the protein gel. The prepared reactions contained 5.8 μ M hHCN1-CTD and 7.2 μ M rNR2A-CTD, resulting in the loading of approximately 4.5 μ g of protein on to the protein gel for analysis. This was almost double the quantity of protein (approximately 2-2.5 μ g) that was analysed in the time course shown in Figure 3.5. GST-YA, rNR2A-CTD and hHCN1-CTD were incubated separately in the presence or absence (negative control) of C- or N1-Src with γ -³²P ATP. Whilst phosphorylation by both C- and N1-Src of the GST-YA positive control was detected by the autoradiograph (M_r ~31.5 kDa), neither the rNR2A-CTD nor hHCN1-CTD were phosphorylated (Figure 3.6, upper panel). The Coomassie stained gels confirmed that equal quantities of each protein were added to the kinase reactions (Figure 3.6, lower panel).

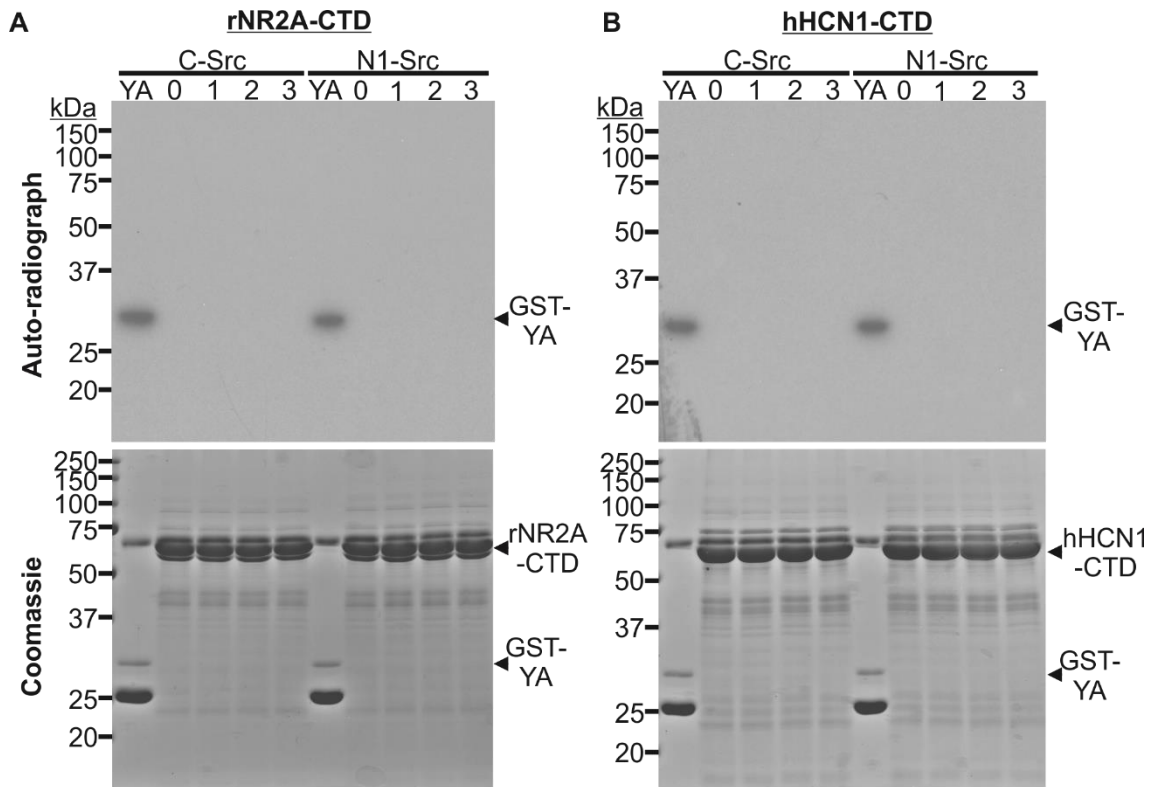


Figure 3.5: Neither rNR2A-CTD nor hHCN1-CTD Phosphorylation by C- or N1- Src were Detected by Autoradiography.

5 μ M rNR2A-CTD (**A**) and hHCN1-CTD (**B**) were incubated with C- or N1-Src at 30 °C for 3 h with γ -³²P ATP. At different time intervals, 10 μ l of the reaction was removed and terminated with 2X Laemmli buffer. Phosphorylation of GST-YA by C- and N1-Src was used as a positive control. Samples were subjected to SDS-PAGE and gels were exposed to X-ray film for 24 h and developed using an X-ray processor (**upper panels**). Gels were also stained with Coomassie to visualise all prominent protein bands (**lower panels**).

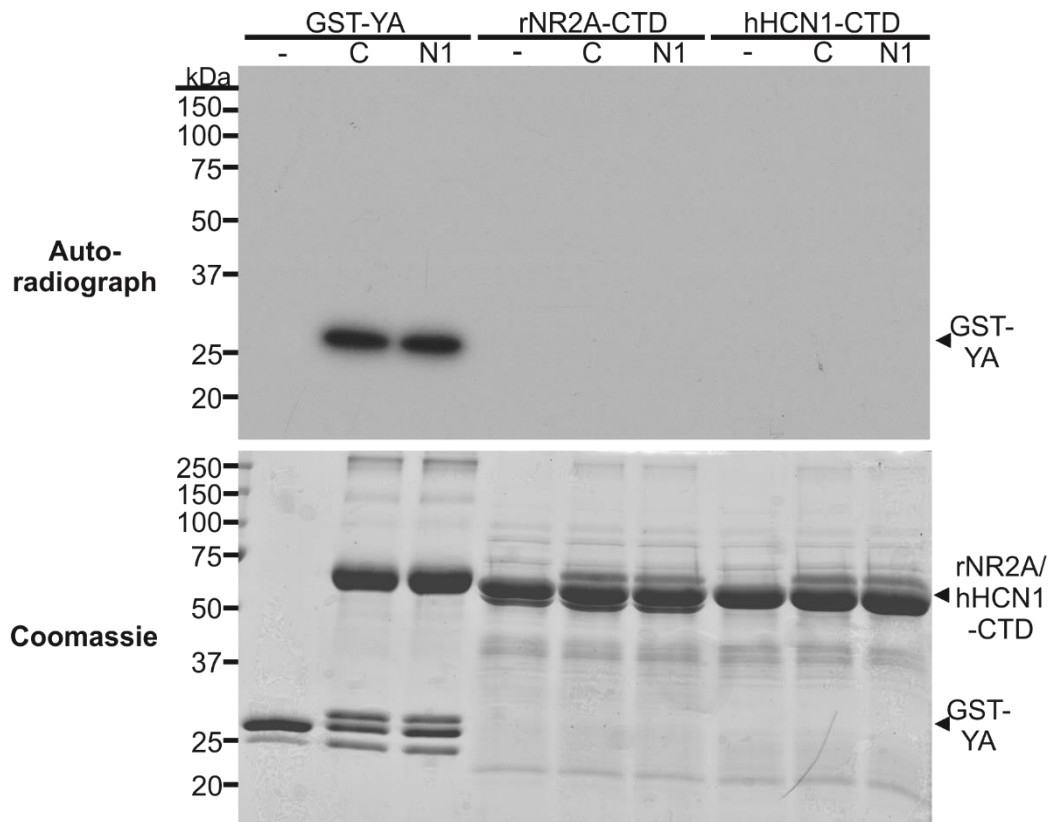


Figure 3.6: Increasing the Reaction Content of rNR2A-CTD and hHCN1-CTD did not Result in Detectable Phosphorylation by C- or N1- Src by Autoradiography.

GST-YA (5 μ M), rNR2A-CTD (7.2 μ M) and hHCN1-CTD (5.8 μ M) were incubated with no kinase, C- or N1-Src at 30 $^{\circ}$ C for 3 h with γ - 32 P ATP. Reactions (25 μ l) were terminated by addition of 2X Laemmli buffer. Samples (30 μ l) were subject to SDS-PAGE and the gel was stained with Coomassie to visualise protein bands (**lower panel**). The gel was exposed to X-ray film for 24 h and developed using an X-ray processor (**upper panel**).

3.2.6 Phosphorylation of the rNR2A- and hHCN1-CTD by PKC was not Detected by Autoradiography.

Since the detectable phosphorylation of the rNR2A-CTD by C- or N1-Src was not achieved, despite utilising published method modifications, a kinase assay using a third enzyme that was known to phosphorylate the rNR2A-CTD and thought to phosphorylate the hHCN1-CTD was performed (Leonard and Hell, 1997, Reetz and Strauss, 2013). Phosphorylation of GST-YA by purified C- and N1-Src suggested that both kinases were active and that it was more likely an issue with the protein substrates. The aim of this experiment was to determine whether this was the case by using an alternative kinase, namely Protein Kinase C (PKC), a serine/threonine kinase known to phosphorylate rNR2A-CTD on at least 3 residues (Figure 3.7A) (Chen and Roche, 2007). In addition to this, it is also thought that PKC phosphorylates the HCN1-CTD, since PKC is a known modulator of HCN1 channel activity and PKC activation corresponds with increased serine phosphorylation of the protein (Reetz and Strauss, 2013, Williams et al., 2015). Myelin basic protein (MBP), a well-known substrate of PKC, was used as a positive control for the experiment, in the event that rNR2A-CTD and hHCN1-CTD were not phosphorylated.

MBP obtained from Sigma, rNR2A-CTD and hHCN1-CTD (5 μ M), were incubated separately in the presence or absence of PKC-zeta and γ -³²P ATP for 3 h (Figure 3.7B). Phosphorylation of the positive control, MBP, was detected, indicated by a band that corresponded with the molecular weight of the protein (18.4 kDa) and the Coomassie stained protein band (Figures 3.7 B). However, phosphorylation of rNR2A-CTD by PKC-zeta was not detected (Figures 3.7 B, upper panel). In addition to this, whilst the full length hHCN1-CTD did not appear to be phosphorylated, there was a faint band at approximately 28 kDa that corresponded to a protein contaminant that originated from the hHCN1-CTD protein preparation. The Coomassie stained SDS-PAGE gel (Figure 3.7 B, lower panels) indicated that equal amounts of protein (MBP, rNR2A-CTD and hHCN1-CTD) were present in the reaction, which were incubated in the presence or absence of PKC-zeta. Given that the rNR2A-CTD positive control was not phosphorylated and the results obtained in the C- and N1-Src kinase assays, no firm conclusions could be drawn from these data with regards to the ability of C- or N1-Src to phosphorylate hHCN1-CTD or rNR2A-CTD.

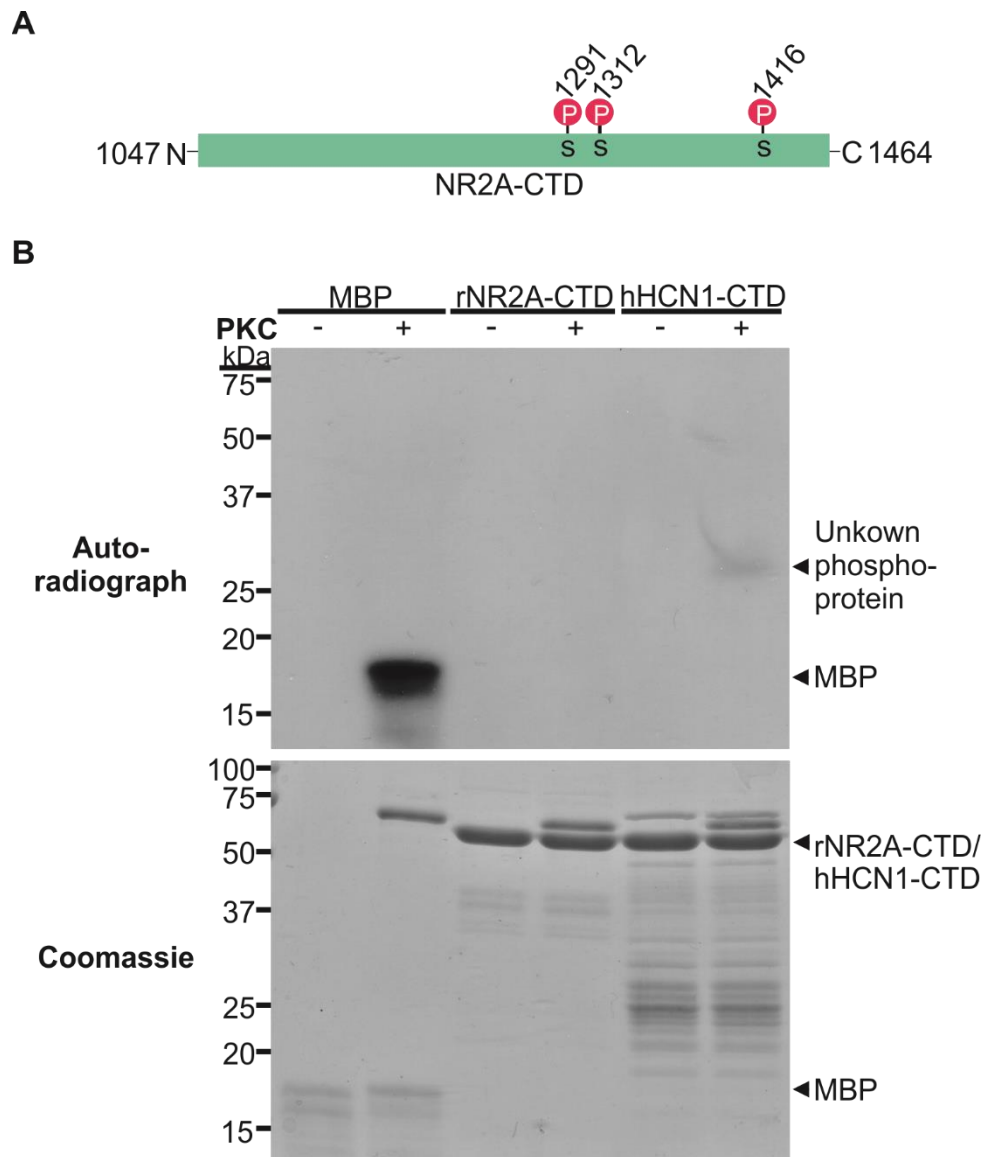


Figure 3.7: Neither Full Length rNR2A-CTD nor hHCN1-CTD were Phosphorylated by PKC-Zeta when Incubated with γ -³²P ATP for 3 h.

(A) Schematic diagram showing residues 1047-1464 of NR2A i.e. the 418 residue NR2A-CTD. Three serine (S) residues (S1291, S1312 and S1416) phosphorylated within NR2A-CTD by PKC are labelled. **(B)** MBP (5 μ M), rNR2A-CTD and hHCN1-CTD were incubated separately with PKC-zeta and γ -³²P ATP at 30 °C for 3 h. Reactions (25 μ l) were terminated by addition of 2X Laemmli buffer and the samples (30 μ l) were subjected to SDS-PAGE. The 10 % gel was stained with Coomassie to visualise protein bands (**lower panel**) and was exposed to X-ray film for 24 h (**upper panel**).

3.2.7 Prospective N1-Src Substrates Identified Through a Peptide Substrate Screen.

Given that the phosphorylation of rNR2A- and hHCN1-CTD was not observed *in vitro*, a different approach, utilising prospective substrates from the bioinformatics screen (described in Section 3.1) was adopted. The aim of this was to identify novel, putative N1-Src substrates, that contained the N1-Src SH3 binding consensus sequence described in Section 3.1. In the second half of this chapter, a phosphorylation screen of peptides whose sequences were selected from prospective substrates of interest and contained the N1-Src consensus motif, was performed.

The phosphorylation of the prospective peptide substrates was compared with the phosphorylation of PD1, a positive control peptide that contained the N1-Src SH3 binding motif, as well as PD1-P5A, the negative control for PD1, in which a critical residue necessary for N1-Src SH3 binding is mutated to alanine (Figure 3.8). Like the ideal Src substrate peptide YA each of the peptides (PD1 and PD1-P5A) were expressed as GST fusions (Figure 3.8). The peptides comprised the ideal Src substrate (AEEEIYGEF), which contained a tyrosine (Y) residue that is phosphorylated by Src, followed by a short linker, and finally the SH3 domain binding motif (Figure 3.8). The latter sequence containing the SH3 binding motif varied between the prospective peptide substrates selected, but most adhered exactly to the established N1-Src consensus motif +XPXXT/AX+ (where + is a positively charged amino acid residue and X can be any residue, see Figure 3.8).

Given that the phosphorylation of the prospective N1-Src peptide substrates was to be compared to the level of PD1 and PD1-P5A phosphorylation, firstly, the concentrations at which PD1 and PD1-P5A phosphorylation differed were established. Since both PD1 and PD1-P5A contain the ideal Src substrate sequence, both GST-fusion peptides are phosphorylated regardless of the presence of the N1-Src SH3 binding motif, which was mutated in PD1-P5A. Therefore, it was necessary to determine a protein concentration at which PD1 phosphorylation by N1-Src exceeded PD1-P5A phosphorylation.

Previous studies in the Evans lab have directly compared the phosphorylation of PD1 by N1-Src to that of YA; the GST-fusion peptide that encodes the ideal Src substrate linked to a mutated C-Src SH3 binding motif, which is similar to PD1-P5A. The K_m for PD1 phosphorylation was significantly lower than that of GST-YA, and it appeared that the greatest differences in phosphorylation occurred between the substrate concentrations of 1-25 μM . PD1-P5A was also shown to be phosphorylated poorly by N1-Src at a concentration of 8.3 μM compared to PD1, which was similar to GST-YA (Keenan, 2012).

In this study, the *in vitro* phosphorylation of PD1-P5A and PD1 were compared at three different concentrations to confirm at which concentration the greatest difference in phosphorylation occurred. PD1 and PD1-P5A were incubated separately with N1-Src kinase and ATP at final concentrations of 1.7, 5 and 15 μM . A Coomassie stained SDS-PAGE gel confirmed equal protein loading between the PD1 and PD1-P5A reactions (Figure 3.9). Western blot data of the same reactions indicated that neither PD1-P5A nor PD1 were phosphorylated at a concentration of 1.7 μM however, PD1 phosphorylation exceeded PD1-P5A phosphorylation at concentrations of 5 and 15 μM . The difference in phosphorylation levels between PD1-P5A and PD1 was greatest at 5 μM , therefore this concentration was carried forward for use in the peptide substrate screen.

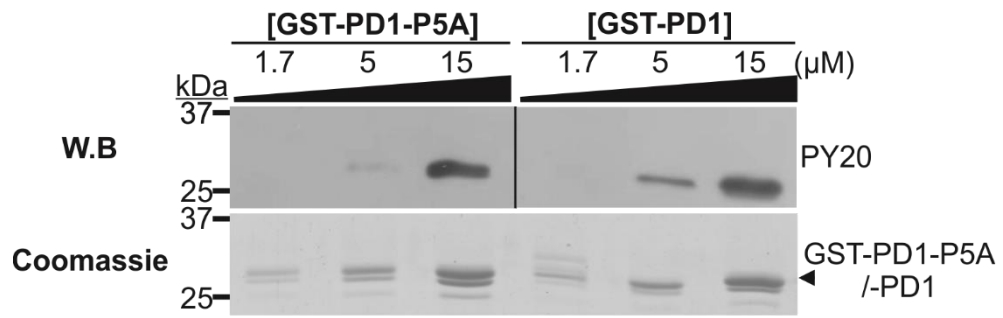


Figure 3.9: Differential Phosphorylation of PD1-P5A and PD1 was Observed at a Substrate Concentration of 5 μM.

A Western blot (W.B) and the corresponding Coomassie stained 15 % gel representing samples (5 μl) from N1-Src kinase assay reactions containing PD1-P5A and PD1. The substrates (1.7, 5 and 15 μM) were incubated in separate reactions with N1-Src (5 nM), ATP (0.5 mM) and MgCl₂ (10 mM) in Tris pH 7.5 (100 mM) for 1.5 h at 30 °C. Reactions were terminated with 2 X Laemmli buffer. Tyrosine phosphorylation of the GST-fusion peptides was detected by Western blotting, using the primary antibody α-PY20 and α-mouse HRP secondary.

Interesting putative N1-Src substrates that fitted the criteria of containing an N1-Src SH3 domain binding motif, as well as being predicted to be tyrosine phosphorylated by Src, were selected for use in the peptide substrate screen (Table 3.1). Since N1-Src is highly expressed in the developing brain and has been implicated to play a role in neuronal development, differentiation and cytoskeletal dynamics (Kotani et al., 2007, Worley et al., 1997, Maness et al., 1988), the majority of the prospective substrates selected for analysis in the screen were linked to these processes.

RACGAP1, ARHGAP1, KALRN, TRIO and ARHGAP5 are a mixture of Rho family GTPase activating proteins (GAPs) and guanine nucleotide exchange factors (GEFs) that regulate actin cytoskeletal dynamics, many of which play a role in neuronal development. Proteins such as ANK2 and RAF1, are linked to the L1-CAM and MAP kinase signalling pathways respectively, which regulate axon outgrowth, whereas NUMB regulates cell differentiation through inhibition of NOTCH signalling. Previous work in the Evans lab has established a link between L1-CAM mediated neurite outgrowth and N1-Src; this will be discussed further in Chapter 4. Other selected targets such as M4K-1, SYNJ1 and AKAP2 and PTPN6 were identified as interesting potential N1-Src substrates that are involved in various signalling processes in the brain or in the latter case, in the regulation of Src itself. Finally, whilst the NMDAR subunit NR2A does not have a consensus motif that conforms exactly with the optimal N1-Src SH3 binding sequence, it has been shown to be phosphorylated by N1-Src (Grovesman et al., 2011). It would therefore be interesting to determine whether the selected peptide enhances phosphorylation of the ideal Src substrate.

Complimentary oligonucleotides that encoded the prospective N1-Src SH3 domain binding peptides were annealed and sub-cloned into pGEX-4T-1 by Dr Gareth Evans. Successful clones encoding the GST-fusion peptides P1-P13 (see Table 3.1) were transformed into BL21 *E. coli* cells. The proteins were expressed (Figure 3.10A) and batch purified using glutathione resin (Section 2.3.2). The concentrations of each protein were determined by Nanodrop and confirmed by the observation of equal loading of 1 ug of each protein on a Coomassie stained gel. Many of the GST-fusion peptides expressed (~31 kDa), including PD1 and PD1-P5A, appeared as doublet bands on the gel (Figure 3.10B). These GST-fusion peptides were carried forward for use in *in vitro* N1-Src kinase assays.

Table 3.1: Prospective N1-Src Substrate Candidates that were Selected for the *In Vitro* Kinase Assay Screen.

Peptide	Protein of origin	Peptide Sequence	Role
P1	M4K-1	ET R PPANTAR L Q	Plays a role in cerebral ischemia, linked with Src (Li et al., 2008b).
P2	ANK2	KE K GPILTQ R EA	Links L1-CAM to the actin cytoskeleton during axon outgrowth (Whittard et al., 2006b).
P3	NR2A	IG R CPSPDY K HS*	NMDA receptor subunit, reportedly phosphorylated by C- and N1-Src (Grovesman et al., 2011, Lau and Huganir, 1995).
P4	RAF1	QP K TPVPAQ R ER	MAPKKK, plays a role in neuronal differentiation and axon outgrowth (Markus et al., 2002).
P5	NUMB	HR R TPSEAD R WL	Part of the notch signalling pathway, regulates in cell differentiation (Wakamatsu et al., 1999).
P6	PTPN6	YL R QPYYAT R VN	Phosphatase involved in Src regulation and regulated by Src itself (Poole and Jones, 2005).
P7	RACGAP1	NL K EPLLTF R LN	Rac GAP, cell differentiation (Kitamura et al., 2001).
P8	ARHGAP1	TQ K SPATAP K PM	Rho GAP, cytoskeletal remodelling (Clay and Halloran, 2013).
P9	AKAP2	V K KNP G IAA K WW	PKA anchoring protein that is enriched in the cerebellum (Wang et al., 2001b).
P10	KALRN	YS K IPLDTS R LA	Rho GEF, dendritic morphogenesis. (Yan et al., 2014, Xie et al., 2010).
P11	TRIO	GP K RP G N T LR K W	Rho GEF, neuronal development (Bateman and Van Vactor, 2001).
P12	ARHGAP5	AA K IPDK T ER L H	Rho GAP, a known C-Src substrate important in the developing brain (Brouns et al., 2001).
P13	SYNJ1	GA R SPAP T R K EF	Synaptic vesicle endocytosis (Slepnev and De Camilli, 2000).

Residues representing the N1-Src SH3 domain binding motif are shown in bold, with positively charged residues highlighted in red. Each peptide (P) was given a number between 1 and 13. *The consensus motif in the NR2A peptide selected, did not adhere exactly to the proposed N1-Src SH3 binding sequence.

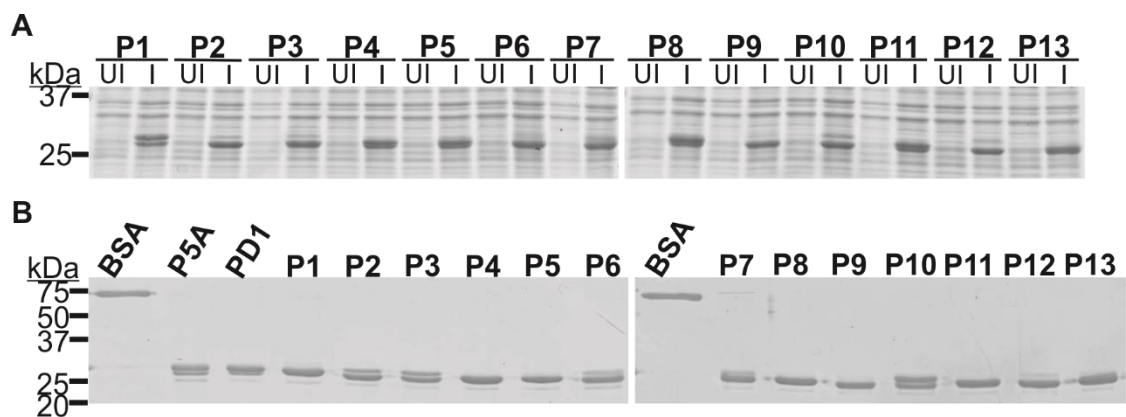


Figure 3.10: Expression and Purification of GST-Fusion Peptides P1-P13.

Coomassie stained, 15 % SDS polyacrylamide gel showing **(A)** samples (2 μ l) of uninduced (UI) and induced (I) BL21 E. coli cells expressing peptides P1-13 that were cultured at 37 °C for 3 h after IPTG induction. **(B)** Samples (1 μ g) of eluted GST-fusion peptides that were isolated from 0.3 L cultures of IPTG-induced BL21 E. coli cells and purified using glutathione resin. The proteins were eluted using glutathione elution buffer, and the concentrations were determined using a Nanodrop spectrophotometer.

The GST-fusion proteins PD1, PD1-P5A and substrates P1-13 (5 μ M) were incubated with N1-Src in a kinase reaction (described in Section 2.3.10). The samples were distributed across two blots, both containing the samples PD1-P5A and PD1, however the first blot contained samples P1-7 and the second represented samples P8-13. A second set of identical protein gels were Coomassie stained, to control for the protein contents of the reactions.

The Western blots presented in Figure 3.11A demonstrate the variability in phosphorylation of the GST-fusion peptides between three experimental replicates of the substrate phosphorylation screen. Whilst PD1 phosphorylation was obviously greater than PD1-P5A phosphorylation for two out of three experimental replicates, there appeared to be a large degree of variability between the differences in phosphorylation on blots within each experiment. In addition, in the case of replicate 2, the bands for PD1 and PD1-P5A were very similar on the blot containing samples P1-7, but this was not reflected by the bands for the same samples present on the second blot. Upon first inspection, replicates 2 and 3 did not appear to produce results that were consistent with the first, or each other. However these observations did not take into account possible fluctuations in the protein contents of the reactions evidenced by the Coomassie stained protein gels (Figure 3.11A; lower panels) or the differences that would inevitably arise from the processing of different blot exposures.

Figure 3.11B represents data that were obtained after performing densitometry on phosphorylated substrate bands (~31 kDa) present on the developed blots (Figure 3.11A), using ImageJ. Since the blots produced within each replicate both contained bands for the PD1 positive control, to facilitate the comparison of substrate phosphorylation between blots, the densitometry values of one blot were adjusted according to the the scale factor obtained from dividing the lowest PD1 densitometry value by the highest. In addition, to account for potential differences in the amount substrate added per reaction, the densitometry bands obtained for each phosphorylated protein were divided by the densitometry values from the corresponding Coomassie stained GST-fusion peptide bands. Finally, to account for potential differences in the processing of blots and Coomassie gels between biological replicates, the values within each experiment were normalised to PD1. Differences between the data values obtained were assessed for significance using a one-way ANOVA.

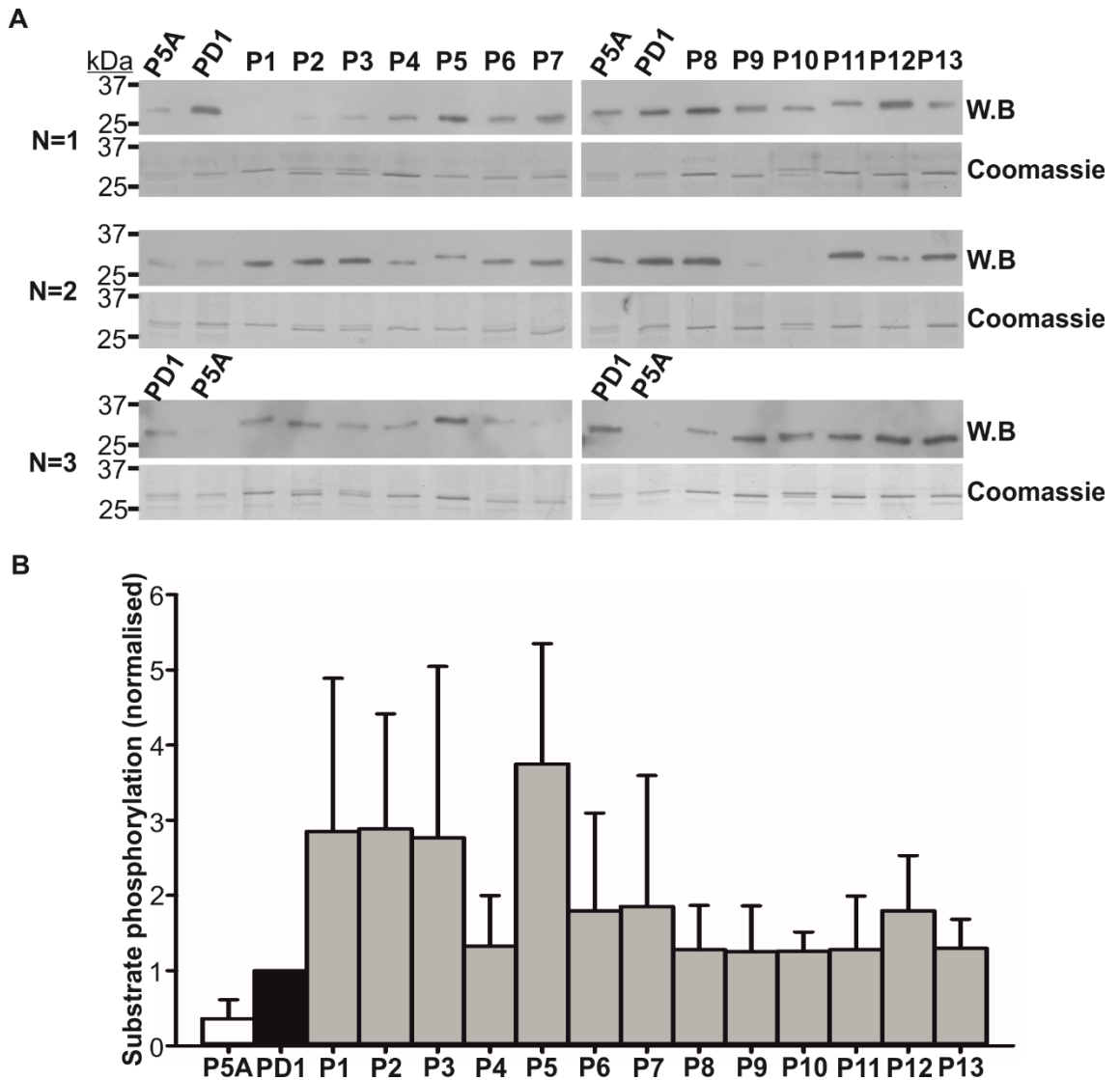


Figure 3.11: Assessment of the Tyrosine Phosphorylation of Putative N1-Src GST-Fusion Peptide Substrates by Western Blotting

(A) Western blots and their corresponding Coomassie stained gels (15 %) representing samples (5 μ l) from N1-Src kinase assay reactions containing the GST-fusion peptide substrates PD1-P5A, PD1 and P1-13 (N=3). GST-fusion peptides (5 μ M) were incubated with N1-Src (5 nM), ATP (0.5 mM) and $MgCl_2$ (10 mM) in Tris pH 7.5 (100 mM) for 1.5 h at 30 $^{\circ}C$. Reactions were terminated by the addition of 2X Laemmli buffer. Tyrosine phosphorylation of the substrates was detected by Western blotting using the primary antibody α -PY20 and α -mouse HRP secondary. **(B)** In ImageJ, substrate phosphorylation was quantified after performing densitometry blots obtained from 3 independent experiments. Within individual replicates, densitometry values were adjusted to account for different PD1 values between blots and the quantity of substrate added to each reaction. The resulting values obtained for each experiment were normalised to the values for PD1. Statistical significance was assessed using a one-way ANOVA.

Densitometry analysis (Figure 3.11B) revealed that whilst the peptide substrates P1-13 appeared to be phosphorylated by N1-Src at comparable or greater levels than PD1, no significant differences between the phosphorylation levels of P1-P13, PD1 or PD1-P5A were observed. However, the error bars, particularly for substrates P1-7, re-affirmed previous observations regarding the reproducibility of the results between replicates. In order for candidate N1-Src substrates to be identified in the future, this assay must be optimised, to reduce the degree of variability between replicates.

3.3 Discussion

3.3.1 A Lack of *In Vitro* Phosphorylation of rNR2A-CTD and hHCN1-CTD by C- and N1-Src.

The primary aim of this chapter was to determine whether the human HCN1-CTD was phosphorylated by N1-Src and to identify the critical residues required for this process. The second aim was to compare C- and N1-Src phosphorylation of the rNR2A-CTD, with a view to pinpointing the phosphorylated residues using mass spectrometry and site directed mutagenesis.

However, after performing *in vitro* kinase assays with both the hHCN1- and rNR2A-CTDs, phosphorylation of both of these proteins could not be detected by either Western blotting or autoradiography. This was particularly surprising in the case of the rNR2A-CTD, which was a positive control for the experiment. In addition, phosphorylation of the rNR2A-CTD by PKC-zeta was not observed, despite this modification being reported previously (Gardoni et al., 2001a, Leonard and Hell, 1997). This suggested that there was a technical problem with the assay used. There are multiple aspects of the experiments performed that could have affected the outcome, which will be discussed below.

Firstly, there is a possibility that there was a problem with the recombinant hHCN1- and rNR2A-CTD proteins, which could have contributed to the negative result of the kinase assays. However, measures were taken to ensure that the recombinant proteins used were comparable to those produced in similar studies. Prior to the expression of the proteins, the nucleotide sequence of both the hHCN1-CTD and the rNR2A-CTD were cloned into pGEX-6P-1 (or 4T-1, depending on the method used) and the construct sequences were verified. This provided confidence that the proteins expressed were the correct proteins, which had no mutations that could affect protein folding or function. In addition to this, mass spectrometry was used to confirm the identity of the proteins. The masses of the Coomassie stained GST-tagged proteins corresponded to the expected masses of GST-hHCN1- and GST-rNR2A-CTD, which were 80.5 and 69.2 kDa respectively. Whilst the coomassie stained GST-cleaved hHCN1-CTD band appeared at the correct mass, that of rNR2A ran slightly higher than expected. However, attempts to identify the exact mass of the protein were unsuccessful due to technical issues. Despite this, it is not uncommon for proteins to run at a slightly different mass than expected, and since the GST-rNR2A-CTD appeared to be the correct molecular weight, and a Coomassie stained GST band (26.4 kDa) was observed in the GST-rNR2A-CTD cleavage reaction (data not shown), it was unlikely that this was a cause for concern.

Notably, the recombinant GST-fusion proteins expressed both contained a ladder of contaminants that were visible on a Coomassie stained gel and were likely a result of protein degradation. It was thought that this could have been due to the fact that mammalian proteins were being expressed in a bacterial system, in which some mammalian codons are rarely used and therefore the correct tRNAs are lacking. As a result, protein translation can be affected. This was primarily tackled by expressing the proteins in *E. coli* strains containing plasmids that encoded tRNAs for some of the codons that are rarely used in bacterial protein translation. However, this did not eradicate protein truncation/degradation. In future, codon optimisation of the nucleotide sequences could be performed to replace rare codons with those that are commonplace in bacteria with the aim of improving protein translation, however double stranded DNA synthesis is costly, and might not resolve the problem of degradation.

Altering the bacterial lysis method from sonication to using a French press appeared to have a mild effect on GST-hHCN1-CTD degradation, yet the greatest effects were observed when the proteins were cleaved from their GST tags. Whilst this did not totally diminish protein degradation, it appeared to be largely reduced. Despite this, improving the purity of the protein expressed had no effect on the outcome of the phosphorylation reactions performed.

Whilst there was a possibility that the degradation products had inhibited the kinase reactions, studies in the literature, in which GST-HCN-CTDs have been shown to be phosphorylated, have used recombinant proteins that had a similar pattern of breakdown products. For example, recombinant HCN2- and HCN4-CTDs were shown to be phosphorylated by *in vitro* C-Src and PKA respectively and suffered a comparable degree of protein degradation (Zong et al., 2005, Liao et al., 2010). In addition, (Santoro et al., 2004) successfully showed an interaction between the HCN1-CTD and Trip8b, irrespective of the degradation products in the protein preparation. In all of these studies, the purification of GST-HCN-CTDs was performed using glutathione resin, the method that was adopted in this study. Furthermore, whilst the *in vitro* phosphorylation of the NR2A-CTD by C-Src was not shown using recombinant proteins, a smaller portion of the GST-NR2A-CTD (residues 1244-1464) including degradation products, was shown to be phosphorylated by α -CAMKII (Gardoni et al., 2001a, Gardoni et al., 2001b). The results from these studies suggested that the presence of protein degradation products affected neither protein phosphorylation nor protein-protein interactions.

The activity of the recombinant Src kinases used in these experiments was confirmed by the successful phosphorylation of the ideal Src substrate (GST-YA). The recombinant kinases, which are routinely used in the Evans lab for *in vitro* kinase assays, have also

been shown to phosphorylate synaptophysin (C-, N1- and N2-Src) and the N-terminal domains of Mint1, 2 and 3 (C-Src only) (Keenan et al., 2015, Dunning et al., 2016). In addition to this, the kinase activity of PKC-zeta was demonstrated by phosphorylating the positive control, MBP. Thus, there is considerable evidence suggesting the kinases used, were capable of phosphorylating both hHCN1- and rNR2A-CTDs.

The composition of the kinase assays used in this study, including the buffer used (100 Mm Tris pH 7.5) and concentration of the co-factors ATP (0.5 mM) and MgCl₂ (10 mM), had been used in previous studies in the Evans lab (Keenan et al., 2015). These conditions were also similar to those used by (Zong et al., 2005) in the phosphorylation of the HCN2-CTD by C-Src, however, the reactions also included 1 mM DTT and 200 μM pervanadate, the latter of which is a phosphatase inhibitor. In addition, the kinase reactions were performed using GST-HCN2-CTD that remained bound to glutathione resin (beads). However, incorporation of these changes into the experiments performed had no effect on the outcome of the GST-rNR2A- and GST-hHCN1-CTD phosphorylation assays. Increasing the sensitivity of the assay by incubating the substrates with γ-³²P ATP also had no effect on the result. One possibility could be that the buffer in which the reactions were performed, negatively affected the reaction outcome. To test this, different buffers that are also commonly used for kinases assays, such as HEPES, MOPS or MES, could be trialled.

Two different methods were used to detect protein phosphorylation in the studies in this chapter. In the first instance, protein phosphorylation was detected via Western Blotting, using a phospho-tyrosine specific primary antibody. This method was adopted since it provides a relatively simple and safe way of achieving selectivity and sensitivity. However, even though the phosphorylation of the YA positive control was achieved, phosphorylation of both the hHCN1- and rNR2A-CTDs was not detected using this technique. Therefore, with the aim of increasing the sensitivity of the phosphorylation detection method, a ³²P kinase assay was designed. Using this method, phosphorylated proteins were radiolabelled with ³²P and protein phosphorylation was directly detected using autoradiography. Therefore, the detection of protein phosphorylation did not rely upon a multi-step method involving different antibody incubations, unlike Western Blotting. This eradicated potential issues that may arise with Western Blotting, such as poor specificity of the phospho-tyrosine primary antibody, which may differ from protein to protein. However, after performing ³²P kinase assays with both hHCN1- and rNR2A-CTD, their phosphorylation was undetected by autoradiography. In addition to this, the phosphorylation of the YA positive control did not exceed and was in some cases lower than the signal that was generated via the Western Blotting of similar control samples. This suggested that this technique did not provide superior sensitivity in the detection of

protein phosphorylation. This could have been because the incorporation of radiolabelled phosphate into the substrate was too low, which could be addressed by increasing the concentration of radiolabelled ATP in the reaction. In addition to this, the sensitivity of the autoradiography detection method could be enhanced by using a phosphorescent intensifying screen. The β -particles emitted by ^{32}P can sometimes pass through X-Ray film without activating the silver halide crystals inside the film, which is required for detection. When a phosphorescent intensifying screen is irradiated by one of these particles, it releases light which in turn activates the crystals in the film, enhancing the sensitivity of the assay.

Other methods that have been used in the phosphorylation of the NR2- and HCN-CTDs include ELISA and the immunoprecipitation of the full length ion channel subunits from heterologous or primary neuronal cells that were either co-expressing a kinase, or incubated with a kinase post-extraction. In studies by Yang and Leonard (2001), phosphorylated NR2A was immunoprecipitated from HEK293 cells that co-expressed V-Src with both the NR2A and NR1 subunits of the NMDAR or NR2A alone. In addition, phosphorylation of the NR2A subunit by PKC has been demonstrated with NMDARs that were solubilised from rat brains and subsequently incubated with PKC *in vitro* (Leonard and Hell, 1997). Multiple other studies involving the phosphorylation of the NR2-CTDs have also used similar approaches with multiple kinases (Lau and Huganir, 1995, Nakazawa et al., 2001). Groveman *et al.*, (2011), used an alternative method to demonstrate the tyrosine phosphorylation of the NR2A-CTD by N1-Src. An ELISA-based assay was used, whereby N1-Src was incubated with Mg^{2+} , Mn^{2+} and ATP in NR2A-CTD coated wells. Phosphorylation of the protein was detected using a HRP-conjugated phosphotyrosine antibody and was shown to increase steadily over a period of 1 h. There is a possibility that this observation could have been a false positive, however, given the precedence for Src phosphorylation of the NR2A subunit and the fact that N1-Src was also shown to bind to the NR2A-CTD, this is unlikely.

To conclude, the experiments performed in this chapter were unable to report a definitive outcome with regard to whether the hHCN1-CTD is a substrate of N1-Src. Despite the fact that hHCN1-CTD was not reported, the lack of phosphorylation of the rNR2A-CTD, which has been shown to be phosphorylated by both C- and N1-Src, meant that firm conclusions could not be derived. Whilst it seems unlikely that the substrate degradation products, kinase activity or reaction buffer contents were the root cause of the problem given the evidence presented from the literature, it is possible that there was an issue regarding the correct folding of the protein substrates.

To determine whether the proteins are folded correctly, a technique called circular dichroism (CD) could be used to derive information regarding the secondary structures of both the hHCN1- and rNR2A-CTDs. The basis of the technique is dependent upon the differential absorption of left and right circularly polarised light by chromophores that possess intrinsic chirality. The CD spectra for peptide bond absorption in the proteins of interest, can provide information regarding the proportion of α -helices, β -pleated sheets and β -turns, which make up the secondary structures of the proteins.

In addition to the use of CD, a functional assay could be used to ensure that the proteins are correctly folded. For example, the cyclic nucleotide binding domain in the HCN1-CTD, is known to bind cyclic adenosine monophosphate (cAMP), which facilitates the voltage-dependent activation of the HCN1 channel (Biel, 2009). A binding assay with the recombinantly expressed hHCN1-CTD and cAMP- conjugated resin could be performed to establish whether the hHCN1-CTD is folded properly. Similarly, the NR2A-CTD has multiple known binding partners, including members of the PSD-95/SAP-97 family, which bind via their PDZ domains to the C-terminal tail of the NR2A-CTD (Niethammer et al., 1996). Such interactions could be exploited in a pull-down assay, to determine whether the recombinantly expressed rNR2A-CTD is functional and folded correctly.

Moving forward from these studies, there are multiple avenues that could be explored in order to try to further optimise the kinase assays, with the aim of achieving rNR2A-CTD phosphorylation by C-, N1-Src and PKC, such as codon optimizing the DNA sequence of the substrates or trialling multiple reaction buffers. However, after taking into account the financial and time costs, it might be more productive to perform these phosphorylation studies by overexpressing the CTDs or full length channel subunits with C- or N1-Src in heterologous cells, and subsequently immunoprecipitating the tyrosine phosphorylated substrates.

3.3.2 The Design of an *In Vitro* Kinase Assay Peptide Substrate Screen to Identify Putative Novel N1-Src Peptides.

In the second part of this chapter, the aim was to design an *in vitro* kinase assay screen to test the ability of peptides selected from putative N1-Src substrates, which contained the N1-Src SH3 binding motif, to enhance the phosphorylation of the ideal Src substrate. Interesting N1-Src substrate candidates that were identified in a bioinformatics study, were selected based on the fact that they were linked to processes in which N1-Src is predicted to play a role (e.g. the regulation of cytoskeletal dynamics during neuronal development; Table 3.1).

The GST-fusion peptides PD1-P5A, PD1 and P1-13 were successfully expressed and purified (Figure 5.10). Although, many of the purified GST-fusion peptides appeared as

doublet or in some cases triplet bands on coomassie stained proteins gels. There are several reasons that may have contributed to this observation. For example, contaminant protease activity or poor protein stability may have led to the breakdown of the proteins.

To facilitate the comparison of the phosphorylation of the different GST-fusion peptides P1-P13 with respect to the positive (PD1) and negative (PD1-P5A) controls, a concentration at which the phosphorylation of PD1 exceeded that of PD1-P5A was determined (μM) and carried forward for use in the N1-Src substrate screen (Figure 3.9). This result was in accordance with a previous result in the Evans lab whereby PD1-P5A was shown to be phosphorylated poorly by N1-Src at a concentration of $8.3 \mu\text{M}$ when compared to PD1. Therefore, an N1-Src substrate screen that compared the phosphorylation of P1-13, to that of both PD1 and PD1-P5A was performed at the selected concentration, to identify potential N1-Src substrates based on the ability of their corresponding predicted N1-Src SH3 binding motif peptides to enhance the phosphorylation of the ideal Src substrate.

The outcome of the experiments performed were inconclusive due to the variability that occurred within and between experimental replicates (Figures 3.11A and B). Phosphorylation of the positive control PD1 was notably greater than PD1-P5A phosphorylation for two out of three experimental replicates, however there was a noticeable degree of variability between the differences in phosphorylation on blots within each experiment. Within replicate two, the bands for PD1 and PD1-P5A were very similar on the blot containing samples P1-7 but this was not the case in the second blot (P1-8), since PD1 phosphorylation exceeded that of PD1-P5A. The densitometry analysis (Figure 3.11B) that compared the phosphorylation of P1-13 to PD1 and PD1-P5A revealed that the degree of error between the experimental replicates was large, particularly for samples P1-7 and no statistically significant differences were observed.

The degree of variability observed, could have been linked to human error or due to issues that occurred during Western blotting, such as uneven transfer. Performing the *in vitro* kinase assays with $\gamma\text{-}^{32}\text{P}$ ATP would prevent any error caused by an uneven transfer, since autoradiography could be used to detect peptide phosphorylation.

Alternatively, in place of using GST-fusion peptides, the phosphorylation of synthesised peptides lacking the GST tag could be compared in an *in vitro* kinase assay with $\gamma\text{-}^{32}\text{P}$ ATP. In this assay, the capture of positively charged phosphopeptides that are pre-treated with phosphoric acid are captured by negatively charged phosphocellulose paper, which can subsequently be subjected to Cerenkov counting. This method was published by Hastie *et al* (2006) and is also commonly used to determine the kinetics of protein kinase reactions. If this assay can be appropriately optimised, for promising

substrate candidates, the kinetics of peptide phosphorylation could be compared to those for PD1 phosphorylation to determine whether the substrates are worth pursuing in further studies.

It should also be noted that the use of phospho-specific antibodies makes the quantification of phosphorylated protein more difficult. This is because it is unlikely that all phosphorylated substrates will be labelled by the antibody and blotting must take place within the linear dynamic range of detection to ensure optimal quantification. These issues could be overcome using radioactive labelling, since a Cerenkov counter could be used to detect and quantify every radio-labelled protein within the samples.

3.3.3 Alternative Methods for Discovering Novel N1-Src Substrates.

Once optimised, the peptide screen described in this chapter could provide valuable information regarding the discovery of novel N1-Src substrates, however the technique presented is relatively low throughput. An alternative *in vitro* approach that has been published by the Schweitzer and Snyder laboratories, would involve the use of a protein microarray to screen hundreds of proteins simultaneously for phosphorylation by the kinase of interest (i.e. N1-Src; (Meng et al., 2008, Mok et al., 2009)). This would involve incubating immobilised functional proteins in solution with recombinant active N1-Src kinase and radiolabelled ATP, which could be subsequently analysed by autoradiography to reveal novel substrates. The main drawback of this method, aside from expense, is that identified targets would then need to be validated *in vivo*.

An additional method, that is more frequently used to identify protein kinase substrates, is called phosphoproteomics (see Roux and Thibault, 2013 for a comprehensive review of methods). Phosphoproteomics generally requires two major steps: 1) the enrichment of phospho-proteins or -peptides from cellular extracts, which are 2) analysed using tandem-mass spectrometry (MS/MS). The data obtained from the MS/MS is used to identify the phosphorylated proteins (i.e. kinase substrates) from large peptide databases. The advantages of this method, are that it can be used to identify substrates from cultured cells and tissue samples, therefore the substrates that are identified are more likely to be physiologically relevant. However, in order to produce optimal results, large amounts of material are required and low abundance phospho-sites are often undetected. In addition to this, phosphoproteomics does not distinguish between proteins that are phosphorylated directly or indirectly by the kinase.

Kevin Shokat's laboratory developed a novel technique for identifying direct kinase substrates using a protein engineering based method (e.g. Blethrow et al., 2008, Ubersax et al., 2003). The technique involves mutating a residue in the ATP-binding pocket of the kinase of interest, in a manner that favours the binding of a radio-labelled

ATP analogue ($[\gamma\text{-}^{32}\text{P}]\text{-N6-cyclopentyl-ATP}$), without compromising catalytic activity. The resultant kinase is then incubated with cellular lysates, in the presence of the ATP analogue, which results in the radiolabelling of target substrates that can subsequently be identified by MS (Blethrow et al., 2008, Ubersax et al., 2003). This approach has been used to successfully engineer mutants of both V-Src (Shah et al., 1997) and Fyn (Liu et al., 1998). It could therefore likely be adopted for N1-Src, since V-Src, Fyn and N1-Src kinases share a conserved catalytic kinase domain. The main disadvantage of this method relates to the physiological relevance of the substrates identified, although this could be confirmed *in vivo* once the initial experiment has been completed.

Chapter 4

The Role of N1-Src in Neuronal Development

Chapter 4. The Role of N1-Src in Neuronal Development

4.1 Introduction

Many of the putative N1-Src substrates that were screened in Chapter 3 had previously been implicated in neuronal morphogenesis. Whilst further method development will be required to validate the putative N1-Src substrates from Chapter 3, limited studies in the literature have also linked N1-Src with neuronal development (Wiestler and Walter, 1988, Kotani et al., 2007, Worley et al., 1997). Chapter 4 will therefore focus on determining the functional effects of N1-Src during neuronal morphogenesis.

4.1.1 N1-Src and Neuronal Development.

Both the existing literature concerning N1-Src (discussed in Section 1.5.1-2) and previous work in the Evans lab link N1-Src function to neuronal development. N1-Src expression is elevated above C-Src levels in mouse brain lysates during early development, from embryonic day nine onwards (Wiestler and Walter, 1988) and conflicting studies have shown that overexpression of N1-Src alters the morphology of several types of neurons after plating (Worley et al., 1997, Kotani et al., 2007). Kotani *et al.*, (2007) found that in transgenic mice overexpressing constitutively active N1-Src, aberrant dendritic morphology occurred in Purkinje neurons and this was less apparent in mice overexpressing the non-mutated (less active) N1-Src. In contrast, Worley *et al.*, (1997) discovered that in *Xenopus* ventral forebrain neurons, N1-Src overexpression increased the length of the longest neurite. However, the same study showed that retinal ganglion cells were unaffected by N1-Src overexpression, yet constitutively active N1-Src stunted axonal outgrowth.

Studies in the Evans lab, which utilised a novel putative peptide inhibitor of N1-Src found that axon number, length and the number of branches per axon decreased in cerebellar granule neurons (CGNs), whereas total neurite length, number of branches per axon and average branch length were reduced in hippocampal neurons (Keenan, 2012). Taken together these findings suggest that N1-Src may play different roles in different subsets of neurons.

4.1.2 The Role of N1-Src in L1-CAM Mediated Neurite Outgrowth.

A role for Src in L1-CAM-mediated neurite outgrowth was previously described by Ignelzi and colleagues using *Src*^{-/-} mice, which did not discriminate between specific isoforms. A possible role for N1-Src in axonal outgrowth in relation to L1CAM signalling was demonstrated in the Evans lab. Cerebellar granule neurons cultured on L1-CAM had reduced axonogenesis and reduced axon length in the presence of a selective N1-Src inhibitor (Keenan, 2012). Also, 6 potential N1-Src targets have been identified, using

bioinformatics (described in Section 3.1.) that are involved in L1CAM signalling, including ankyrin B, which anchors L1CAM to the cytoskeleton, modulating L1CAM dependent cytoskeletal remodelling (Keenan, 2012).

4.1.3 Using Rodent Model Systems for Studying the Effects of N1-Src on Neuronal Morphology.

The N1-Src 18 bp mini-exon is conserved in rodents (Martinez et al., 1987, Cartwright et al., 1987), thus mouse and rat models provide useful mammalian tools for investigating the functions of neuronal Src. The primary cell culture of multiple types of neurons derived from juvenile rodent brain tissue has been well documented and is widely used experimentally (e.g. (Costa et al., 2016, Smothers et al., 2016, Winkle et al., 2016). In this study, hippocampal neurons were used to dissect the role of N1-Src during neuronal morphogenesis for two reasons. Firstly, N1-Src expression has previously been detected in hippocampal tissue, therefore manipulations of this experimental system are physiologically relevant (Sugrue et al., 1990). This also enables the endogenous expression of N1-Src to be targeted by RNA silencing methods. Secondly, hippocampal neurons develop a more complex neuronal morphology in culture, compared to some other commonly utilised cell types such as CGNs. Hippocampal neurons exhibit branched neurites; therefore, more complex information can be derived from morphological studies.

When cultured *in vitro*, hippocampal neurons undergo a well characterised series of morphological changes, which ultimately result in polarised mature neurons (Figure 4.1). Upon plating, the neurons are spherical in shape, with a lamellipodium surrounding the periphery of the cell (Figure 4.1; stage 1). At stage two, the cells extend multiple short neurites, which undergo cycles of extension and retraction until one of the neurites begins to grow rapidly during stage 3. This neurite will eventually become the axon. After this stage, the remaining shorter neurites develop into dendrites (stage 4) and after approximately one week in culture, the functional polarisation of the axon and dendrites occurs and synapses are created (Dotti et al., 1988, Tahirovic and Bradke, 2009). In the majority of the neuronal experiments performed in this chapter, the cells were fixed 2 days post transfection (DPT), approximately stage 4 of the polarisation process, therefore the effects of N1-Src on the early stages of neuronal morphogenesis could be assessed.

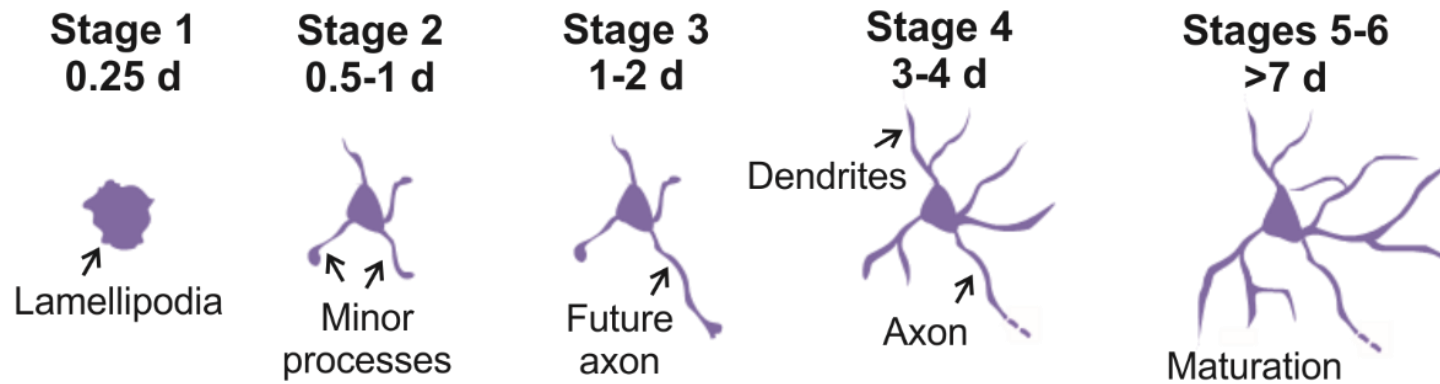


Figure 4.1: The Neuronal Polarization of Rat Hippocampal Neurons in Culture (Dotti's Classification System).

Adapted from (Baj et al., 2014) and (Tahirovic and Bradke, 2009). In culture, hippocampal neurons follow a distinct pattern of development (Dotti et al., 1988). Upon plating, the rounded cells extend lamellipodia from the cell periphery (stage 1). After 0.5-1 days (d) in culture, several dynamic minor processes protrude from the cell body (stage 2), one of which, later (1-2 d) begins to rapidly elongate; this process will become the future axon (stage 3). At stage 4, the shorter processes grow and develop into dendrites, after which the cells continue to mature and create synaptic connections with other neurons (stages 5-6).

4.1.4 Aims

The ability to specifically knockdown the neuronal splice variants of C-Src has not previously been achieved and in the literature, only overexpression studies have been reported, delivering conflicting results (Kotani et al., 2007 and Worley et al., 1997). Therefore, there are gaps in the field relating to the specific role of N1-Src. This study aimed to resolve this controversy by performing both the overexpression and knockdown of N1-Src in the same neuronal model (rat hippocampal neurons).

Ignelzi et al. (1997) demonstrated that Src was required for L1-CAM mediated neurite outgrowth, however the specific isoform of Src (C-/N1-/N2-Src) involved was unclear. Previous work in the Evans lab suggested a link between N1-Src and L1-CAM-mediated neurite outgrowth in CGNs, but whether L1-CAM homophilic or heterophilic interactions were involved in the pathway was not investigated. Further experiments were performed using a fibroblast model, to determine whether N1-Src mediates process extension via L1-CAM homophilic or heterophilic interactions.

4.2 Results

4.2.1 Measuring the Morphological Parameters of Rat Hippocampal Neurons.

In order to quantify changes in neuronal morphology, the NeuronJ plugin for the image analysis software ImageJ was used throughout this chapter. NeuronJ provides a semi-automatic method for tracing neurons in captured microscope images, and facilitates the labelling and measurement of different neuronal features including neurites, primary, secondary and tertiary branches (Figure 4.2A).

In this study, the overexpression and shRNA knockdown of N1-Src were performed in neurons dissociated from the hippocampi of new-born Wistar rats that were transfected after 1 day *in vitro* (DIV) and fixed and imaged after 2 DPT. Therefore, the effects of N1-Src on the initial processes of neurite outgrowth could be analysed. At this stage in development (stage 4), the major process that will form the axon has begun to grow rapidly and outgrowth of the remaining 'minor' processes that will form the dendrites has also started. Despite this, at this stage the molecular distinction between the axon and dendrites can only be determined for approximately 70 % of cultured neurons (Baj et al., 2014). For this reason, the parameters measured in these studies describe neuronal morphology in terms of neurites, for example total length of neurites and length of longest neurite (Figure 4.2B). Since, the mechanisms governing neurite branching are different to those for neurite outgrowth (Gallo, 2011), parameters describing the primary, secondary and tertiary branching of neurites were also measured (Figure 4.2B).

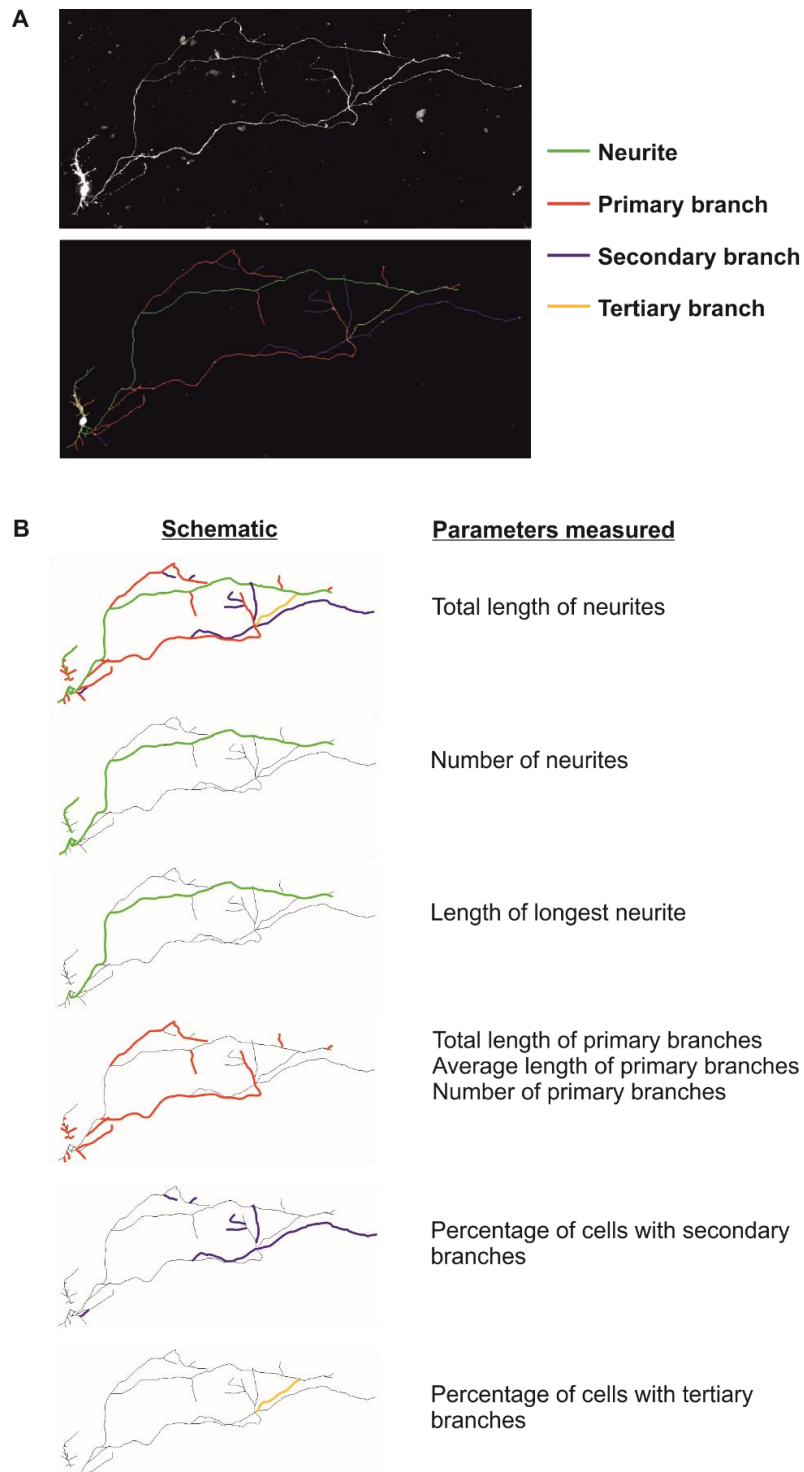


Figure 4.2: Schematic Diagram Depicting the Method of Hippocampal Neuronal Morphology Analysis Using NeuronJ.

(A) An example of a neuronal tracing drawn over a 5 DIV hippocampal neuron that was transfected with pSuper after 1 DIV. Tracings were drawn using the NeuronJ plugin for ImageJ. Different features of the neurons including neurites (green) and primary (red), secondary (purple) and tertiary (yellow) branches are highlighted. **(B)** Schematics of the different combinations of tracings that were used to calculate parameters, which describe multiple morphological features of the neurons *in vitro*.

From the raw neuronal morphology data, it was apparent that there was significant variation between the data values obtained for different rat hippocampal neuron preparations. This might be attributable to the fact that neurons from each biological replicate were cultured from the dissociated hippocampi of individual rat litters that descended from different parents. Therefore, it is feasible that natural variation between rat litters was responsible for the differences observed between cultures. Alternatively, there is a possibility that a variation in the conditions, in which the experiments were performed is accountable for the results observed, given that each biological replicate was completed independently on different days.

Figure 4.3 gives an example of control data, where neurons were transfected with the empty vector pSuper-CFP and the average total length of neurites per cell was measured. In this example, there was a significant difference in mean total neurite length occurring between replicates 1-3 and replicate 4 (Figure 4.3A). This is reflected in the frequency distribution plot, where there is a shift towards shorter total neurite lengths for replicate 4 (Figure 4.3B). To account for these inherent differences between cultures, the values for each treatment were normalised to the average control value for each parameter.

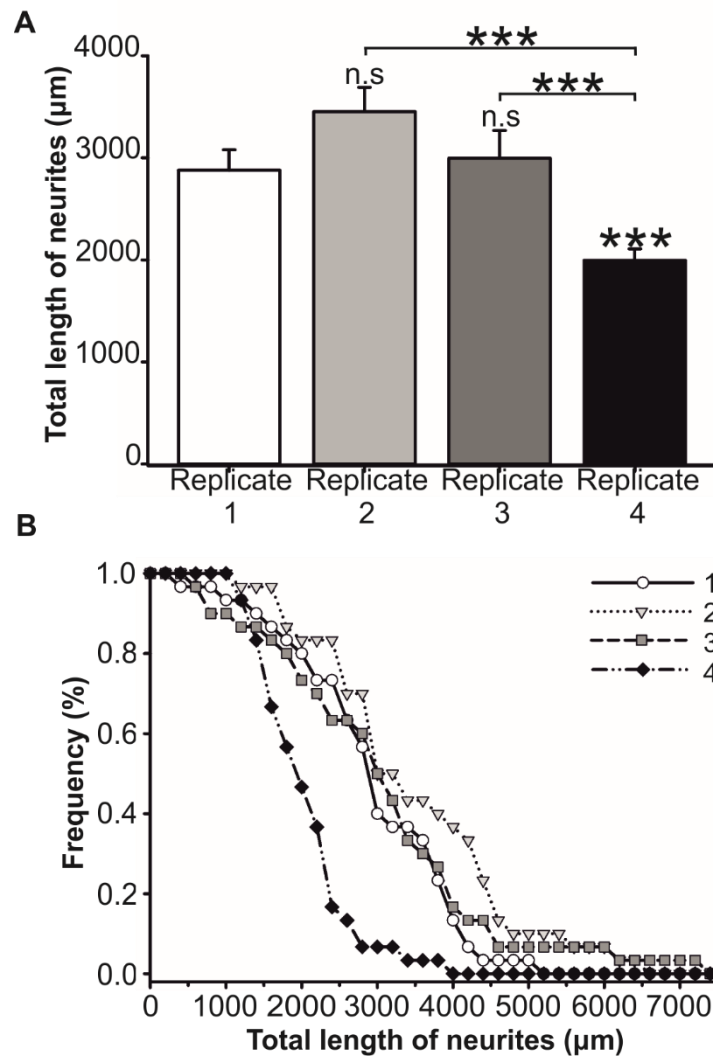


Figure 4.3: The Length of Rat Hippocampal Neurons Varied Between Cultures.

Rat hippocampal neurons (1DIV) were transfected with pSuper-CFP (control) for 48 h and processed for immunofluorescence. Using a Zeiss slide scanner, images of four whole coverslips were captured per condition from which 30 images of individual neurons were randomly selected. In ImageJ, the NeuronJ plugin was used to trace and measure neurites. The mean values (**A**) and frequency distribution (**B**) of the total length of neurites are presented.

4.2.2 N1-Src Overexpression in Hippocampal Neurons Leads to Aberrant Neuronal Morphology.

Previous studies characterising N1-Src overexpression *in vivo* have produced conflicting results with regards to the function of N1-Src (Section 4.1.1). In addition to this, overexpression of N1-Src in *Xenopus* epithelial cells (Worley et al., 1997) as well as the monkey fibroblast cell line COS7 (Keenan, 2012, Lewis, 2014) leads to the formation of neurite-like processes, suggesting N1-Src facilitates process extension. To begin characterising the role of N1-Src in the neuronal morphogenesis of rat hippocampal neurons, N1-Src-mCherry was overexpressed. N1-Src and C-Src overexpression were compared to determine the functional differences, if any, between the kinases.

To analyse the neuronal morphology of the pmCherry, C- or N1-Src-mCherry transfected cells (Figure 4.4), neurites were traced and measured in NeuronJ (as described in Section 4.2.1) and the average number of neurites, total length of neurites and length of longest neurite per cell were analysed for three biological replicates (Figure 4.5).

Hippocampal neurons overexpressing N1-Src displayed aberrant neuronal morphology when compared to control and C-Src overexpressing neurons, with the majority of neurons appearing smaller and underdeveloped (Figure 4.4). In contrast, neurons overexpressing C-Src were similar to control neurons, if not larger. These findings were supported by the quantification of neurite lengths (Figure 4.5). The mean number of neurites was significantly reduced in N1-Src overexpressing neurons compared control cells ($p=0.032$ *, Figure 4.5A). In addition, there was a marked significant decrease in the mean total length of neurites ($p= <0.001$ ***, Figure 4.5C) and the length of the longest neurite ($p= <0.001$ ***, Figure 4.5E) in N1- Src overexpressing neurons compared to control cells. These data were also depicted in frequency plots, which clearly showed that the distribution of values for mean total neurite length and length of longest neurite particularly, were shifted towards lower values (left) for N1-Src expressing cells (Figure 4.5 B, D and F.)

In comparison to control cells, C-Src overexpression resulted in elevated values for all the parameters measured, however these differences were not significant (Figure 4.5 A,C and E). These results were reflected in the frequency plots, where C-Src curves were slightly shifted to the right (Figure 4.5 B, D and F). However, the decrease in average number of neurites, total length of neurites and length of longest neurite in N1-Src overexpressing cells compared to C-Src were highly significant ($p <0.001$ *** for all parameters), indicating that C- and N1-Src have hugely different effects when overexpressed in hippocampal neurons.

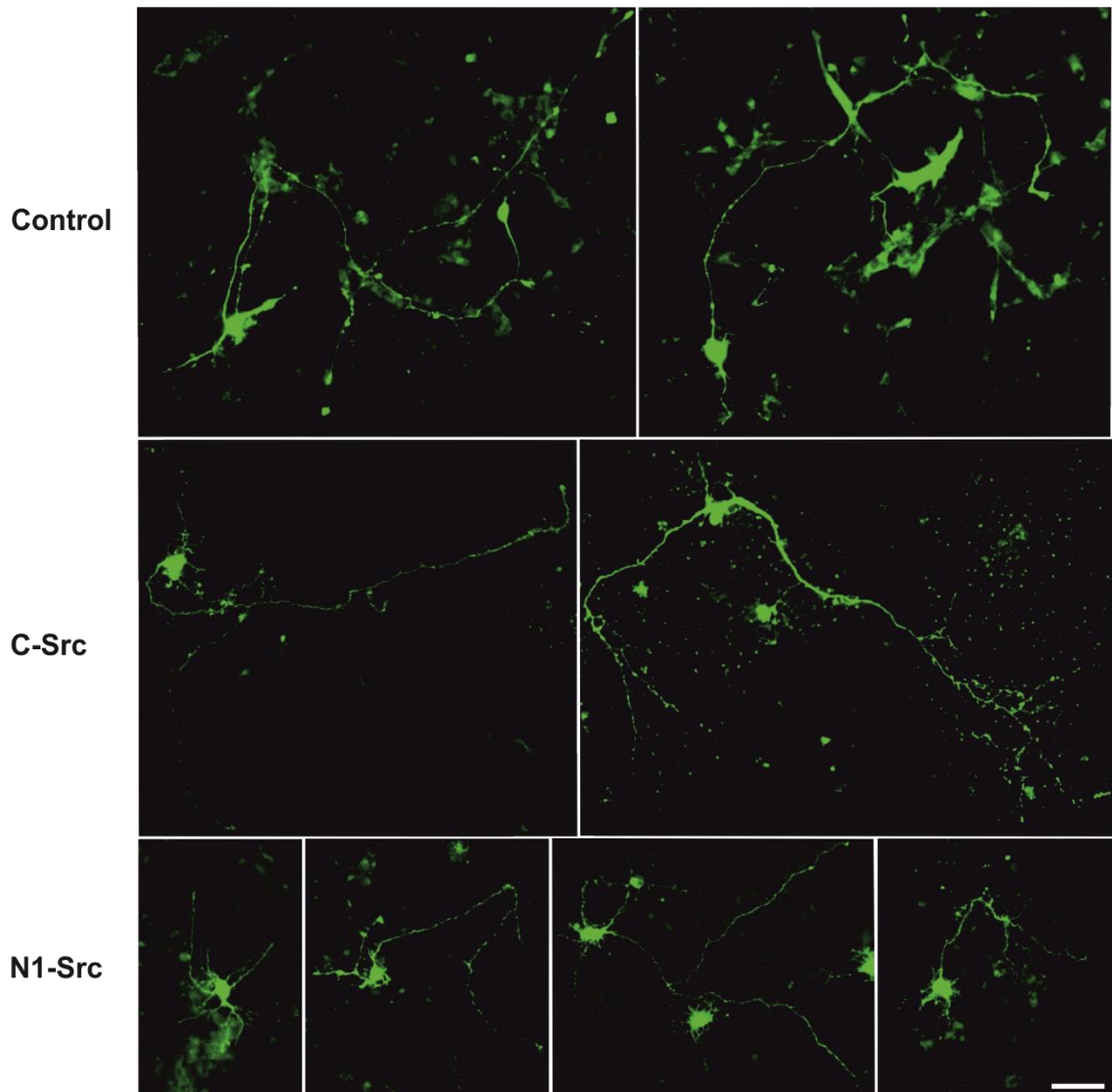


Figure 4.4: Overexpression of N1-Src-mCherry in Hippocampal Neurons Resulted in Aberrant Neuronal Morphology.

Representative images from an N = 3 experiment, displaying the effects of the overexpression of C-Src- and N1-Src-mCherry on cell morphology in comparison to the empty vector control (pmCherry). 1 DIV rat hippocampal neurons were transfected for 48 h and processed for immunofluorescence. Using a fluorescence microscope, 25-30 images were captured per condition across 3 coverslips. The Stitching plugin for ImageJ was used to overlay multiple images taken of the same neuron. The expression of mCherry and mCherry-Src kinases are displayed in green. N=3, scale bar = 50 μ m.

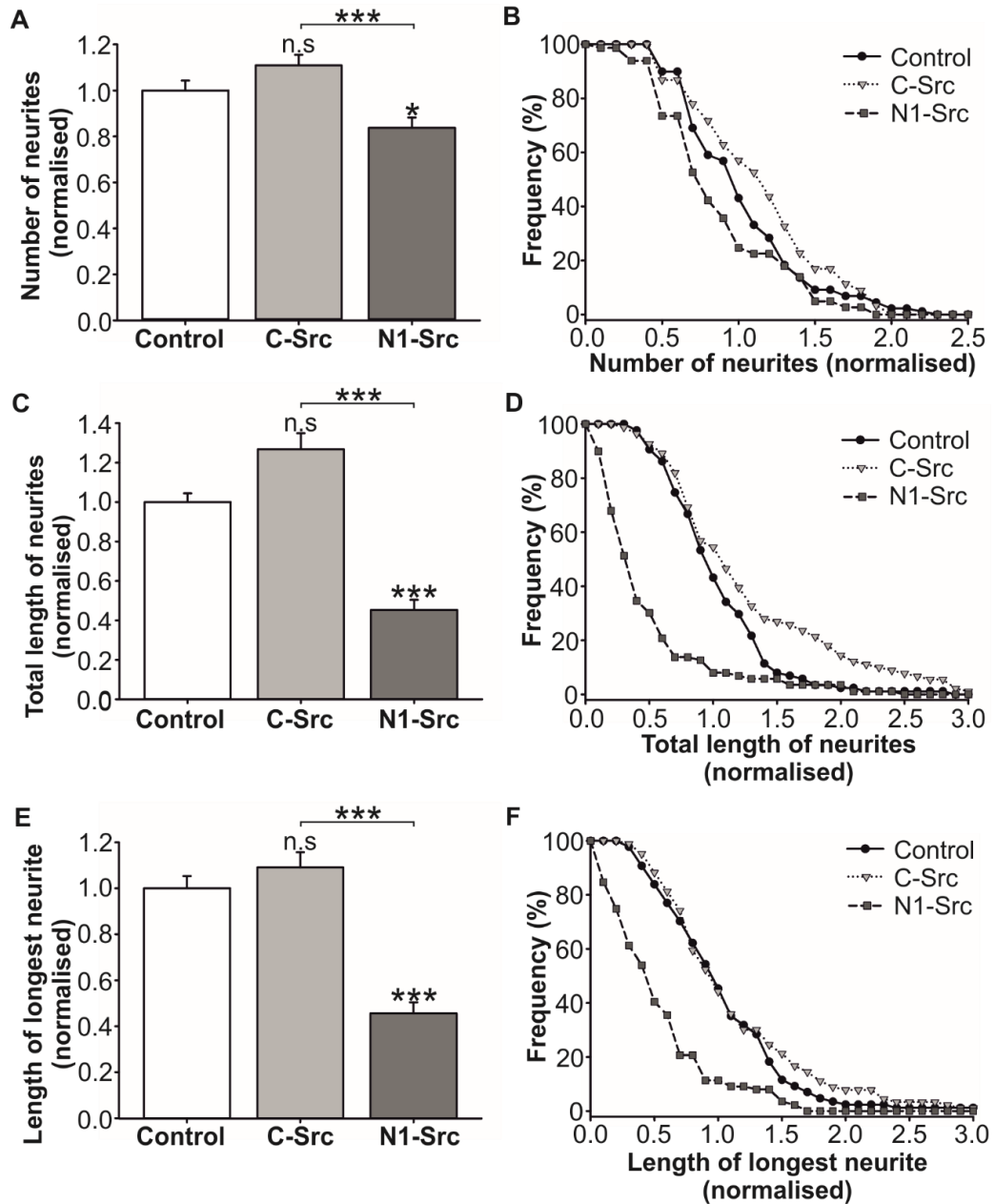


Figure 4.5: N1-Src-mCherry Overexpression in Hippocampal Neurons Resulted in Aberrant Neurite Outgrowth.

1 DIV rat hippocampal neurons were transfected with empty pmCherry (control), C-Src-mCherry or N1-Src-mCherry for 48 h and processed for immunofluorescence. Using a fluorescence microscope, 26-30 images were captured per condition across 3 coverslips. In ImageJ, the NeuronJ plugin was used to trace and measure neurites. The mean values and frequency distribution were assessed for the following parameters: the number of neurites (A, B), total length of neurites (C, D), and length of longest neurite (E, F). C-Src and N1-Src data were normalised to the mean value of the control for each replicate. The experiment was performed 3 times and statistical significance of the pooled data (n=84-88) was assessed in SPSS (*p<0.05, ***p<0.001). Control n=88, C-Src n=87, N1-Src n=84.

4.2.3 N1-Src Overexpression Affects the Development of Cultured Rat Hippocampal Neurons.

After analysing the morphology of the neurons overexpressing mCherry, C-Src- and N1-Src-mCherry, there were apparent differences in the developmental stages of the transfected neurons between conditions. Therefore, using Dotti's classification system, depicted in Figure 4.1, the developmental stages of the neurons were determined. The percentage of cells at stages 1, 2 or 3 and above was calculated for each condition and the statistical significance between the values obtained for each developmental stage was determined using a one-way ANOVA, followed by a post-hoc Tukey's test (Figure 4.6).

The analysis revealed that 100 % of the control and C-Src-mCherry expressing cells were at stage 3 or above. This meant that the cells had at least reached the stage at which the rapid elongation of one of the 'minor neurites' (the future axon) had begun. However, in N1-Src-mCherry transfected cells, there was a significant decrease (35 %) in the number of cells at stage 3 or above in comparison to Control and C-Src-mCherry transfected cells which corresponded to a significant increase (31 %) in the percentage of cells that were at stage 2 (minor processes only). These data implied that the overexpression of N1-Src in hippocampal neurons had a marked effect on developmental progression.

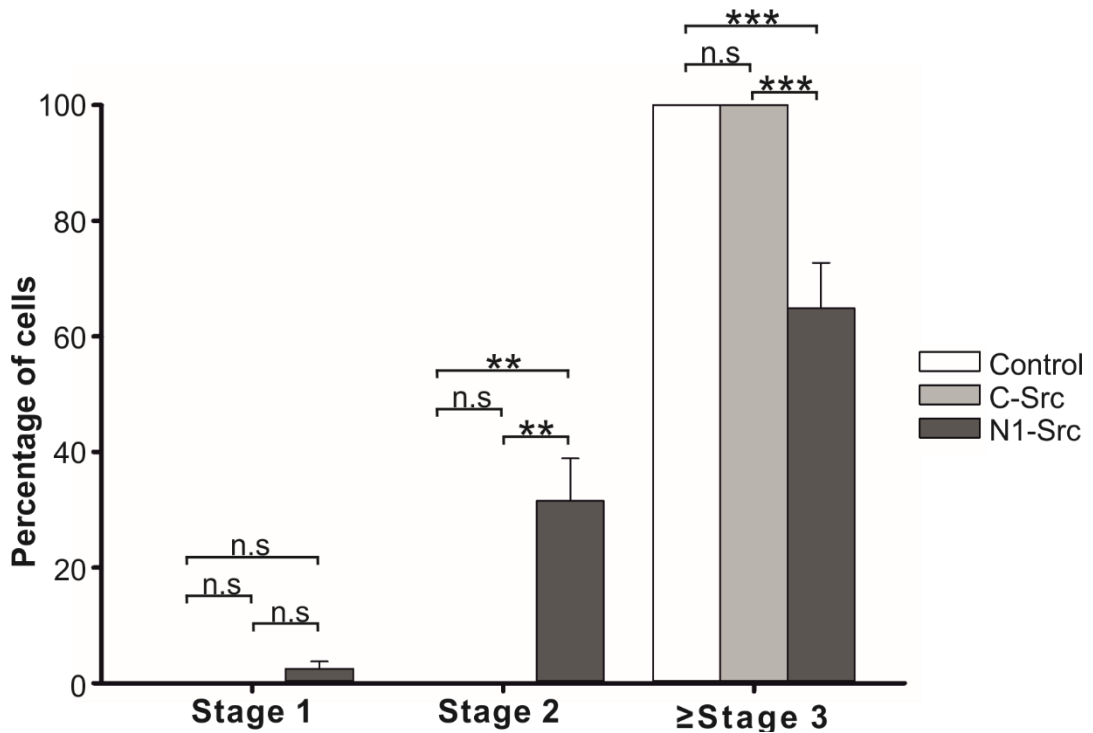


Figure 4.6: The Overexpression of N1-Src-mCherry Disrupted Hippocampal Neuron Development in Culture.

1 DIV rat hippocampal neurons were transfected for 48 h with pmcherry (Control), p-C-Src-mcherry (C-Src) and p-N1-Src-mcherry (N1-Src), fixed and processed for immunofluorescence. Using a fluorescence microscope, 25-30 images were captured per condition across 3 coverslips. The Stitching plugin for ImageJ was used to overlay multiple images taken of the same neuron. The developmental stage of the neurons was determined using Dotti's classification system (Dotti et al., 1988). N=3, n=25-30, **p<0.01, ***p<0.001.

4.2.4 N1-Src can be Specifically Knocked Down Using shRNA.

Whilst overexpressing the kinase is one means of gaining information about the function of N1-Src, manipulating the endogenous protein could provide more physiologically relevant information about the role of the kinase. Two common methods that would achieve such a result are 1.) the inhibition of kinase activity or 2.) the knock-down of protein expression in cells. Unfortunately, current commercial inhibitors of N1-Src are non-specific and target all SFKs, including C-Src (Kim et al., 2009). Therefore, it is impossible to assign specific functions to N1-Src using these inhibitors. For this reason, the approach used to manipulate endogenous levels of N1-Src concentrated upon achieving the specific knockdown of N1-Src kinase levels in neurons.

In this study, two independent shRNAs, designed to specifically knock-down the expression of N1-Src were used (Figure 4.7). Given that N1-Src only differs from C-Src by an 18 base pair (or 6 amino acid) insert in the SH3 domain, the design of the shRNAs was limited to correspond to that area of the gene (Figure 4.7A). Since, the N2-Src SH3 insert incorporates the first 17 base pairs as of the N1-Src SH3 insert, to ensure N1-Src specificity, it was important that the shRNAs not only incorporated the sequence of the SH3 insert, but also overlapped with the flanking sequence in Exon4 (Figure 4.7A). The shRNAs (designed by Dr Gareth Evans) were cloned into the pSuper-CFP vector by Katarina Mahal. The pSuper RNA interference (RNAi) system used, facilitates the production of shRNA molecules, which trigger the down-regulation of the target gene, in this case N1-Src.

Given that there are no effective, commercially available antibodies to detect N1-Src, the specificity and efficacy of the N1-Src shRNAs A and B were tested by co-expressing FLAG-tagged N1-, N2- or C-Src with the individual shRNAs, in the monkey fibroblast cell line COS7 (Figure 4.7B). This method proved successful as each of the FLAG-tagged kinases could be detected by Western blot and therefore the effect of shRNA A and B on Flag-kinase expression levels could be assessed. The bands were subjected to densitometry analysis (Figure 4.7C) which illustrated the effects of shRNAs A and B on the expression of Flag-tagged C-, N1- and N2-Src with respect to the pSuper-CFP control. shRNA A predominantly affected N1-Src expression, causing a 68 % reduction in N1-Src protein levels. However, C- and N2-Src expression were also reduced, albeit to a lesser degree than N1-Src, by 16 and 35 % respectively. In contrast, shRNA B largely knocked down N2-Src, resulting in a 96 % reduction in protein expression. N1-Src expression was relatively unaffected by shRNA B (reduced by 9 %), whereas there

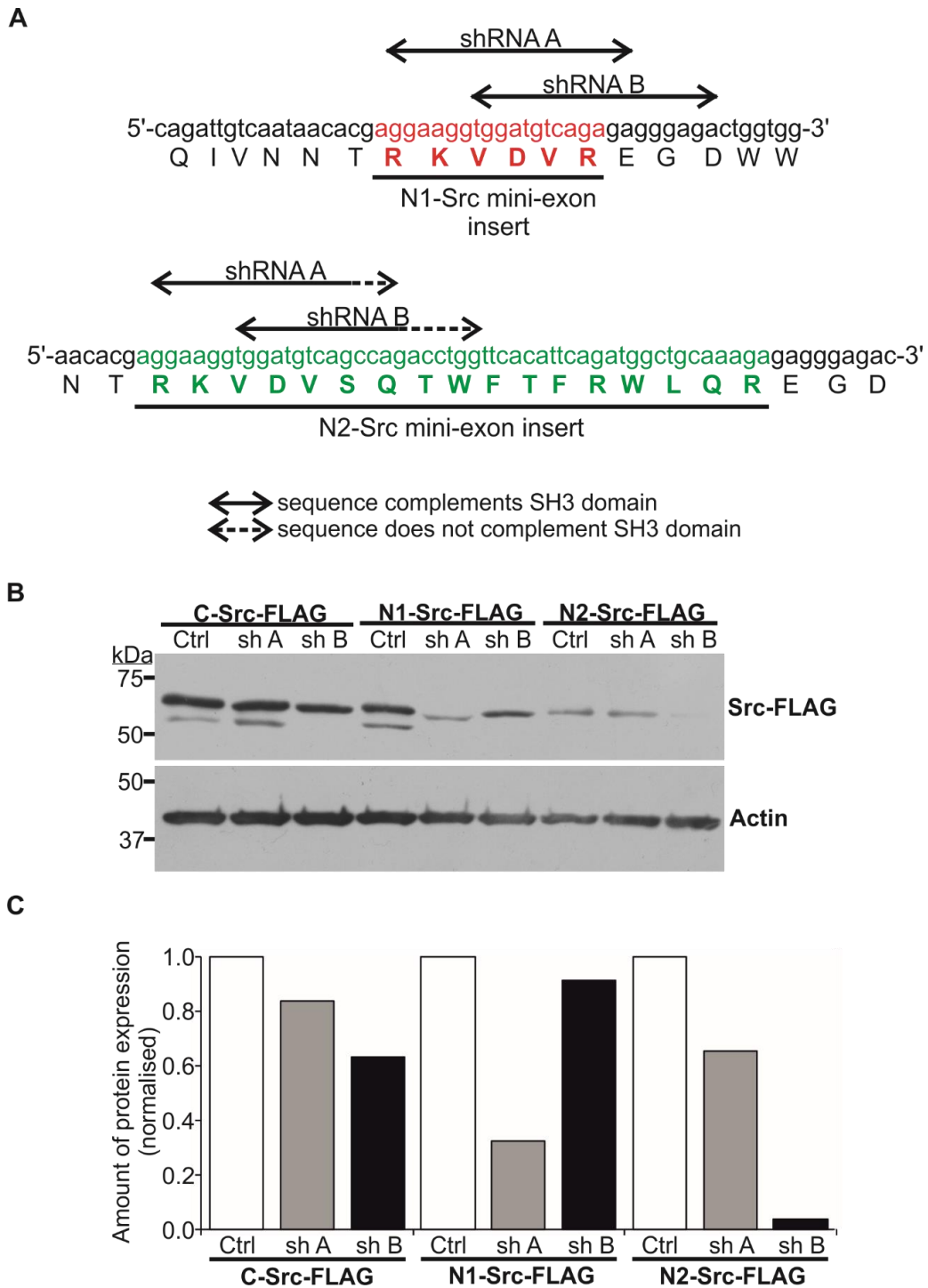


Figure 4.7: shRNAs A and B Largely Depleted N1- and N2-Src Expression Respectively.

(A) shRNAs A and B were designed to target N1-Src expression, however there was also a high degree of sequence complementarity with N2-Src. **(B)** COS7 cells were co-transfected with C-, N1- or N2-Src-FLAG and empty pSuper-CFP, shRNA A or shRNA B. Cells were lysed in 2X Laemmli buffer after 4 h and samples were resolved by SDS-PAGE, transferred to PVDF and analysed by Western blotting using an α -FLAG primary, followed by an α -mouse HRP secondary. **(C)** Src-FLAG bands from a data set of $n=1$, were subject to densitometry analysis using ImageJ and normalised to the densitometry values of the B-actin bands.

was a partial depletion in C-Src expression by 37 %. Together, these results suggested that shRNA A and B were capable of depleting the expression of multiple Src splice variants. However, whilst shRNA A mostly targeted N1-Src, the main target of shRNA B was N2-Src resulting in an almost complete knockdown.

4.2.5 Knockdown of N1-Src with shRNA A Reduces the Length of Longest Neurite.

After testing the shRNAs in COS7 cells, the shRNA constructs were transfected into hippocampal neurons to assess the effect of downregulating N1- and N2-Src expression on neuronal morphology.

Figure 4.8 depicts representative images of control, shRNA A and shRNA B transfected neurons. On first inspection, pSuper-CFP-shRNA-A transfected neurons appear smaller, and the length of the longest neurite was shorter, in comparison to control and p-Super-CFP-shRNA-B transfected neurons. This observation was supported by the morphological data gathered (Figure 4.9). In comparison to control cells, those expressing shRNA A exhibited a significant decrease (11.7%) in the mean number of neurites per cell ($p=0.045$ *). This result was significantly different to that obtained for cells expressing shRNA B, in which there was a significant increase in the number of neurites (15.8%, ($p<0.001$ ***), compared to control cells (Figure 4.9A). The corresponding representative frequency plot (Figure 4.9B) supported these findings. In addition, whilst shRNA B had little effect on the mean total length of neurites per cell (Figure 4.9C) and mean length of longest neurite (Figure 4.9E), in cells containing shRNA A there was a significant decrease in both parameters, by 21 % and 28 % respectively, in comparison to control cells ($p<0.001$ ***). In the frequency plots, the overall distribution of values was shifted to the left of the control and shRNA B curves (Figure 4.9 D and F).

Taken together, these results suggested that the down-regulation of N1-Src expression by shRNA A negatively affected neurite outgrowth, in particular, the length of longest neurite and number of neurites produced. Whereas the effects of shRNA B differed, resulting in an increased mean number of neurites per cell.

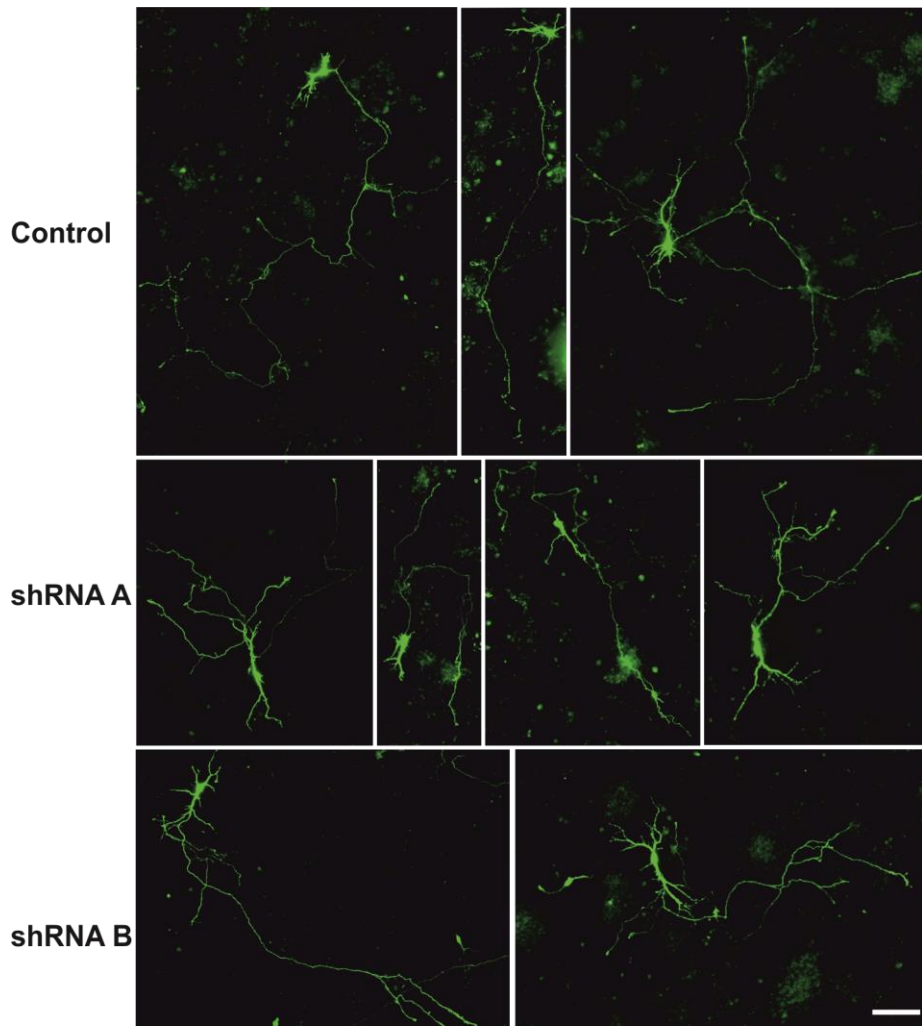


Figure 4.8: Representative Images of the Morphological Effects of shRNAs A and B in Hippocampal Neurons.

Rat hippocampal neurons were transfected at 1DIV with pSuper-CFP, shRNA A or shRNA B and fixed after 48 h. The cells were processed for immunofluorescence. Using a Zeiss slidescanner, images of four whole coverslips were captured per condition from which 30 images of individual neurons were randomly selected. Representative images are shown from N=3. Scale bar = 50 μ m.

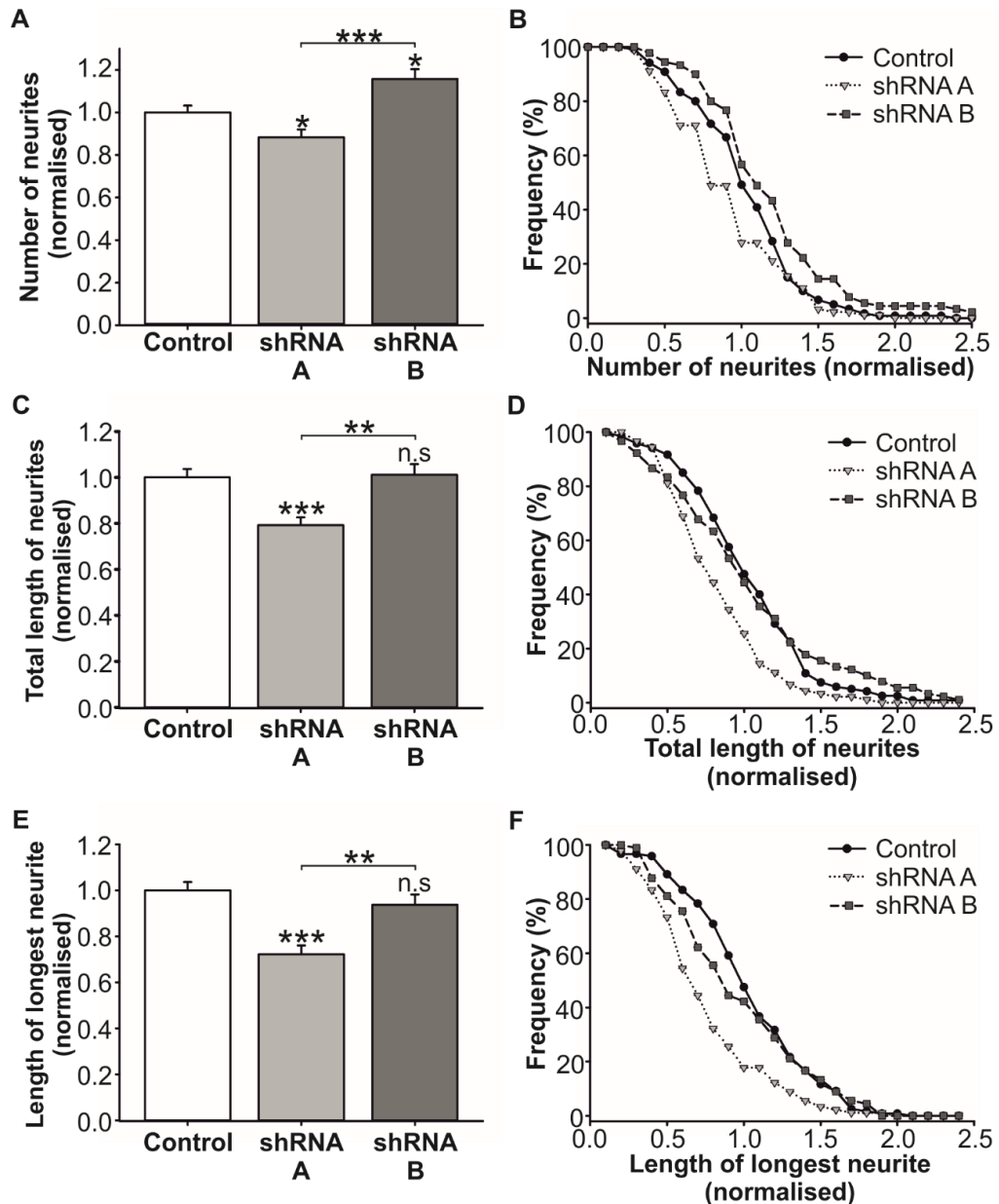


Figure 4.9: Knockdown of N1-Src by Two Independent shRNAs (A and B) Resulted in Atypical Neuronal Morphology.

Rat hippocampal neurons (1DIV) were transfected with pSuper-CFP (control), pSuper-CFP-shRNA-A or p-Super-CFP-shRNA-B for 48 h and fixed in 4 % PFA. The cells were processed for immunofluorescence and using a Zeiss slide scanner, images of four coverslips were captured per condition, from which 30 images of individual neurons were randomly selected. In ImageJ, the NeuronJ plugin was used to trace and measure neurites. The mean values and frequency distribution were assessed for the following parameters: the number of neurites (A,B), total length of neurites (C,D), and length of longest neurite (E,F). shRNA A and B data were normalised to the mean value of the pSuper-CFP control for each replicate. The experiment was performed 3 times and statistical significance of the pooled data (n=90) was assessed in SPSS (*p<0.05, **p<0.01, ***p<0.001).

4.2.6 N2-Src shRNA B Increases Neurite Branching

After determining the effects of a reduction of N1-Src expression on neurite outgrowth, the effects on neurite branching were assessed. Whilst shRNA A had no significant effect on the primary branching of neurites compared to control cells, a slight decrease in the mean number of primary branches (reduced by 6.2 %, Figure 4.10A), total length of primary branches (reduced by 14.9 %, Figure 4.10C) and average length of primary branches (reduced by 8.9 %, Figure 4.10E) was observed. This was reflected in the frequency plots for shRNA A, where the curves were shifted left, in comparison to the control curves (Figure 4.10B, D and F). In contrast, for cells transfected with shRNA B, there was no significant change in the mean total length of primary branches (Figure 4.10C and D), however there was a striking and significant increase (40 %) in the mean number of primary branches ($p < 0.001$ ***, Figure 4.10A). This can be visualised further in the frequency plot, where the shRNA B values are shifted to the right (Figure 4.10B). In addition to this, there is a significant decrease in the average length of primary branches compared to control cells ($p = 0.025$ *, Figure 4.10E), however this does not vary significantly from shRNA A transfected cells (Figure 4.10E).

In addition to studying the growth of primary branches, the percentage of cells with secondary (Figure 4.11A) or tertiary (Figure 4.11B) branches was determined. The average percentage of cells with secondary or tertiary branches was not significantly altered in either shRNA A or shRNA B transfected cells in comparison to the pSuper-CFP control.

Overall, these data suggest that the downregulation of N1-Src by shRNA A had no effect on the primary branching of neurites in 2 DPT rat hippocampal neurons. However, cells transfected with shRNA B displayed increased primary branching of neurites, with a shorter average length, but the mean total length of neurites was unaffected. The percentage of cells with secondary and tertiary branching was unaffected in cells transfected with either shRNA.

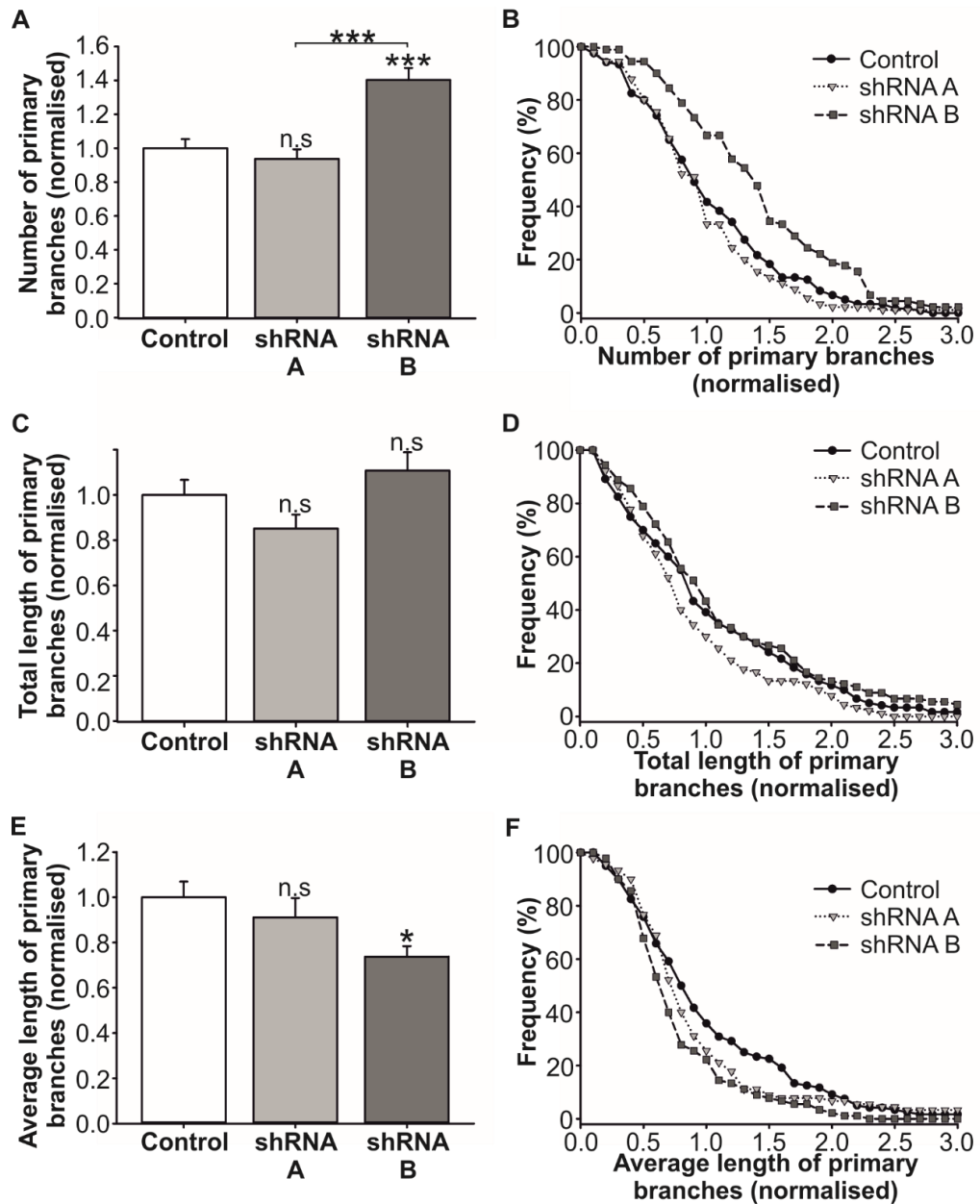


Figure 4.10: N1-Src Knockdown by Two Independent shRNAs had Little Effect on the Primary Branching of Neurites in Hippocampal Neurons.

In ImageJ, the NeuronJ plugin was used to trace and measure the primary branches of neurites from 2 DPT hippocampal neurons that were transfected with the pSuper (control) or N1-Src shRNA A or B. The mean values and frequency distribution were analysed respectively for the following parameters: the number of primary branches (A,B), total length of primary branches (C,D), and the average length of primary branches/cell (E,F). Across 3-4 coverslips, 30 cells per condition were analysed from images captured using a slide scanner. The shRNA A and B data were normalised to the mean value of the control for each replicate. The experiment was performed 3 times and statistical significance of the pooled data (n=90) was assessed in SPSS (*p<0.05, ***p<0.005).

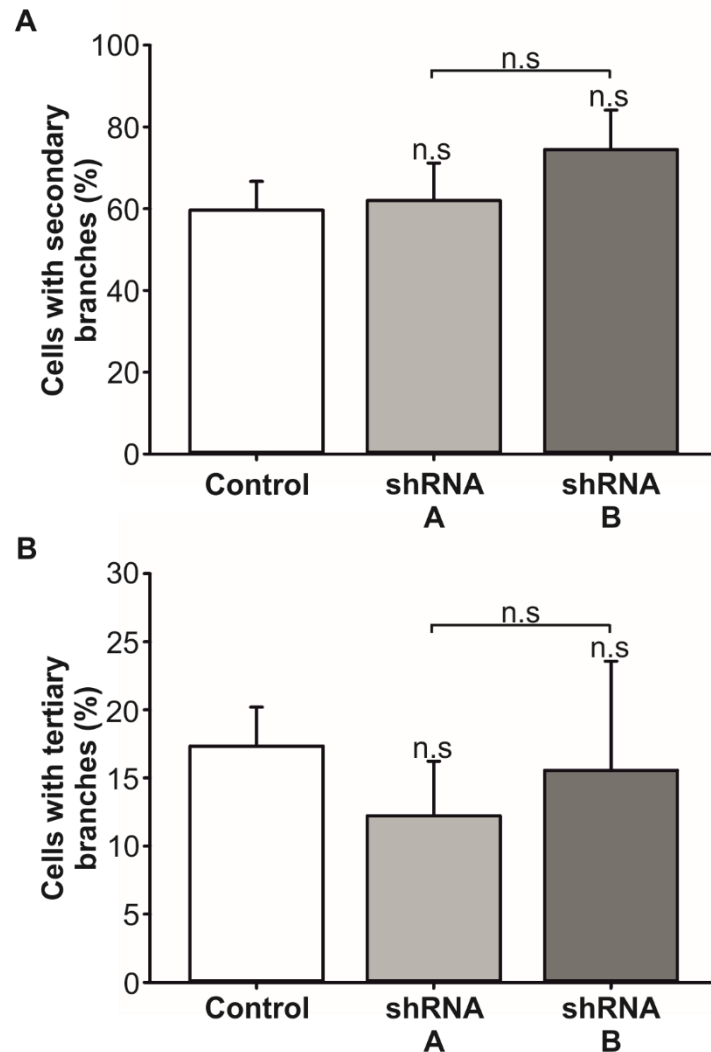


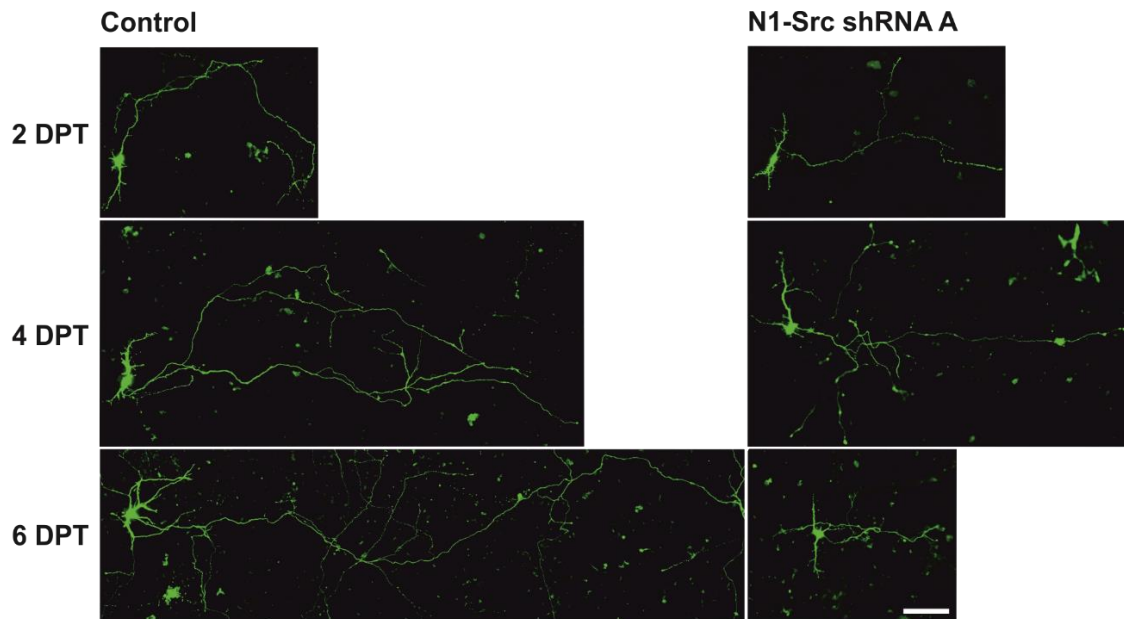
Figure 4.11: N1-Src Knockdown by Two Independent shRNAs did not Affect the Percentage of Hippocampal Neurons with Secondary and Tertiary Branches

In ImageJ, the NeuronJ plugin was used to trace the secondary and tertiary branches of 3 DIV hippocampal neurons that were transfected with pSuper-CFP (Control) or pSuper-CFP-N1-Src-shRNA-A or -B. The average percentage of cells with secondary (**A**) and tertiary (**B**) branches were calculated. Across 3-4 coverslips, 30 cells per condition were analysed from images captured using a slide scanner. The experiment was performed 3 times and statistical significance was assessed in SPSS using a one-way ANOVA (n.s. = not significant).

4.2.7 A Time-course of N1-Src Shrna Transfection Reveals the Length of Longest Neurite Further Decreases with Time.

In Section 4.2.4, the transfection of pSuper-CFP: shRNA-A into 1 DIV rat hippocampal neurons, which predominantly targeted N1-Src expression, resulted in a significant reduction in the length of longest neurite (Figure 4.10E). To determine whether this effect changed with respect to time, a time course was performed comparing the effect of shRNA A on the length of longest neurite, with that of the pSuper-CFP control. Similar to previous experiments, within each biological replicate, the values for the length of longest neurite were normalised to the mean value measured for pSuper-CFP at 2 DPT. The data presented incorporated two biological repeats, therefore statistical analysis was not performed on the data.

In Figure 4.12A, representative images illustrate the profound effect of shRNA A on the length of longest neurite with respect to time, compared to control cells. shRNA A greatly reduced the length of longest neurite when compared to control cells and the decrease between control and shRNA A transfected cells became greater over time, from 21 % to 64 % (Figure 4.12B). In addition to this, whilst the length of longest neurite in control cells increased with respect to time, this was also the case for shRNA A transfected cells up until 4 DPT, after which the length of longest neurite decreased by 47 % (Figure 4.12B). These data strongly indicate that the depletion of N1-Src by shRNA A reduces the length of longest neurite and that this effect becomes greater with time.



B

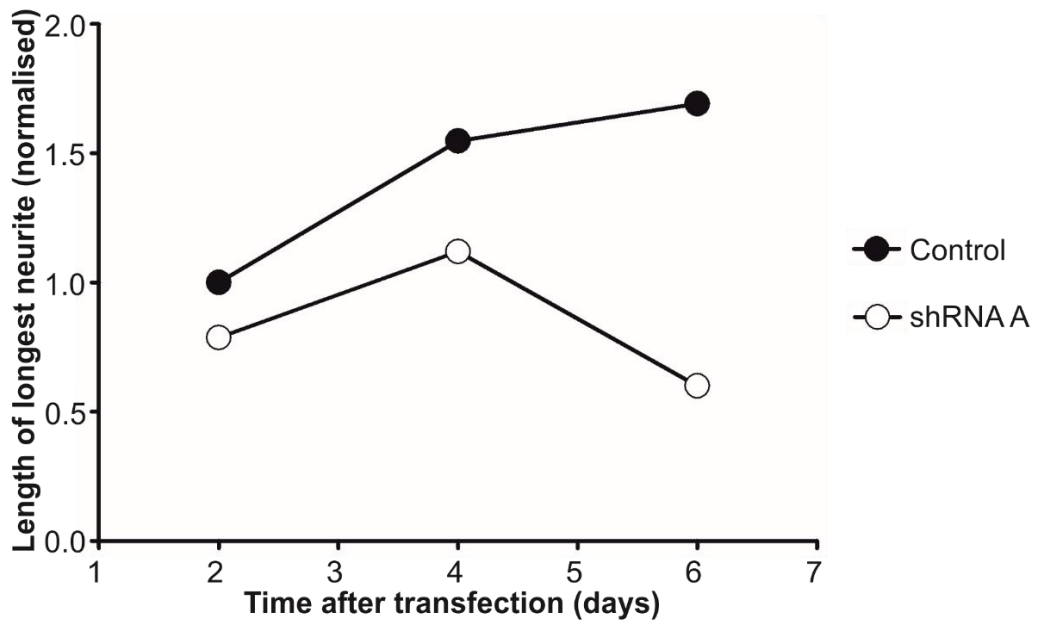


Figure 4.12: The Effect of N1-Src Depletion by shRNA A on the Length of Longest Neurite Increased with Respect to Time.

(A) Representative images showing the effect of shRNA A over time after, in comparison to the empty vector control (pSuper). Rat hippocampal neurons were transfected at 1DIV and fixed after 2, 4 or 6 h. The cells were processed for immunofluorescence. Using a Zeiss slidescanner, images of four whole coverslips were captured per condition from which 30 images of individual neurons were randomly selected. Scale bar = 50 μ m. **(B)** In ImageJ, the NeuronJ plugin was used to trace and measure the length of longest neurite and the mean values were plotted as a function of time for control and shRNA A transfected cells. All data points were normalised to the mean value of the 2 DPT control time point for each replicate. N=2.

4.2.8 The Role of N1-Src in L1-CAM Mediated Neurite Outgrowth.

The results from the shRNA experiments (Sections 4.2.4-6) established a potential role for N1-Src in neurite outgrowth. N1-Src shRNA A, the most potent of the two shRNAs, evoked a significant reduction in the length of longest neurite (Figure 4.9E). The magnitude of this effect increased with respect to time up to 6 DPT (Figure 4.12). Since cultured hippocampal neurons are known to develop an axon after 3-4 DIV, this suggested that N1-Src plays a role in axon outgrowth in developing hippocampal neurons. One mechanism through which N1-Src could regulate axon outgrowth is via the L1-CAM signalling pathway. Ignelzi *et al.*, (1994) demonstrated that impaired neurite outgrowth occurred in *Src*^{-/-} CGNs cultured on L1-CAM. Whilst this study did not directly implicate N1-Src, in the *Src*^{-/-} mice, C-, N1- and N2-Src expression were abolished, therefore this function could be linked to the neuronal kinases, which are the predominant isoforms of Src in the developing brain (Wiestler and Walter, 1988). In addition to this, studies in the Evans lab specifically pointed to a role for N1-Src in L1-mediated neurite outgrowth in CGNs. These studies, however, did not address whether L1-CAM homophilic or heterophilic interactions were responsible for the effects observed.

Since preliminary data from the Evans lab showed that N1-Src induces the formation of neurite-like processes in the fibroblast cell line COS7, this concept was used to develop an assay to test the effects of N1-Src within L1-CAM signalling pathways. In order to develop a model for N1-Src-mediated process outgrowth triggered by extracellular L1-CAM, process outgrowth was analysed in COS7 cells overexpressing mCherry (Control) or N1-Src-mCherry that were plated in control or L1-CAM substrate (L1-Fc) coated wells. To determine whether L1-CAM homophilic interactions were necessary for this process, N1-Src-mCherry was co-expressed with human L1-CAM in the presence or absence of L1-Fc.

The data presented (Figures 4.13 and 4.14) represent a single biological replicate. In order to draw firm conclusions from these data, further biological repeats must be performed, however, early indications of the appropriateness of this model and preliminary findings could be examined.

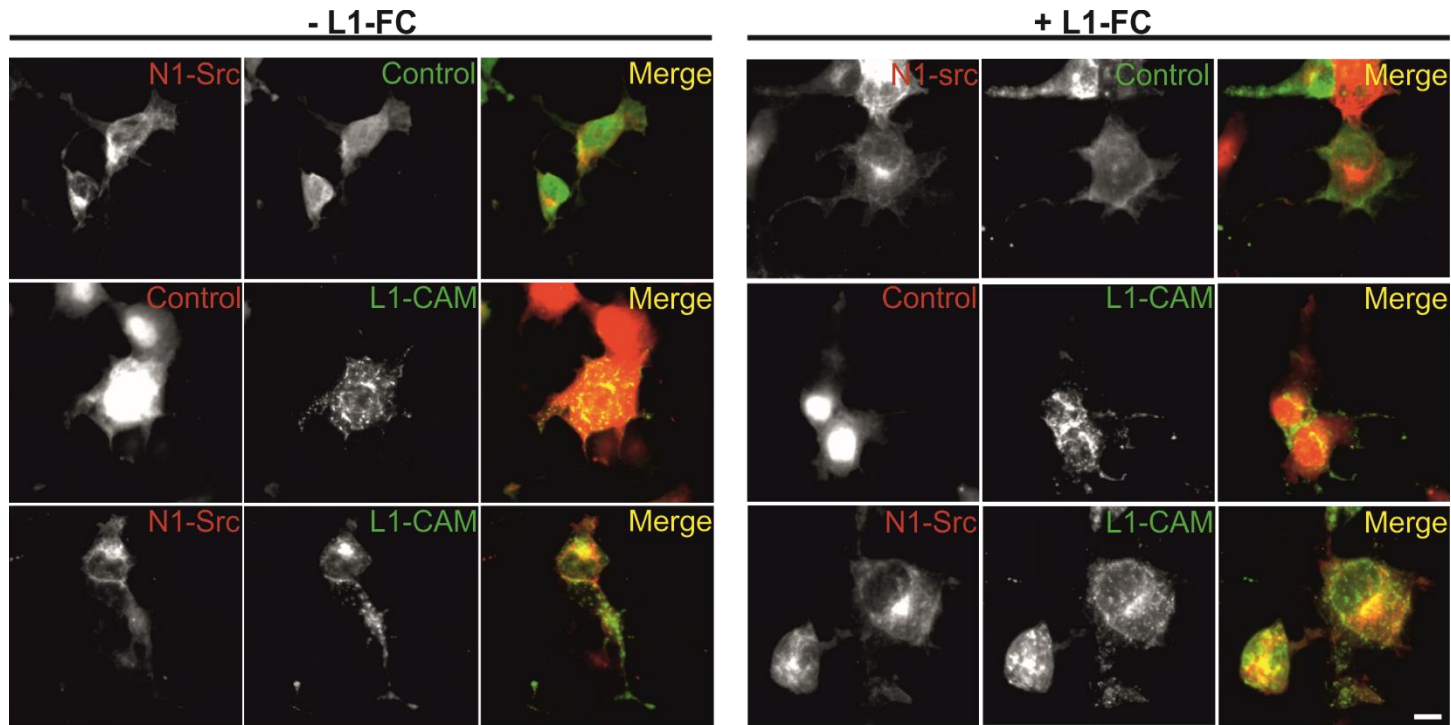


Figure 4.13: N1-Src-mCherry Co-localised with L1-CAM in the Perinuclear Region of COS7 Cells that were Grown in the Absence or Presence of L1-Fc.

Representative images showing the localization of N1-Src-mCherry and L1-CAM in COS7 cells, grown in the absence or presence of L1-Fc. COS7 cells were cultured in control or L1-Fc coated wells for 24 hours prior to being cotransfected with combinations of pmCherry (Control, red) or p-N1-Src-mCherry (N1-Src, red) and pcDNA5-CFP (Control, green) or pcDNA5-L1-CAM (L1CAM, green). The amount of co-localisation (yellow) was assessed when images were merged. The cells were fixed 48 h post-transfection and processed for immunofluorescence using a rabbit anti-sera raised against CFP, a mouse anti L1-CAM antibody and the relevant AlexaFluor488 secondary antibodies. Images were captured (30 fields of view) using a fluorescence microscope with a 40 X objective lens. Scalebar= 20 μ m, N=1.

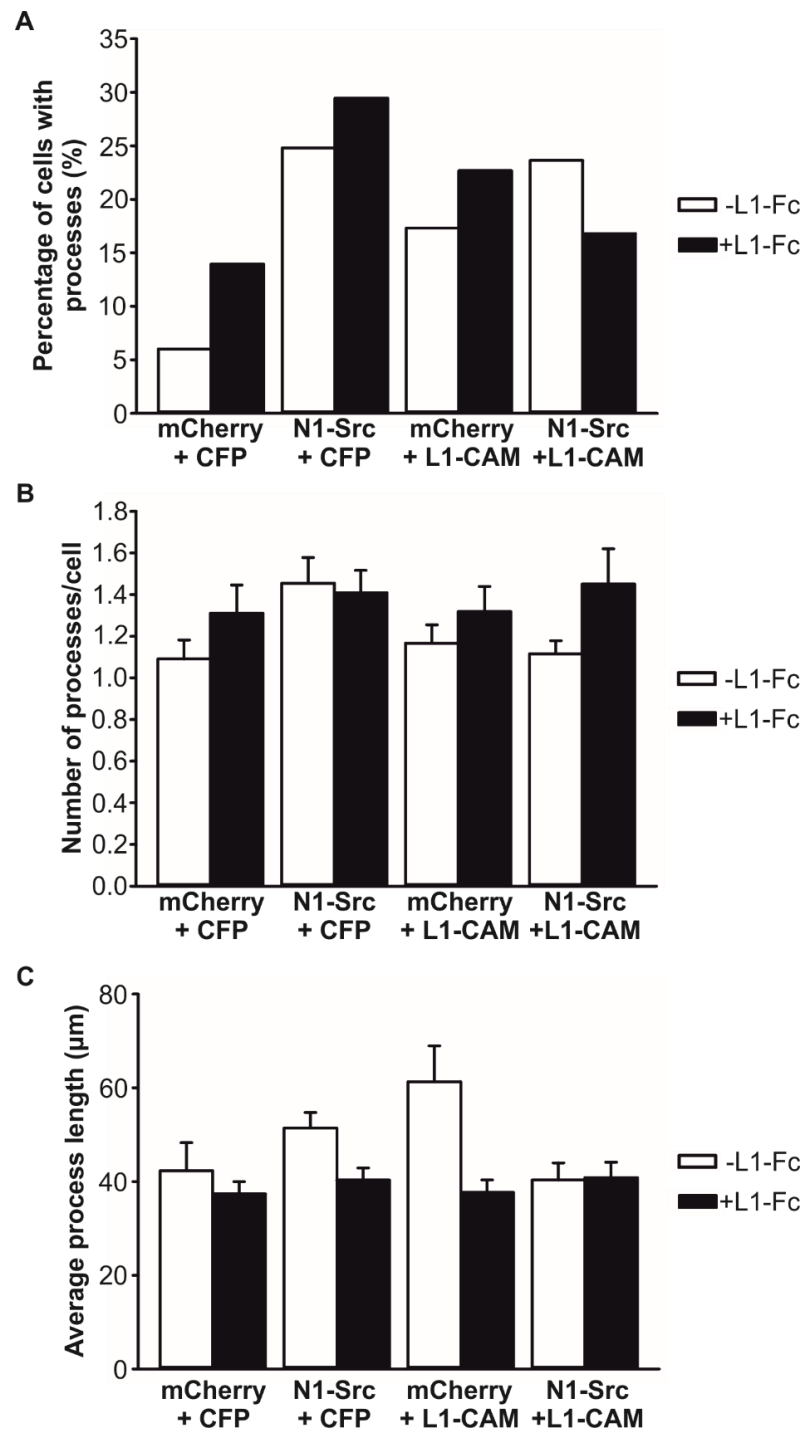


Figure 4.14: Preliminary Results Indicated that Homophilic L1-CAM Signalling did not Enhance Process Outgrowth in COS7 Cells.

COS7 cells that were cultured in control or L1-Fc coated wells, were co-transfected with combinations of pmCherry or p-N1-Src-mCherry and pcDNA5-CFP or pcDNA5-L1-CAM. The cells were fixed 48 h post-transfection and processed for immunofluorescence. Images were captured using a fluorescence microscope with a 40 X objective lens and the percentage of cells with processes was calculated from the cells present in 30 fields of view (n=97-208) **(A)**. Of the cells that had processes (n=11-43) the number of processes per cell **(B)** and the average process per cell (μm) were measured **(C)**. N=1.

Figure 4.13 shows representative images of cells transfected with the different combinations of conditions plated in control and L1-Fc coated wells. In cells that expressed N1-Src-mCherry and CFP, plated under control conditions, N1-Src accumulated in the perinuclear region and appeared diffuse throughout the cell. This distribution of N1-Src-mCherry appeared the same when cells transfected with the same constructs were plated on L1-Fc. In contrast, when L1-CAM was expressed in control cells alongside mCherry, whilst there was some perinuclear localization of the protein, the staining revealed the presence of multiple puncta distributed throughout the cytosol. A similar pattern of expression was visible in cells grown on L1-Fc substrate. Upon expression of both N1-Src-mCherry and L1-CAM together in either control or L1-Fc coated wells, both proteins appeared to co-localise in the perinuclear region, however there was no obvious co-localization between the L1-CAM puncta in the cytosol and N1-Src-mCherry.

To assess the effects of N1-Src-mCherry and L1-CAM expression on process extension in cells plated both in the absence or presence of L1-Fc, multiple parameters were quantified (Figure 4.14). These included the percentage of cells with processes (Figure 4.14A), the average number of processes (Figure 4.14B) and the average length of processes (Figure 4.14C). In cells co-expressing mCherry and CFP, the percentage of cells extending processes was low (6.02 %) when grown in the absence of L1-Fc and this increase more than doubled in the presence of L1-Fc (13.94 %) (Figure 4.14A). There was little change in the average number and length of neurites (Figure 4.14B and C) in these cells.

In contrast, co-expression of N1-Src-mCherry and CFP in control wells resulted in an increased proportion of cells (24.81 %) with processes (Figure 4.14A). This has been observed in previous studies in the Evans lab and notably in Section 5.2.1-2. This has contributed to the hypothesis that N1-Src plays a role in cytoskeletal re-modelling and process formation/extension. There was only a small increase in the percentage of cells with processes (4.64 %) in N1-Src-mCherry and CFP expressing cells grown on L1-Fc, with little change observed in the average number and length of processes.

In addition to expressing mCherry or N1-Src-mCherry with CFP (control), these proteins were also co-expressed with full length L1-CAM, with the aim of further understanding whether N1-Src regulates process outgrowth via an L1-L1 homophilic interaction stimulated signalling pathway.

In mCherry and L1-CAM expressing cells grown in control wells, there was an 11.29 % increase in the percentage of cells with processes compared to mCherry and CFP

expressing cells (Figure 4.14A). Whilst the average number of processes remained the same (Figure 4.14B), there was a 45 % increase in the average process length (Figure 4.14C). This suggested that L1-CAM expression in COS7 cells may enhance process outgrowth. When grown in L1-Fc coated wells, there was a slight increase (5.37 %) in the percentage of cells with processes, in comparison to control wells (Figure 4.14A). There was little change in the average number of neurites (Figure 4.14B), however the average length of neurites was reduced by 40 % back to the levels in control cells co-expressing mCherry and CFP (Figure 4.14C).

The difference in the percentage of cells with processes in N1-Src-mCherry and CFP or L1-CAM expressing cells was virtually unchanged in control wells. However, there was a decrease in cells with processes from 23.64 % to 16.81 % when those cells were grown on L1-Fc (Figure 4.14A). Whilst there was an increase in the average number of processes per cell from 1.11 to 1.45 (Figure 4.14B), the average length of neurites per cell remained unaltered (Figure 4.14C).

4.3 Discussion

The studies conducted in Chapter 4 sought to gain further insight into the functional role of N1-Src during neuronal morphogenesis. To address this, two main approaches were employed; 1) the overexpression and 2) shRNA knockdown of the kinase. These experiments provided evidence to support the hypothesis that N1-Src is involved in neurite outgrowth and could play a major role in axonal elongation. The first direct comparison between the roles of N1- and N2-Src during neuronal development demonstrated different functions for the kinases. Since previous data from the Evans lab suggested that N1-Src may act downstream of L1-CAM signalling to promote axon extension, further experiments were aimed at developing a model for L1-CAM mediated N1-Src signalling in the heterologous fibroblast cell line COS7. Whilst further biological repeats are required to draw firm conclusions from the data, preliminary results suggested that N1-Src did not evoke downstream signalling that enhanced the formation or elongation of neurite-like processes. However, the data suggested that L1-L1 homophilic signalling may have had an inhibitory effect via N1-Src signalling.

4.3.1 The Experimental Use of Primary Hippocampal Neurons.

Whilst there are many advantages to using cultured hippocampal neurons experimentally (discussed in Section 4.1.3), there are also certain caveats. The main limitation to consider when using dissociated hippocampal neurons is the resulting heterogeneous cell populations obtained. These contain both CA1 and CA3 glutamatergic pyramidal neurons, as well as various types of GABAergic interneurons (Benson et al., 1994). It is important to note that data outputs from experiments using these cells incorporated the results from the whole cell population, since it is difficult to tease apart differences between cells after 3 DIV (Figure 4.1). Despite this, pyramidal neurons are thought to comprise approximately 85-90 % of the total cell population, therefore the results obtained could be largely attributed to these types of neurons (Schlessinger et al., 1978, Boss et al., 1987). Since dentate granule cells develop postnatally, these cells were not present in the P0 hippocampal preparations used in the experiments described in this chapter.

There were also significant differences in the morphological parameters of control cells between different biological replicates, most noticeably between replicate 4 and the other replicates (Figure 4.3). This is likely attributed to the occurrence of natural variation between different rat litters. To account for these differences, individual values for each parameter measured in shRNA A or shRNA B expressing cells, were normalised to the average value of the control (pSuper-CFP transfected cells) (Figures 4.9 and 4.10). This

approach to data analysis has been adopted in many other studies, most notably by Vance Lemmon, whose pioneering work on L1-CAM mediated neurite outgrowth is referenced throughout this thesis (Cheng et al., 2005, Blackmore et al., 2010).

4.3.2 N1-Src Overexpression Resulted in Aberrant Neurite Outgrowth.

Overexpression of N1-Src in hippocampal neurons resulted in a highly significant reduction in the average total length of neurites and average length of longest neurite, as well as a reduction in the average number of neurites per cell (Figures 4.4 and 4.5). This indicated that the overexpression of the kinase had a severe effect on the development of hippocampal neuron morphology. After 3 DIV, 100 % of mCherry and C-Src-mCherry expressing cells were at stage three or above in the developmental sequence of events undertaken by hippocampal neurons in culture (described in Figure 4.1), which meant that the neurons were polarised since one of the minor neurites had been selected to become the axon. However, approximately half of N1-Src expressing cells appeared to not have progressed past stage two (Figure 4.6). This suggested that N1-Src-mCherry overexpression had affected the polarization of the neurons. In these experiments, the neurons were transfected after 1 DIV, at which point the cells measured were expected to have been at the developmental stages two or three. Therefore, one possible explanation for the results observed could be that the overexpression of N1-Src-mCherry prevented the progression of the neurons from stage two to stage three, whereas the neurons that were already at stage three at the time of transfection subsequently suffered stunted neurite outgrowth. To test this theory, it would be useful to track the development of N1-Src-mCherry overexpressing neurons in real time using live imaging. To understand whether N1-Src-mCherry overexpression, is either delaying or blocking developmental progression, a timecourse overexpressing the kinase over a longer period of time could be performed.

The results of N1-Src-mCherry overexpression on neuronal development observed in this study (Figures 4.4-4.6) have some similarities and differences when compared to the two N1-Src overexpression studies that have previously been published (Kotani et al., 2007, Worley et al., 1997). Kotani *et al.*, (2007) used an L7 promoter to drive the overexpression of constitutively active N1-Src (Y535F) in Purkinje neurons of transgenic mice. Whilst N1-SrcY535F had little effect in P3-P5 cells, surprisingly at P7, many of the Purkinje neurons appeared less polarised compared to control cells and displayed aberrant dendritic morphology, retaining multiple dendritic shafts and forming abnormal dendritic branches. These defects however, were not observed in P10 mice and onwards, implying that another mechanism may compensate for the effect observed (Kotani et al., 2007). Although the results in this chapter did not report phenotypic

changes relating solely to dendritic structures, the results did suggest that overexpression of the kinase resulted in defects in neuronal polarization. Unlike this study, Kotani *et al.*, (2007) did not report any findings relating to alterations in neurite length, nor did they discuss an axon-related phenotype, but it is unclear whether this was investigated. A further study by Worley *et al.*, (1997) found that the axonal lengths of *Xenopus* ventral forebrain neurons increased in N1-Src overexpressing cells, contradicting the findings in this chapter. It is important to note, however, that the number of neurons measured by Worley *et al.*, (1997) was of a very small sample size (n=5) whereas the results shown in Figure 4.5 were generated using a larger sample size (n=84-88 across 3 biological replicates).

Overexpression of C-Src-mCherry in hippocampal neurons had little effect on neuronal morphology compared to control cells (Figure 4.4), with no significant changes in the average number of neurites, total length of neurites and length of longest neurite (Figure 4.5). However, the differences in these parameters between C- and N1-Src-mCherry expressing cells were highly significant, given the aberrant morphology observed in N1-Src-mCherry cells. Although C-Src has been linked to neurite outgrowth in numerous studies, the lack of phenotype observed in this work could be attributed to the fact that C-Src has relatively low constitutive activity, especially in comparison to the N-Srcs (Ignelzi Jr *et al.*, 1994, Brouns *et al.*, 2001, Keenan *et al.*, 2015). In the various studies in the literature, C-Src mediated neurite outgrowth is placed in the context of a signalling mechanism, therefore, it is likely that C-Src activity must be triggered by a suitable stimulus to evoke changes in neurite outgrowth (Ignelzi Jr *et al.*, 1994). Since it has been shown that N1-Src has much higher constitutive activity than C-Src, this could explain the severe changes in neurite outgrowth attributable to N1-Src overexpression (Keenan *et al.*, 2015). To understand further the potential differences between C- and N1-Src function, it could be useful to compare the effects of the overexpression of constitutively active C-Src with wild type or constitutively active N1-Src.

Taken together, these results suggested that N1-Src overexpression in hippocampal neurons leads to aberrant neuronal development by disrupting neuronal polarization as well as causing stunted neurite outgrowth. N1-Src-mCherry overexpression also had a much greater effect on neuronal morphology than C-Src-mCherry, which could be attributed to the differences in constitutive activity between C- and N1-Src reported in other studies, or differences in substrate specificity. In addition, N1-Src overexpression appeared to have different effects in different cell types, which suggests that N1-Src has cell type specific functions. Alternatively, overexpression of the kinase could lead to the occurrence of non-physiological effects, caused by aberrant signalling. This is a

possibility given the high constitutive activity of the kinase. For this reason, shRNA knockdown studies (Figures 4.7-4.12) were performed to shed further light on the physiological roles of N1-Src and will be the subject of discussion in the sections that follow.

It should be noted that in order to link the effects of the overexpression of C-, N1- and N2-Src directly to the catalytic activity of the kinases, the experiment should be repeated using kinase-null mutants as an additional control. By including this control, the possibility that the kinases mediate their effects through the formation of protein-protein interactions or other means, could be ruled out. In addition to this, a second control should be included to assess the protein levels of the overexpressed kinases. The performance of this control is necessary to show that the differences between the effects of C-Src and N1-/N2-Src can be specifically attributed to the individual functions of the kinases and are not caused by differences in their expression levels. In the overexpression study performed in this chapter, the transfection efficiency of the neurons used was too low to be able to perform an accurate quantification of the kinase expression levels. However, this could be overcome by using a lentiviral gene delivery system to greatly improve the transfection efficiency of the neurons. In order to be able to deduce firm conclusions from these data in the future, the experiment should be repeated using both of these controls.

4.3.3 The Specificity of the N1-Src Targeting shRNAs.

Two independent shRNAs were designed with the aim of specifically depleting the expression of N1-Src. Given that N1- and N2-Src differ from each other and C-Src via small mini-exon inserts in their SH3 domains (illustrated in Figure 4.7A), the scope for designing N1-Src specific shRNAs was limited. The difficulty of this task was reflected by the results obtained after testing the efficacy of the shRNAs in COS7 cells (Figures 4.7B and C). Whilst shRNA A was largely specific to N1-Src, depleting N1-Src protein levels by approximately 70 %, N2-Src by 35 % and C-Src by only 15 %, shRNA B was largely specific to N2-Src, depleting N2-Src protein levels by approximately 95 %, C-Src by 37 % and N1-Src by less than 10 %. These represent data from an n=1, since the results from additional experimental repeats were invalid due to technical faults. However, the outcome of the experiment is supported by the initial shRNA efficacy experiments performed by Katharina Mahal, who also cloned the shRNAs (Mahal, 2010).

The depletion of C- and N2-Src protein levels by both shRNAs is likely due to the partial sequence complementarity shared between the shRNAs and the mRNA's of the kinases, however the fact that shRNA B depleted N2-Src protein by much greater levels was

surprising, since shRNA A shared greater sequence complementarity with N2-Src compared to shRNA B.

Ideally the efficacy of the shRNA's would have been tested in hippocampal neurons however, the fact that there are no commercially available antibodies for N1-Src and the neuronal transfection efficiency using Lipofectamine was poor, meant that this was not a feasible option. To overcome these issues, the effect of the shRNAs on the levels of C-, N1- and N2-Src mRNA could be assessed using reverse-transcription PCR (rt-PCR), although a much greater neuronal transfection efficiency would need to be achieved. This could be addressed by using a highly efficient lentiviral system, to deliver the siRNA into the hippocampal neurons. In addition, an experiment similar to the one performed in this chapter in COS7 cells could be performed with hippocampal neurons, using the lentiviral system to improve transfection efficiency.

4.3.4 Depletion of N1-Src Expression by shRNA A Resulted in Reduced Neurite Outgrowth.

Depletion of N1-Src expression by shRNA A had a significant effect on neurite outgrowth in cultured hippocampal neurons. The average number of neurites, total length of neurites and length of longest neurite were significantly reduced (Figure 4.9), whereas neurite branching was unaffected (Figures 4.10 and 4.11). This study was the first of its kind, to predominantly target the knockdown of N1-Src expression, with respect to C- and N2-Src and suggested that N1-Src may play a role in the formation and extension of neurites. The impaired outgrowth of the longest neurite mediated by shRNA A, worsened with respect to time (Figure 4.12) implying that N1-Src expression was vital to the mechanisms that governed neurite outgrowth. Since the neurons analysed were fixed between 2-6 DPT, and 100 % of the cells were observed to have reached stage 3 or above using Dotti's classification system (Figure 4.1) of hippocampal neuron development, it was likely that N1-Src depletion by shRNA A particularly inhibited axonal outgrowth. Furthermore, the decrease in the length of longest neurite between shRNA A transfected cells fixed at 4 and 6 DPT, suggested that in addition to inhibiting the mechanisms that drive neurite extension, exposure of the cells to shRNA A for this period of time, could have ultimately led to neurite retraction. In order to determine the statistical significance of the data, a third biological repeat should be performed.

Whilst there are no studies that directly link N1-Src knockdown to neurite outgrowth, (Ignelzi Jr et al., 1994) found that neurite outgrowth was impaired in CGN's cultured from Src^{-/-} mice that were grown on the neuronal cell adhesion molecule L1-CAM. The mouse knockout used was not specific to a single splice variant of Src, and therefore the

expression of C-, N1- and N2-Src kinases would have been abolished in the neurons used. Therefore, it is plausible that this phenotype could be at least partially assigned to N1-Src, which would support the findings of the shRNA A transfection. However, in the Ignelzi study (1994), impaired neurite outgrowth was observed in CGNs that were cultured on L1-CAM, whereas *Src*^{-/-} cells grown on laminin, which stimulates integrin mediated neurite outgrowth, were not affected. This suggested that Src facilitated neurite outgrowth via an L1-CAM dependent pathway.

In the studies carried out in this thesis, hippocampal neurons were grown on poly D-lysine (PDL), a commonly used synthetic polyamino acid, which facilitated the adherence and growth of cells on glass. Therefore, in the absence of external extracellular matrix signalling cues, including cell adhesion molecules and integrins, depletion of N1-Src still resulted in reduced neurite outgrowth. This could suggest that N1-Src drives neurite outgrowth via an intrinsic mechanism that operates in the absence of external factors. One possible explanation for this could be the high constitutive kinase activity that N1-Src possesses.

Src has also been linked to the regulation of neurite outgrowth in conjunction with p190RhoGAP, which regulates actin cytoskeletal dynamics via the GTPase RhoA. Overexpression of p190RhoGAP promotes neurite outgrowth in neuroblastoma cells, which is similar to the effects of N1-Src overexpression in fibroblasts (Brouns et al., 2001, Worley et al., 1997). In addition, p190RhoGAP was also shown to be the most prominent tyrosine phosphorylated protein in whole mouse brain lysates, which was reduced in *Src*^{-/-} mice and almost completely abolished in *Src*^{-/-}/*Fyn*^{-/-} double knock out mice (Brouns et al., 2001). Thus, it appears that both Src and Fyn are regulators of p190RhoGAP in the brain. Whilst C-Src has been shown to phosphorylate p190RhoGAP in fibroblasts, the possibility that N1-Src could regulate the protein has not been explored (Roof et al., 1998). Brouns *et al.*, (2001) also demonstrated that p190RhoGAP was localised to the distal tips of neurites, alongside F-actin, in hippocampal neurons (E18.5) cultured on PDL and interestingly, biochemical studies have also shown that N1-Src is present in neuronal growth cone membranes in developing rat brain. Whether C- or N1-Src directly phosphorylates and regulates p190RhoGAP to promote neurite outgrowth in primary neurons still remains to be shown

Unpublished work in the Evans lab established an N1-Src inhibitor called PD1, through the development of an N1-Src specific SH3 binding motif (Keenan, 2012). N1-Src inhibition by PD1 in hippocampal neurons resulted in a decrease in the primary branching of neurites, but had no effect on the average number of neurites formed or neurite

lengths. However, the outcomes of the shRNA A depletion of N1-Src did not support these findings, and pointed towards a role for N1-Src in neurite formation and extension. This could be explained by the occurrence of off target effects in either the PD1 or shRNA studies, or may be due to the differences between the methods used. As a competitive inhibitor of N1-Src, PD1 elicits an acute response, whereas shRNAs act to prevent protein synthesis by targeting mRNA for degradation. To confirm the differences in the functions ascribed to N1-Src and provide greater confidence in the shRNA knockdown, it would be useful to perform this study with a second N1-Src specific shRNA.

Given that there was only a partial depletion in the expression of C- (12 %) and N2-Src (35 %) by shRNA A, it seemed that neither of the kinases were able to functionally compensate for the effect of the ~ 70 % depletion of N1-Src expression up to 6 DPT. This suggests that the kinases have different functional roles. This is in part, supported by the outcome of the shRNA B transfection in which N2-Src expression was predominantly depleted and a different morphological phenotype was observed (discussed in Section 4.3.5). Since the sequence, of C-Src is fully conserved with N1- and N2-Src, with the exception of the n-Src loop, it would be difficult to establish the specific functional role of C-Src in neurons, without resorting to overexpression techniques, which cannot always be relied upon to determine physiological function.

4.3.5 The Overexpression and Knockdown of N1-Src Display Similar Effects on Neuronal Morphology.

Interestingly, both the overexpression of N1-Src and the knockdown of N1-Src by shRNA A yielded similar results, in that both experiments resulted in a reduction in neurite outgrowth. This observation is likely attributable to the fact that the overexpression of a kinase can cause aberrant signalling. There are multiple explanations why this might occur (reviewed by Prelich, 2012). For example, the overexpression of the kinase might disrupt the formation of multi-protein complexes, in which N1-Src is a key component. This may be due to the formation of subassemblies that include N1-Src bound to one or more of the other complex components, but which do not form the whole functional complex, leading to the loss of function of the kinase. A further explanation could be that the overexpression of the kinase may result in the aberrant phosphorylation of cellular proteins, which results in the inhibition of neurite outgrowth. In addition to this, it is possible that overexpressing the kinase results in the sequestration of signalling components into complexes with N1-Src, preventing such components from interacting with other proteins that are also necessary for the regulation of neurite outgrowth.

4.3.6 The Effect of shRNA B on the Primary Branching of Neurites.

Originally shRNA B was designed to knockdown N1-Src expression, however testing of the shRNA in COS7 cells revealed that shRNA B was in fact extremely effective at knocking down N2-Src expression and partially reduced C-Src levels by 37 % (Figure 4.7). Interestingly, the results obtained from shRNA B transfected cells were different to shRNA A transfected cells. shRNA B transfection resulted in a highly significant increase in the average number of primary branches as well as a decrease in the average length of primary branches, with little change in the total length of primary branches per cell (Figure 4.10). An increase in the average number of neurites was also observed (Figure 4.9). These results suggested that N2-Src may play a role in the primary branching of neurites, serving to inhibit or regulate primary branching events, and potentially regulating branch extension.

To date, there are no studies in the literature describing the function or substrates of N2-Src in primary neurons. However, N2-Src has been linked to a positive prognosis in the childhood cancer neuroblastoma, in which tumour cells spontaneously differentiate into benign neuronal cells (Matsunaga et al., 1998, Terui et al., 2005). Whilst there is precedence in the literature for a role of N2-Src in neuronal differentiation, any potential effects that could have altered the cell fate of the hippocampal neurons could not have been detected in these experiments, since the fate of the cells used had already been determined. In addition to this, 100 % of the cells transfected with shRNA B that were analysed (n=90) had successfully polarised.

Taken together, the shRNA results presented in this chapter indicate different roles for N1- and N2-Src in neuronal morphogenesis. Whilst shRNA A demonstrated a partial knockdown of N2-Src by 35 %, given there was no correlation with the results for shRNA B, which primarily depleted N2-Src protein levels, it is likely that the partial knockdown of N2-Src was not great enough to cause a significant effect. Taking this into account, since N2-Src protein levels were depleted by 96 % by shRNA B, whereas C-Src and N1-Src levels were reduced by 37 % and 9 % respectively (Figure 4.7), it is reasonable to assume that the effects of this shRNA could be largely attributed to the role of N2-Src. Therefore, this study provides the first comparative analysis of the effects of both N1- and N2-Src on neuronal morphogenesis, and suggests that the kinases have different functions. N1-Src appeared to play a role in neurite extension, whereas N2-Src regulated the formation of primary branches (Figure 4.10). To confirm the validity of these effects, a second shRNA targeting each kinase should be tested. This would discount the possibility that off-target effects contributed to these results.

Chapter 5

Dissecting the Role of N1-Src in RhoA Signalling

Chapter 5. Dissecting the Role of N1-Src in RhoA Signalling

5.1 Introduction

In Chapter 4, N1-Src was implicated in the mechanisms governing neurite outgrowth and in particular, regulation of the average number of neurites and length of longest neurite. Rho GTPases are key players in directing cytoskeletal dynamics during neurite outgrowth (reviewed in (Stankiewicz and Linseman, 2014) and mounting evidence suggests that there could be a potential link between N1-Src activity and RhoA signalling.

Firstly, bioinformatics studies in the Evans lab have identified several putative N1-Src substrates involved in RhoA signalling, including p190RhoGAP, ARHGAP1, TRIO and KALIRIN (Keenan, 2012). In addition to this, N1-Src has also been shown to interact with DAAM1 *in vitro*, which is a known effector of RhoA and has been shown to mediate the formation of branched protrusions in fibroblasts, in a C-Src dependent manner (Aspenstrom et al., 2006).

There have also been multiple reports linking C-Src and RhoA, including a study that identified p190RhoGAP as the principal substrate for C-Src and Fyn in the brain (Brouns et al., 2001) and a separate study, which reported that C-Src can directly phosphorylate and regulate RhoA activity *in vitro* (Uezu et al., 2012). With this in mind, Chapter 5 will focus on investigating a potential role for N1-Src in RhoA signalling, with the aim of providing further insight into the role of N1-Src in neurite outgrowth.

5.1.1 RhoA as a Regulator of Cell Morphology

Of the many processes that Rho GTPases regulate, perhaps their role in the regulation of cell morphology and motility, via the control of the actin cytoskeleton, are the most widely studied. To date, there are 20 known Rho GTPases amongst which RhoA, Rac1 and Cdc42 are the best characterised. The role of RhoA was first demonstrated in fibroblasts, where RhoA activation resulted in the formation of stress fibres (contractile actin-myosin filaments) and focal adhesion complexes in response to various extracellular stimuli (Ridley and Hall, 1992). Whilst activation of RhoA promotes cell contraction and rounding, inactivation of this GTPase promotes membrane protrusion. This is also the case in neurons, where RhoA activation stimulates neurite retraction and rounding of the cell body and inactivation enhances neurite outgrowth (Kozma et al., 1997).

5.1.2 The Molecular Mechanism and Regulation of the Small GTPase RhoA

Rho GTPases, share a common mechanism of action and are often referred to as 'molecular switches', alternating between their 'on' (active) and 'off' (inactive) states, enabling the tight regulation of downstream signalling pathways (Figure 5.1).

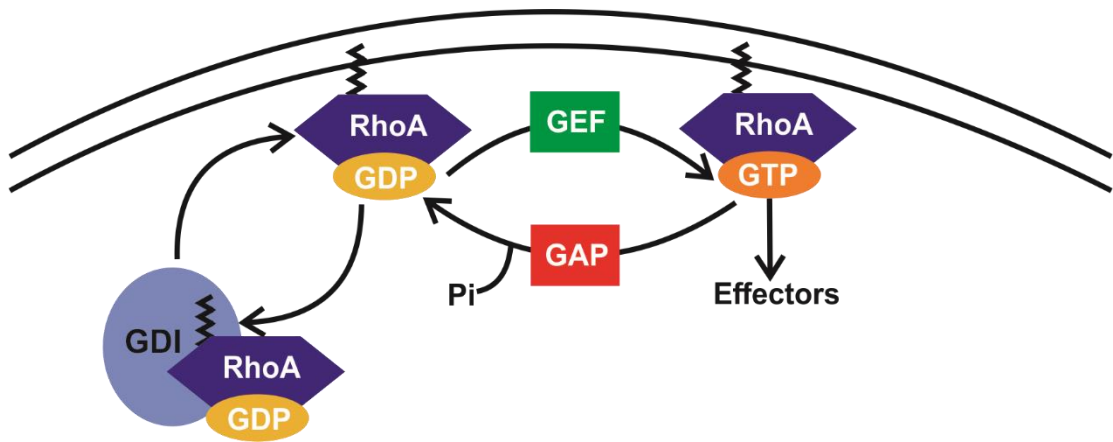


Figure 5.1: Schematic Diagram Illustrating the Mechanism of RhoA Activation and Inactivation.

RhoA operates as a molecular switch, which alternates between an 'on' (active) or 'off' (inactive) state. When bound to GDP, RhoA is rendered inactive, whereas GTP-bound RhoA is active. When the RhoA is active and GDP-bound, this enables effector binding and facilitates downstream signalling pathways. The cycling between RhoA-GDP and RhoA-GTP is facilitated by GEFs, which activate the GTPase and GAPs, which inactivate the GTPase. The C-terminus of RhoA is prenylated, which facilitates the attachment of active RhoA to the plasma membrane and intracellular membrane compartments. RhoGDIs bind to the lipid modification on RhoA and sequesters RhoA in the cytosol, effectively inactivating the GTPase.

When active, Rho GTPases are bound to guanosine triphosphate (GTP), which facilitates the conformation dependent binding of effector proteins. Upon hydrolysis of GTP to guanosine diphosphate (GDP), the GTPase switches to its inactive, GDP bound state, which prevents effectors binding and effectively 'switches off' downstream signalling events.

There are two classes of proteins, namely guanine nucleotide-exchange factors (GEFs) and GTPase activating proteins (GAPs), which catalyse the 'activation' (GTP bound) and 'inactivation' (GDP bound) of Rho GTPases, respectively (Figure 5.1). GEFs act by catalysing the exchange of GDP for GTP, whereas GAPs induce GTPase activity that results in GTP hydrolysis, yielding the GDP bound form (Fritz and Pertz, 2016).

The regulation of RhoA is an extremely complex process that involves multiple inputs. In the human genome, whilst there are 20 members of the Rho GTPase family, there are 83 known activators (GEFs) and 67 known inactivators (GAPs). Therefore, a single Rho GTPase can be regulated by multiple GAPs and GEFs. Some GAPs and GEFs also exhibit a degree of promiscuity and are capable of regulating more than one Rho GTPase. For example, the GEF Vav2 is known to activate RhoA, Cdc42 and Rac1 (Abe et al., 2000). In turn, the activity of Rho GAPs and GEFs can also be modulated by post-translational modifications (e.g. (Uezu et al., 2012).

In addition to GAP and GEF activity, a further mode of RhoA regulation occurs via the interaction of RhoA with a Rho guanine dissociation inhibitor (RhoGDI; Figure 5.1). The C-terminus of RhoA is prenylated, which facilitates the attachment of active RhoA to the plasma membrane and intracellular membrane compartments. RhoGDIs bind to the lipid modification on RhoA, effectively forming inactive complexes that are soluble in the cytosol (Cherfils and Zeghouf, 2013).

The direct regulation of RhoA by post-translational modifications has also been reported. RhoA can be targeted for degradation upon the ubiquitination of Lys-6 and -7 or Lys-135 by the E3 ubiquitin ligases Smurf1 and FBX119, respectively (Wang et al., 2006a, Wei et al., 2013).

Furthermore, RhoA activity can be regulated by direct phosphorylation of the protein. Protein kinase A (PKA) and Protein kinase G (PKG) phosphorylate RhoA at Ser-188, which promotes the inactivation of RhoA by sequestering the protein into a complex with RhoGDI (Ellerbroek et al., 2003). This modification is also thought to protect RhoA from ubiquitin-mediated degradation as well as disrupt the interaction between RhoA and ROCK, a major effector that binds to RhoA (Rolli-Derkinderen et al., 2005). C-Src has

been shown to phosphorylate RhoA at Tyr-34 and -66, which is also proposed to disrupt effector binding and therefore downstream signalling processes (Uezu et al., 2012).

5.1.3 Aims

Since there is evidence to suggest that N1-Src may play a role in RhoA signalling, the aim of this study was to determine whether N1-Src drives cytoskeletal dynamics via a RhoA dependent signalling mechanism. This work was carried out using a fibroblast model (also used in Chapter 5), in which N1-Src overexpression has previously been shown to increase process formation and reduce cell area in COS7 cells (Keenan, 2012). The hypothesis underpinning this work is that N1-Src will serve to promote the inactivation or act downstream of inactivated RhoA, which will ultimately lead to increased process formation and outgrowth in COS7 cells. This was investigated using a variety of cell biology and biochemical techniques.

5.2 Results

5.2.1 Dissecting the Role of N1-Src in RhoA Signalling Using RhoA Mutants.

In this chapter, a fibroblast model was employed to address the hypothesis that N1-Src regulates neurite outgrowth via the inhibition of RhoA. As previously described in Chapter 4, the overexpression of N1-Src-mCherry in COS7 cells results in the formation of neurite-like processes in a portion of cells, which suggests that N1-Src regulates conserved cytoskeletal mechanisms that direct changes in cell morphology. This phenotype is not commonly observed in COS7 control cells ($\leq 10\%$) and therefore provides a simpler model for investigating manipulations of N1-Src signalling, as subtle effects on neurite outgrowth in hippocampal neurons can often be difficult to detect. A further advantage of using the COS7 cell line for studying N1-Src signalling is that these cells can be cultured and transfected more easily than neurons.

In this study, the morphology of COS7 cells overexpressing N1-Src-mCherry alongside wild type (WT), constitutively active (Q63L) and dominant negative (T19N) GFP-RhoA was analysed. RhoA Q63L is a mutant that is unable to hydrolyse GTP and is therefore locked in the GTP-bound active state, whereas RhoA T19N acts by sequestering upstream GEFs, thus preventing exchange of GDP for GTP, rendering the protein inactive (Figure 5.2).

The RhoA proteins were N-terminally-tagged with GFP, therefore an empty vector GFP control was used as a negative control. In addition to this, the GFP and RhoA constructs were co-transfected with plasmids expressing C-Src-mCherry (to compare with N1-Src-mCherry) and mCherry (a control for the Src-mCherry constructs). Multiple morphological parameters were measured, including the percentage of cells with processes (Figure 5.4A), cell area (Figure 5.6A) and the circularity of the cells (Figure 5.6B).

Representative images indicated that, for all three GFP-RhoA constructs (WT, Q63L and T19N), the proteins were largely localised in the perinuclear region of COS7 cells (Figure 5.3). They also appeared diffuse within the cytosol with some protein concentrated within small puncta. In the case of GFP-RhoA-WT and -Q63L, some protein was localised at the plasma membrane (Figure 5.3). When co-expressed with C-Src-mCherry, GFP-RhoA-WT, -Q63L and -T19N appeared to co-localise with C-Src-mCherry in the perinuclear region (Figure 5.3B). This was also the case for N1-Src-mCherry co-expressed with GFP-RhoA-WT and -T19N, but was less apparent in GFP-RhoA-Q63L transfected cells, where the RhoA mutant appeared more diffuse throughout the cells (Figure 5.3C). Upon first inspection, the morphology of cells expressing GFP-RhoA-Q63L was more compact and rounded. Whereas in GFP-RhoA-WT and -T19N

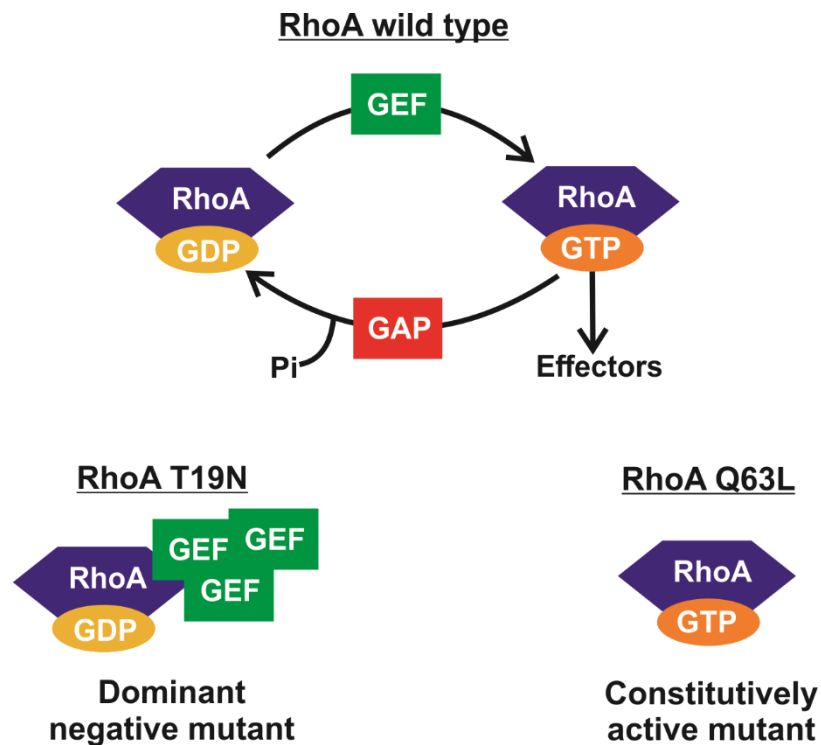


Figure 5.2: Schematic Diagram Illustrating the Dominant Negative and Constitutively Active RhoA Mutants.

RhoA wild type (WT) is capable of cycling between inactive GDP-bound and active GTP-bound RhoA and vice versa, which is facilitated by GEFs and GAPs. The dominant negative RhoA mutant (T19N) is GDP bound, since the protein sequesters Rho GEFs, preventing the exchange of GDP for GTP. This protein can also interfere with other Rho GTPase signalling pathways since some GEFs are capable of regulating more than one GTPase. Constitutively active RhoA is continuously locked in the GTP bound active form and sequesters effector proteins, triggering downstream signalling events.

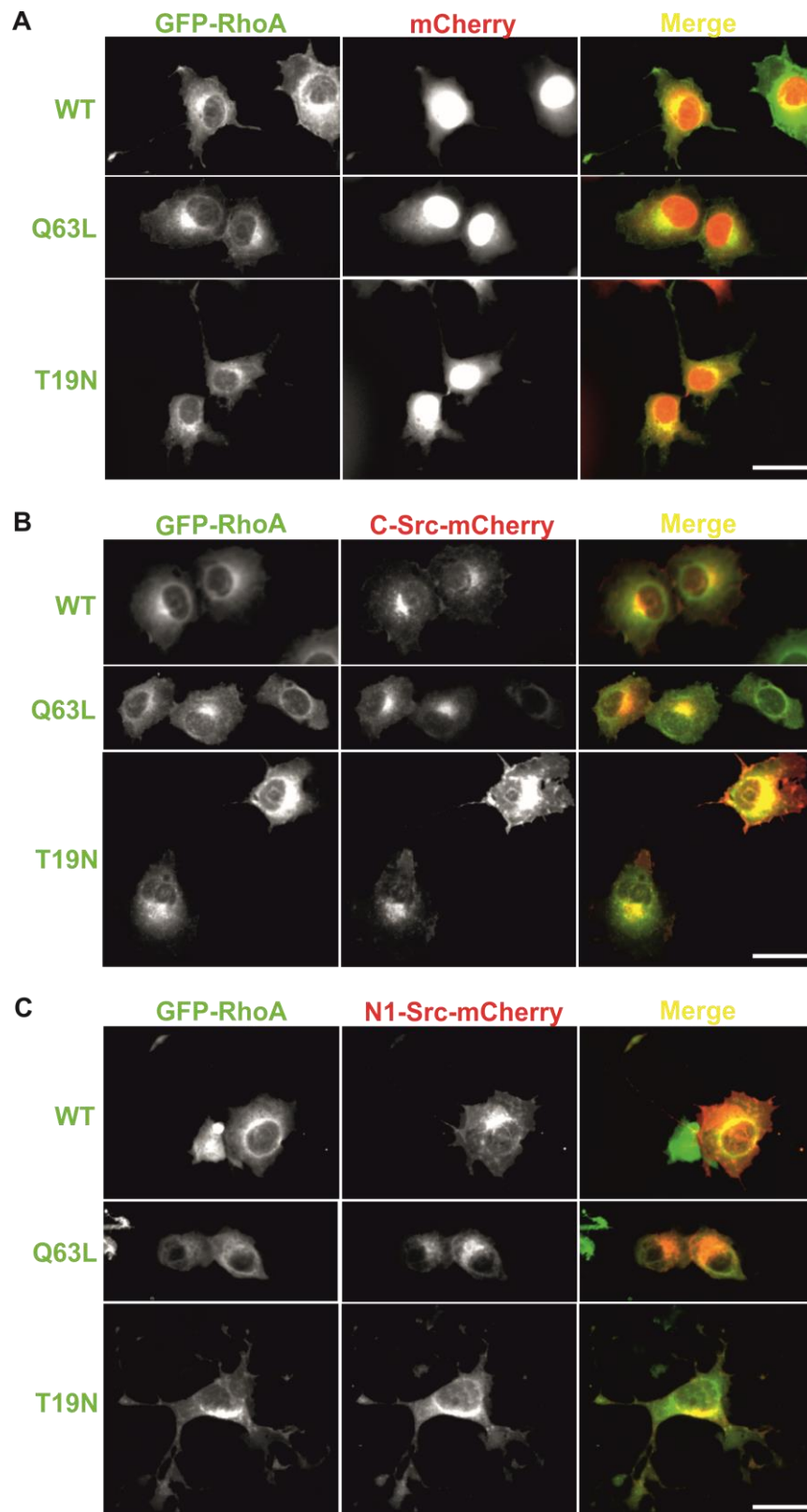


Figure 5.3: N1-Src Co-localises with RhoA WT and T19N in the Perinuclear Region of COS7 Cells, which is Less Apparent in RhoA Q63L Expressing Cells.

Representative images of COS7 cells co-transfected with empty- (A), C-Src (B) or N1-Src-mCherry (C) and RhoA WT, Q63L or T19N. Cells were transfected for 48 h fixed and processed for immunofluorescence. Images were captured of 15 fields of view per condition using a fluorescence microscope. N=3, scale bar= 50 μ m.

transfected cells, a greater number of cells appeared to project neurite-like processes, particularly when co-transfected with mCherry or N1-Src-mCherry (Figures 5.3 A and C).

To assess the differential effects of the GFP-RhoA constructs on the ability of COS7 cells to form neurite-like processes in the presence of mCherry, C-Src- or N1-Src-mCherry, the percentage of cells with processes and average number of processes per cell were quantified (Figure 5.4). Statistical analysis revealed that the percentage of cells with processes for GFP, GFP-RhoA-WT, -Q63L and -T19N expressing cells, was not dependent upon the Src-mCherry construct that was co-expressed, despite the fact that N1-Src-mCherry overexpression in control (GFP) and GFP-RhoA-T19N expressing cells resulted in an elevation in the percentage of cells with processes with respect to the corresponding mCherry expressing cells (Figure 5.4A). However, statistical analysis of the data did indicate that the overall average of the percentage of cells with processes in N1-Src-mCherry expressing cells was significantly higher in comparison to mCherry ($p=0.049$ *) and C-Src-mCherry ($p<0.001$ ***) expressing cells (statistics for averaged data not shown on graph). In addition to this, the ability of cells overexpressing GFP-RhoA-WT and -T19N to form processes (Figure 5.4A) was significantly elevated with respect to GFP-RhoA-Q63L ($p=0.037$ * and <0.001 ***, respectively) and GFP (T19N only; $p=0.005$ **) cells (statistics for averaged data not shown on graph).

Figure 5.4B shows data depicting the average number of processes per cell, which follows the same trend as the percentage of cells with processes data (Figure 5.4A). Statistical analysis of these data indicated that process formation in the GFP-RhoA construct transfected cells was dependent on the presence of the Src-mCherry construct.

The data highlighted that in GFP-RhoA-T19N cells co-expressing mCherry, there was a significant increase in the average number of processes per cell in comparison to GFP and GFP-RhoA-Q63L transfected cells (Figure 5.4B). The phenotype of RhoA WT transfected cells appeared to lie somewhere between that of GFP-RhoA-Q63L and -T19N cells. Whilst the values obtained for C-Src-mCherry did not vary widely with respect to mCherry transfected cells, N1-Src-mCherry promoted process formation (Figure 5.4B).

The increase in the average number of processes in cells co-expressing N1-Src-mCherry and GFP was close to significance ($p=0.061$) when compared to mCherry containing cells. In addition to this, process formation was significantly higher in N1-Src-mCherry and GFP-RhoA-T19N expressing cells with respect to their mCherry and C-Src-mCherry expressing counterparts ($p>0.001$ ***). Whereas in GFP-RhoA-Q63L expressing cells process formation was comparable across mCherry, C-Src-mCherry and N1-Src-mCherry expressing cells.

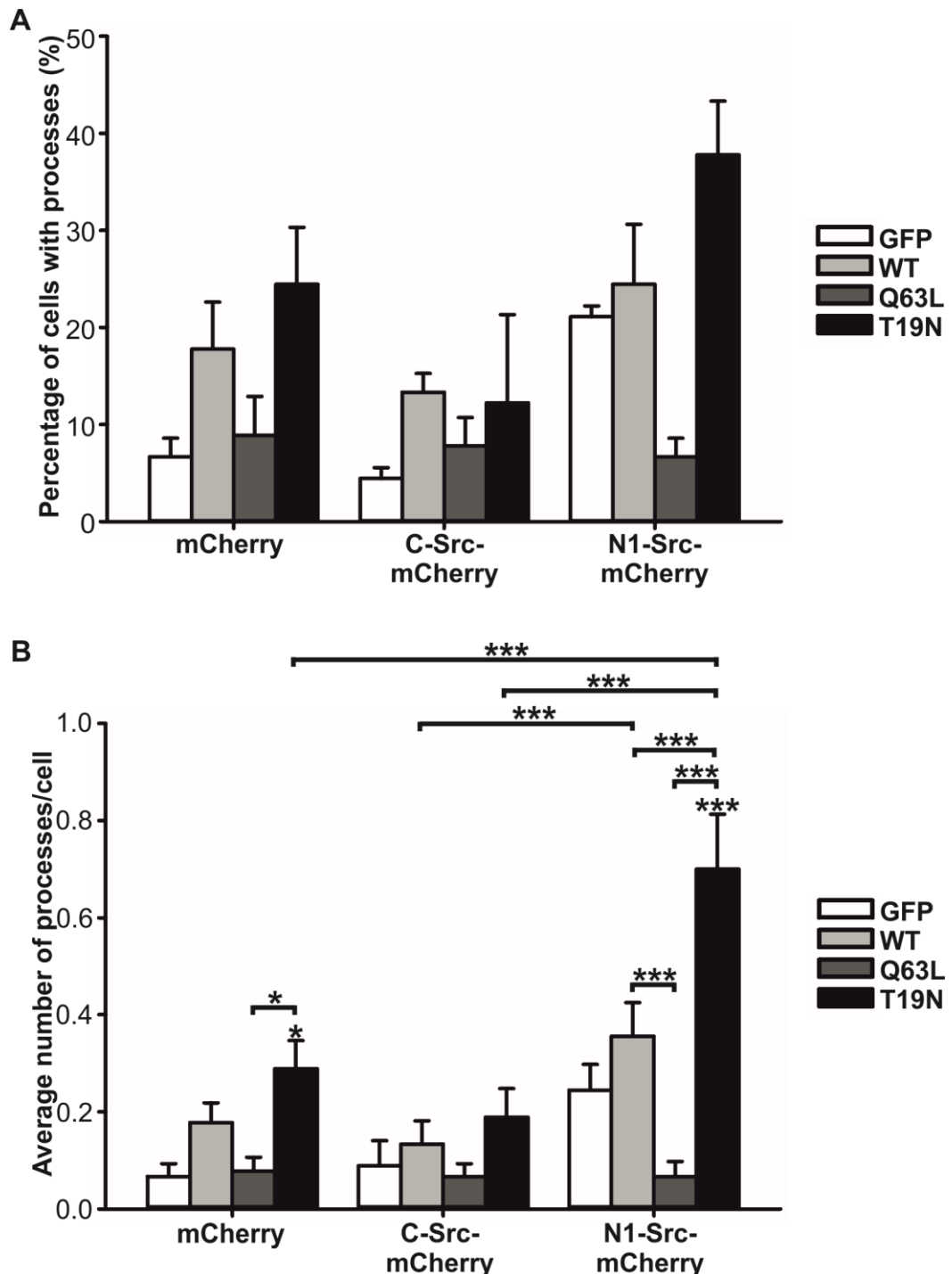


Figure 5.4: The Effects N1-Src-mCherry and the GFP-RhoA Mutants on Process Extension in COS7 Cells.

The percentage of cells with processes (**A**) and average number of processes per cell (**B**) were determined from images of COS7 cells that were co-transfected with mCherry, C-Src- or N1-Src-mCherry plasmids and constructs expressing GFP, GFP-RhoA-WT, -Q63L or -T19N. The cells were transfected for 48 h, fixed and processed for immunofluorescence. The analysis was performed on 30 cells per condition, from a maximum of 15 fields of view. The experiments were performed 3 times and statistical analysis of the average number of processes per cell was performed on pooled data (n=90) using a two-way ANOVA. (* $p < 0.05$, ** $p < 0.01$, *** $p < 0.001$).

Although process extension by N1-Src-mCherry and GFP-RhoA-Q63L cells was not significantly different from their GFP transfected counterparts, it was significantly reduced in comparison to GFP-RhoA-WT ($p=0.001$ ***) and -T19N ($p<0.001$ ***) expressing cells. This indicated that N1-Src-mCherry was unable to promote process formation in the presence of GFP-RhoA-Q63L.

With the aim of further understanding the effects of N1-Src-mCherry on process outgrowth, a more in depth morphological analysis was performed on the conditions that resulted in more than 20 % of the cells producing neurite-like processes (Figure 5.5).

When N1-Src-mCherry was co-expressed with GFP-RhoA-T19N, there was a significant increase in the average number of processes (Figure 5.5A) and total length of processes per cell (Figure 5.5B), when compared to GFP ($p=0.01$ ** and 0.007 **, respectively) and GFP-RhoA-WT (total length of processes only; $p=0.022$ *) cells (Figure 5.5B). However, there was no significant change in the length of the longest process (Figure 5.5C), average process length (data not shown) or the number of branches per cell (Figure 5.5D). Furthermore, when comparing the same morphological parameters in mCherry or N1-Src-mCherry cells co-expressing GFP-RhoA-T19N, it was apparent that N1-Src-mCherry activity significantly enhanced the effects of GFP-RhoA-T19N process outgrowth (Figure 5.5E, $p=0.008$ **) and branching (Figure 5.5H, $p=0.02$ *), which resulted in an increase in the total length of processes (Figure 5.5F, $p=0.009$ **). Once again, the length of the longest process and average process length (data not shown) remained unaffected.

The area of cells co-expressing WT RhoA and mCherry was comparable to GFP expressing cells. However, GFP-RhoA-Q63L expression triggered a significant decrease in cell area with respect to GFP or GFP-RhoA-WT cells (Figure 5.6A, $p=0.008$ ** and 0.006 **, respectively). In addition, there was a close to significant or significant reduction in the area of GFP-RhoA-T19N expressing cells in comparison to control (GFP; $p=0.058$) and GFP-RhoA-WT ($p=0.042$ *) cells, respectively. In terms of cell area, C-Src expressing cells behaved similarly to mCherry expressing cells, with the exception of GFP-RhoA-T19N, in which the area remained unchanged in relation to GFP and GFP-RhoA-WT cells (Figure 5.6A). Therefore, there was a significant increase in the average area of GFP-RhoA-T19N cells expressing C-Src-mCherry, compared to mCherry ($p=0.006$ **).

Amongst N1-Src-mCherry transfected cells, the area of GFP, GFP-RhoA-WT and -T19N containing cells was comparable, however GFP-RhoA-Q63L induced a significant reduction in the average cell area with respect to GFP-RhoA-WT ($p=0.015$ *) and -T19N

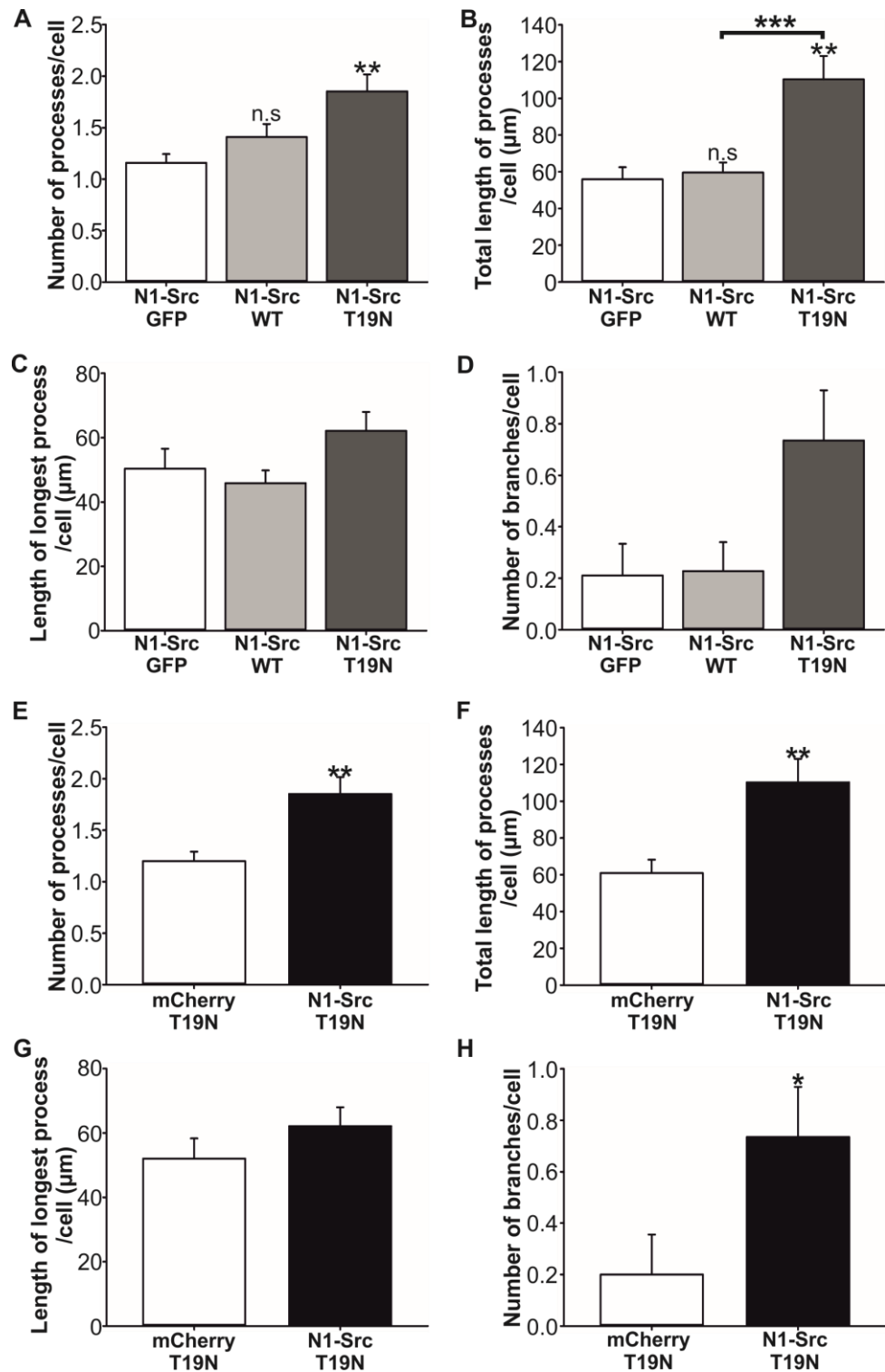


Figure 5.5: Process and Branch Formation is Enhanced in Cells Co-expressing N1-Src-mCherry and GFP-RhoA-T19N.

The average number of processes, total length of processes, length of longest process and number of branches per cell were determined for cells that were identified as extending processes and that were transfected with constructs encoding either N1-Src-mCherry and GFP (n=19), GFP-RhoA-WT (n=22) or -T19N (n=34; A-D), or GFP-RhoA-T19N and mCherry (n=20) or N1-Src-mCherry (n=34; E-H). The analysis was performed on data obtained from three experiments and statistical analyses were performed on the pooled data (see n numbers above) (* p<0.05, ** p<0.01, *** p<0.001).

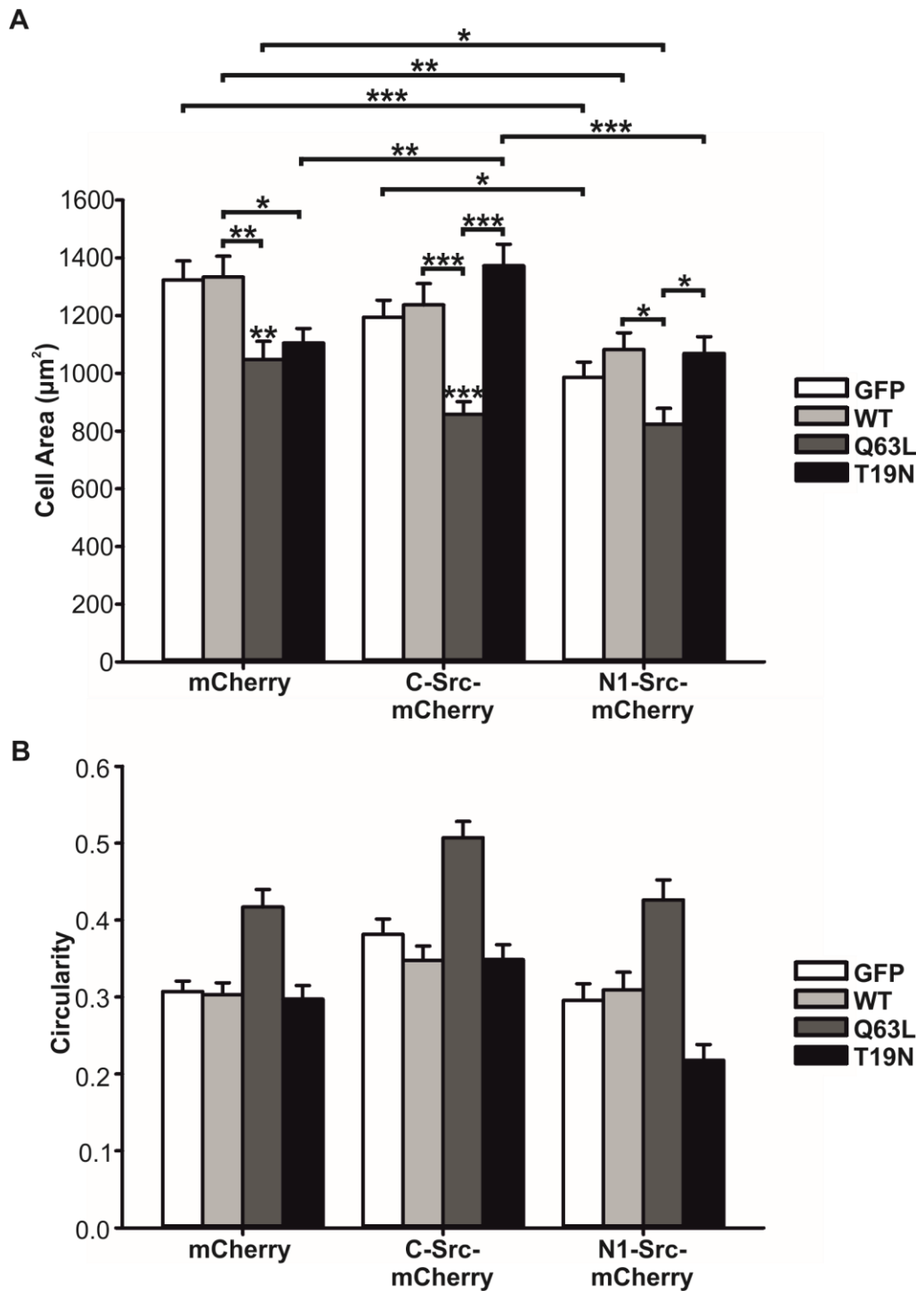


Figure 5.6: The Effects of N1-Src-mCherry and the GFP-RhoA Mutants on the Cell Area and Circularity of COS7 Cells.

The average cell area (**A**) and circularity (**B**) of cells were determined in ImageJ after tracing the perimeter of cells that were co-transfected with mCherry, C-Src- or N1-Src-mCherry and GFP, GFP-RhoA-WT, -Q63L or -T19N. The cells were transfected for 48 h, fixed and processed for immunofluorescence. The analysis was performed on 30 cells per condition, from a maximum of 15 fields of view. The experiments were performed 3 times and statistical analysis was performed on pooled data (n=90) using a two-way ANOVA. (* p<0.05, ** p<0.01, *** p<0.001).

($p=0.024$ *) (Figure 5.6A). In cells co-expressing N1-Src-mCherry and GFP, GFP-RhoA-WT or -Q63L, there was a significant reduction in cell area with respect to their mCherry expressing counterparts ($p<0.001$ ***, 0.011 *, 0.026 *, respectively). Whereas in GFP-RhoA-T19N expressing cells, the cell area was consistent with the corresponding mCherry control (Figure 5.6A).

In comparison to C-Src-mCherry cells co-expressing GFP or GFP-RhoA-T19N, there was a significant decrease in the cell area of the equivalent cells expressing N1-Src-mCherry ($p=0.045$ * and $p<0.001$ ***, respectively).

Taken together, these data indicated that in mCherry expressing cells, both GFP-RhoA-Q63L and -T19N reduced cell area in comparison to control and GFP-RhoA-WT cells. In addition, the results emphasised the fact that N1-Src-mCherry overexpression with GFP and the RhoA constructs reduced cell area with respect to their mCherry expressing counterparts, with exception of GFP-RhoA-T19N cells, which remained unchanged.

To further understand the effects of the RhoA constructs on cell morphology, in the presence or absence of C- and N1-Src-mCherry, the circularity of the cells was measured (Figure 5.6B). The data obtained indicated that the circularity of the cells expressing the different RhoA constructs was not dependent on the expression of the Src-mCherry construct.

In general, the circularity of the cells expressing GFP, GFP-RhoA-WT, -Q63L or -T19N appeared similar regardless of the presence of the mCherry constructs. However, it should be noted that the difference in the overall mean values of circularity were significantly different for C-Src-mCherry expressing cells with respect to mCherry and N1-Src-mCherry expressing cells. This reflects the slight increase in the circularity of C-Src-mCherry transfected cells in comparison to mCherry and N1-Src-mCherry transfected cells (Figure 5.6B). In addition to this, there was a statistically significant increase ($p<0.001$ ***) in the average circularity values of GFP-RhoA-Q63L expressing cells, with respect to the other Rho constructs (GFP, GFP-RhoA-WT and -T19N) (Figure 5.6B). It should also be noted that the circularity of cells co-expressing GFP-RhoA-T19N and N1-Src-mCherry, was reduced by approximately 30 and 40 % compared to their corresponding cells expressing mCherry and C-Src-mCherry, respectively (Figure 5.6B).

Overall these data suggested that whilst C-Src-mCherry expressing cells behaved similarly to mCherry expressing cells, N1-Src-mCherry appeared to promote process outgrowth and reduce cell area in GFP, GFP-RhoA-WT and -T19N cells (Figure 5.6A). A closer inspection of the morphology of process-extending cells provided additional evidence indicating that N1-Src-mCherry overexpression enhanced GFP-RhoA-T19N-

mediated process and branch formation. However, the Q63L RhoA mutant prevented N1-Src-mCherry-mediated process formation, increased cell circularity and decreased cell area further.

5.2.2 Manipulating RhoA-N1-Src Signalling via the Inhibition of Rho.

With the aim of providing further insight into the role of N1-Src in Rho signalling pathways, a selective inactivator of Rho isoforms A, B and C was used. Exoenzyme C3 transferase (C3) ADP-ribosylates an asparagine residue (Asp 41) in the effector binding region of Rho. This modification serves to inhibit the activation of Rho proteins via GEFs and results in the sequestration of ADP-ribosylated Rho-GDP in the Rho-GDI complex, in the cytosol (Figure 5.7, (Aktories et al., 2004)). Apart from also inactivating Rho B and C, this differs to the dominant negative RhoA mutation (T19N) because although RhoA is locked into the inactive GDP-bound form, T19N also sequesters RhoA GEFs, which might also interfere with the activation of other Rho family GTPases. In these studies, C- and N1-Src-mCherry were co-expressed with C3, to assess whether the kinases enhanced or reduced the effects of C3 inactivation.

Empty mCherry, C-Src- and N1-Src-mCherry constructs were co-transfected into COS7 cells with the empty vector pLINK or the Rho inhibitor C3 (pLINK-C3) to determine the effect of N1- and C-Src-mCherry on process outgrowth in cells containing inactivated RhoA, B, C.

Upon first inspection, cells co-transfected with pLINK and N1-Src-mCherry appeared smaller with many extending neurite-like processes from the cell body, whereas mCherry and C-Src-mCherry expressing cells were larger and more spread (Figure 5.8A). Both C- and N1-Src-mCherry were largely co-localised to the perinuclear regions of the cell (Figure 5.8A). However, when mCherry or the Src-mCherry constructs were co-expressed with C3, a large proportion of the cells exhibited a decrease in the area of the cell body, which also extended one or more neurite-like processes.

To quantify the effects of C3 on process formation in the presence of C- and N1-Src-mCherry, firstly, the percentage of cells with processes under each condition was analysed (Figure 5.8B). The analysis revealed that in control cells (pLINK) expressing N1-Src-mCherry, the percentage of cells with processes was significantly higher (28.9 %) than in mCherry (8.9 %; $p=0.004$ **) and C-Src-mCherry (7.8 %; $p=0.003$ **) expressing cells. When mCherry and C-Src-mCherry were co-expressed with C3, the RhoA/B/C inhibitor; there was a highly significant increase in the percentage of cells with processes from 8.9 % to 45.6 % ($p <0.001$ ***) and 7.8 % to 50 % ($p <0.001$ ***), respectively. Similarly, there was a large increase in C3 and N1-Src-mCherry expressing

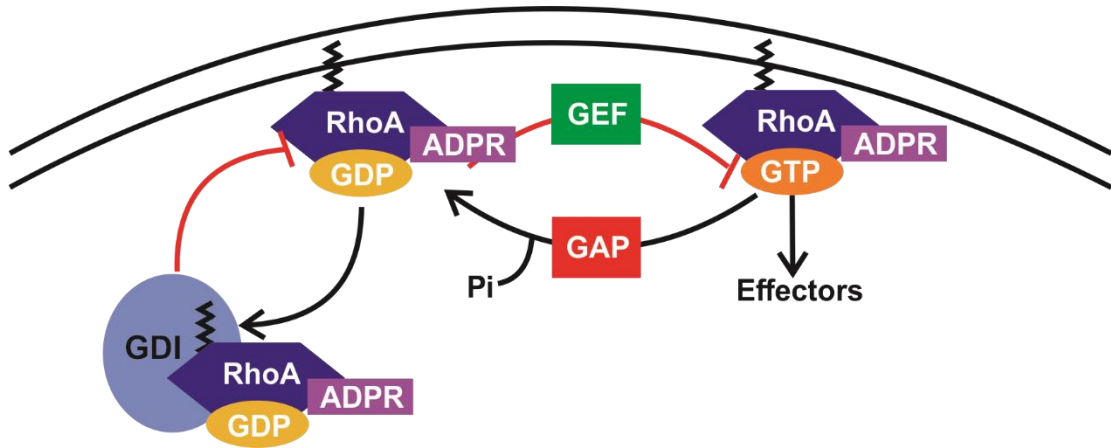


Figure 5.7: Schematic Diagram Illustrating the Inhibition of RhoA-C by C3.

The exoenzyme C3 transferase ADP-ribosylates RhoA at Asp-41. This modification inhibits Rho A, B and C by preventing the activation of Rho via GEFs and leading to the sequestration of ADP-ribosylated Rho-GDP in the Rho-GDI complex in the cytosol. (Adapted from Aktories *et al.*, 2004).

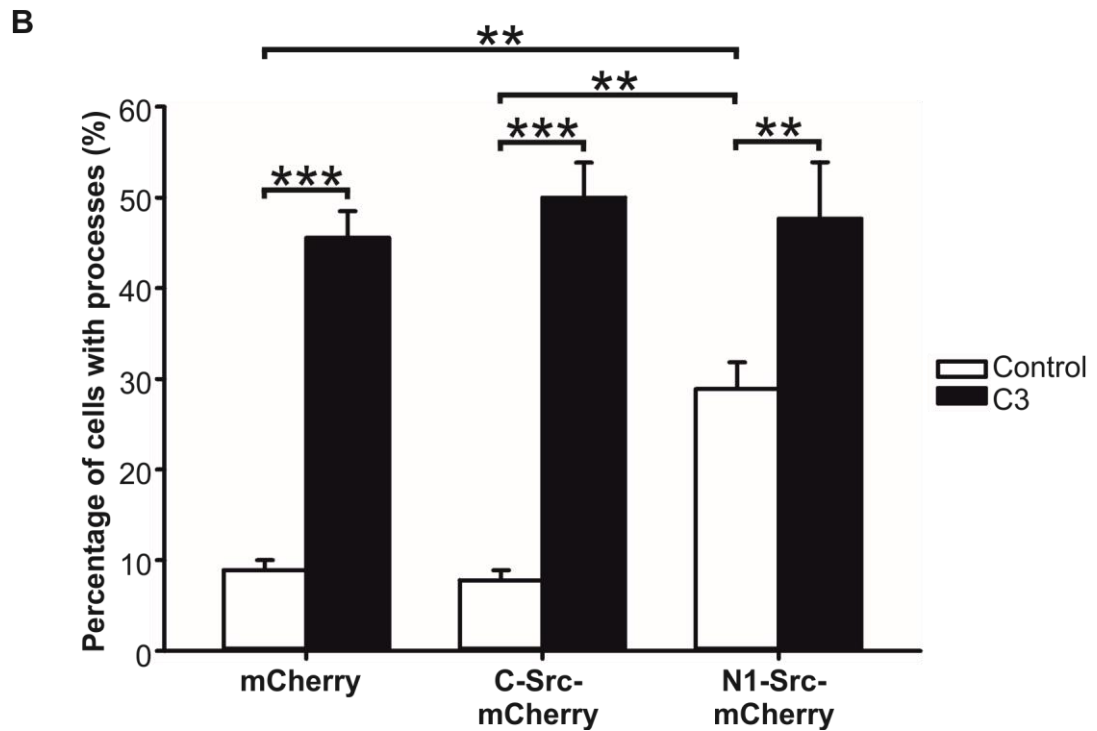
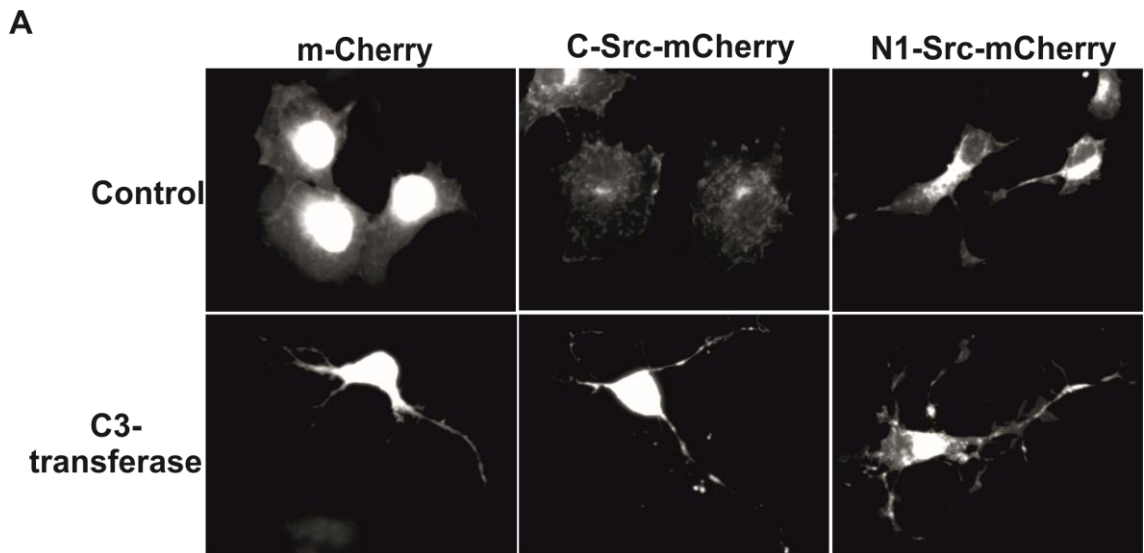


Figure 5.8: Overexpression of N1-Src-mCherry did not Enhance C3 Mediated Process Formation.

(A) Representative images of COS7 cells co-transfected with empty-, C-Src or N1-Src-mCherry and pLINK or pLINK-C3 (C3). Cells were transfected for 48 h, fixed and processed for immunofluorescence. Images were captured of 15 fields of view per condition using a fluorescence microscope. N=3, scale bar= 50 μ m. **(B)** The percentage of cells with processes was determined from 30 cells per condition, from a maximum of 15 fields of view. The experiments were performed 3 times and statistical analysis was determined using a two-way ANOVA (* $p < 0.05$, *** $p < 0.001$).

cells compared to control cells from 28.9 % to 47.2% ($p=0.003$ **). However, when comparing the percentage of C3 expressing cells with processes between groups, i.e. mCherry, C-Src- and N1-Src-mCherry expressing cells, there was very little difference (45.6, 50, and 47.2 %, respectively).

In addition to this, exactly the same data trends were observed when analysing the average number of processes per cell (data not shown).

These data demonstrated that both N1-Src and inactive Rho were capable of individually promoting process formation in control cells (i.e. pLink or mCherry expressing cells respectively), however N1-Src-mCherry was unable to further drive process outgrowth in cells containing inactive Rho above the levels observed in both mCherry and C-Src-mCherry expressing cells.

To further understand the effects of N1-Src-mCherry in C3 expressing cells, further morphological analysis was performed on the conditions that resulted in greater than 20 % of cells producing neurite-like processes (Figure 5.9). Of the cells co-expressing N1-Src-mCherry and C3 that formed processes, the average number of processes ($p=0.002$ **, Figure 5.9A), total length of processes ($p=0.006$ **, Figure 5.9B) and number of branches ($p=0.005$ **, Figure 5.9D) per cell were significantly elevated with respect to the corresponding GFP expressing cells, whereas process length remained unchanged (Figure 5.9C). However, when the same properties were compared amongst C3 expressing cells containing mCherry, C-Src- or N1-Src-mCherry, there were no significant changes (Figures 5.9 E-H). This suggested that N1-Src-mCherry overexpression did not enhance the effects of C3 on process or branch formation in COS7 cells.

In control (pLINK transfected) cells, there was a significant decrease in the mean area of cells expressing N1-Src-mCherry with respect to mCherry ($p < 0.001$ ***) and C-Src-mCherry ($p < 0.001$ ***) containing cells, which were comparable (Figure 5.10A). Interestingly, when mCherry and C-Src-mCherry were co-expressed with C3, the area of the transfected cells was significantly reduced to similar levels by approximately 40 % ($p < 0.001$ ***) (Figure 5.10A). Whilst the area of N1-Src-mCherry and C3 transfected cells decreased a further 22 % in comparison to control cells ($p=0.017$ *), the average cell area was not significantly different to cells co-expressing both C3 and mCherry or C-Src-mCherry (Figure 5.10A).

The trends in the differences in the circularity of the cells analysed (Figure 5.10B) were very similar to those observed with cell area. N1-Src-mCherry overexpression in control

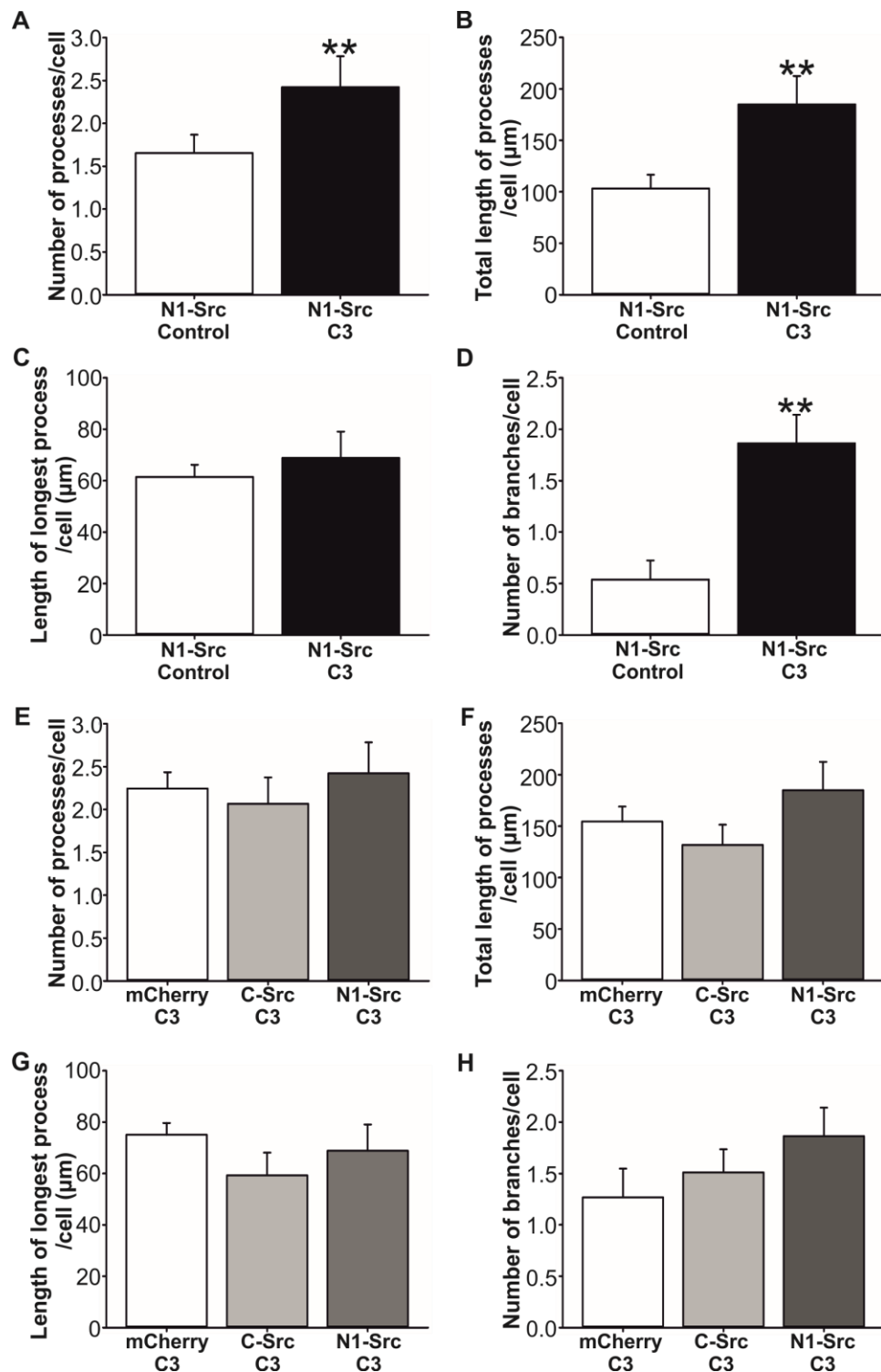


Figure 5.9: Process and Branch Formation, as well as the Length of Longest Process was Comparable in Cells Co-expressing C3 and empty-, C- or N1-Src-mCherry.

The average number of processes, total length of processes, length of longest process and number of branches per cell were determined for cells that were identified as extending processes and that were transfected with either N1-Src-mCherry and pLINK (n=26) or C3 (n= 45; A-D), or C3 and mCherry (n=41), C- (n=45) or N1-Src-mCherry (n=45; E-H) constructs. The analysis was performed on data obtained from three experiments and statistical analyses were performed on the pooled data (** p<0.01).

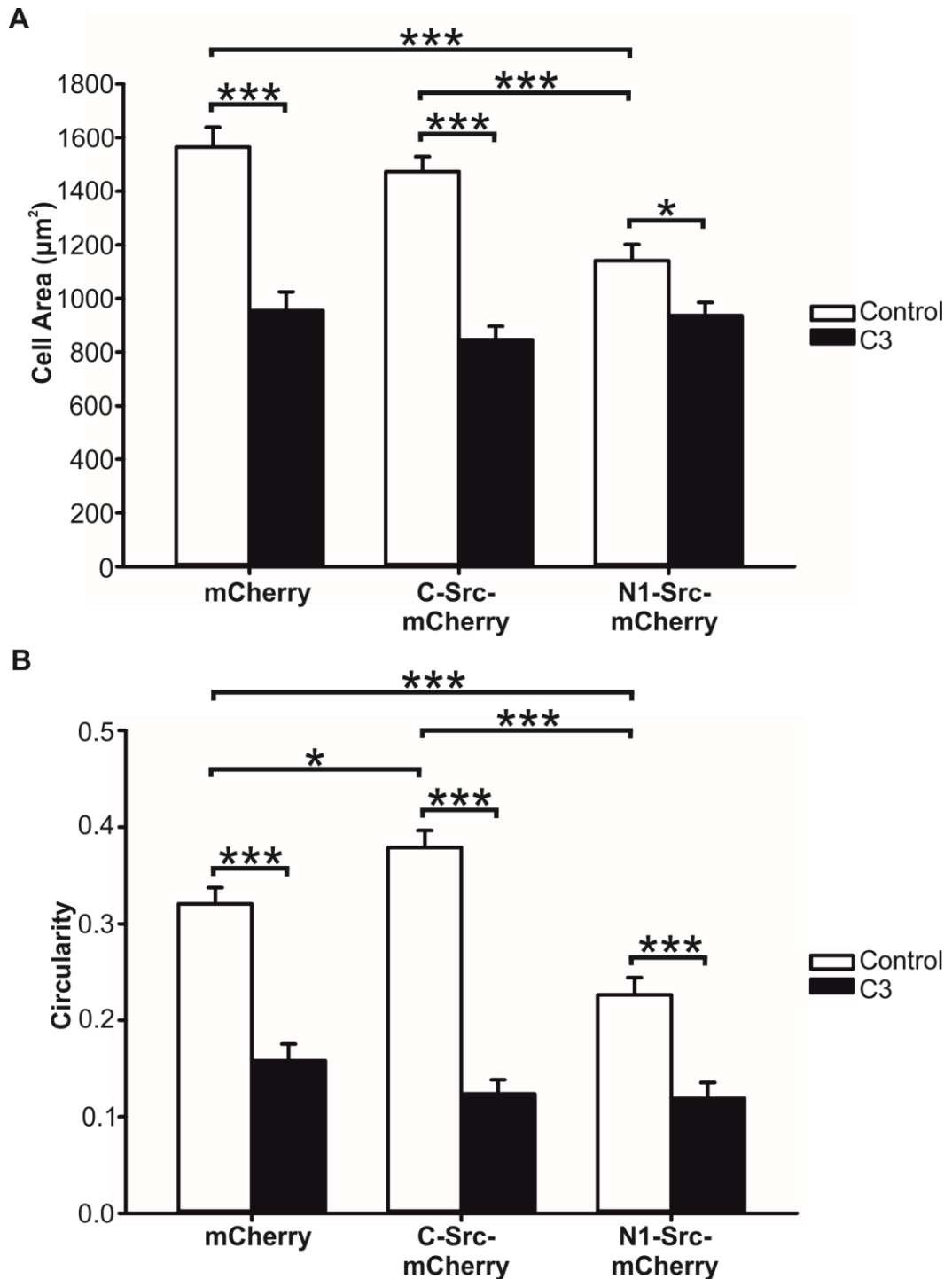


Figure 5.10: The Effects of the mCherry-Srcs and C3 Inactivation of Rho on the Cell Area and Circularity of COS7 Cells.

The average cell area (**A**) and circularity (**B**) of cells were determined in ImageJ after tracing the perimeter of cells that were co-transfected with mCherry, C-Src- or N1-Src-mCherry constructs and pLINK (control) or pLINK-C3 (C3). The cells were transfected for 48 h, fixed and processed for immunofluorescence. The analysis was performed on 30 cells per condition, from a maximum of 15 fields of view. The experiments were performed 3 times and statistical analysis was performed on pooled data (n=90) using a two-way ANOVA. (* p<0.05, *** p<0.001).

(pLINK) cells resulted in a significant reduction in circularity of the cells with respect to mCherry and C-Src-mCherry transfected cells ($p < 0.001$ ***), indicating the shape of the cells expressing N1-Src-mCherry were more elongated, which is visible in Figure 5.8A. Notably, in C-Src-mCherry expressing cells, there was a significant increase in circularity with respect to mCherry expressing cells ($p < 0.038$ *). When co-expressed with C3, the circularity in mCherry, C- or N1-Src-mCherry expressing cells was significantly reduced ($p < 0.001$ ***) to similar levels, in comparison to control cells (Figure 5.10B).

Taken together, these results indicated that the overexpression of N1-Src-mCherry in COS7 cells results in a similar, yet weaker phenotype to the inactivation of RhoA by C3. N1-Src-mCherry overexpression in pLINK transfected cells resulted in an increase in the percentage of cells with processes (Figure 5.8B) and a decrease in cell circularity (Figure 5.10B) as well as cell area (Figure 5.10A) compared to mCherry containing cells. Cells overexpressing C-Src-mCherry largely resembled mCherry expressing cells with the exception that C-Src-mCherry containing cells had a higher circularity. Irrespective of the presence of C- or N1-Src-mCherry, the percentage of cells with processes (Figure 5.8), circularity and cell area (Figure 5.10) was comparable in C3 expressing cells. A more in depth analysis of the cells extending processes also revealed that C3 had the same effects on the average number of processes (Figure 5.9E), total length of processes (Figure 5.9F), length of longest process (Figure 5.9G) and number of branches per cell (Figure 5.9H) in mCherry, C-Src and N1-Src-mCherry containing cells. This indicated that N1-Src-mCherry did not enhance the effects of C3 within this experimental system. This result was different to that in Figure 5.4, where N1-Src-mCherry enhanced process outgrowth above control levels in GFP-RhoA-T19N (dominant negative) transfected cells.

5.2.3 Overexpression of GFP-RhoA-WT, -Q63L and -T19N did not Affect N1-Src-FLAG Activity in COS7 Cells.

The effect of the overexpression of GFP-RhoA-WT, -Q63L and -T19N on the activation status of N1-Src- in comparison to C-Src-FLAG was explored to determine whether the kinase acts downstream of RhoA under basal conditions (Figure 5.11). Phosphorylation of the kinase on Tyr-416 (Y416) in the active site is a marker of kinase activity. The different GFP-RhoA constructs (including GFP) were co-expressed with either C- or N1-Src-FLAG and kinase activity was detected via Western Blotting.

Phosphorylation of C-Src-FLAG at Tyr-416 was elevated in the presence of GFP-RhoA-WT in comparison to cells overexpressing GFP alone. However, the GFP-RhoA-Q63L and -T19N mutants did not enhance C-Src-FLAG activity over the levels observed in GFP and C-Src-FLAG expressing cells. It should be noted that expression of levels of

the different RhoA mutants varied, which may account for the reduced C-Src activity seen in GFP-RhoA-mutant and C-Src-FLAG expressing cells. Upon first inspection, N1-Src-FLAG activity, in cells co-expressing N1-Src-FLAG and GFP-RhoA Q63L, appeared reduced compared to GFP, GFP-RhoA-WT and -T19N expressing cells. However, the amount of N1-Src-FLAG also appears reduced, which could account for this observation. Therefore, overall, N1-Src-FLAG activity did not appear to be affected by GFP-RhoA-WT, -Q63L or -T19N.

In figure 5.11B, the levels of Tyr-416 phosphorylation were quantified by performing densitometry analysis of the protein bands from three biological replicates. Since the protein levels of Src-FLAG and the GFP-RhoA mutants appeared to vary between conditions, phosphorylation of Tyr-416 was normalised to the amounts of both Src-FLAG and RhoA-GFP.

In C-Src-FLAG transfected cells, the results indicated that Tyr-416 phosphorylation appeared slightly higher when cells were co-transfected with GFP-RhoA-WT or -Q63L in comparison to control cells. Whereas C-Src-FLAG and GFP-RhoA-T19N co-transfected cells displayed even higher levels of kinase activity with respect to control cells. However, statistical analysis of these data confirmed that these observations were insignificant. In cells co-transfected with N1-Src-FLAG and GFP, GFP-RhoA-WT or -Q63L, the level of Tyr-416 phosphorylation was similar between conditions. This was slightly elevated in N1-Src-FLAG cells co-expressing GFP-RhoA-T19N, although this observation was not significant. Overall, these data indicated that the co-expression of neither C- nor N1-Src-FLAG with the GFP-RhoA mutants resulted in significant changes to the activity of the kinases.

It should also be noted that the baseline level of Tyr-416 phosphorylation in N1-Src-FLAG transfected cells was elevated, when compared to C-Src transfected cells. However, the error bars on the N1-Src data points were particularly large, indicating that a high degree of variation occurred within the three biological replicates. In addition, there was no significant interaction between the C-Src- and N1-Src-FLAG data. Further repeats of this data set should be performed in order to determine the potential differences between the kinase activity of C-Src- and N1-Src-FLAG in COS7 cells.

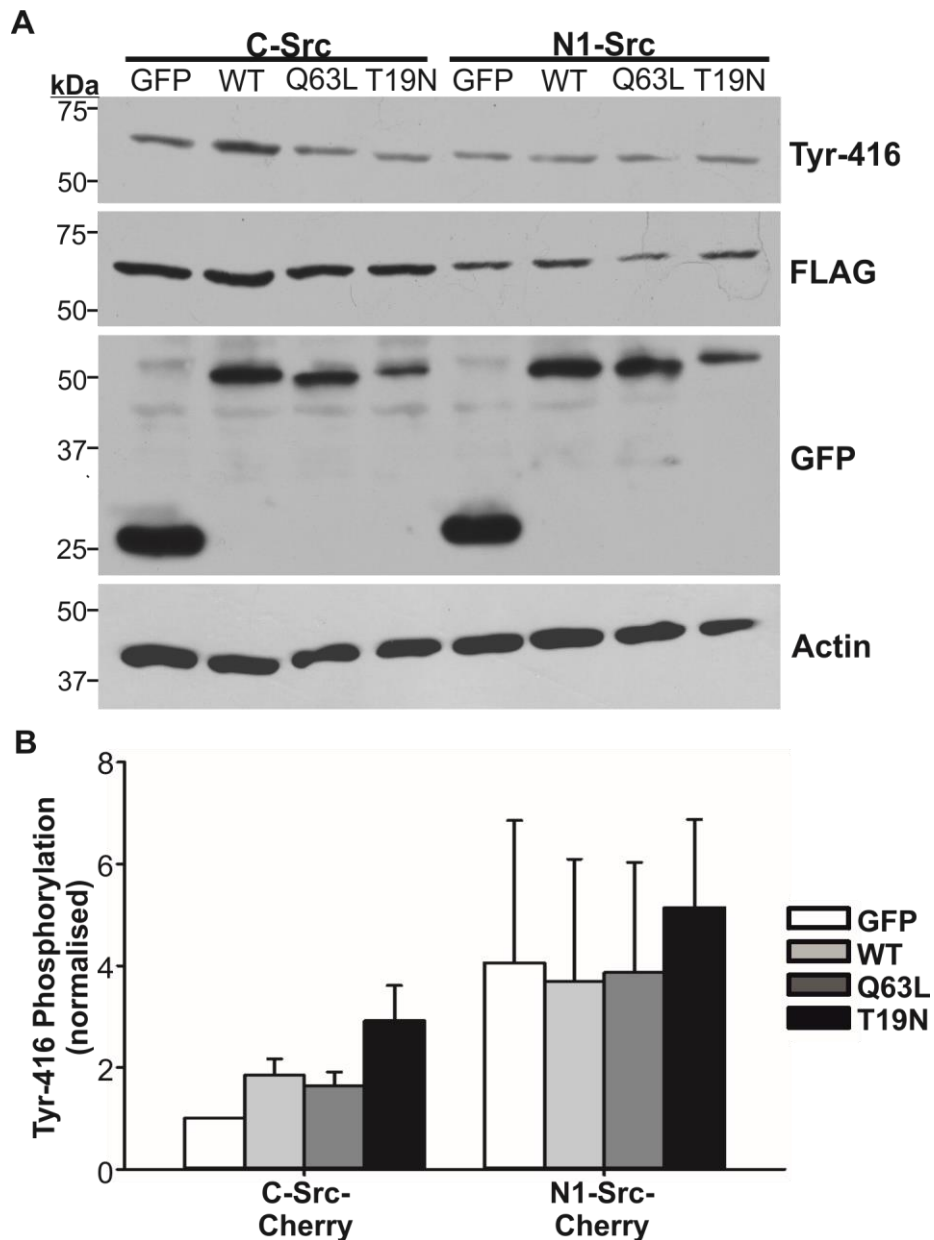


Figure 5.11: Overexpression of GFP-RhoA-WT, -Q63L or -T19N had Little Effect on C- or N1-Src-FLAG Activity.

COS7 cells were co-transfected with C-Src- or N1-Src-FLAG and GFP, GFP-RhoA-WT, -Q63L or -T19N. The cells were transfected for 48 h, lysed, separated by SDS PAGE and subject to Western blot analysis. Kinase activity was assessed by monitoring the phosphorylation of Tyr-416. The blots shown are a representative of n=3. B) Tyr-416 phosphorylation was quantified by performing densitometry in ImageJ. Phosphorylation of Tyr-416 was normalised to the amounts of Src-FLAG and GFP-RhoA and statistical analysis of the data (n=3) was performed using a two-way ANOVA.

5.2.4 N1-Src and C-Src-FLAG Interacted with Active GFP-RhoA-WT in COS7 Cells.

Since N1-Src appeared to co-localise with GFP-RhoA-WT and -T19N (Figure 5.3), the possibility that N1-Src interacts with RhoA was investigated. An immunoprecipitation (IP) using α -GFP conjugated resin that bound the GFP-tagged RhoA-WT was performed to determine whether N1-Src-FLAG could be pulled-down with the GTPase in COS7 cells (Figure 5.12). Further negative controls were performed to confirm that N1-Src-FLAG did not interact with GFP and that GFP-RhoA-WT did not interact FLAG alone. Whilst these controls were verified, N1-Src-FLAG did not appear to be pulled-down by GFP-RhoA-WT.

As p190RhoGAP has previously been shown to interact with RhoA, as a positive control, the blot was probed with a p190RhoGAP specific antibody, however the protein could not be detected in either the input or pull-down lanes (data not shown).

The overexpression of constitutively active C-Src has previously been linked to RhoA phosphorylation in mouse 3T3 cells and directly inactivates RhoA activity (Uezu et al., 2012). However, GFP-RhoA-WT did not appear to be phosphorylated in N1-Src-FLAG overexpressing cells (Figure 5.12). It should also be noted that in the input lanes for the cell lysates containing N1-Src-FLAG, bands representing a phospho-tyrosine modified protein, which corresponded to the molecular weight of N1-Src, were present. However, this was not detected in the GFP-RhoA-WT/N1-Src-FLAG IP lane (Figure 5.12). Together these results suggested that N1-Src neither phosphorylates nor interacts with RhoA WT. However, the inclusion of a further positive control to demonstrate that GFP-RhoA-WT interacts with known binding partners (e.g. p190rhoGAP) will be required to verify the latter result.

5.2.4 C- and N1-Src-FLAG Evoked Differential Effects on the Activation of GFP-RhoA-WT.

Previous experiments have suggested that N1-Src-FLAG does not bind to or phosphorylate GFP-RhoA-WT under basal cellular conditions, however, these studies did not provide evidence regarding the effect of the kinase on GTPase activity. Therefore, to assess the effect of both C- and N1-Src-FLAG on RhoA activity, a commercial RhoA GTPase activation assay kit was used.

The basis of this assay relies upon the well characterised interaction between the RhoA binding domain (RBD) of Rhotekin (a RhoA effector) and RhoA-GTP. The kit consists of a pull-down assay that can be used to indicate the levels of GTP-bound RhoA in treated

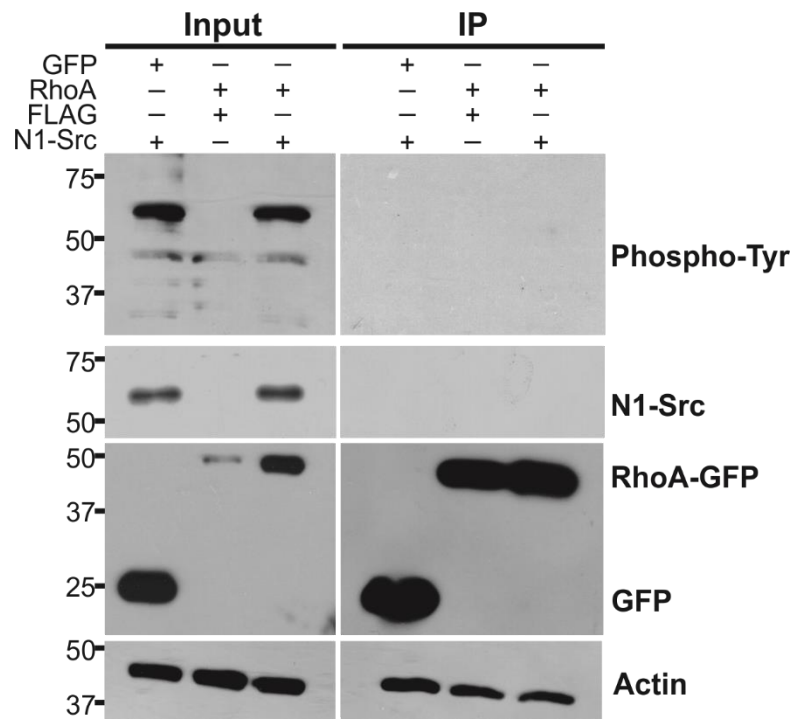


Figure 5.12: N1-Src-FLAG neither Interacted with nor Phosphorylated GFP-RhoA-WT.

COS7 cells were co-transfected with Empty- or N1-Src-FLAG and GFP or GFP-RhoA-WT constructs for 48 h. The cells were lysed in RIPA buffer and GFP or GFP-RhoA-WT was immunoprecipitated from cell lysates using an α -GFP resin. Input (1 %) and immunoprecipitation (IP) samples were separated by SDS-PAGE and subject to Western blot analysis. The blots shown are representative of the results obtained for n=3.

cells. The advantage of using this kit is that it is designed to monitor the activation status of endogenous cellular RhoA, however this proved technically difficult. Whilst GTP loaded RhoA was easily detected (positive control), in two separate experiments, either trace levels or no active RhoA were detected in cell lysates containing Empty-, C-Src- or N1-Src-FLAG. Therefore, it was difficult to deduce any conclusions from these data regarding the effects of the kinases (data not shown).

Taking this into account, the experiment was repeated in cells that were transfected with GFP-RhoA-WT (Figure 5.13). In addition to controls, whereby cells were loaded with either GDP (negative) and GTP (positive), which confirmed the GFP-tagged GTPase was functional, further controls, were transfected with either GFP-RhoA-Q63L (positive) or -T19N (negative). In the case of GFP-RhoA-T19N expressing cells, no signal indicating the presence of GFP-RhoA-GTP was detected, whereas a large signal was observed for the cells that contained GFP-RhoA-Q63L (Figure 5.13).

The result observed for the GFP-RhoA-T19N negative control implied that the GFP tag had no affinity for the GST-Rhotekin RBD resin. In comparison to cells that co-expressed both GFP-RhoA-WT and an empty FLAG construct, C-Src-FLAG appeared to evoke an increase in the amount of GTP-bound GFP-RhoA-WT. This was also true for N1-Src-FLAG expressing cells but to a lesser extent than for C-Src. The PVDF membrane containing the pull-down samples was probed with an α -FLAG antibody to determine whether the kinases co-purified with GFP-RhoA-GTP. Both C-Src- and a small amount N1-Src-FLAG were detected in the pull-downs.

Taken together, these results suggested that both C- and N1-Src-FLAG activate GFP-RhoA-WT under basal cellular conditions and interact with GFP-RhoA-GTP but this interaction is much weaker in N1-Src-FLAG transfected cells. In order to confirm the results obtained in this assay, replicate experiments must be performed. In order to confirm the results obtained in this assay, replicate experiments must be performed. In addition, a further negative control that would involve a GST-Rhotekin pulldown in the absence of GFP-RhoA-WT should be included, to discount the possibility that C- or N1-Src could be binding to Rhotekin .

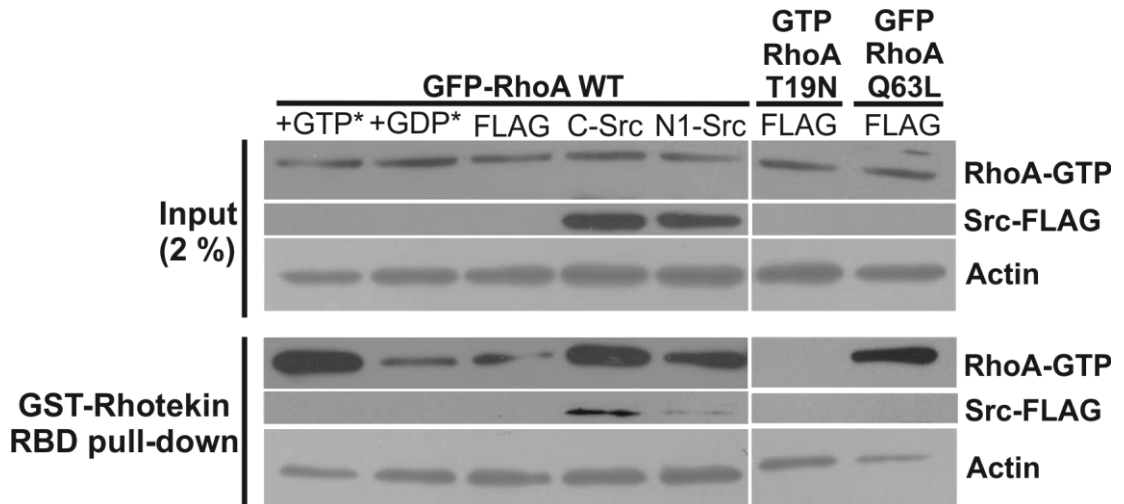


Figure 5.13: C- and N1-Src have Differential Effects on the Activation Status of GFP-RhoA.

COS7 cells were co-transfected with Empty-, C-Src or N1-Src-FLAG and GFP-RhoA-WT, -T19N (negative control) or -Q63L (positive control) constructs for 48 h. In the first two lanes, cell lysates were pre-loaded with either GTP (positive control) or GDP (negative control). Using a RhoA GTPase kit, the cells were lysed and samples were incubated with GST-Rhotekin-RBD resin to pull-down active GTP-bound GFP-RhoA. Input (2 %) and pull-down samples were separated by SDS-PAGE and subject to Western blot analysis. N=1, *cells were co-transfected with an Empty FLAG vector.

5.3 Discussion

5.3.1 Dissecting the Role of N1-Src and RhoA in the Regulation of Process Outgrowth in COS7 Cells.

The studies conducted in Chapter 5 sought to determine whether N1-Src-mediated process outgrowth in COS7 cells is dependent upon RhoA inactivation. Using a combination of RhoA mutants and a RhoA inhibitor in COS7 cells, as well as biochemical approaches, the role of N1-Src in RhoA signalling was dissected. The outcomes of these experiments are discussed below.

5.3.1.1 *The Effect of N1-Src-mCherry on Cell Morphology*

When overexpressed in COS7 cells, N1-Src-mCherry promotes process formation; this was demonstrated in Figures 5.4 and 5.8 and has previously been shown in the Evans lab (Keenan, 2012). Despite the fact that there was not a statistically significant difference in the percentage of cells with processes between the cells co-expressing either of the Src-mCherry and GFP-RhoA constructs (Figure 5.4A), the overall mean percentage of cells with processes for N1-Src-mCherry transfected cells was significantly higher than that of mCherry and C-Src-mCherry expressing cells. In addition to increasing process formation, N1-Src-mCherry overexpression also resulted in a significant reduction in cell area (Figure 5.6A) and in some cases, circularity (Figure 5.10B). This model was used, in conjunction with biochemical studies, to test the hypothesis that N1-Src regulates cell morphology of COS7 cells (in particular process formation) via the inhibition of RhoA.

To test the effects of N1-Src on RhoA signalling (or vice versa), N1-Src-mCherry was overexpressed with different GFP-RhoA constructs and a RhoA inhibitor (C3). Overexpression of the GFP-RhoA-mutants and C3 had distinct effects on cell morphology themselves (Figures 5.3-6 and 5.8-10) and will be discussed in Section 5.3.1.2-4 to follow.

5.3.1.2 *The Effect of RhoA Inactivation on Cell Morphology*

GFP-RhoA-T19N (dominant negative mutant) expression resulted in an elevation of process formation (Figure 5.4), a reduction in cell area (Figure 5.6A), but cell circularity remained unaffected (Figure 5.6B). This mimicked the effects of N1-Src-mCherry overexpression, suggesting that signalling resulting from GFP-RhoA inactivation (T19N) and via N1-Src worked towards a common goal. This was supported by the observation that inhibition of all three Rho proteins (A, B and C) also resulted in elevated process outgrowth (Figure 5.8).

Analysis of process formation in cells co-expressing N1-Src-mCherry and GFP-RhoA-T19N in comparison to the corresponding mCherry or GFP expressing cells, produced conflicting results (Figure 5.4). The percentage of cells with processes in cells co-expressing mCherry and GFP-RhoA-T19N or N1-Src-mCherry and GFP were very similar (~20-25 %). When N1-Src-mCherry and GFP-RhoA-T19N were expressed together the effect on the percentage of cells with processes was almost additive (~40 %), which suggested that N1-Src-mCherry and GFP-RhoA-T19N act through separate pathways (Figure 5.4A).

However, when quantifying the average number of processes per cell (Figure 5.4B), the effect appeared synergistic (more than additive), which would suggest that both GFP-RhoA-T19N and N1-Src-mCherry were working together to enhance process formation (Figure 5.4B). However, this would be unlikely to be as a result of N1-Src-mCherry inhibiting the GTPase, since the T19N construct is dominant negative, thus RhoA is already inactivated.

An in depth analysis of the cells that contained the construct combinations that produced greater than 20 % of cells with processes (Figure 5.5), revealed that whilst the average number of processes was significantly higher in N1-Src-mCherry and GFP-RhoA-T19N co-transfected cells, the effect appeared to be additive, rather than synergistic (Figure 5.5A). This agreed with the data presented in Figure 5.4A, which suggested that N1-Src and RhoA act via separate pathways to drive process formation in COS7 cells. The presence of N1-Src-mCherry in GFP-RhoA-T19N expressing cells, had a significant impact on the number of branches per cell (~0.7 branches per cell), compared to GFP-RhoA-T19N cells expressing the mCherry control (~0.2 branches per cell, Figure 5.5H). Comparing this result to the number of branches per cell observed for GFP and N1-Src-mCherry expressing cells (~0.2 branches per cell, Figure 5.5D) the effect of N1-Src-mCherry and GFP-RhoA-T19N together appeared to be synergistic. However, confidence in this result should be improved by increasing the sample size, since the error bars were very large.

5.3.1.3 The Effect of the RhoA/B/C Inhibition on Cell Morphology

A further experiment that was aimed at understanding the potential interplay between N1-Src and RhoA GDP-mediated process outgrowth, was performed using the RhoA/B/C inhibitor C3 (Figures 5.8-10). In this experiment, almost 50 % of cells transfected with pLINK-C3 produced processes regardless of the Src-mCherry status of the cells (Figure 5.8B). However, the percentage of cells with processes when N1-Src-mCherry was co-expressed with pLINK-C3 did not appear to be the result of an additive effect of the percentages of cells with processes when mCherry and C3 or N1-Src-

mCherry and pLINK (control) were co-expressed (Figure 5.8B). This result differed from the additive effect seen when N1-Src-mCherry and GFP-RhoA-T19N were co-expressed (Figure 5.5A), which suggested that both N1-Src and inactive RhoA work via separate pathways. There are multiple explanations that could explain this outcome.

Firstly, since all of the cell parameters that were measured were comparable in C3 expressing cells (Figure 5.8B), it is possible that within the experimental system used, maximal phenotypic effects were observed and therefore the effects of additional stimulators of process outgrowth (i.e. N1-Src) were not clearly represented. A second theory is that N1-Src-mCherry drives RhoB or C inactivation, which is why an additive effect on neurite outgrowth was not observed, since the Rho GTPases were inhibited by C3. Alternatively, the opposite could have occurred, whereby inactive Rho B or C antagonised N1-Src-mCherry mediated process formation. However, it seems unlikely that inactive Rho would serve to inhibit N1-Src, when they are working towards a common goal and this also appears to be the function of active RhoA (discussed in Section 5.3.1.5).

Before a valid conclusion can be deduced from the C3 data, a dose response experiment using a commercial cell permeable C3 protein should be performed to ascertain the upper boundaries of the model, and determine the validity of the results obtained. Alternatively, a similar titration could be performed using a small molecule inhibitor of RhoA, namely Rhosin (Merck Millipore, Watford, UK)(Shang et al., 2012).

5.3.1.4 The Effect of Constitutively Active RhoA on Cell Morphology.

In cells overexpressing GFP-RhoA-Q63L (constitutively active mutant), process formation remained comparable to the GFP control (Figure 5.4), whereas cell area decreased (Figure 5.6A) and circularity increased (Figure 5.6B). This was in line with the known function of active RhoA, which promotes stress fibre formation and acto-myosin contractility.

The data for the co-expression of N1-Src-mCherry with GFP-RhoA-Q63L, suggested that this RhoA mutation prevented N1-Src mediated process formation (Figure 5.4). In addition to this, the circularity of N1-Src-mCherry and GFP-RhoA-Q63L co-expressing cells (Figure 5.6B) was equivalent to the cells co-expressing GFP-RhoA-Q63L and the mCherry control, whereas cell area was significantly reduced (Figure 5.6A) when N1-Src-mCherry was present versus mCherry alone. However, there was not a significant difference in cell area when GFP or GFP-RhoA-Q63L were co-expressed with N1-Src-mCherry. The constitutive activation of RhoA probably inhibited N1-Src mediated process outgrowth via cross-talk with the N1-Src signalling pathway. Co-expression of N1-Src-mCherry with GFP-RhoA-Q63L did not appear to directly affect N1-Src activity,

however this does not discount the fact that RhoA-Q63L could disrupt a signalling pathway downstream of N1-Src.

5.3.1.5 The Effect of N1-Src-on the Activation of RhoA

Under basal conditions, in cells containing GFP-RhoA-WT, there is a mixture of GDP- and GTP-bound RhoA, which was evidenced by the RhoA GTPase activation assay (Figure 5.13). This could explain the fact that the GFP-RhoA-WT cell morphological phenotype lay somewhere in between that of GFP-RhoA-Q63L and-T19N when co-expressed with the mCherry control. The opposing roles of GDP- and GTP-bound RhoA, the latter of which was demonstrated to be enhanced by N1-Src-FLAG expression (Figure 5.13), could also account for the phenotype observed in cells co-expressing GFP-RhoA-WT and N1-Src-mCherry, whereby neither the percentage of cells with processes (Figure 5.4A), nor the average number of processes per cell (Figure 5.4B) were altered with respect to the cells co-expressing N1-Src-mCherry and the GFP control.

Finally, the RhoA GTPase activation assay revealed that in cells transfected with N1-Src-FLAG and GFP-RhoA-WT, the kinase promoted the activation of RhoA and some N1-Src-FLAG was pulled down with active (GTP-bound) RhoA (Figure 5.13). Whilst this experiment needs to be repeated, one explanation for N1-Src serving to activate RhoA, could be that the kinase forms part of a negative feedback loop modelled in Figure 5.14. This would involve the self-regulation of N1-Src mediated process outgrowth. This type of regulation is not uncommon, and since COS7 cells would not ordinarily form neurite-like processes, the existence of a negative feedback regulatory step could be feasible. Since small amounts of N1-Src-FLAG appeared to be pulled down with GFP-RhoA-WT-GTP, it is possible that N1-Src could form part of a complex with RhoA-GTP, in which it serves to regulate the activity of a Rho GEF to facilitate RhoA activation. In order to test this, it would be interesting to perform mass spectrometry on the proteins that are pulled-down in complex with RhoA, to identify candidate substrates.

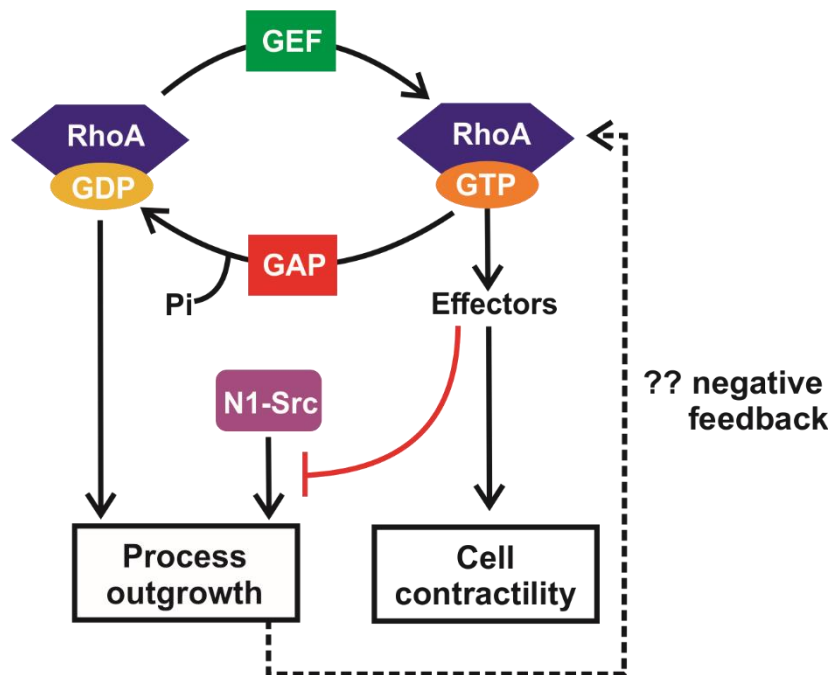


Figure 5.14: Schematic of the Proposed N1-Src/RhoA Signalling Pathway Regulating COS7 Cell Morphology.

Both GDP-bound RhoA and N1-Src promote process outgrowth in COS7 cells, whereas activation of RhoA results in stress fibre formation and acto-myosin contractility and inhibits N1-Src mediated process outgrowth. In a proposed negative feedback loop, N1-Src mediated process outgrowth may be self-regulated by activating RhoA.

5.3.2 The Alternate Roles of C- and N1-Src in RhoA Signalling

For the most part of this chapter, the roles of both C- and N1-Src-mCherry in RhoA signalling were investigated, enabling a comparison of the two kinases. In Figure 5.9B (C3 experiment), there was a significantly reduced proportion of cells extending processes amongst control cells (pLINK transfected) expressing C-Src-mCherry in comparison to N1-Src-mCherry. This data was also supported by the data in Figure 5.4, in which the overall average percentage of cells with processes in cells overexpressing C-Src-mCherry and the RhoA constructs, was also significantly reduced with respect to the corresponding N1-Src-mCherry expressing cells. In addition to this, the overall average value of circularity (Figure 5.10B) for C-Src-mCherry transfected cells was significantly higher in comparison to Empty- and N1-Src-mCherry containing cells. Since increased circularity is a feature of GFP-RhoA-Q63L expressing cells (Figure 5.6B), this observation could be in part related to the fact that C-Src-FLAG overexpression appeared to activate GFP-RhoA-WT in COS7 cells, under basal cellular conditions (Figure 5.13).

The average area of the cells co-expressing C-Src-mCherry and GFP was similar to their mCherry expressing counterparts, however the cell area of N1-Src-mCherry containing cells was significantly reduced (Figure 5.6A). When combined, these data highlighted the opposing roles of C- and N1-Src in the regulation of cell morphology. Whilst C-Src-mCherry expressing cells appeared more rounded and spread, N1-Src-mCherry promoted process outgrowth and shrinking of the cell body.

In C-Src-mCherry transfected cells, process formation did not vary significantly in GFP-RhoA-WT, -Q63L and -T19N cells in comparison to the GFP control (Figure 5.4). There was also no observable difference in process formation between C-Src-mCherry cells co-expressing either GFP-RhoA-Q63L or -T19N. In contrast, a significant difference in the average number of processes per cell was observed between the GFP-RhoA-Q63L and -T19N cells co-expressing either mCherry or N1-Src-mCherry (Figure 5.4B). However, the error bar for the percentage of cells with processes in C-Src-mCherry and GFP-RhoA-T19N co-transfected cells was particularly large (Figure 5.4A), therefore further repeats of this dataset would increase confidence in this outcome. Despite this large error bar, these data further emphasised the difference between the effects of C- and N1-Src-mCherry on process outgrowth in COS7 cells, whereby C-Src-mCherry had little effect on process formation and cells behaved similarly to mCherry control cells.

5.3.2.1 The Differential Activation of RhoA by N1 and C-Src

Surprisingly, preliminary data suggested that C-Src activated RhoA to a greater extent than N1-Src under basal cellular conditions (Figure 5.13). Whilst it seems sensible that

C-Src would activate RhoA more so than N1-Src, given the role of N1-Src in process outgrowth, the majority of the literature linking C-Src with RhoA, conclude that C-Src serves to inactivate RhoA (Arthur et al., 2000, Brouns et al., 2001).

In neurons, the inactivation of RhoA via p190RhoGAP, which has been shown to be a major substrate of Src in the brain, promotes axon outgrowth and fasciculation and formed part of the basis for the investigation in this chapter (Brouns et al., 2001). Moreover, in non-neuronal cells types, C-Src-mediated inactivation of RhoA via the stimulation of p190RhoGAP activity in response to integrin engagement, has been widely studied and plays a key role in the regulation of cell-matrix adhesion, cell spreading and migration (reviewed in Huveneers and Danen, 2009). Although it should be noted that in the latter studies, this mechanism was dependent on the engagement of integrins via an extracellular stimulus, whereas the studies in this chapter were performed under basal conditions.

One possible pathway through which C-Src could promote RhoA activation is via the regulation of RhoGDI. RhoGDI binds inactive RhoA, prevents activation of the GTPase and sequesters the protein into the cytosol. Co-transfection of constitutively active C-Src and RhoGDI in HeLa cells revealed that the kinase phosphorylates RhoGDI under basal conditions (DerMardirossian et al., 2006). This was shown to largely reduce the amounts of RhoA, Rac1 and Cdc42 in complex with RhoGDI, resulting in an increase in membrane localised RhoGDI.

Although the direct effects on Rho GTPase activation were not shown biochemically, diminished levels of the RhoA, Rac1 and Cdc42 in complex with RhoGDI appeared to increase cell spreading and membrane ruffling; functions that are associated with the activation of Rho GTPases.

5.3.3 RhoA as a Binding Partner for N1-Src

Preliminary data also suggested that both C- and N1-Src-FLAG interacted with GFP-RhoA-GTP and that this interaction appeared proportional to the degree of RhoA activation (Figure 5.13). Although this interaction needs to be confirmed by repeating the experiment with further controls, this observation could potentially reinforce the idea that C-Src substrates bind poorly to and are weakly phosphorylated by N1-Src. This phenomenon was proposed by Keenan *et al.*, (2015) and has also been alluded to in multiple other studies, whereby the N1-Src SH3 domain has been shown to bind multiple proteins including CR16, Synapsin and DAAM1 with reduced affinity in comparison to C-Src (Weiler et al., 1996, Onofri et al., 1997, Aspenstrom et al., 2006). In addition to this, other studies have shown that some C-Src SH3 binding partners, such as SNP70,

ASAP1 and RICH1, are unable to bind N1-Src (Richnau and Aspenstrom, 2001, Craggs et al., 2001, Brown et al., 1998).

Taking the above evidence into account, it is possible that both C- and N1-Src-FLAG activated GFP-RhoA-WT by modulating the same substrate. If this was the case, how the interaction between both C- or N1-Src with active RhoA, could relate to a potential mechanism involving the phosphorylation of RhoGDI is unclear, and should be the subject of future studies. Alternatively, N1-Src could be acting via a completely separate mechanism to C-Src. To address this, it would be interesting to perform mass spectrometry on the Src-RhoA-GTP complexes to identify and compare the potential binding partners and substrates of the kinases.

5.3.4 Concluding Remarks

The RhoA mutant data presented in this chapter suggest a potential role for N1-Src in process outgrowth via a signalling pathway that is independent of RhoA-GDP related signalling. However, in order to determine whether this observation is correct, further clarification of the effect of N1-Src in C3 treated cells is required. If this role is confirmed, the hypothesis underpinning this work, which stated that N1-Src regulates process outgrowth by inactivating RhoA, would be disproved. Further data suggested that N1-Src could form part of a negative feedback loop, whereby stimulation of process outgrowth by N1-Src enhanced RhoA activation, which subsequently served to prevent N1-Src mediated process outgrowth. However, further experiments should be performed to confirm these proposals. Preliminary data also indicated that both N1- and C-Src interacted with RhoA GTP but to different extents, providing further biochemical evidence for the differences between C- and N1-Src.

Whilst further repeats of some datasets are required, these results have provided new insights into the regulation of N1-Src mediated process outgrowth in COS7 cells. Future work should be directed towards investigating the role of N1-Src in other Rho GTPase signalling pathways, such as Rac1 and Cdc42, which have also been implicated in neurite outgrowth (Hoshino and Nakamura, 2003). Whilst monitoring the role of N1-Src in the basal signalling pathways of COS7 cells has provided a good starting point for studying N1-Src effects in heterologous cells, moving forwards, identifying the external cues that trigger downstream N1-Src signalling pathways in neurons should be a priority.

Chapter 6

Conclusions and Future Directions

Chapter 6. Conclusions and Future Directions

The work presented in this thesis provides a thorough characterisation of the cell functions of N1-Src during neuronal development and incorporates the first mechanistic insight into N1-Src signalling. In addition, progress was also made towards the development of an *in vitro* peptide phosphorylation screen for identifying putative N1-Src substrates, which could provide a useful tool for future studies. The specific outcomes of this thesis are discussed below.

6.1 N1-Src as a Regulator of Ion Channel Signalling

With a dearth of N1-Src substrates in the literature, HCN1, which was identified in a N1-SH3 yeast 2-hybrid screen, appeared to be an excellent candidate for further study (Santoro et al., 1997). There is precedence of a role for N1-Src in ion channel signalling, given that N1-Src has been shown to bind and phosphorylate the NR2A subunit of the NMDAR (Grovesman et al., 2011). In addition, the phosphorylation and regulation of related HCN channels (2 and 4) by C-Src has previously been demonstrated (Zong et al., 2005, Li et al., 2008a). With this in mind, *in vitro* phosphorylation assays with the intracellular HCN1-CTD were performed.

Whilst the phosphorylation of the HCN1-CTD could not be detected from *in vitro* kinase assays, the fact that the NR2A-CTD positive control was not phosphorylated either, meant that no firm conclusions could be derived from these data. Therefore, HCN1- and NR2A-CTD could not be ruled out as N1-Src substrates, especially since the phosphorylation of NR2A has been demonstrated previously (Grovesman et al., 2011).

C-Src is not thought to regulate HCN1 channel activity, since studies in the Yu lab indicated that HCN1 channel currents expressed in HEK293 cells were unaffected by SFK inhibition, whereas HCN2 channel activation was inhibited, despite the fact that C-Src is co-immunoprecipitated with both channels (Yu et al., 2004). The addition of N1-Src into a similar system would be a simple way of determining the physiological effects of N1-Src on channel regulation, as a secondary approach. It would be interesting to perform immunoprecipitation assays with both C- and N1-Src, comparing both the binding affinities for HCN1 and the channel phosphorylation status. It is possible that the HCN1 channel could be a weaker substrate for C-Src than N1-Src. Sequence analysis of the HCN1-CTD revealed that it does not contain a N1-Src SH3 binding motif, however it does contain several PXXP motifs, which should be explored if the phosphorylation of the channel is demonstrated in cells.

Grovesman *et al.*, (2011) demonstrated that the NR2A-CTD of the NMDAR was phosphorylated *in vitro* by N1-Src and also showed that NR1/NR2A receptor currents

were enhanced in HEK-293 cells when co-expressed with N1-Src. Whilst N1-Src served as a positive control in the experiments carried out in this thesis, the ultimate aim, if phosphorylation had been demonstrated, was to identify and compare the tyrosine residues phosphorylated by N1-Src to those of C-Src, using mass spectrometry and to subsequently confirm these findings using site directed mutagenesis. A peptide selected from the NR2A tail (RCPSDPYK) was also included in the GST-fusion peptide substrate screen, since it largely conformed to the N1-Src SH3 binding consensus motif that was previously identified in the Evans lab by Dr Sarah Keenan (Keenan, 2012). When this peptide screen is optimised, the results could provide evidence this region binds to N1-Src and the mutagenesis of critical residues of the NR2A subunit could be performed to potentially abolish this interaction in cells.

Both NMDARs and the HCN1 channel are vital for correct brain function. Indeed, the dysregulation of these channels has severe implications in health and disease. For example, the improper regulation of the NMDAR has been linked with neurodegenerative disease (Mota et al., 2014a, Mota et al., 2014b), schizophrenia (Cohen et al., 2015) and ischemic stroke (Knox et al., 2013). One method through which N1-Src might be implicated in the damaging effects of cerebral ischaemia, is through the stimulation of the M4K-1 pathway via NMDAR activation. Li *et al.*, (2008b) demonstrated that the application of the generic SFK inhibitor PP2, resulted in the decreased activation of M4K-1, which subsequently downregulated the MLK3/JNK3/c-jun pathway, known to mediate ischemic effects. This was thought to be mediated via SFK activation of the NMDAR. The same inhibitor was subsequently shown to protect neuronal cells against ischaemic mediated-cell death. This theory would align with the observation by Groveman *et al.*, (2011) that N1-Src activates NMDARs, although both C-Src and Fyn are also capable of activating them. The indiscriminate effects of PP2 on SFKs, makes it difficult to pin-point the kinase involved and requires further investigation. However encouragingly, M4K-1 was also identified as a potential N1-Src substrate that was included in the in GST-fusion peptide screen in Chapter 3. The potential phosphorylation of M4K-1 could provide a further layer of kinase regulation in response to cerebral ischemia.

6.2 The Role of N1-Src in Neuronal Development and Cytoskeletal Dynamics

In this study, the effects of N1-Src on primary rat hippocampal neuronal morphology were determined. The shRNA-mediated knockdown of N1-Src impaired neurite outgrowth, particularly with respect to the length of longest neurite. In addition, there was also a significant reduction in the number of neurites per cell. Together these data not only implicated N1-Src in axon outgrowth, but also suggest that N1-Src plays a role in neurite formation.

The striking effects of N1-Src on neuronal morphology implied that N1-Src is involved in the regulation of neuronal cytoskeletal dynamics. The combined effects of both actin and microtubule dynamics drive axon outgrowth: microtubule polymerization creates a pushing force originating from the axon shaft, whereas the retrograde flow of actin at the leading edge of the growth cone creates a pulling force. The signalling mechanisms that ultimately coordinate these actions are diverse and complex. A comprehensive view outlining these pathways is reviewed in (Lewis et al., 2013).

For several reasons this study focused on the potential role of N1-Src in RhoA GTPase-mediated neurite outgrowth. Many of the GST-fusion peptides that were screened in Chapter 3 were derived from multiple Rho GTPase GAPs or GEFs that had previously been demonstrated to play a role in neuronal development. For example, p190BRhoGAP, whose role is to inactivate RhoA, had previously been demonstrated to promote axonal outgrowth and guidance (Brouns et al., 2001). In addition, Src and Fyn has been identified as the main kinase that phosphorylates the GAP in the developing brain. Whilst, C-Src has been shown to phosphorylate p190RhoGAP in non-neuronal cells, the presence of a putative N1-Src SH3 binding motif on the GAP suggested this protein could also be under the regulation of N1-Src.

Although the results of the N1-Src substrate screen were inconclusive, a complimentary study was performed to determine the effects of N1-Src on RhoA signalling in COS7 cells. The data suggested that whilst the inactivation of RhoA enhanced process formation in COS7 cells under basal cellular conditions, N1-Src did not mediate these effects. Although, the constitutive activation of RhoA prevented N1-Src mediated process formation and surprisingly, N1-Src appeared to enhance RhoA activation, which I speculated could form part of a negative feedback loop.

The overexpression of N1-Src also resulted in impaired neurite outgrowth, with a significant proportion of cells failing to polarise. The conflicting results obtained for the shRNA and overexpression studies suggested that the dysregulation of N1-Src when overexpressed, resulted in non-physiological effects. A previous study by Kotani and colleagues (2007), who overexpressed N1-Src in cerebellar Purkinje neurons, also noted defects in neuronal polarisation since the multiple dendritic shafts characteristic of earlier stages in development, failed to converge into a single shaft. They linked this to the aberrant arrangement of microtubules, visible by EM, present in the dendritic shafts of the unpolarised neurons (Kotani et al., 2007). In hippocampal neurons, microtubule stabilization in one of the minor neurites formed in the early stages of development occurs prior to axon specification and outgrowth (Witte et al., 2008). However, when neurons are treated with the microtubule stabilising reagent taxol, the resultant effect is

aberrant neuronal polarization (Conde and Caceres, 2009). Given that the overexpression of N1-Src has been demonstrated to negatively affect neuronal polarisation, investigating the role of N1-Src in the regulation of microtubule dynamics could provide an interesting line of inquiry.

6.3 Different Roles of C-, N1- and N2-Src

The work carried out in Chapters 4 and 5 highlighted the different functions of the three Src isoforms. Whilst the overexpression of C-Src had no effects on cultured hippocampal neuronal morphology, the overexpression of N1-Src resulted in aberrant neuronal polarization and neurite outgrowth. The second major difference observed between C- and N1-Src was the differential activation of RhoA, under basal cellular conditions. Whilst the latter result requires further confirmation, the differences observed provide specific examples that highlight how the small structural difference in the n-Src loop of the SH3 domain of N1-Src, is capable of altering both phenotype and signal transduction with respect to C-Src. In addition, the first direct comparison of the functions of N1- and N2-Src during the neuronal morphogenesis of hippocampal neurons *in vitro* was performed. shRNA knockdown of both kinases revealed that whilst N1-Src plays a critical role in driving neurite outgrowth, N2-Src appears to play a role in the regulation of neurite branching. In conclusion, these studies have provided direct evidence, suggesting that all three Src isoforms regulate different cellular processes.

6.4 Future Directions

The N1-Src and N2-Src shRNAs characterised in this study provide a useful tool for dissecting the roles of N-Src in neuronal development. To take this research one step further, the splice variant specific shRNAs could be used to generate N1- and N2-Src specific knockout mice. Although firstly, the phenotypic effects of these shRNAs should be confirmed by testing a second set of shRNAs targeting the two splice variants. This technique, which has previously been demonstrated by (Tiscornia et al., 2003), would involve generating transgenic mice that constitutively express the shRNAs. Since both the N1- and N2-Src genes incorporate the N1 mini-exon insert, knocking down N1-Src would also result in the loss of N2-Src. Therefore, using shRNAs to constitutively knockdown the kinases would overcome this issue.

The previously generated C-Src^{-/-} mice were deficient in C-, N1- and N2-Src expression, making it impossible to assign any phenotypes observed to C-Src only. The literature indicated that no obvious neurological phenotypes arose in the absence of the kinases, which was thought to be in part due to the functional redundancy between Src kinases (Soriano et al., 1991). It's also possible that other signalling pathways could compensate for the loss of Src, for example during neurite outgrowth. However, Ignelzi and

colleagues (1994) demonstrated that neurite outgrowth was impaired in cultured cerebellar granule neurons from C-Src^{-/-} mice that were grown on L1-CAM, which has since been demonstrated in the Evans lab to be potentially regulated by N1-Src (Keenan, 2012).

The generation of an N1-Src deficient mouse would facilitate a more in depth analysis of the effects of N1-Src at a phenotypic level but perhaps more importantly at the molecular level. It would enable the analysis of multiple neuronal types in the brain and help produce a more comprehensive picture of the cell type-specific functions of N1-Src during neuronal morphogenesis. In addition, the analysis of brain tissue slices, could be used to determine the physiological relevance of N1-Src mediated effects, by assessing the native biological architecture of neuronal networks. The dissection of N1-Src signalling pathways with respect to external stimuli (e.g. growth factors or cell adhesion signalling) and downstream targets (e.g. Rho GTPases) could feasibly be carried out in neurons, in place of simpler models, eliminating the obstacle of poor transfection efficiency.

In conclusion, this study has been instrumental in providing a platform for future lines of investigation into the roles of N1-Src. The key to advancing the findings reported in this thesis, will involve the further integration of both phenotypic studies and those seeking to de-lineate the signalling transduction pathways through which N1-Src operates in neurons.

Abbreviations

Abbreviations

3'	Three prime
5'	Five prime
aa	Amino acid(s)
AMPAR	α -amino-3-hydroxy-5-methyl-4-isoxazolepropionic acid receptor
APS	Ammonium persulfate
Arg	Arginine
ATP	Adenosine triphosphate
BSA	Bovine serum albumin
C	Carboxyl
°C	Degrees centigrade
cDNA	Copy deoxyribonucleic acid
CGNs	Cerebellar granule neurons
CNS	Central nervous system
Cos-7	African green monkey kidney fibroblasts
CTD	C-terminal domain
dH₂O	Distilled water
DIV	Days <i>in vitro</i>
DMEM	Dulbecco's modified Eagle's medium
DMSO	Dimethyl sulfoxide
DNA	Deoxyribonucleic acid
dNTPs	Deoxynucleoside triphosphates
DPT	Days post-transfection
DRD1	Dopamine 1 receptor
DTT	Dithiothreitol
E	Embryonic
ECL	Enhanced chemiluminescence
ECM	Extracellular matrix
<i>E. coli</i>	<i>Escherichia coli</i>
EDTA	Ethylenediaminetetraacetic acid
EGFR	Epidermal growth factor receptor
EGTA	Ethylene glycol tetraacetic acid

ERK	Extracellular signal-regulated kinase
EVL	Ena/Vasp-like protein
FAK	Focal adhesion kinase
FBS	Foetal bovine serum
g	Grams
g	Gravitational force
GABA	γ -aminobutyric acid
GAP	GTPase activating protein
GDP	Guanosine diphosphate
GFP	Green fluorescent protein
GPCR	G-protein coupled receptor
GST	Glutathione-S-transferase
GTP	Guanosine-5'-triphosphate
HCN(1)	Hyperpolarisation-activated cyclic nucleotide-gated (channel 1)
HIS	Epitope tag consisting of histidine residues
HRP	Horseradish peroxidase
I_h	Hyperpolarisation activated current
IPTG	Isopropyl- β -D-1-thiogalactopyranoside
kbp	Kilobase pairs
kDa	Kilodaltons
L	Litre(s)
L1-CAM	L1-cell adhesion molecule
LB	Lysogeny broth
LTD	Long-term depression
LTP	Long-term potentiation
μg	Microgram(s)
μg μl⁻¹	Microgram(s) per microlitre
μg ml⁻¹	Microgram(s) per millilitre
μm	Micrometre(s)
μm²	Micrometre(s) squared
μM	Micromolar
M	Molar

mg	Milligram(s)
mGluR	Metabotropic glutamate receptors
mg ml⁻¹	Milligrams(s) per millilitre
ml	Millilitre(s)
mm	Millimetre(s)
mM	Millimolar
MBP	Myelin binding protein
min	Minute(s)
MW	Molecular weight
N	Amino
NEB	New England Biolabs
ng	Nanogram(s)
NMDAR	N-methyl-D-aspartate receptor
O.D₆₀₀	Optical density measured at 600 nm
Oligos	Oligonucleotides
ORF(s)	Open reading frame(s)
P	Postnatal
PAC1	Pituitary adenylate cyclase activating peptide 1 receptor
PBS	Phosphate buffered saline
PCR	Polymerase chain reaction
PDGFR	Platelet derived growth factor receptor
PDL	Poly-D-lysine
PenStrep	Penicillin-streptomycin
pH	-log ₁₀ concentration of hydrogen ions
PI3K	Phosphoinositide 3-kinase
PKC	Protein kinase C
PKL	Paxillin kinase linker
PMSF	Phenylmethanesulfonylfluoride
PP2	(+/-butyl)pyrazolo[3,4-d]pyrimidine
Pro	Proline
PTB	Polypyrimidine tract binding protein
PTM	Post translational modification

PVDF	Polyvinylidene fluoride membrane
RhoA	Ras homolog gene family member A
RIPA	Radioimmunoprecipitation assay
RBD	RhoA binding domain
RNA	Ribonucleic acid
RSV	Rous sarcoma virus
RTK	Receptor tyrosine kinase
RTPs	Receptor tyrosine phosphatases
S	Seconds
SDM	Site directed mutagenesis
SDS	Sodium dodecyl sulphate
SDS-PAGE	Sodium dodecyl sulphate polyacrylamide gel electrophoresis
Ser	Serine
SH2	Src homology 2
SH3	Src homology 3
ShRNA	Short hairpin RNA
SFK	Src family kinase
TAE	Tris-acetate-EDTA
TBS	Tris buffered saline
TBST	Tris buffered saline containing Tween-20
TEMED	Tetramethylethylenediamine
Thr	Threonine
tRNA	Transfer RNA
U	Units
Uml⁻¹	Units per ml
V	Volts
v/v	Volume per volume
WT	Wild type
w/v	Weight per volume

References

References

- ABE, K., ROSSMAN, K. L., LIU, B., RITOLA, K. D., CHIANG, D., CAMPBELL, S. L., BURRIDGE, K. & DER, C. J. 2000. Vav2 is an activator of Cdc42, Rac1, and RhoA. *J Biol Chem*, 275, 10141-9.
- AKTORIES, K., WILDE, C. & VOGELSGESANG, M. 2004. Rho-modifying C3-like ADP-ribosyltransferases. *Rev Physiol Biochem Pharmacol*, 152, 1-22.
- ALEXANDROPOULOS, K., CHENG, G. & BALTIMORE, D. 1995. Proline-rich sequences that bind to Src homology 3 domains with individual specificities. *Proc Natl Acad Sci U S A*, 92, 3110-4.
- AMATA, I., MAFFEI, M. & PONS, M. 2014. Phosphorylation of unique domains of Src family kinases. *Front Genet*, 5, 181.
- ARINSBURG, S. S., COHEN, I. S. & YU, H. G. 2006. Constitutively active Src tyrosine kinase changes gating of HCN4 channels through direct binding to the channel proteins. *J Cardiovasc Pharmacol*. United States.
- ARTHUR, W. T., PETCH, L. A. & BURRIDGE, K. 2000. Integrin engagement suppresses RhoA activity via a c-Src-dependent mechanism. *Curr Biol*, 10, 719-22.
- ASPENSTROM, P., RICHNAU, N. & JOHANSSON, A. S. 2006. The diaphanous-related formin DAAM1 collaborates with the Rho GTPases RhoA and Cdc42, CIP4 and Src in regulating cell morphogenesis and actin dynamics. *Exp Cell Res*, 312, 2180-94.
- BAJ, G., PATRIZIO, A., MONTALBANO, A., SCIANCALEPORE, M. & TONGIORGI, E. 2014. Developmental and maintenance defects in Rett syndrome neurons identified by a new mouse staging system in vitro. *Front Cell Neurosci*, 8, 18.
- BARNEKOW, A., JAHN, R. & SCHARTL, M. 1990. Synaptophysin: a substrate for the protein tyrosine kinase pp60c-src in intact synaptic vesicles. *Oncogene*, 5, 1019-24.
- BATEMAN, J. & VAN VACTOR, D. 2001. The Trio family of guanine-nucleotide-exchange factors: regulators of axon guidance. *Journal of Cell Science*, 114, 1973-1980.
- BELFIELD, J. L., WHITTAKER, C., CADER, M. Z. & CHAWLA, S. 2006. Differential Effects of Ca²⁺ and cAMP on Transcription Mediated by MEF2D and cAMP-response Element-binding Protein in Hippocampal Neurons. *Journal of Biological Chemistry*, 281, 27724-27732.
- BENQUET, P., GEE, C. E. & GERBER, U. 2002. Two distinct signaling pathways upregulate NMDA receptor responses via two distinct metabotropic glutamate receptor subtypes. *J Neurosci*. United States.
- BENSON, D. L., WATKINS, F. H., STEWARD, O. & BANKER, G. 1994. Characterization of GABAergic neurons in hippocampal cell cultures. *J Neurocytol*, 23, 279-95.
- BETZ, W. J. 1970. Depression of transmitter release at the neuromuscular junction of the frog. *J Physiol*, 206, 629-44.
- BIEL, M. 2009. Cyclic nucleotide-regulated cation channels. *J Biol Chem*, 284, 9017-21.
- BJELFMAN, C., HEDBORG, F., JOHANSSON, I., NORDENSKJÖLD, M. & PÅHLMAN, S. 1990. Expression of the Neuronal Form of pp60c-src in Neuroblastoma in Relation to Clinical Stage and Prognosis. *Cancer Research*, 50, 6908-6914.
- BJORGE, J. D., PANG, A. & FUJITA, D. J. 2000. Identification of Protein-tyrosine Phosphatase 1B as the Major Tyrosine Phosphatase Activity Capable of Dephosphorylating and Activating c-Src in Several Human Breast Cancer Cell Lines. *Journal of Biological Chemistry*, 275, 41439-41446.
- BLACK, D. L. 1991. Does steric interference between splice sites block the splicing of a short c-src neuron-specific exon in non-neuronal cells? *Genes & Development*, 5, 389-402.
- BLACKMORE, M. G., MOORE, D. L., SMITH, R. P., GOLDBERG, J. L., BIXBY, J. L. & LEMMON, V. P. 2010. High content screening of cortical neurons identifies novel regulators of axon growth. *Molecular and Cellular Neuroscience*, 44, 43-54.
- BLETHROW, J. D., GLAVY, J. S., MORGAN, D. O. & SHOKAT, K. M. 2008. Covalent capture of kinase-specific phosphopeptides reveals Cdk1-cyclin B substrates. *Proc Natl Acad Sci U S A*, 105, 1442-7.

- BOGGON, T. J. & ECK, M. J. 2004. Structure and regulation of Src family kinases. *Oncogene*, 23, 7918-27.
- BOSS, B. D., TURLEJSKI, K., STANFIELD, B. B. & COWAN, W. M. 1987. On the numbers of neurons on fields CA1 and CA3 of the hippocampus of Sprague-Dawley and Wistar rats. *Brain Research*, 406, 280-287.
- BRÁBEK, J., MOJŽITA, D., NOVOTNÝ, M., PŮTA, F. & FOLK, P. 2002. The SH3 domain of Src can downregulate its kinase activity in the absence of the SH2 domain-pY527 interaction. *Biochemical and Biophysical Research Communications*, 296, 664-670.
- BRADFORD, M. M. 1976. A rapid and sensitive method for the quantitation of microgram quantities of protein utilizing the principle of protein-dye binding. *Anal Biochem*, 72, 248-54.
- BRADSHAW, J. M., MITAXOV, V. & WAKSMAN, G. 1999. Investigation of phosphotyrosine recognition by the SH2 domain of the Src kinase1. *Journal of Molecular Biology*, 293, 971-985.
- BREITENLECHNER, C. B., KAIRIES, N. A., HONOLD, K., SCHEIBLICH, S., KOLL, H., GREITER, E., KOCH, S., SCHÄFER, W., HUBER, R. & ENGH, R. A. 2005. Crystal Structures of Active Src Kinase Domain Complexes. *Journal of Molecular Biology*, 353, 222-231.
- BRIGGS, S. D. & SMITHGALL, T. E. 1999. SH2-kinase linker mutations release Hck tyrosine kinase and transforming activities in Rat-2 fibroblasts. *J Biol Chem*, 274, 26579-83.
- BROUNS, M. R., MATHESON, S. F. & SETTLEMAN, J. 2001. p190 RhoGAP is the principal Src substrate in brain and regulates axon outgrowth, guidance and fasciculation. *Nat Cell Biol*, 3, 361-367.
- BROWN, M. T., ANDRADE, J., RADHAKRISHNA, H., DONALDSON, J. G., COOPER, J. A. & RANDAZZO, P. A. 1998. ASAP1, a phospholipid-dependent arf GTPase-activating protein that associates with and is phosphorylated by Src. *Mol Cell Biol*, 18, 7038-51.
- BRUGGE, J. S., COTTON, P. C., QUERAL, A. E., BARRETT, J. N., NONNER, D. & KEANE, R. W. 1985. Neurons express high levels of a structurally modified, activated form of pp60c-src. *Nature*, 316, 554-7.
- BURNETT, G. & KENNEDY, E. P. 1954. The enzymatic phosphorylation of proteins. *J Biol Chem*, 211, 969-80.
- BUSS, J. E., KAMPS, M. P. & SEFTON, B. M. 1984. Myristic acid is attached to the transforming protein of Rous sarcoma virus during or immediately after synthesis and is present in both soluble and membrane-bound forms of the protein. *Molecular and Cellular Biology*, 4, 2697-2704.
- CALALB, M. B., POLTE, T. R. & HANKS, S. K. 1995. Tyrosine phosphorylation of focal adhesion kinase at sites in the catalytic domain regulates kinase activity: a role for Src family kinases. *Molecular and Cellular Biology*, 15, 954-63.
- CALALB, M. B., ZHANG, X., POLTE, T. R. & HANKS, S. K. 1996. Focal Adhesion Kinase Tyrosine-861 Is a Major Site of Phosphorylation by Src. *Biochemical and Biophysical Research Communications*, 228, 662-668.
- CANTLEY, L. C. 2002. The phosphoinositide 3-kinase pathway. *Science*, 296, 1655-7.
- CARROLL, R. C., LISSIN, D. V., VON ZASTROW, M., NICOLL, R. A. & MALENKA, R. C. 1999. Rapid redistribution of glutamate receptors contributes to long-term depression in hippocampal cultures. *Nat Neurosci*, 2, 454-60.
- CARTWRIGHT, C. A., SIMANTOV, R., COWAN, W. M., HUNTER, T. & ECKHART, W. 1988. pp60c-src expression in the developing rat brain. *Proceedings of the National Academy of Sciences*, 85, 3348-3352.
- CARTWRIGHT, C. A., SIMANTOV, R., KAPLAN, P. L., HUNTER, T. & ECKHART, W. 1987. Alterations in pp60c-src accompany differentiation of neurons from rat embryo striatum. *Mol Cell Biol*, 7, 1830-40.
- CATALDI, M., TAGLIALATELA, M., GUERRIERO, S., AMOROSO, S., LOMBARDI, G., DI RENZO, G. & ANNUNZIATO, L. 1996. Protein-tyrosine Kinases Activate while Protein-tyrosine

- Phosphatases Inhibit L-type Calcium Channel Activity in Pituitary GH Cells. *Journal of Biological Chemistry*, 271, 9441-9446.
- CHAN, R. C. & BLACK, D. L. 1997. The polypyrimidine tract binding protein binds upstream of neural cell-specific c-src exon N1 to repress the splicing of the intron downstream. *Molecular and Cellular Biology*, 17, 4667-76.
- CHEN, B.-S. & ROCHE, K. W. 2007. Regulation of NMDA receptors by phosphorylation. *Neuropharmacology*, 53, 362-368.
- CHENG, L., ITOH, K. & LEMMON, V. 2005. L1-Mediated Branching Is Regulated by Two Ezrin-Radixin-Moesin (ERM)-Binding Sites, the RSLE Region and a Novel Juxtamembrane ERM-Binding Region. *The Journal of Neuroscience*, 25, 395-403.
- CHERFILS, J. & ZEGHOUF, M. 2013. Regulation of Small GTPases by GEFs, GAPs, and GDIs. *Physiological Reviews*, 93, 269-309.
- CHODNIEWICZ, D. & KLEMKE, R. L. 2004. Regulation of integrin-mediated cellular responses through assembly of a CAS/Crk scaffold. *Biochimica et Biophysica Acta (BBA) - Molecular Cell Research*, 1692, 63-76.
- CHOI, C. W., KIM, Y. H., SOHN, J. H., LEE, H. & KIM, W. S. 2015. Focal adhesion kinase and Src expression in premalignant and malignant skin lesions. *Exp Dermatol*, 24, 361-4.
- CHOU, M.-Y., UNDERWOOD, J. G., NIKOLIC, J., LUU, M. H. T. & BLACK, D. L. 2000. Multisite RNA Binding and Release of Polypyrimidine Tract Binding Protein during the Regulation of c-src Neural-Specific Splicing. *Molecular Cell*, 5, 949-957.
- CICCHETTI, P., MAYER, B., THIEL, G. & BALTIMORE, D. 1992. Identification of a protein that binds to the SH3 region of Abl and is similar to Bcr and GAP-rho. *Science*, 257, 803-806.
- CLAY, M. R. & HALLORAN, M. C. 2013. Rho activation is apically restricted by Arhgap1 in neural crest cells and drives epithelial-to-mesenchymal transition. *Development*, 140, 3198-3209.
- COHEN, S. M., TSIEN, R. W., GOFF, D. C. & HALASSA, M. M. 2015. The impact of NMDA receptor hypofunction on GABAergic neurons in the pathophysiology of schizophrenia. *Schizophr Res*, 167, 98-107.
- COLLETT, J. W. & STEELE, R. E. 1992. Identification and developmental expression of src+ mRNAs in *Xenopus laevis*. *Developmental Biology*, 152, 194-198.
- CONDE, C. & CACERES, A. 2009. Microtubule assembly, organization and dynamics in axons and dendrites. *Nat Rev Neurosci*, 10, 319-32.
- COSTA, L. G., TAGLIAFERRI, S., ROQUÉ, P. J. & PELLACANI, C. 2016. Role of glutamate receptors in tetrabrominated diphenyl ether (BDE-47) neurotoxicity in mouse cerebellar granule neurons. *Toxicology Letters*, 241, 159-166.
- CRAGGS, G., FINAN, P. M., LAWSON, D., WINGFIELD, J., PERERA, T., GADHER, S., TOTTY, N. F. & KELLIE, S. 2001. A Nuclear SH3 Domain-binding Protein That Colocalizes with mRNA Splicing Factors and Intermediate Filament-containing Perinuclear Networks. *Journal of Biological Chemistry*, 276, 30552-30560.
- CROSSIN, K. L. & KRUSHEL, L. A. 2000. Cellular signaling by neural cell adhesion molecules of the immunoglobulin superfamily. *Dev Dyn*. United States: 2000 Wiley-Liss, Inc.
- DERMARDIROSIAN, C., ROCKLIN, G., SEO, J. Y. & BOKOCH, G. M. 2006. Phosphorylation of RhoGDI by Src regulates Rho GTPase binding and cytosol-membrane cycling. *Mol Biol Cell*, 17, 4760-8.
- DOTTI, C. G., SULLIVAN, C. A. & BANKER, G. A. 1988. The establishment of polarity by hippocampal neurons in culture. *J Neurosci*, 8, 1454-68.
- DUNNING, C. J. R., BLACK, H. L., ANDREWS, K. L., DAVENPORT, E. C., CONBOY, M., CHAWLA, S., DOWLE, A. A., ASHFORD, D., THOMAS, J. R. & EVANS, G. J. O. 2016. Multisite tyrosine phosphorylation of the N-terminus of Mint1/X11 α by Src kinase regulates the trafficking of amyloid precursor protein. *Journal of Neurochemistry*, n/a-n/a.
- ECK, M. J., SHOELSON, S. E. & HARRISON, S. C. 1993. Recognition of a high-affinity phosphotyrosyl peptide by the Src homology-2 domain of p56lck. *Nature*, 362, 87-91.

- ELLERBROEK, S. M., WENNERBERG, K. & BURRIDGE, K. 2003. Serine Phosphorylation Negatively Regulates RhoA in Vivo. *Journal of Biological Chemistry*, 278, 19023-19031.
- ENGEN, J. R., WALES, T. E., HOCHREIN, J. M., MEYN, M. A., 3RD, BANU OZKAN, S., BAHAR, I. & SMITHGALL, T. E. 2008. Structure and dynamic regulation of Src-family kinases. *Cell Mol Life Sci*, 65, 3058-73.
- ENGLISH, J., PEARSON, G., WILSBACHER, J., SWANTEK, J., KARANDIKAR, M., XU, S. & COBB, M. H. 1999. New insights into the control of MAP kinase pathways. *Exp Cell Res*, 253, 255-70.
- ERREGER, K., DRAVID, S. M., BANKE, T. G., WYLLIE, D. J. & TRAYNELIS, S. F. 2005. Subunit-specific gating controls rat NR1/NR2A and NR1/NR2B NMDA channel kinetics and synaptic signalling profiles. *J Physiol*, 563, 345-58.
- EVANS, A. E., D'ANGIO, G. J. & RANDOLPH, J. 1971. A proposed staging for children with neuroblastoma. Children's cancer study group A. *Cancer*, 27, 374-378.
- EVANS, G. J. O. & COUSIN, M. A. 2005. Tyrosine phosphorylation of synaptophysin in synaptic vesicle recycling. *Biochemical Society Transactions*, 33, 1350-1353.
- FADOOL, D. A., HOLMES, T. C., BERMAN, K., DAGAN, D. & LEVITAN, I. B. 1997. Tyrosine Phosphorylation Modulates Current Amplitude and Kinetics of a Neuronal Voltage-Gated Potassium Channel. *Journal of Neurophysiology*, 78, 1563-1573.
- FALK, J., BECHARA, A., FIORE, R., NAWABI, H., ZHOU, H., HOYO-BECERRA, C., BOZON, M., ROUGON, G., GRUMET, M., PUSCHEL, A. W., SANES, J. R. & CASTELLANI, V. 2005. Dual functional activity of semaphorin 3B is required for positioning the anterior commissure. *Neuron*, 48, 63-75.
- FELSENFELD, D. P., SCHWARTZBERG, P. L., VENEGAS, A., TSE, R. & SHEETZ, M. P. 1999. Selective regulation of integrin--cytoskeleton interactions by the tyrosine kinase Src. *Nat Cell Biol*, 1, 200-6.
- FENG, S., CHEN, J., YU, H., SIMON, J. & SCHREIBER, S. 1994. Two binding orientations for peptides to the Src SH3 domain: development of a general model for SH3-ligand interactions. *Science*, 266, 1241-1247.
- FENG, S., KASAHARA, C., RICKLES, R. J. & SCHREIBER, S. L. 1995. Specific interactions outside the proline-rich core of two classes of Src homology 3 ligands. *Proc Natl Acad Sci U S A*, 92, 12408-15.
- FILIPPAKOPOULOS, P., MULLER, S. & KNAPP, S. 2009. SH2 domains: modulators of nonreceptor tyrosine kinase activity. *Curr Opin Struct Biol*, 19, 643-9.
- FINAN, P. M., HALL, A. & KELLIE, S. 1996. Sam68 from an immortalised B-cell line associates with a subset of SH3 domains. *FEBS Letters*, 389, 141-144.
- FOSTER-BARBER, A. & BISHOP, J. M. 1998. Src interacts with dynamin and synapsin in neuronal cells. *Proceedings of the National Academy of Sciences*, 95, 4673-4677.
- FRITZ, R. D. & PERTZ, O. 2016. The dynamics of spatio-temporal Rho GTPase signaling: formation of signaling patterns. *F1000Res*, 5.
- FUKUDA, K., GUPTA, S., CHEN, K., WU, C. & QIN, J. 2009. The pseudoactive site of ILK is essential for its binding to alpha-Parvin and localization to focal adhesions. *Mol Cell*, 36, 819-30.
- FULTS, D. W., TOWLE, A. C., LAUDER, J. M. & MANESS, P. F. 1985. pp60c-src in the developing cerebellum. *Molecular and Cellular Biology*, 5, 27-32.
- GALLO, G. 2011. The cytoskeletal and signaling mechanisms of axon collateral branching. *Developmental Neurobiology*, 71, 201-220.
- GARDONI, F., BELLONE, C., CATTABENI, F. & DI LUCA, M. 2001a. Protein Kinase C Activation Modulates α -Calmodulin Kinase II Binding to NR2A Subunit of N-Methyl-D-Aspartate Receptor Complex. *Journal of Biological Chemistry*, 276, 7609-7613.
- GARDONI, F., SCHRAMA, L. H., KAMAL, A., GISPEN, W. H., CATTABENI, F. & DI LUCA, M. 2001b. Hippocampal synaptic plasticity involves competition between Ca²⁺/calmodulin-dependent protein kinase II and postsynaptic density 95 for binding to the NR2A subunit of the NMDA receptor. *J Neurosci*, 21, 1501-9.

- GATTA, E., LEFEBVRE, T., GAETANI, S., DOS SANTOS, M., MARROCCO, J., MIR, A. M., CASSANO, T., MACCARI, S., NICOLETTI, F. & MAIRESSE, J. 2016. Evidence for an imbalance between tau O-GlcNAcylation and phosphorylation in the hippocampus of a mouse model of Alzheimer's disease. *Pharmacol Res*, 105, 186-97.
- GIL, O. D., SAKURAI, T., BRADLEY, A. E., FINK, M. Y., CASSELLA, M. R., KUO, J. A. & FELSENFELD, D. P. 2003. Ankyrin binding mediates L1CAM interactions with static components of the cytoskeleton and inhibits retrograde movement of L1CAM on the cell surface. *J Cell Biol*. United States.
- GLENNEY, J. R. & ZOKAS, L. 1989. Novel tyrosine kinase substrates from Rous sarcoma virus-transformed cells are present in the membrane skeleton. *The Journal of Cell Biology*, 108, 2401-2408.
- GOULD, K. L. & HUNTER, T. 1988. Platelet-derived growth factor induces multisite phosphorylation of pp60c-src and increases its protein-tyrosine kinase activity. *Mol Cell Biol*, 8, 3345-56.
- GRANT, E. R., BACSKAI, B. J., ANEGAWA, N. J., PLEASURE, D. E. & LYNCH, D. R. 1998. Opposing Contributions of NR1 and NR2 to Protein Kinase C Modulation of NMDA Receptors. *Journal of Neurochemistry*, 71, 1471-1481.
- GROVEMAN, B. R., XUE, S., MARIN, V., XU, J., ALI, M. K., BIENKIEWICZ, E. A. & YU, X.-M. 2011. Roles of the SH2 and SH3 domains in the regulation of neuronal Src kinase functions. *FEBS Journal*, 278, 643-653.
- HARDER, K. W., MOLLER, N. P. H., PEACOCK, J. W. & JIRIK, F. R. 1998. Protein-tyrosine Phosphatase α Regulates Src Family Kinases and Alters Cell-Substratum Adhesion. *Journal of Biological Chemistry*, 273, 31890-31900.
- HASTIE, C. J., MCLAUCHLAN, H. J. & COHEN, P. 2006. Assay of protein kinases using radiolabeled ATP: a protocol. *Nat Protoc*, 1, 968-71.
- HEIDINGER, V., MANZERRA, P., WANG, X. Q., STRASSER, U., YU, S. P., CHOI, D. W. & BEHRENS, M. M. 2002. Metabotropic glutamate receptor 1-induced upregulation of NMDA receptor current: mediation through the Pyk2/Src-family kinase pathway in cortical neurons. *J Neurosci*. United States.
- HOEY, J. G., SUMMY, J. & FLYNN, D. C. 2000. Chimeric constructs containing the SH4/Unique domains of cYes can restrict the ability of Src527F to upregulate heme oxygenase-1 expression efficiently. *Cellular Signalling*, 12, 691-701.
- HORWITZ, G. C., RISNER-JANICZEK, J. R., JONES, S. M. & HOLT, J. R. 2011. HCN channels expressed in the inner ear are necessary for normal balance function. *J Neurosci*. United States.
- HOSHINO, M. & NAKAMURA, S. 2003. Small GTPase Rin induces neurite outgrowth through Rac/Cdc42 and calmodulin in PC12 cells. *J Cell Biol*, 163, 1067-76.
- HUNTER, T. 2009. Tyrosine phosphorylation: thirty years and counting. *Curr Opin Cell Biol*, 21, 140-6.
- HUSE, M. & KURIYAN, J. 2002. The Conformational Plasticity of Protein Kinases. *Cell*, 109, 275-282.
- HUVENEERS, S. & DANEN, E. H. J. 2009. Adhesion signaling – crosstalk between integrins, Src and Rho. *Journal of Cell Science*, 122, 1059-1069.
- IGNELZI JR, M. A., MILLER, D. R., SORIANO, P. & MANESS, P. F. 1994. Impaired neurite outgrowth of src-minus cerebellar neurons on the cell adhesion molecule L1. *Neuron*, 12, 873-884.
- IMAMOTO, A. & SORIANO, P. 1993. Disruption of the csk gene, encoding a negative regulator of Src family tyrosine kinases, leads to neural tube defects and embryonic lethality in mice. *Cell*, 73, 1117-24.
- ISHIZAWAR, R. & PARSONS, S. J. 2004. c-Src and cooperating partners in human cancer. *Cancer Cell*, 6, 209-14.
- JONES, R. J., AVIZIENYTE, E., WYKE, A. W., OWENS, D. W., BRUNTON, V. G. & FRAME, M. C. 2002. Elevated c-Src is linked to altered cell-matrix adhesion rather than proliferation in KM12C human colorectal cancer cells. *Br J Cancer*, 87, 1128-35.

- JURA, N., SHAN, Y., CAO, X., SHAW, D. E. & KURIYAN, J. 2009. Structural analysis of the catalytically inactive kinase domain of the human EGF receptor 3. *Proc Natl Acad Sci U S A*, 106, 21608-13.
- KANG, T. H. & KIM, K. T. 2008. VRK3-mediated inactivation of ERK signaling in adult and embryonic rodent tissues. *Biochim Biophys Acta*, 1783, 49-58.
- KANNER, S. B., REYNOLDS, A. B., VINES, R. R. & PARSONS, J. T. 1990. Monoclonal antibodies to individual tyrosine-phosphorylated protein substrates of oncogene-encoded tyrosine kinases. *Proceedings of the National Academy of Sciences*, 87, 3328-3332.
- KAPLAN, K. B., BIBBINS, K. B., SWEDLOW, J. R., ARNAUD, M., MORGAN, D. O. & VARMUS, H. E. 1994. Association of the amino-terminal half of c-Src with focal adhesions alters their properties and is regulated by phosphorylation of tyrosine 527. *EMBO J*, 13, 4745-56.
- KAPLAN, K. B., SWEDLOW, J. R., MORGAN, D. O. & VARMUS, H. E. 1995. c-Src enhances the spreading of src^{-/-} fibroblasts on fibronectin by a kinase-independent mechanism. *Genes Dev*, 9, 1505-17.
- KARACHALIOU, N., CHAIB, I., PILOTTO, S., CODONY, J., CAI, X., LI, X., MARIN, S., ZHOU, C., CAO, P. & ROSELL, R. 2016. 76P An innovative co-targeting of signal transducer and activator of transcription 3 (STAT3) and Src-YAP pathways in EGFR mutant non-small cell lung cancer (NSCLC). *J Thorac Oncol*, 11, S87-8.
- KÄRKKÄINEN, S., HIIPAKKA, M., WANG, J. H., KLEINO, I., VÄHÄ-JAANKOLA, M., RENKEMA, G. H., LISS, M., WAGNER, R. & SAKSELA, K. 2006. Identification of preferred protein interactions by phage-display of the human Src homology-3 proteome. *EMBO reports*, 7, 186-191.
- KASHIWABUCHI, N., IKEDA, K., ARAKI, K., HIRANO, T., SHIBUKI, K., TAKAYAMA, C., INOUE, Y., KUTSUWADA, T., YAGI, T., KANG, Y., AIZAWA, S. & MISHINA, M. 1995. Impairment of motor coordination, Purkinje cell synapse formation, and cerebellar long-term depression in GluR δ 2 mutant mice. *Cell*, 81, 245-252.
- KATZ, B. & MILEDI, R. 1968. The role of calcium in neuromuscular facilitation. *J Physiol*, 195, 481-92.
- KAY, B. K., WILLIAMSON, M. P. & SUDOL, M. 2000. The importance of being proline: the interaction of proline-rich motifs in signaling proteins with their cognate domains. *Faseb j*, 14, 231-41.
- KEENAN, S. 2012. Structure-function studies of the neuronal Src kinases *Thesis, University of York*.
- KEENAN, S., LEWIS, P. A., WETHERILL, S. J., DUNNING, C. J. R. & EVANS, G. J. O. 2015. The N2-Src neuronal splice variant of C-Src has altered SH3 domain ligand specificity and a higher constitutive activity than N1-Src. *Febs Letters*, 589, 1995-2000.
- KELLY, L., FARRANT, M. & CULL-CANDY, S. G. 2009. Synaptic mGluR activation drives plasticity of calcium-permeable AMPA receptors. *Nat Neurosci*, 12, 593-601.
- KHANNA, S., ROY, S., PARK, H. A. & SEN, C. K. 2007. Regulation of c-Src activity in glutamate-induced neurodegeneration. *J Biol Chem*, 282, 23482-90.
- KIM, L. C., SONG, L. & HAURA, E. B. 2009. Src kinases as therapeutic targets for cancer. *Nat Rev Clin Oncol*, 6, 587-595.
- KITAMURA, T., KAWASHIMA, T., MINOSHIMA, Y., TONOZUKA, Y., HIROSE, K. & NOSAKA, T. 2001. Role of MgcRacGAP/Cyk4 as a Regulator of the Small GTPase Rho Family in Cytokinesis and Cell Differentiation. *Cell Structure and Function*, 26, 645-651.
- KNIGHTON, D. R., ZHENG, J. H., TEN EYCK, L. F., ASHFORD, V. A., XUONG, N. H., TAYLOR, S. S. & SOWADSKI, J. M. 1991. Crystal structure of the catalytic subunit of cyclic adenosine monophosphate-dependent protein kinase. *Science*, 253, 407-14.
- KNOLL, B. & DRESCHER, U. 2004. Src family kinases are involved in EphA receptor-mediated retinal axon guidance. *J Neurosci*, 24, 6248-57.
- KNOX, R., ZHAO, C., MIGUEL-PEREZ, D., WANG, S., YUAN, J., FERRIERO, D. & JIANG, X. 2013. Enhanced NMDA receptor tyrosine phosphorylation and increased brain injury following

- neonatal hypoxia-ischemia in mice with neuronal Fyn overexpression. *Neurobiol Dis*, 51, 113-9.
- KOEGEL, M., ZLATKINE, P., LEY, S. C., COURTNEIDGE, S. A. & MAGEE, A. I. 1994. Palmitoylation of multiple Src-family kinases at a homologous N-terminal motif. *Biochemical Journal*, 303, 749-753.
- KOHR, G. & SEEBURG, P. H. 1996. Subtype-specific regulation of recombinant NMDA receptor-channels by protein tyrosine kinases of the src family. *J Physiol*, 492 (Pt 2), 445-52.
- KOTANI, T., MORONE, N., YUASA, S., NADA, S. & OKADA, M. 2007. Constitutive activation of neuronal Src causes aberrant dendritic morphogenesis in mouse cerebellar Purkinje cells. *Neuroscience Research*, 57, 210-219.
- KOZMA, R., SARNER, S., AHMED, S. & LIM, L. 1997. Rho family GTPases and neuronal growth cone remodelling: relationship between increased complexity induced by Cdc42Hs, Rac1, and acetylcholine and collapse induced by RhoA and lysophosphatidic acid. *Mol Cell Biol*, 17, 1201-11.
- LAKKAKORPI, P. T., NAKAMURA, I., YOUNG, M., LIPFERT, L., RODAN, G. A. & DUONG, L. T. 2001. Abnormal localisation and hyperclustering of $(\alpha)(V)(\beta)(3)$ integrins and associated proteins in Src-deficient or tyrphostin A9-treated osteoclasts. *J Cell Sci*, 114, 149-160.
- LAMBRECHTS, A., KWIATKOWSKI, A. V., LANIER, L. M., BEAR, J. E., VANDEKERCKHOVE, J., AMPE, C. & GERTLER, F. B. 2000. cAMP-dependent Protein Kinase Phosphorylation of EVL, a Mena/VASP Relative, Regulates Its Interaction with Actin and SH3 Domains. *Journal of Biological Chemistry*, 275, 36143-36151.
- LAU, L. F. & HUGANIR, R. L. 1995. Differential tyrosine phosphorylation of N-methyl-D-aspartate receptor subunits. *J Biol Chem*, 270, 20036-41.
- LE BEAU, J. M., WIESTLER, O. D. & WALTER, G. 1987. An altered form of pp60c-src is expressed primarily in the central nervous system. *Molecular and Cellular Biology*, 7, 4115-4117.
- LEMMON, M. A. & SCHLESSINGER, J. 2010. Cell signaling by receptor tyrosine kinases. *Cell*, 141, 1117-34.
- LEONARD, A. S. & HELL, J. W. 1997. Cyclic AMP-dependent protein kinase and protein kinase C phosphorylate N-methyl-D-aspartate receptors at different sites. *J Biol Chem*, 272, 12107-15.
- LEVY, J. B. & BRUGGE, J. S. 1989. Biological and biochemical properties of the c-src+ gene product overexpressed in chicken embryo fibroblasts. *Mol Cell Biol*, 9, 3332-41.
- LEVY, J. B., DORAI, T., WANG, L. H. & BRUGGE, J. S. 1987. The structurally distinct form of pp60c-src detected in neuronal cells is encoded by a unique c-src mRNA. *Mol Cell Biol*, 7, 4142-5.
- LEWIS, P. 2014. The role of N-Src kinases in neuronal differentiation *Thesis, University of York*.
- LEWIS, T. L., COURCHET, J. & POLLEUX, F. 2013. Cellular and molecular mechanisms underlying axon formation, growth, and branching. *The Journal of Cell Biology*, 202, 837-848.
- LI, C. H., ZHANG, Q., TENG, B., MUSTAFA, S. J., HUANG, J. Y. & YU, H. G. 2008a. Src tyrosine kinase alters gating of hyperpolarization-activated HCN4 pacemaker channel through Tyr531. *Am J Physiol Cell Physiol*. United States.
- LI, T., YU, X.-J. & ZHANG, G.-Y. 2008b. Tyrosine phosphorylation of HPK1 by activated Src promotes ischemic brain injury in rat hippocampal CA1 region. *FEBS Letters*, 582, 1894-1900.
- LIAO, Z., LOCKHEAD, D., LARSON, E. D. & PROENZA, C. 2010. Phosphorylation and modulation of hyperpolarization-activated HCN4 channels by protein kinase A in the mouse sinoatrial node. *The Journal of General Physiology*, 136, 247-258.
- LIU, G., BEGGS, H., JURGENSEN, C., PARK, H.-T., TANG, H., GORSKI, J., JONES, K. R., REICHARDT, L. F., WU, J. & RAO, Y. 2004. Netrin requires focal adhesion kinase and Src family kinases for axon outgrowth and attraction. *Nat Neurosci*, 7, 1222-1232.
- LIU, X. J., GINGRICH, J. R., VARGAS-CABALLERO, M., DONG, Y. N., SENGAR, A., BEGGS, S., WANG, S. H., DING, H. K., FRANKLAND, P. W. & SALTER, M. W. 2008. Treatment of inflammatory

- and neuropathic pain by uncoupling Src from the NMDA receptor complex. *Nat Med*. United States.
- LIU, Y., SHAH, K., YANG, F., WITUCKI, L. & SHOKAT, K. M. 1998. Engineering Src family protein kinases with unnatural nucleotide specificity. *Chem Biol*, 5, 91-101.
- LU, W. Y., XIONG, Z. G., LEI, S., ORSER, B. A., DUDEK, E., BROWNING, M. D. & MACDONALD, J. F. 1999. G-protein-coupled receptors act via protein kinase C and Src to regulate NMDA receptors. *Nat Neurosci*, 2, 331-8.
- LUTTRELL, L. M., FERGUSON, S. S., DAAKA, Y., MILLER, W. E., MAUDSLEY, S., DELLA ROCCA, G. J., LIN, F., KAWAKATSU, H., OWADA, K., LUTTRELL, D. K., CARON, M. G. & LEFKOWITZ, R. J. 1999. Beta-arrestin-dependent formation of beta2 adrenergic receptor-Src protein kinase complexes. *Science*, 283, 655-61.
- MACDONALD, D. S., WEERAPURA, M., BEAZELY, M. A., MARTIN, L., CZERWINSKI, W., RODER, J. C., ORSER, B. A. & MACDONALD, J. F. 2005. Modulation of NMDA Receptors by Pituitary Adenylate Cyclase Activating Peptide in CA1 Neurons Requires Gαq, Protein Kinase C, and Activation of Src.
- MAFFEI, M., ARBESÚ, M., LE ROUX, A.-L., AMATA, I., ROCHE, S. & PONS, M. 2015. The SH3 Domain Acts as a Scaffold for the N-Terminal Intrinsically Disordered Regions of c-Src. *Structure*, 23, 893-902.
- MAGLEBY, K. L. & ZENGEL, J. E. 1975. A quantitative description of tetanic and post-tetanic potentiation of transmitter release at the frog neuromuscular junction. *J Physiol*, 245, 183-208.
- MAHAL, K. 2010. Specific splice variant silencing of neuronal Srcs. *Thesis, University of York*.
- MALENKA, R. C. 1994. Synaptic plasticity in the hippocampus: LTP and LTD. *Cell*, 78, 535-8.
- MALINOW, R. & MALENKA, R. C. 2002. AMPA receptor trafficking and synaptic plasticity. *Annu Rev Neurosci*, 25, 103-26.
- MAMMOTO, T., JIANG, A., JIANG, E. & MAMMOTO, A. 2016. The Role of Twist1 Phosphorylation in Tumor Angiogenesis in Lung Cancer. *The FASEB Journal*, 30, 439.4.
- MANESS, P. F., AUBRY, M., SHORES, C. G., FRAME, L. & PFENNINGER, K. H. 1988. c-src gene product in developing rat brain is enriched in nerve growth cone membranes. *Proceedings of the National Academy of Sciences*, 85, 5001-5005.
- MANESS, P. F., SHORES, C. G. & IGNELZI, M. 1989. Localization of the Normal Cellular SRC Protein to the Growth Cone of Differentiating Neurons in Brain and Retina. In: LAUDER, J. M., PRIVAT, A., GIACOBINI, E., TIMIRAS, P. S. & VERNADAKIS, A. (eds.) *Molecular Aspects of Development and Aging of the Nervous System*. Boston, MA: Springer US.
- MANESS, P. F., SORGE, L. K. & FULTS, D. W. 1986. An early developmental phase of pp60c-src expression in the neural ectoderm. *Developmental Biology*, 117, 83-89.
- MANNING, G., WHYTE, D. B., MARTINEZ, R., HUNTER, T. & SUDARSANAM, S. 2002. The protein kinase complement of the human genome. *Science*, 298, 1912-34.
- MARCOUX, N. & VUORI, K. 2003. EGF receptor mediates adhesion-dependent activation of the Rac GTPase: a role for phosphatidylinositol 3-kinase and Vav2. *Oncogene*, 22, 6100-6106.
- MARKUS, A., ZHONG, J. & SNIDER, W. D. 2002. Raf and Akt Mediate Distinct Aspects of Sensory Axon Growth. *Neuron*, 35, 65-76.
- MARTINEZ, R., MATHEY-PREVOT, B., BERNARDS, A. & BALTIMORE, D. 1987. Neuronal pp60c-src contains a six-amino acid insertion relative to its non-neuronal counterpart. *Science*, 237, 411-415.
- MATSUNAGA, T., SHIRASAWA, H., ENOMOTO, H., YOSHIDA, H., IWAI, J., TANABE, M., KAWAMURA, K., ETOH, T. & OHNUMA, N. 1998. Neuronal src and trk A protooncogene expression in neuroblastomas and patient prognosis. *International Journal of Cancer*, 79, 226-231.
- MAYER, B. J. 2001. SH3 domains: complexity in moderation. *J Cell Sci*, 114, 1253-63.

- MEIJERING, E., JACOB, M., SARRIA, J. C., STEINER, P., HIRLING, H. & UNSER, M. 2004. Design and validation of a tool for neurite tracing and analysis in fluorescence microscopy images. *Cytometry A*, 58, 167-76.
- MENG, L., MICHAUD, G. A., MERKEL, J. S., ZHOU, F., HUANG, J., MATTOON, D. R. & SCHWEITZER, B. 2008. Protein kinase substrate identification on functional protein arrays. *BMC Biotechnol*, 8, 22.
- MESSA, M., CONGIA, S., DEFRANCHI, E., VALTORTA, F., FASSIO, A., ONOFRI, F. & BENFENATI, F. 2010. Tyrosine phosphorylation of synapsin I by Src regulates synaptic-vesicle trafficking. *Journal of Cell Science*, 123, 2256-2265.
- MESSINA, S., ONOFRI, F., BONGIORNO-BORBONE, L., GIOVEDI, S., VALTORTA, F., GIRAULT, J. A. & BENFENATI, F. 2003. Specific interactions of neuronal focal adhesion kinase isoforms with Src kinases and amphiphysin. *J Neurochem*, 84, 253-65.
- MIYAGI, Y., YAMASHITA, T., FUKAYA, M., SONODA, T., OKUNO, T., YAMADA, K., WATANABE, M., NAGASHIMA, Y., AOKI, I., OKUDA, K., MISHINA, M. & KAWAMOTO, S. 2002. Delphilin: a novel PDZ and formin homology domain-containing protein that synaptically colocalizes and interacts with glutamate receptor delta 2 subunit. *J Neurosci*, 22, 803-14.
- MODAFFERI, E. F. & BLACK, D. L. 1997. A complex intronic splicing enhancer from the c-src pre-mRNA activates inclusion of a heterologous exon. *Molecular and Cellular Biology*, 17, 6537-45.
- MOK, J., IM, H. & SNYDER, M. 2009. Global identification of protein kinase substrates by protein microarray analysis. *Nat. Protocols*, 4, 1820-1827.
- MORO, L., DOLCE, L., CABODI, S., BERGATTO, E., ERBA, E. B., SMERIGLIO, M., TURCO, E., RETTA, S. F., GIUFFRIDA, M. G., VENTURINO, M., GODOVAC-ZIMMERMANN, J., CONTI, A., SCHAEFER, E., BEGUINOT, L., TACCHETTI, C., GAGGINI, P., SILENGO, L., TARONE, G. & DEFILIPPI, P. 2002. Integrin-induced Epidermal Growth Factor (EGF) Receptor Activation Requires c-Src and p130Cas and Leads to Phosphorylation of Specific EGF Receptor Tyrosines. *Journal of Biological Chemistry*, 277, 9405-9414.
- MOSS, S. J., GORRIE, G. H., AMATO, A. & SMART, T. G. 1995. Modulation of GABAA receptors by tyrosine phosphorylation. *Nature*, 377, 344-8.
- MOTA, S. I., FERREIRA, I. L. & REGO, A. C. 2014a. Dysfunctional synapse in Alzheimer's disease - A focus on NMDA receptors. *Neuropharmacology*, 76 Pt A, 16-26.
- MOTA, S. I., FERREIRA, I. L., VALERO, J., FERREIRO, E., CARVALHO, A. L., OLIVEIRA, C. R. & REGO, A. C. 2014b. Impaired Src signaling and post-synaptic actin polymerization in Alzheimer's disease mice hippocampus--linking NMDA receptors and the reelin pathway. *Exp Neurol*, 261, 698-709.
- MUKHERJEE, A., ARNAUD, L. & COOPER, J. A. 2003. Lipid-dependent recruitment of neuronal Src to lipid rafts in the brain. *J Biol Chem*, 278, 40806-14.
- MUKHERJEE, S. & MANAHAN-VAUGHAN, D. 2013. Role of metabotropic glutamate receptors in persistent forms of hippocampal plasticity and learning. *Neuropharmacology*, 66, 65-81.
- MULKEY, R. M., HERRON, C. E. & MALENKA, R. C. 1993. An essential role for protein phosphatases in hippocampal long-term depression. *Science*, 261, 1051-5.
- MUSACCHIO, A., SARASTE, M. & WILMANN, M. 1994. High-resolution crystal structures of tyrosine kinase SH3 domains complexed with proline-rich peptides. *Nat Struct Biol*, 1, 546-51.
- NADA, S., SHIMA, T., YANAI, H., HUSI, H., GRANT, S. G., OKADA, M. & AKIYAMA, T. 2003. Identification of PSD-93 as a substrate for the Src family tyrosine kinase Fyn. *J Biol Chem*, 278, 47610-21.
- NAGARAJ, K. & HORTSCH, M. 2006. Phosphorylation of L1-type cell-adhesion molecules--ankyrins away! *Trends Biochem Sci*. England.
- NAKAMURA, M., ZHAI, P., DEL RE, D. P., MAEJIMA, Y. & SADOSHIMA, J. 2016. Mst1-mediated phosphorylation of Bcl-xL is required for myocardial reperfusion injury. *JCI Insight*, 1.
- NAKAZAWA, T., KOMAI, S., TEZUKA, T., HISATSUNE, C., UMEMORI, H., SEMBA, K., MISHINA, M., MANABE, T. & YAMAMOTO, T. 2001. Characterization of Fyn-mediated Tyrosine

- Phosphorylation Sites on GluR ϵ 2 (NR2B) Subunit of the N-Methyl-D-aspartate Receptor. *Journal of Biological Chemistry*, 276, 693-699.
- NEET, K. & HUNTER, T. 1996. Vertebrate non-receptor protein-tyrosine kinase families. *Genes Cells*, 1, 147-69.
- NIETHAMMER, M., KIM, E. & SHENG, M. 1996. Interaction between the C terminus of NMDA receptor subunits and multiple members of the PSD-95 family of membrane-associated guanylate kinases. *J Neurosci*, 16, 2157-63.
- NISHIMURA, K., YOSHIHARA, F., TOJIMA, T., OOASHI, N., YOON, W., MIKOSHIBA, K., BENNETT, V. & KAMIGUCHI, H. 2003. L1-dependent neuriteogenesis involves ankyrinB that mediates L1-CAM coupling with retrograde actin flow. *J Cell Biol.* United States.
- NOBLE, M. E., MUSACCHIO, A., SARASTE, M., COURTNEIDGE, S. A. & WIERENGA, R. K. 1993. Crystal structure of the SH3 domain in human Fyn; comparison of the three-dimensional structures of SH3 domains in tyrosine kinases and spectrin. *The EMBO Journal*, 12, 2617-2624.
- NOLAN, M. F., MALLERET, G., DUDMAN, J. T., BUHL, D. L., SANTORO, B., GIBBS, E., VRONSKAYA, S., BUZSAKI, G., SIEGELBAUM, S. A., KANDEL, E. R. & MOROZOV, A. 2004. A behavioral role for dendritic integration: HCN1 channels constrain spatial memory and plasticity at inputs to distal dendrites of CA1 pyramidal neurons. *Cell.* United States.
- NOLAN, M. F., MALLERET, G., LEE, K. H., GIBBS, E., DUDMAN, J. T., SANTORO, B., YIN, D., THOMPSON, R. F., SIEGELBAUM, S. A., KANDEL, E. R. & MOROZOV, A. 2003. The hyperpolarization-activated HCN1 channel is important for motor learning and neuronal integration by cerebellar Purkinje cells. *Cell.* United States.
- NOLEN, B., TAYLOR, S. & GHOSH, G. 2004. Regulation of protein kinases; controlling activity through activation segment conformation. *Mol Cell*, 15, 661-75.
- OBARA, Y., LABUDDA, K., DILLON, T. J. & STORK, P. J. S. 2004. PKA phosphorylation of Src mediates Rap1 activation in NGF and cAMP signaling in PC12 cells. *Journal of Cell Science*, 117, 6085-6094.
- OLSEN, J. V., BLAGOEV, B., GNAD, F., MACEK, B., KUMAR, C., MORTENSEN, P. & MANN, M. 2006. Global, in vivo, and site-specific phosphorylation dynamics in signaling networks. *Cell*, 127, 635-48.
- ONOFRI, F., GIOVEDÌ, S., VACCARO, P., CZERNIK, A. J., VALTORTA, F., DE CAMILLI, P., GREENGARD, P. & BENFENATI, F. 1997. Synapsin I interacts with c-Src and stimulates its tyrosine kinase activity. *Proceedings of the National Academy of Sciences*, 94, 12168-12173.
- OSUSKY, M., TAYLOR, S. J. & SHALLOWAY, D. 1995. Autophosphorylation of purified c-Src at its primary negative regulation site. *J Biol Chem*, 270, 25729-32.
- OTTILIE, S., RAULF, F., BARNEKOW, A., HANNIG, G. & SCHARTL, M. 1992. Multiple src-related kinase genes, srk1-4, in the fresh water sponge *Spongilla lacustris*. *Oncogene*, 7, 1625-30.
- PAIGE, L. A., NADLER, M. J., HARRISON, M. L., CASSADY, J. M. & GEAHLEN, R. L. 1993. Reversible palmitoylation of the protein-tyrosine kinase p56lck. *Journal of Biological Chemistry*, 268, 8669-74.
- PÉREZ, Y., GAIRÍ, M., PONS, M. & BERNADÓ, P. 2009. Structural Characterization of the Natively Unfolded N-Terminal Domain of Human c-Src Kinase: Insights into the Role of Phosphorylation of the Unique Domain. *Journal of Molecular Biology*, 391, 136-148.
- PEREZ, Y., MAFFEI, M., IGEA, A., AMATA, I., GAIRI, M., NEBREDA, A. R., BERNADO, P. & PONS, M. 2013. Lipid binding by the Unique and SH3 domains of c-Src suggests a new regulatory mechanism. *Sci Rep*, 3, 1295.
- PICON-RUIZ, M., PAN, C., DREWS-ELGER, K., JANG, K., BESSER, A. H., ZHAO, D., MORATA-TARIFA, C., KIM, M., INCE, T. A., AZZAM, D. J., WANDER, S. A., WANG, B., ERGONUL, B., DATAR, R. H., COTE, R. J., HOWARD, G. A., EL-ASHRY, D., TORNE-POYATOS, P., MARCHAL, J. A. & SLINGERLAND, J. M. 2016. Interactions between Adipocytes and Breast Cancer Cells

- Stimulate Cytokine Production and Drive Src/Sox2/miR-302b-Mediated Malignant Progression. *Cancer Res*, 76, 491-504.
- PLAYFORD, M. P. & SCHALLER, M. D. 2004. The interplay between Src and integrins in normal and tumor biology. *Oncogene*, 23, 7928-46.
- POOLE, A. W. & JONES, M. L. 2005. A SHPing tale: Perspectives on the regulation of SHP-1 and SHP-2 tyrosine phosphatases by the C-terminal tail. *Cellular Signalling*, 17, 1323-1332.
- PREIBISCH, S., SAALFELD, S. & TOMANCAK, P. 2009. Globally optimal stitching of tiled 3D microscopic image acquisitions. *Bioinformatics*, 25, 1463-5.
- PRELICH, G. 2012. Gene overexpression: uses, mechanisms, and interpretation. *Genetics*, 190, 841-54.
- PYPER, J. M. & BOLEN, J. B. 1989. Neuron-specific splicing of C-SRC cDNA RNA in human brain. *Journal of Neuroscience Research*, 24, 89-96.
- PYPER, J. M. & BOLEN, J. B. 1990. Identification of a novel neuronal C-SRC exon expressed in human brain. *Mol Cell Biol*, 10, 2035-40.
- RAULF, F., ROBERTSON, S. M. & SCHARTL, M. 1989. Evolution of the neuron-specific alternative splicing product of the c-src proto-oncogene. *Journal of Neuroscience Research*, 24, 81-88.
- REETZ, O. & STRAUSS, U. 2013. Protein Kinase C Activation Inhibits Rat and Human Hyperpolarization Activated Cyclic Nucleotide Gated Channel (HCN)1 - Mediated Current in Mammalian Cells. *Cellular Physiology and Biochemistry*, 31, 532-541.
- REGEHR, W. G. 2012. Short-term presynaptic plasticity. *Cold Spring Harb Perspect Biol*, 4, a005702.
- REN, R., MAYER, B., CICHETTI, P. & BALTIMORE, D. 1993. Identification of a ten-amino acid proline-rich SH3 binding site. *Science*, 259, 1157-1161.
- REN, X. D., KIOSSES, W. B., SIEG, D. J., OTEY, C. A., SCHLAEPFER, D. D. & SCHWARTZ, M. A. 2000. Focal adhesion kinase suppresses Rho activity to promote focal adhesion turnover. *Journal of Cell Science*, 113, 3673-3678.
- RESH, M. D. 1994. Myristylation and palmitoylation of Src family members: The fats of the matter. *Cell*, 76, 411-413.
- REYNOLDS, A. B., VILA, J., LANSING, T. J., POTTS, W. M., WEBER, M. J. & PARSONS, J. T. 1987. Activation of the oncogenic potential of the avian cellular src protein by specific structural alteration of the carboxy terminus. *EMBO J*, 6, 2359-64.
- REYNOLDS, C. H., GARWOOD, C. J., WRAY, S., PRICE, C., KELLIE, S., PERERA, T., ZVELEBIL, M., YANG, A., SHEPPARD, P. W., VARNDILL, I. M., HANGER, D. P. & ANDERTON, B. H. 2008. Phosphorylation Regulates Tau Interactions with Src Homology 3 Domains of Phosphatidylinositol 3-Kinase, Phospholipase C γ 1, Grb2, and Src Family Kinases. *Journal of Biological Chemistry*, 283, 18177-18186.
- RICHNAU, N. & ASPENSTROM, P. 2001. Rich, a rho GTPase-activating protein domain-containing protein involved in signaling by Cdc42 and Rac1. *J Biol Chem*, 276, 35060-70.
- RICKLES, R. J., BOTFIELD, M. C., ZHOU, X. M., HENRY, P. A., BRUGGE, J. S. & ZOLLER, M. J. 1995. Phage display selection of ligand residues important for Src homology 3 domain binding specificity. *Proceedings of the National Academy of Sciences*, 92, 10909-10913.
- RIDLEY, A. J. & HALL, A. 1992. The small GTP-binding protein rho regulates the assembly of focal adhesions and actin stress fibers in response to growth factors. *Cell*, 70, 389-399.
- ROLLI-DERKINDEREN, M., SAUZEAU, V., BOYER, L., LEMICHEZ, E., BARON, C., HENRION, D., LOIRAND, G. & PACAUD, P. 2005. Phosphorylation of Serine 188 Protects RhoA from Ubiquitin/Proteasome-Mediated Degradation in Vascular Smooth Muscle Cells. *Circulation Research*, 96, 1152-1160.
- ROOF, R. W., HASKELL, M. D., DUKES, B. D., SHERMAN, N., KINTER, M. & PARSONS, S. J. 1998. Phosphotyrosine (p-Tyr)-Dependent and -Independent Mechanisms of p190 RhoGAP-p120 RasGAP Interaction: Tyr 1105 of p190, a Substrate for c-Src, Is the Sole p-Tyr Mediator of Complex Formation. *Molecular and Cellular Biology*, 18, 7052-7063.

- ROSKOSKI, R., JR. 2004. Src protein-tyrosine kinase structure and regulation. *Biochem Biophys Res Commun*, 324, 1155-64.
- ROSKOSKI, R., JR. 2012. MEK1/2 dual-specificity protein kinases: structure and regulation. *Biochem Biophys Res Commun*, 417, 5-10.
- ROSS, C. A., WRIGHT, G. E., RESH, M. D., PEARSON, R. C. & SNYDER, S. H. 1988. Brain-specific src oncogene mRNA mapped in rat brain by in situ hybridization. *Proceedings of the National Academy of Sciences*, 85, 9831-9835.
- ROUX, P. P. & THIBAUT, P. 2013. The coming of age of phosphoproteomics--from large data sets to inference of protein functions. *Mol Cell Proteomics*, 12, 3453-64.
- RUDOLPH, P., LAPPE, T., HERO, B., BERTHOLD, F., PARWARESCH, R., HARMS, D. & SCHMIDT, D. 1997. Prognostic significance of the proliferative activity in neuroblastoma. *Am J Pathol*, 150, 133-45.
- RUEST, P. J., SHIN, N. Y., POLTE, T. R., ZHANG, X. & HANKS, S. K. 2001. Mechanisms of CAS substrate domain tyrosine phosphorylation by FAK and Src. *Mol Cell Biol*, 21, 7641-52.
- SADOWSKI, I., STONE, J. C. & PAWSON, T. 1986. A noncatalytic domain conserved among cytoplasmic protein-tyrosine kinases modifies the kinase function and transforming activity of Fujinami sarcoma virus P130gag-fps. *Molecular and Cellular Biology*, 6, 4396-4408.
- SAITO, Y., INOUE, T., ZHU, G., KIMURA, N., OKADA, M., NISHIMURA, M., MURAYAMA, S., KANEKO, S., SHIGEMOTO, R., IMOTO, K. & SUZUKI, T. 2012. Hyperpolarization-activated cyclic nucleotide gated channels: a potential molecular link between epileptic seizures and Abeta generation in Alzheimer's disease. *Mol Neurodegener*. England.
- SALTER, M. W. & KALIA, L. V. 2004. Src kinases: a hub for NMDA receptor regulation. *Nat Rev Neurosci*, 5, 317-28.
- SANTORO, B., GRANT, S. G., BARTSCH, D. & KANDEL, E. R. 1997. Interactive cloning with the SH3 domain of N-src identifies a new brain specific ion channel protein, with homology to eag and cyclic nucleotide-gated channels. *Proc Natl Acad Sci U S A*, 94, 14815-20.
- SANTORO, B., LEE, J. Y., ENLOT, D. J., GILDERSLEEVE, S., PISKOROWSKI, R. A., SIEGELBAUM, S. A., WINAWER, M. R. & BLUMENFELD, H. 2010. Increased seizure severity and seizure-related death in mice lacking HCN1 channels. *Epilepsia*. United States.
- SANTORO, B., WAINGER, B. J. & SIEGELBAUM, S. A. 2004. Regulation of HCN channel surface expression by a novel C-terminal protein-protein interaction. *J Neurosci*, 24, 10750-62.
- SANZ-CLEMENTE, A., NICOLL, R. A. & ROCHE, K. W. 2013. Diversity in NMDA receptor composition: many regulators, many consequences. *Neuroscientist*. United States.
- SATO, I., OBATA, Y., KASAHARA, K., NAKAYAMA, Y., FUKUMOTO, Y., YAMASAKI, T., YOKOYAMA, K. K., SAITO, T. & YAMAGUCHI, N. 2009. Differential trafficking of Src, Lyn, Yes and Fyn is specified by the state of palmitoylation in the SH4 domain. *Journal of Cell Science*, 122, 965-975.
- SAYA, H., LEE, P. S. Y., NISHI, T., IZAWA, I., NAKAJIMA, M., GALLICK, G. E. & LEVIN, V. A. 1993. Bacterial expression of an active tyrosine kinase from a protein A/truncated c-src fusion protein. *FEBS Letters*, 327, 224-230.
- SCHAEFER, A. W., KAMEI, Y., KAMIGUCHI, H., WONG, E. V., RAPOPORT, I., KIRCHHAUSEN, T., BEACH, C. M., LANDRETH, G., LEMMON, S. K. & LEMMON, V. 2002. L1 endocytosis is controlled by a phosphorylation-dephosphorylation cycle stimulated by outside-in signaling by L1. *J Cell Biol*. United States.
- SCHALLER, M. D., HILDEBRAND, J. D. & PARSONS, J. T. 1999. Complex Formation with Focal Adhesion Kinase: A Mechanism to Regulate Activity and Subcellular Localization of Src Kinases. *Molecular Biology of the Cell*, 10, 3489-3505.
- SCHALLER, M. D., HILDEBRAND, J. D., SHANNON, J. D., FOX, J. W., VINES, R. R. & PARSONS, J. T. 1994. Autophosphorylation of the focal adhesion kinase, pp125FAK, directs SH2-dependent binding of pp60src. *Molecular and Cellular Biology*, 14, 1680-1688.
- SCHARTL, M. & BARNEKOW, A. 1984. Differential expression of the cellular src gene during vertebrate development. *Developmental Biology*, 105, 415-422.

- SCHINDLER, T., SICHERI, F., PICO, A., GAZIT, A., LEVITZKI, A. & KURIYAN, J. 1999. Crystal Structure of Hck in Complex with a Src Family–Selective Tyrosine Kinase Inhibitor. *Molecular Cell*, 3, 639-648.
- SCHLESSINGER, A. R., COWAN, W. M. & SWANSON, L. W. 1978. The time of origin of neurons in Ammon's horn and the associated retrohippocampal fields. *Anat Embryol (Berl)*, 154, 153-73.
- SCHNEIDER, C. A., RASBAND, W. S. & ELICEIRI, K. W. 2012. NIH Image to ImageJ: 25 years of image analysis. *Nat Methods*, 9, 671-5.
- SHAH, K., LIU, Y., DEIRMENGIAN, C. & SHOKAT, K. M. 1997. Engineering unnatural nucleotide specificity for Rous sarcoma virus tyrosine kinase to uniquely label its direct substrates. *Proc Natl Acad Sci U S A*, 94, 3565-70.
- SHALLOWAY, D., ZELENETZ, A. D. & COOPER, G. M. 1981. Molecular cloning and characterization of the chicken gene homologous to the transforming gene of rous sarcoma virus. *Cell*, 24, 531-541.
- SHANG, X., MARCHIONI, F., SIPES, N., EVELYN, C. R., JERABEK-WILLEMSEN, M., DUHR, S., SEIBEL, W., WORTMAN, M. & ZHENG, Y. 2012. Rational design of small molecule inhibitors targeting RhoA subfamily Rho GTPases. *Chem Biol*, 19, 699-710.
- SHENOY-SCARIA, A. M., DIETZEN, D. J., KWONG, J., LINK, D. C. & LUBLIN, D. M. 1994. Cysteine3 of Src family protein tyrosine kinase determines palmitoylation and localization in caveolae. *The Journal of Cell Biology*, 126, 353-363.
- SHENOY, S., CHACKALAPARAMPIL, I., BAGRODIA, S., LIN, P. H. & SHALLOWAY, D. 1992. Role of p34cdc2-mediated phosphorylations in two-step activation of pp60c-src during mitosis. *Proceedings of the National Academy of Sciences*, 89, 7237-7241.
- SHI, S. H., HAYASHI, Y., PETRALIA, R. S., ZAMAN, S. H., WENTHOLD, R. J., SVOBODA, K. & MALINOW, R. 1999. Rapid spine delivery and redistribution of AMPA receptors after synaptic NMDA receptor activation. *Science*, 284, 1811-6.
- SICHERI, F., MOAREFI, I. & KURIYAN, J. 1997. Crystal structure of the Src family tyrosine kinase Hck. *Nature*, 385, 602-9.
- SILVERMAN, L., SUDOL, M. & RESH, M. D. 1993. Members of the src family of nonreceptor tyrosine kinases share a common mechanism for membrane binding. *Cell Growth Differ*, 4, 475-82.
- SLEPNEV, V. I. & DE CAMILLI, P. 2000. Accessory factors in clathrin-dependent synaptic vesicle endocytosis. *Nat Rev Neurosci*, 1, 161-172.
- SMOTHERS, C. T., SZUMLINSKI, K. K., WORLEY, P. F. & WOODWARD, J. J. 2016. Altered NMDA receptor function in primary cultures of hippocampal neurons from mice lacking the Homer2 gene. *Synapse*, 70, 33-39.
- SODERLING, T. R. & DERKACH, V. A. 2000. Postsynaptic protein phosphorylation and LTP. *Trends Neurosci*, 23, 75-80.
- SOMANI, A.-K., BIGNON, J. S., MILLS, G. B., SIMINOVITCH, K. A. & BRANCH, D. R. 1997. Src Kinase Activity Is Regulated by the SHP-1 Protein-tyrosine Phosphatase. *Journal of Biological Chemistry*, 272, 21113-21119.
- SONGYANG, Z., CARRAWAY, K. L., ECK, M. J., HARRISON, S. C., FELDMAN, R. A., MOHAMMADI, M., SCHLESSINGER, J., HUBBARD, S. R., SMITH, D. P. & ENG, C. 1995. Catalytic specificity of protein-tyrosine kinases is critical for selective signalling. *Nature*, 373, 536-539.
- SONGYANG, Z., SHOELSON, S. E., MCGLADE, J., OLIVIER, P., PAWSON, T., BUSTELO, X. R., BARBACID, M., SABE, H., HANAFUSA, H. & YI, T. 1994. Specific motifs recognized by the SH2 domains of Csk, 3BP2, fps/fes, GRB-2, HCP, SHC, Syk, and Vav. *Molecular and Cellular Biology*, 14, 2777-2785.
- SOPKO, R. & ANDREWS, B. J. 2008. Linking the kinome and phosphorylome--a comprehensive review of approaches to find kinase targets. *Mol Biosyst*, 4, 920-33.
- SORIANO, P., MONTGOMERY, C., GESKE, R. & BRADLEY, A. 1991. Targeted disruption of the c-src proto-oncogene leads to osteopetrosis in mice. *Cell*, 64, 693-702.

- SOUTHAN, A. P., MORRIS, N. P., STEPHENS, G. J. & ROBERTSON, B. 2000. Hyperpolarization-activated currents in presynaptic terminals of mouse cerebellar basket cells. *J Physiol*, 526 Pt 1, 91-7.
- STANKIEWICZ, T. R. & LINSEMAN, D. A. 2014. Rho family GTPases: key players in neuronal development, neuronal survival, and neurodegeneration. *Front Cell Neurosci*, 8, 314.
- STEHELIN, D., VARMUS, H. E., BISHOP, J. M. & VOGT, P. K. 1976. DNA related to the transforming gene(s) of avian sarcoma viruses is present in normal avian DNA. *Nature*, 260, 170-173.
- STEIN, P. L., VOGEL, H. & SORIANO, P. 1994. Combined deficiencies of Src, Fyn, and Yes tyrosine kinases in mutant mice. *Genes Dev*, 8, 1999-2007.
- SUBAUSTE, M. C., VON HERRATH, M., BENARD, V., CHAMBERLAIN, C. E., CHUANG, T.-H., CHU, K., BOKOCH, G. M. & HAHN, K. M. 2000. Rho Family Proteins Modulate Rapid Apoptosis Induced by Cytotoxic T Lymphocytes and Fas. *Journal of Biological Chemistry*, 275, 9725-9733.
- SUGIMOTO, Y., ERIKSON, E., GRAZIANI, Y. & ERIKSON, R. L. 1985. Inter- and intramolecular interactions of highly purified Rous sarcoma virus-transforming protein, pp60v-src. *J Biol Chem*, 260, 13838-43.
- SUGRUE, M., BRUGGE, J., MARSHAK, D., GREENGARD, P. & GUSTAFSON, E. 1990. Immunocytochemical localization of the neuron-specific form of the c-src gene product, pp60c-src(+), in rat brain. *The Journal of Neuroscience*, 10, 2513-2527.
- SUMMY, J. M., QIAN, Y., JIANG, B.-H., GUAPPONE-KOAY, A., GATESMAN, A., SHI, X. & FLYNN, D. C. 2003. The SH4-Unique-SH3-SH2 domains dictate specificity in signaling that differentiate c-Yes from c-Src. *Journal of Cell Science*, 116, 2585-2598.
- SUN, L., WANG, D., LI, X., ZHANG, L., ZHANG, H. & ZHANG, Y. 2016. Extracellular matrix protein ITGBL1 promotes ovarian cancer cell migration and adhesion through Wnt/PCP signaling and FAK/SRC pathway. *Biomedicine & Pharmacotherapy*, 81, 145-151.
- TAHIROVIC, S. & BRADKE, F. 2009. Neuronal polarity. *Cold Spring Harb Perspect Biol*, 1, a001644.
- TAKEYA, T. & HANAFUSA, H. 1983. Structure and sequence of the cellular gene homologous to the RSV src gene and the mechanism for generating the transforming virus. *Cell*, 32, 881-890.
- TAYLOR, S. S. & KORNEV, A. P. 2010. Yet another "active" pseudokinase, Erb3. *Proc Natl Acad Sci U S A*, 107, 8047-8.
- TEN KLOOSTER, J. P., JAFFER, Z. M., CHERNOFF, J. & HORDIJK, P. L. 2006. Targeting and activation of Rac1 are mediated by the exchange factor β -Pix. *The Journal of Cell Biology*, 172, 759-769.
- TERUI, E., MATSUNAGA, T., YOSHIDA, H., KOUCHI, K., KURODA, H., HISHIKI, T., SAITO, T., YAMADA, S.-I., SHIRASAWA, H. & OHNUMA, N. 2005. Shc Family Expression in Neuroblastoma: High Expression of shcC Is Associated with a Poor Prognosis in Advanced Neuroblastoma. *Clinical Cancer Research*, 11, 3280-3287.
- TIGARET, C. M., OLIVO, V., SADOWSKI, J. H., ASHBY, M. C. & MELLOR, J. R. 2016. Coordinated activation of distinct Ca(2+) sources and metabotropic glutamate receptors encodes Hebbian synaptic plasticity. *Nat Commun*, 7, 10289.
- TISCORNIA, G., SINGER, O., IKAWA, M. & VERMA, I. M. 2003. A general method for gene knockdown in mice by using lentiviral vectors expressing small interfering RNA. *Proc Natl Acad Sci U S A*, 100, 1844-8.
- TRAYNELIS, S. F., WOLLMUTH, L. P., MCBAIN, C. J., MENNITI, F. S., VANCE, K. M., OGDEN, K. K., HANSEN, K. B., YUAN, H., MYERS, S. J. & DINGLELINE, R. 2010. Glutamate receptor ion channels: structure, regulation, and function. *Pharmacol Rev*, 62, 405-96.
- TREPANIER, C., LEI, G., XIE, Y. F. & MACDONALD, J. F. 2013. Group II metabotropic glutamate receptors modify N-methyl-D-aspartate receptors via Src kinase. *Sci Rep*, 3, 926.
- TSUI-PIERCHALA, B. A., ENCINAS, M., MILBRANDT, J. & JOHNSON JR, E. M. 2002. Lipid rafts in neuronal signaling and function. *Trends in Neurosciences*, 25, 412-417.

- UBERSAX, J. A., WOODBURY, E. L., QUANG, P. N., PARAZ, M., BLETHROW, J. D., SHAH, K., SHOKAT, K. M. & MORGAN, D. O. 2003. Targets of the cyclin-dependent kinase Cdk1. *Nature*, 425, 859-64.
- UEZU, A., OKADA, H., MURAKOSHI, H., DEL VESCOVO, C. D., YASUDA, R., DIVIANI, D. & SODERLING, S. H. 2012. Modified SH2 domain to phototrap and identify phosphotyrosine proteins from subcellular sites within cells. *Proc Natl Acad Sci U S A*, 109, E2929-38.
- WAHL-SCHOTT, C. & BIEL, M. 2009. HCN channels: structure, cellular regulation and physiological function. *Cell Mol Life Sci*, 66, 470-94.
- WAKAMATSU, Y., MAYNARD, T. M., JONES, S. U. & WESTON, J. A. 1999. NUMB localizes in the basal cortex of mitotic avian neuroepithelial cells and modulates neuronal differentiation by binding to NOTCH-1. *Neuron*, 23, 71-81.
- WAKSMAN, G., SHOELSON, S. E., PANT, N., COWBURN, D. & KURIYAN, J. 1993. Binding of a high affinity phosphotyrosyl peptide to the Src SH2 domain: Crystal structures of the complexed and peptide-free forms. *Cell*, 72, 779-790.
- WALKER, F., DEBLAQUIERE, J. & BURGESS, A. W. 1993. Translocation of pp60c-src from the plasma membrane to the cytosol after stimulation by platelet-derived growth factor. *Journal of Biological Chemistry*, 268, 19552-19558.
- WALLAR, B. J. & ALBERTS, A. S. 2003. The formins: active scaffolds that remodel the cytoskeleton. *Trends in Cell Biology*, 13, 435-446.
- WANG, D., HUANG, X.-Y. & COLE, P. A. 2001a. Molecular Determinants for Csk-Catalyzed Tyrosine Phosphorylation of the Src Tail. *Biochemistry*, 40, 2004-2010.
- WANG, H. R., OGUNJIMI, A. A., ZHANG, Y., OZDAMAR, B., BOSE, R. & WRANA, J. L. 2006a. Degradation of RhoA by Smurf1 Ubiquitin Ligase. *Methods in Enzymology*. Academic Press.
- WANG, K., HACKETT, J. T., COX, M. E., VAN HOEK, M., LINDSTROM, J. M. & PARSONS, S. J. 2004. Regulation of the Neuronal Nicotinic Acetylcholine Receptor by Src Family Tyrosine Kinases. *Journal of Biological Chemistry*, 279, 8779-8786.
- WANG, L., SUNAHARA, R. K., KRUMINS, A., PERKINS, G., CROCHIERE, M. L., MACKEY, M., BELL, S., ELLISMAN, M. H. & TAYLOR, S. S. 2001b. Cloning and mitochondrial localization of full-length D-AKAP2, a protein kinase A anchoring protein. *Proceedings of the National Academy of Sciences*, 98, 3220-3225.
- WANG, Y. H., AYRAPETOV, M. K., LIN, X. & SUN, G. 2006b. A new strategy to produce active human Src from bacteria for biochemical study of its regulation. *Biochem Biophys Res Commun*, 346, 606-11.
- WANG, Y. T. & SALTER, M. W. 1994. Regulation of NMDA receptors by tyrosine kinases and phosphatases. 369, 233-235.
- WEI, J., MIALKI, R. K., DONG, S., KHOO, A., MALLAMPALLI, R. K., ZHAO, Y. & ZHAO, J. 2013. A new mechanism of RhoA ubiquitination and degradation: Roles of SCFFBXL19 E3 ligase and Erk2. *Biochimica et Biophysica Acta (BBA) - Molecular Cell Research*, 1833, 2757-2764.
- WEILER, M., SMITH, J. & MASTERS, J. 1996. CR16, a novel proline-rich protein expressed in rat brain neurons, binds to SH3 domains and is a MAP kinase substrate. *Journal of Molecular Neuroscience*, 7, 203-215.
- WENG, Z., RICKLES, R. J., FENG, S., RICHARD, S., SHAW, A. S., SCHREIBER, S. L. & BRUGGE, J. S. 1995. Structure-function analysis of SH3 domains: SH3 binding specificity altered by single amino acid substitutions. *Mol Cell Biol*, 15, 5627-34.
- WHISSTOCK, J. C. & LESK, A. M. 1999. SH3 domains in prokaryotes. *Trends Biochem Sci*, 24, 132-3.
- WHITTARD, J. D., SAKURAI, T., CASSELLA, M. R., GAZDOIU, M. & FELSENFELD, D. P. 2006a. MAP kinase pathway-dependent phosphorylation of the L1-CAM ankyrin binding site regulates neuronal growth. *Mol Biol Cell*. United States.

- WHITTARD, J. D., SAKURAI, T., CASSELLA, M. R., GAZDOIU, M. & FELSENFELD, D. P. 2006b. MAP Kinase Pathway-dependent Phosphorylation of the L1-CAM Ankyrin Binding Site Regulates Neuronal Growth. *Molecular Biology of the Cell*, 17, 2696-2706.
- WIESTLER, O. D. & WALTER, G. 1988. Developmental expression of two forms of pp60c-src in mouse brain. *Mol Cell Biol*, 8, 502-4.
- WILLIAMS, A. D., JUNG, S. & POOLOS, N. P. 2015. Protein kinase C bidirectionally modulates Ih and hyperpolarization-activated cyclic nucleotide-gated (HCN) channel surface expression in hippocampal pyramidal neurons. *The Journal of Physiology*, 593, 2779-2792.
- WILLIAMS, J. C., WEIJLAND, A., GONFLONI, S., THOMPSON, A., COURTNEIDGE, S. A., SUPERTI-FURGA, G. & WIERENGA, R. K. 1997. The 2.35 Å crystal structure of the inactivated form of chicken Src: a dynamic molecule with multiple regulatory interactions. *J Mol Biol*, 274, 757-75.
- WINKLE, C. C., HANLIN, C. C. & GUPTON, S. L. 2016. Utilizing Combined Methodologies to Define the Role of Plasma Membrane Delivery During Axon Branching and Neuronal Morphogenesis. e53743.
- WITTE, H., NEUKIRCHEN, D. & BRADKE, F. 2008. Microtubule stabilization specifies initial neuronal polarization. *J Cell Biol*, 180, 619-32.
- WORLEY, T. L., CORNEL, E. & HOLT, C. E. 1997. Overexpression of c-src and n-src in the DevelopingXenopusRetina Differentially Impairs Axonogenesis. *Molecular and Cellular Neuroscience*, 9, 276-292.
- XIAO, J., DUAN, Q., WANG, Z., YAN, W., SUN, H., XUE, P., FAN, X., ZENG, X., CHEN, J., SHAO, C. & ZHU, F. 2016. Phosphorylation of TOPK at Y74, Y272 by Src increases the stability of TOPK and promotes tumorigenesis of colon. *Oncotarget*.
- XIE, Z., CAHILL, M. E. & PENZES, P. 2010. Kalirin loss results in cortical morphological alterations. *Molecular and Cellular Neuroscience*, 43, 81-89.
- XU, W., HARRISON, S. C. & ECK, M. J. 1997. Three-dimensional structure of the tyrosine kinase c-Src. *Nature*, 385, 595-602.
- YAMAGUCHI, H. & HENDRICKSON, W. A. 1996. Structural basis for activation of human lymphocyte kinase Lck upon tyrosine phosphorylation. *Nature*, 384, 484-489.
- YAN, Y., EIPPER, B. A. & MAINS, R. E. 2014. Kalirin-9 and Kalirin-12 Play Essential Roles in Dendritic Outgrowth and Branching. *Cerebral Cortex*.
- YANG, K., TREPANIER, C., SIDHU, B., XIE, Y. F., LI, H., LEI, G., SALTER, M. W., ORSER, B. A., NAKAZAWA, T., YAMAMOTO, T., JACKSON, M. F. & MACDONALD, J. F. 2012. Metaplasticity gated through differential regulation of GluN2A versus GluN2B receptors by Src family kinases. *EMBO J*. England.
- YANG, M. & LEONARD, J. P. 2001. Identification of mouse NMDA receptor subunit NR2A C-terminal tyrosine sites phosphorylated by coexpression with v-Src. *J Neurochem*, 77, 580-8.
- YANG, X. M., MARTINEZ, R., LE BEAU, J., WIESTLER, O. & WALTER, G. 1989. Evolutionary expression of the neuronal form of the src protein in the brain. *Proceedings of the National Academy of Sciences*, 86, 4751-4755.
- YU, H.-G., LU, Z., PAN, Z. & COHEN, I. 2004. Tyrosine kinase inhibition differentially regulates heterologously expressed HCN channels. *Pflügers Archiv*, 447, 392-400.
- YU, H., ROSEN, M., SHIN, T., SEIDEL-DUGAN, C., BRUGGE, J. & SCHREIBER, S. 1992. Solution structure of the SH3 domain of Src and identification of its ligand-binding site. *Science*, 258, 1665-1668.
- YU, X. M., ASKALAN, R., KEIL, G. J., 2ND & SALTER, M. W. 1997. NMDA channel regulation by channel-associated protein tyrosine kinase Src. *Science*, 275, 674-8.
- ZARRINPAR, A., BHATTACHARYYA, R. P. & LIM, W. A. 2003. The structure and function of proline recognition domains. *Sci STKE*, 2003, Re8.

- ZEQIRAJ, E., FILIPPI, B. M., DEAK, M., ALESSI, D. R. & VAN AALTEN, D. M. 2009. Structure of the LKB1-STRAD-MO25 complex reveals an allosteric mechanism of kinase activation. *Science*, 326, 1707-11.
- ZEQIRAJ, E. & VAN AALTEN, D. M. 2010. Pseudokinases-remnants of evolution or key allosteric regulators? *Curr Opin Struct Biol*, 20, 772-81.
- ZHANG, S. Q., YANG, W., KONTARIDIS, M. I., BIVONA, T. G., WEN, G., ARAKI, T., LUO, J., THOMPSON, J. A., SCHRAVEN, B. L., PHILIPS, M. R. & NEEL, B. G. 2004. Shp2 Regulates Src Family Kinase Activity and Ras/Erk Activation by Controlling Csk Recruitment. *Molecular Cell*, 13, 341-355.
- ZHAO, W., CAVALLARO, S., GUSEV, P. & ALKON, D. L. 2000. Nonreceptor tyrosine protein kinase pp60c-src in spatial learning: Synapse-specific changes in its gene expression, tyrosine phosphorylation, and protein-protein interactions. *Proceedings of the National Academy of Sciences*, 97, 8098-8103.
- ZHENG, X. M., RESNICK, R. J. & SHALLOWAY, D. 2000. A phosphotyrosine displacement mechanism for activation of Src by PTP α . *The EMBO Journal*, 19, 964-978.
- ZHOU, S., SHOELSON, S. E., CHAUDHURI, M., GISH, G., PAWSON, T., HASER, W. G., KING, F., ROBERTS, T., RATNOFSKY, S., LECHLEIDER, R. J., NEEL, B. G., BIRGE, R. B., FAJARDO, J. E., CHOU, M. M., HANAFUSA, H., SCHAFFHAUSEN, B. & CANTLEY, L. C. 1993. SH2 domains recognize specific phosphopeptide sequences. *Cell*, 72, 767-778.
- ZONG, X., ECKERT, C., YUAN, H., WAHL-SCHOTT, C., ABICHT, H., FANG, L., LI, R., MISTRİK, P., GERSTNER, A., MUCH, B., BAUMANN, L., MICHALAKIS, S., ZENG, R., CHEN, Z. & BIEL, M. 2005. A Novel Mechanism of Modulation of Hyperpolarization-activated Cyclic Nucleotide-gated Channels by Src Kinase. *Journal of Biological Chemistry*, 280, 34224-34232.